CVR JOURNAL OF SCIENCE AND TECHNOLOGY

Vol.No. 17, December 2019
P-ISSN 2277 - 3916

DOI 10.32377/CVRJST17
E-ISSN 2581 - 7957

CVR COLLEGE OF ENGINEERING

In Pursuit of Excellence

PATRONS

Dr. Raghava V. Cherabuddi, President & Chairman

Dr. K. Rama Sastri, Director

Dr. K.S. Nayanathara, Principal

Editor : **Dr. K. Lal Kishore, Professor and Dean- Research, CVRCE**

Associate Editor : **Dr. S. Venkateshwarlu, Professor & Head, Dept. of EEE**

Editorial Board :

Dr.M.V. Seshagiri Rao	Professor & Dean-Planning & Coordination, CVRCE
Prof. L.C. Siva Reddy	Professor & Vice-Principal, CVRCE
Dr. Rameshwar Rao	Professor & Dean- Projects & Consultancy, CVRCE
Dr. N.V. Rao	Professor & Dean-Academics, CVRCE
Dr. T. Muralidhara Rao	Professor & Head, Dept. of Civil Engg., CVRCE
Dr. K. Venkateswara Rao	Professor & Head, Dept. of CSE, CVRCE
Dr.K. Lalithendra	Professor & Head, Dept. of ECE, CVRCE
Dr. S. Harivardhagini	Professor & Head, Dept. of EIE, CVRCE
Dr. Bipin Bihari Jayasingh	Professor & Head, Dept. of IT, CVRCE
Dr. M. Venkata Ramana	Professor & Head, Dept. of Mech. Engg., CVRCE
Dr. H.N. Lakshmi	Professor & Head, Dept. of CSIT, CVRCE
Dr. G. Bikshamaiah	Professor & Head, Dept. of H&S, CVRCE

International Review Board:

Prof. Tzung-Pei Hong	Chair Professor, Dept. of CSI Engg., AI Research Center National University of Kaohsiung 811, Taiwan
Dr. Tomonobu Senjyu	Professor, Department of Electrical Engineering, University of the Ryukyus, Nishihara-cho, Nakagami Okinawa, Japan
Dr Masoud Mohammadian	Assoc. Professor, Faculty of Science and Technology, University of Canberra, Australia
Dr. Rubén Ruiz García	Full Professor, Head of the Applied Optimization Systems Group, Department of Applied Statistics, Universitat Politècnica de València, Camino de Vera, Spain
Dr. Ray-Hwa Wong	Professor, Department of Mech. Engg., Hwa-Hsia University of Technology, Taipei, Taiwan
Dr. Stefan Talu	Faculty of Mech. Engineering, DMCDI, The Technical University of Cluj-Napoca, B-dul Muncii Street, No. 103-105, Cluj-Napoca, 400641, Romania
Assoc. Prof. Ir. Dr. Norhaliza Abdul Wahab	Director, Control & Mechatronics Engg. Dept., Faculty of Electrical Engineering, UTM Skudai 81310 Johor
Dr. R. Venkata Rao	Professor, Department of Mech Engg., Sardar Vallabhbhai National Institute of Technology (SVNIT), Surat, Gujarat State – 395 007, India
Dr. Vijay Janyani	Professor Dept. of ECE, Malaviya National Institute of Technology (MNIT), Jaipur - 302017 (Rajasthan)
Dr.V. Prasanna Venkatesan	Prof. & Head, Department of Banking Technology, School of Management, R.V.Nagar, Kalapet, Pondicherry University, Puducherry

CVR JOURNAL OF SCIENCE AND TECHNOLOGY

Indexed by

- Google Scholar
- Directory of Research Journals Indexing (DRJI)
- Scientific Indexing Services (SIS)
- International Institute of Organised Research (I2OR)
- Scholar Impact - Journal Index
- Citefactor
- Member Crossref / DOI

NIRF Ranking of 132 in the Country

Accredited by NAAC with 'A' GRADE

CVR COLLEGE OF ENGINEERING

(UGC Autonomous - Affiliated to JNTU Hyderabad)
Mangalpalli (V), Ibrahimpatnam (M),
R.R. District, Telangana. – 501510
http://cvr.ac.in

EDITORIAL

We are glad to bring out Volume – 17 of the Biannual Journal- CVR Journal of Science and Technology, due in December 2019. This Volume has DOI number and e-ISSN number along with print ISSN number on the cover page. Every research article published is given DOI number and they can be accessed on- line. On line portal is also created for the Journal. This Volume is also brought out in time, with the co-operation of all the authors and editorial team, despite some issues with Anti-plagiarism software. We are thankful to the Management for supporting this activity, and permitting to publish the journal in colour print, using quality printing paper.

The Volume covers research articles in the following branches of engineering. The breakup of papers among various branches is:

CIVIL – 5, ECE – 5, CSE– 4, EEE – 5, EIE – 3, MECH – 3.

In this issue, total number of research articles published is increased to 25.

This issue has an article on Strength and Durability Studies on Steel Fibre Reinforced Self Compacting Concrete. On similar lines another article on Self-cured High Strength Concrete is also published. In the field of communications, an article on Automatic Aircraft Tracking with RTL-SDR is also published. For Future Ultra-Wideband Applications, a Semi-circular Slotted Monopole Antenna is proposed, and an article is published regarding the same. In another article related to LVDT, an Efficient Approach for Optimization of Nonlinearity Response is explained. On Robotics, Virtually Transcribed and Restrained System is described in one article. Another article on Brain Image Registration using Evolve Contourlet Transform - An Efficient way to Register the Monomodal MRI-T2 Images, is published which has medical applications. Similarly, there are 25 such articles in different branches of engineering. Hope these articles make an interesting reading for researchers.

The college has many accomplishments and to name a few, it obtained **NBA Tier 1 accreditation for its UG Programs, NAAC 'A' grade**, **UGC autonomous status**, **National Employability Award** for seventh year in a row and received a very high rating by several ranking agencies including the most recent Education World ranking of third best college in Telangana and Outlook magazine, rating CVR CE, one among the **top 100 colleges in the country**, and **AAAA grade** from Careers 360. The college received the **ISTE Best Engineering College award.** The college received Rs. 2.87 crores from New Gen IEDC of DST.

I am thankful to all the members of the Editorial Board for their help in reviewing and short listing the research papers for inclusion in the current Volume of the journal. I wish to thank **Dr. S. Venkateshwarlu, HOD, EEE** for the effort made in bringing out this Volume. Thanks are due to **HOD, H & S, Dr. G. Bhikshamaiah** and the staff of English Department for reviewing the papers. I am also thankful to **Smt. A. Sreedevi**, **DTP Operator** in the Office of Dean Research for the effort put, in the preparation of the papers in Camera Ready form.

For further clarity on waveforms, graphs, circuit diagrams and figures, readers are requested to browse the soft copy of the journal, available on the college website **www.cvr.ac.in** wherein a link is provided. Authors can also submit their papers through our online open journal system(OJS) **www.ojs.cvr.ac.in** or **www.cvr.ac.in/ojs**

Prof. K. Lal Kishore

CONTENTS

E-ISSN 2581 – 7957
P-ISSN 2277 – 3916

CVR Journal of Science and Technology, Volume 17, December 2019
DOI: 10.32377/cvrjst1701

Strength and Durability Studies on Steel Fibre Reinforced Self Compacting Concrete

Dr. M.V. Seshagiri Rao[1] and Md. Pasha Junead[2]
[1]Professor, CVR College of Engineering/ Civil Engg. Department, Hyderabad, India.
Email: rao_vs_meduri@yahoo.com
[2]PG Scholar, CVR College of Engineering/Civil Engg. Department, Hyderabad, India.
Email: m.p.junead786@gmail.com

Abstract: **This paper presents the studies on the strength and durability properties of Steel Fibre Reinforced Self Compacting Concrete (SFRSCC) of different grades. Compressive strength and durability performance of Steel Fibre Reinforced Self Compacting Concrete (SFRSCC) using hooked end steel fibres is reported in terms of Chemical Resistance, Initial Absorption Test (ISAT). The rational mix design procedure is used for designing the SCC mixes satisfying the EFNARC (2005) guidelines. In the first phase, the mechanical properties like compressive strength and in the second phase durability properties like Acid-Durability factors, sorptivity were studied for the Plain SCC (SCCP) and Steel Fibre Reinforced SCC (SFRSCC) and comparisons are made. Based on the studies, it is observed that the compressive strengths of the SFRSCC were found to be about 2% to 10% more compared to SCCP. The Sorptivity of SFRSCC is found to be reduced, with the addition of steel fibres and increase in the grade of concrete. Acid weight loss factor, the loss of dimension stability, acid strength loss percentage decreases with increase in grade of concrete. With increase in the period of immersion of the concrete in 5% concentration of acids and sulphates like Na2SO4, HCL, H2SO4, there was a damage of concrete near the corners of the cubes and such disruption in SFRSCC was less than that in SCCP. When compared to the plain SCC, the SFRSCC was found to be more durable against both acids and sulphates.**

Index Terms: Acid durability factor, Steel Fibres, Acid attack factor, Durability, Self Compacting Concrete, Strength and Sorpitivity.

I. Introduction

Self compacting concrete or self consolidating concrete is defined as a concrete, which has ability to flow under its self weight and to fill every corner of the formwork evenly without any external vibration, while maintaining its homogeneity.

The concept of self compacting concrete is proposed by Professor Hajme Okamura of Japan in 1986 to overcome some of the problems associated with fresh concrete like skill of workers, type and shape of structural section, complexity of reinforcement , segregation, pumpability and compaction. But the prototype was first developed by Professor Ozawa of Japan in 1989.

The BIS has not brought out any standard mix procedure, even though number of agencies and researchers carried out several investigations to establish rational mix design procedure and self compatibility testing methods. The self compacting concrete consists of cement, fine and coarse aggregates, water, mineral and chemical admixtures whose composition is similar to normal concrete. The notable difference between self compacting concrete and normal concrete is that, the self compacting concrete has more fines content, high range water reducing agents and Viscosity Modifying Agent (VMA). Mineral Admixtures are used as extra fine material besides cement, and some cases, they replace cement. The admixtures are used to improve strength and durability properties of concrete.

II. Literature Review

Cunha W.V.M.C.F, Barros J.A.O and Sena-Cruz J.M. (2011) [1] presented the work carried out to develop numerical model for the tensile behaviour of SFRSCC. They have assumed SFRSCC as two phase material. The nonlinear material behaviour of self-compacting concrete is given in 3-D smeared crack model. The numerical model showed good correlation with experimental values.

Chandrasekhar M, Seshagiri Rao M V, Janardhana Maganti (2012) et al. [2] Behavior of Fibre Reinforced Self Compacting Concrete and its application as Wall Panels developed by the above authors. In this investigation, Cubes of 100mm x 100mm x 100mm and cylinders of 150mm diameter x 300mm length were cast for obtaining the compressive strength and stress-strain behaviour of both plain M30 grade SCC and M30 grade SFRSCC separately. The compressive strengths of the FRSCC design mixes are found to have increased by the addition of fibres. However, it is observed in improvement of stress values for the same strains because of addition of fibres.

The stress - strain behaviour of FRSCC and SCC mixes was found to be almost similar. However, it is observed that the addition of fibres has improved the stress values for the same strains. The increase in strain values was observed at peak stresses in all FRSCC mixes and rom the stress-strain behaviour of all types of FRSCC, it is concluded that the ultimate load- carrying capacity and strains at peak stresses are more in SFRSCC and HFRSCC for mixes upto 1.062% confinement. The hybridization of SCC with glass and steel fibres has shown superior performance amongst all FRSCC mixes.

E-ISSN 2581 – 7957
P-ISSN 2277 – 3916

DOI: 10.32377/cvrjst1701

W Zhu J Quinn & P.J.M Bartos (2002) et al. [3] (Aspects of Durability Of Self Compacting Concrete). In the present study, gas permeability, capillary water absorption and chloride diffusivity, which are important indicators for concrete durability performance, of various types of SCC and conventional vibrator reference concrete mixes were assessed and compared.

The SCC mixes have shown significant lower values of sorptivity and coefficient of permeability when compared to the traditional vibrated reference mixes of the same strength grade. The SCC mixes have also shown almost same chloride diffusivity to those of vibrated mixes. However, the chloride diffusivity was found to be very much dependant on the types of powder used in concrete. Both the reference and SCC mixes containing PFA showed much lower values of coefficient of chloride migration than the other mixes. Among the three different SCC mixes, it appeared that the SCC mix containing no additional powder but using the viscosity agent to maintain stability of the fresh mix had the highest permeability, sorptivity and chloride diffusivity, thus less resistant to ingress of aggressive fluids.

S Shrihari and Seshgiri Rao M V (2016) *et al*. [4] The authors developed Strength and Durability properties of SCC with GBFS and Meta Kaolin. In this development, test results of compressive strength of cubes and cylinders are on lower side with the use of 100% river sand and the Strength increased where 40% of GBFS with 10% of Meta Kaolin were replaced with the river sand.

The physical and chemical properties of GIBFS are suitable for the production of concrete mix. The rapid chloride permeability test and water absorption was conducted, with the use of Meta Kaolin and increasing % of fly ash with GBFS an improvement in the impermeability of concrete and also the compressive strength and split tensile strength are lower for 0% replacement. Percentage of water absorption gradually decreases with the use of GIBFS with Meta Kaolin, the replacement of cement by MK leads to decrease in pore space.

N Venkat Rao, M Rajasekhar, Mohd Mujeebuddin Ahmed (2013) The above authors have explained about an Experimental Study on Durability of High Strength Self Compacting Concrete (HSSCC). The test specimens of 10cmX10cmX10cm cubes were immersed in 5 % of Sodium sulphate solution over a period of time. The performance and properties of concrete that can be affected by sulphate attack were identified. The amount of attack by H2SO4 is comparatively more when compared with that of HCL and Na2SO4.

The percentage reduction in compressive strength of the specimens with and without immersion in acids (HCL, H2SO4) and sulphate (Na2SO4) solutions of 5 % concentration after 28 days was found to be 16.31 %, 47.07 % and 19.86 % respectively. It is noticed that the attack intensity by H2SO4 is comparatively more than that of HCL and Na2SO4. The reduction of strength due to the effect of H2SO4 on the concrete is more significant.

III. Experimental Programme

The experimental programme consisted of casting and testing SCC specimens. The mixes were designed with rational mix design method and several trials were made in producing SCC satisfying the EFNARC specifications (EFNARC, 2005). A total of four grades of concrete were investigated. A total of forty standard cubes of size 150mmX150mmX150mm for SCCP, 40 standard cubes for SFRSCC for acid attack, sulphate attack and eight specimens each for SCCP and SFRSCC of size 100mm×100mm for sorptivity studies, were cast and tested.

IV. Materials and Properties

Cement

Ordinary Portland Cement of 53 grade is used in this investigation. The Cement used was tested as per IS 4031-1988 and found to be satisfying the specifications of 12269-1987.The specific gravity was 3.2 and fineness was 2.38%.

Coarse Aggregate

Crushed angular granite of 10 mm size from a local market was used as coarse aggregate. The specific gravity and fineness modulus were 2.65 and 6.7 respectively.

Fine Aggregate

River sand was used as fine aggregate. The specific gravity is 2.60 and fineness modulus is 2.79.

Fly Ash

Type-II fly ash was used in the present investigation. The properties of fly ash is confirms to I.S. 3812 – 2002.

Steel Fibres

Hooked end steel fibres of 0.4mm diameter and Aspect ratio of 30 and 12mm length were used.

Super Plasticizer

Super Plasticizer (Conplast :SP430) having specific gravity 1.22 to 1.225 at 30^0C and pH value as 7 ± 1 , brown colour with no Chloride Content is used.

Viscosity Modifying Agent

Viscosity modifying agent used is colourless, in liquid form. It is having a Specific of gravity 1.02 ± 0.01 @ 25^0C and pH value as 8 ± 1 with no Chloride Content is used.

Acids and sulphates

The properties of the constituent acids and sulphate used in the present investigation are LR (laboratory grade) hydrochloric acid 35–38% with specific gravity 1.18, LR sulphuric acid 98%, 98.07 g/mol with specific gravity 1.835 and sodium sulphate with specific gravity of 1.464, molecular weight 142.036 g/mol. The concentrations of both acids and sulphate are 5%.

E-ISSN 2581 – 7957
P-ISSN 2277 – 3916

DOI: 10.32377/cvrjst1701

V. Mix Proportions

The Rational mix design methods was used (SV Rao et al., 2010). The details of the mix proportions are shown in Table 1, The fresh properties of the four grades of concrete and the compressive strength of the four grades of concrete were shown.

VI. Strength Studies

Before investigating the strength properties of SCC and SFRSCC, the fresh properties of concrete like slump flow T50cm, V-Funnel, L-Box Test were calculated. Later the compressive strength of cubes for 7 days and 28 days were calculated for different grades of SCC and SFRSCC.

VII. Durability Studies

Tests for acid attack and sorptivity were conducted for different grades of SCCP and SFRSCC.

Tests for acid attack on SCCP and SFRSCC

After 28 days of water curing, each cube was tested for compressive strength and weight. The specimens of different grades viz. M20, M30, M40 and M60 were exposed to 5% solutions of Sulfuric acid, Hydrochloric acid and Sodium Sulphate for 28 days and 56 days. The response of the specimens to the solutions was evaluated through change in appearance, weight, compressive strength and dimensions of solid diagonals. Before testing, each specimen was removed and brushed and cleaned with water.The resistance of concrete specimens to aggressive environment such as acid attack, durability attack factors such as acid strength loss factor (ASLF), acid attacking factor (AAF), acid weight loss factor (AWLF) and acid durability loss factor (ADLF) (Venkateswara Rao, 2010) are evaluated as per ASTM C 666–1997 (ASTM, 1997).

ASLF gives relative performance of concrete before and after immersion in different acids and Sulphates. The factor also depends on the period of immersion of the specimen in solution. ASLF can be calculated as

Acid strength loss factor (ASLF) = Sr × (N/M)

Where Sr is relative strength at N days (%), N is number of days at which the durability factor is required; M is number of days at which the exposure is to be terminated. A lower value of ASLF indicates greater stability towards acid attack.

AAF is meant to determine indirectly the disruption of concrete near the corners of the cube by way of measuring the change in the length of diagonal (referred to as diagonal loss) in a typical concrete cube after immersion in acids and Sulphate for a certain period of time.

A higher value of AAF indicates that the dimensional stability is lower.

AWLF is calculated after immersing the cubes in different solutions for different periods.

A higher value of the AWLF indicates that the weight loss is greater.

In order to have a unified factor describing durability, these factors are combined to derive a factor termed the ADLF.

ADLF = ASLF × AAF × AWLF

Test for Sulphate Attack on SCC and SFRSCC

Resistance of concrete to the attack has been tested by immersing concrete cubes in the solution of 5 % Sodium Sulphate. The effect of chemical attack has been determined by measuring change of mass into consideration. The test specimens of 100mm×100mm×100 mm were immersed in 5 % of Sodium Sulphate solution for different periods ie.28 and 56 days and the effect of Sulphate attack on performance properties of concrete are obtained. The resistance of concrete to the Sulphate attack has been estimated by considering changes in their dynamic modulus of elasticity. Even from the visual observation also the intensity of Sulphate attack on disintegration is noticed.

Tests for Sorptivity

Sorptivity is transport of moisture into unsaturated specimens. Sorptivity is as an important index of concrete durability because the test method used for the determination of Sorptivity reflects the way in which different solutions will penetrate into the concrete. Sorptivity tests were carried out on cubes of size 100 mm × 100 mm × 100 mm on the basis of Hall's method (Hall, 1989).
The Sorptivity Co-efficient (S) was calculated using the following expression

$S = i/t1/2, i = \Delta W/Ad$

Where ΔW is the amount of water absorbed (kg); A is the cross-section of specimen that was in contact with water (m2); d is the density of the medium in which the specimen was dipped (d = 1, as the medium used was water); t = time (min). The unit of s is kg/(m2 min1/2).

The variation of i against t1/2 was plotted.

VIII. Test Results and Discussions

Durability studies

The durability of different grades SCC and SFRSCC was studied. A total number of 80 cubes were cast and after 56 days of acid environment curing with distilled water. The cubes were tested for compressive strength. From the studies on acid effect on SCC and SFRSCC specimens, it was noted that most of the SFRSCC specimens performed well compared with SCC specimens. To estimate the effects of acid on SCC and SFRSCC, certain factors are determined, as explained in the following paragraphs.
When the specimens were kept in an acid environment, the net loss in strength, physical change in the dimensions of the cube and weight loss were noted. All of these can be considered to derive a unique factor typically depicting the various losses due to acid attack and termed as ADLF (Venkateswara Rao, 2010). The different losses are individually quantified in terms of different factors.

Acid Strength Loss Factor

The ASLF indicates the variation in the compressive strength of SCC and SFRSCC when kept in different acidic environments, namely HCl and H2SO4 at 5 %

E-ISSN 2581 – 7957
P-ISSN 2277 – 3916

DOI: 10.32377/cvrjst1701

concentrations. Figure 1 shows the variation of ASLF in SCC and SFRSCC for 56 days of immersion in acids. The figure indicates that the SCC and SFRSCC showed more or less similar percentage loss in strength for the different grades of concrete. Furthermore, it is observed that as the strength grade increased there is a slight increase in percentage loss of strength in both SCC and SFRSCC. This justifies the notion that increase in strength may not bring increase in durability, as interpreted from the loss of strength, because, it can be based on performance design rather than the strength-based design of concrete. The ASLF is less for SFRSCC than SCC for 5% HCl and the rate of increase of ASLF is greater in sulfuric acid solution.

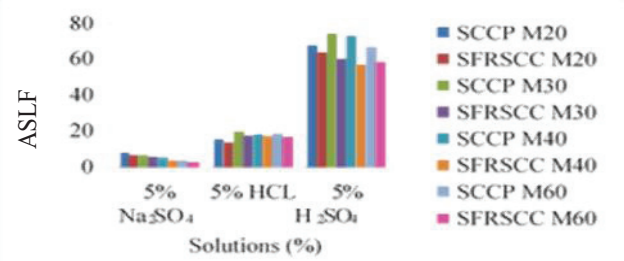

Figure 1. Acid Strength Loss Factors (ASLF) for SCCP and SFRSCC at 56 Days

Acid Attacking Factor

The AAF gives an idea of the disruption in the geometry of the specimen due to an acidic environment. This is determined by measuring the loss in the diagonals of standard test specimens. The average loss in the diagonals was measured for all the specimens immersed in acid at the end of 28 days and 56 days. The comparison for all the grades of concrete between SCC and SFRSCC revealed that SFRSCC specimens performed better than SCC specimens. Figure 2 shows the variation of AAF in SCC and SFRSCC for 56 days of immersion in acids. This indicates that there is less loss of diagonal (i.e. greater dimensional stability) in SFRSCC mixes than in SCC mixes.

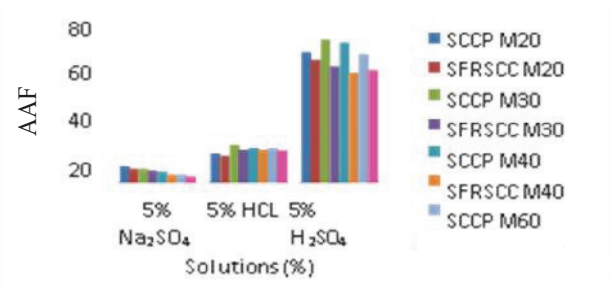

Figure 2. Acid attack factor of SCC and SFRSCC at 56 days of immersion

Acid Weight Loss Factor

Because of the acidic environment, the pH of the concrete decreases; at the same time, the cement and the mortar parts breakdown by the acid. This results in decrease in the weight of the specimen. It can be noted in general that the loss is greater with 5% H2SO4 than with HCl. Figure 3 shows the variation of AWLF in SCC and SFRSCC for 56 days of immersion in acids.

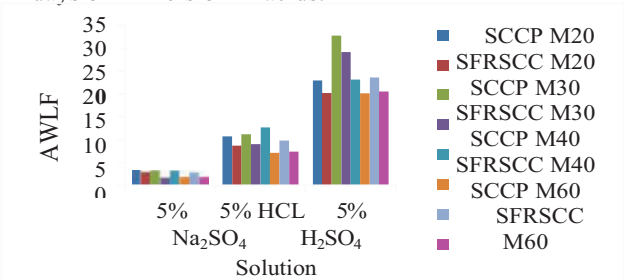

Figure 3. Acid weight loss factors (AWLF) for SCC and SFRSCC at 56 days of immersion

Acid Durability Loss Factor

As mentioned in previous section losses in strength, weight and geometry are combined to obtain a durability factor termed ADLF. Figure 4 shows the variation of ADLF in SCC and SFRSCC for 56 days of immersion in acids. It can be noted that the losses are greater in SCC specimens than in SFRSCC specimens. Hence, it can be said at this stage that the SFRSCC specimens are more durable compared to SCC. In the present study, four grades of concrete and two types of acids (HCl and H2SO4) and one type of Sulphate with concentration of 5% were considered. The ADLF values were calculated from the loss factors of ASLF, AAF and AWLF. The average ADLF values are given in Table 2. Figure 4 shows the variation in average ADLF with acid concentration for both SCC and SFRSCC.

The figure reveals that for HCL and Na2SO4 concentrations the SCC and SFRSCC behaved similarly, but as the H2SO4 concentration increased the SCC showed higher damage levels than SFRSCC. This indicates that the performance of SFRSCC is better than that of SCC under acidic and Sulphate environmental conditions. It also supports the use of SFRSCC in acidic and Sulphate environments.

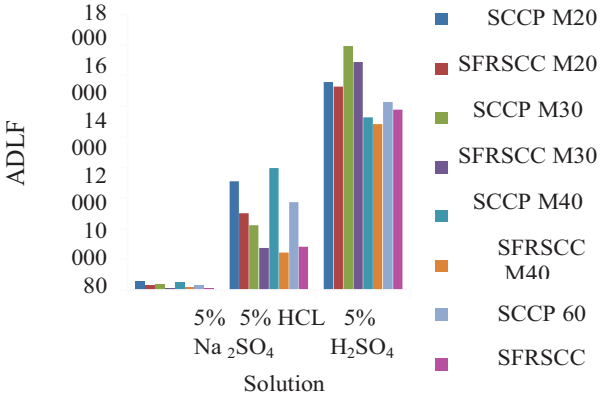

Figure 4. Acid Durability Loss Factors (ADLF) for SCCP and SFRSCC at 56 Days of immersion

Sorptivity Studies on SCP and SFRSCC

Sorptivity is the absorption and transmission of water by capillary action (Pereira de Oliveira et al., 2006). Table 4 shows the details of the water absorbed due to capillary action and Sorptivity coefficient for SCC and SFRSCC. Figures 5 & 6 show the variation of absorbed water per unit area, i against t1/2: The cumulative water absorption was less for SFRSCC than for SCC with the increase in time. This is true for all grades of concrete. For the Sorptivity coefficient, asymptotic behaviour was observed for both SCC and SFRSCC mixes. It can be noted from the above tables and figures, that as the grade of concrete increases the water absorption decreases, and the values of water absorption in SCC are much lower than that of SFRSCC.

E-ISSN 2581 – 7957
P-ISSN 2277 – 3916

DOI: 10.32377/cvrjst1701

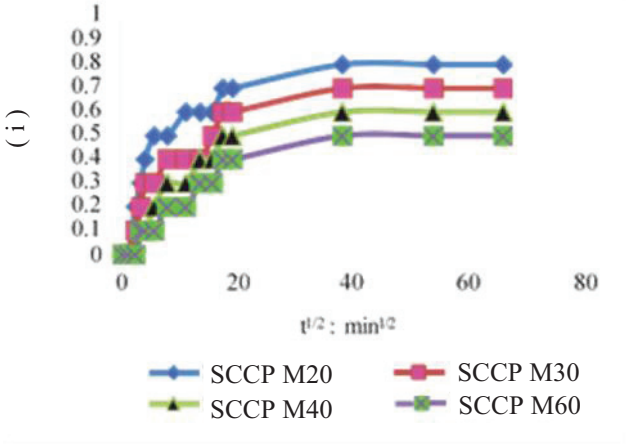

Figure 5. Absorbed water per unit area (i) against time ($t^{1/2}$) for SCCP

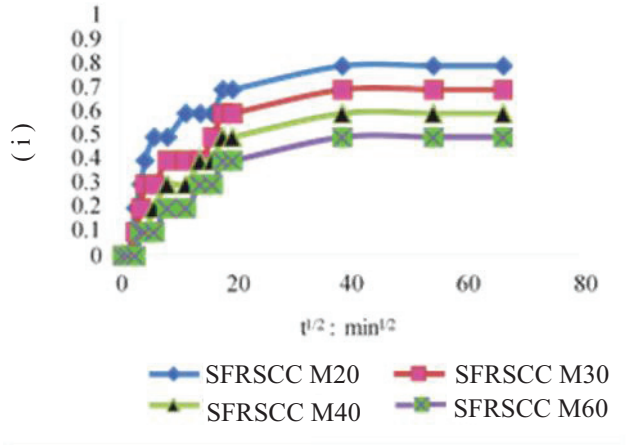

Figure 6. Absorbed water per unit area (i) against time ($t^{1/2}$) for SFRSCC

IX. Conclusions

The following conclusions are drawn based on the studies on SCC and SFRSCC mixes of different grades

1. Fibre reinforced self-compacting concrete can be produced by incorporating Steel fibres to improve its performance. However, the use of appropriate dosages of super plasticizer and viscosity modifying agent are essential to maintain the fresh properties of self-compacting concrete.
2. In the case of Steel fibres, a dosage of 31 kilo grams of fibres/m^3 of concrete is found as the optimum dosage by suitably adjusting the dosages of admixtures.
3. With the increase of fibre dosage, the workability decreases. This problem of workability and flow properties of concrete can be overcome by adding superplastizers and VMA.
4. With the increase in the grade of concrete, the Sorptivity of Steel Fibre Reinforced SCC is found to be decreasing.
5. With the increase in period of immersion of the concrete in 5% concentration of acids like Na2SO4, HCl and H2SO4, there was a damage of concrete near the corners of the standard cube .Such disruption in SFRSCC was observed to be less than in SCC, indicating superior durability of SFRSCC.
6. The SFRSCC has shown 3% more resistance to weight loss, compared to plain SCC.
7. The acid durability loss factor decreases with increase in grade of concrete.When compared to the plain SCC, the SFRSCC was found to be more durable against both acids and sulphates.
8. The acid weight loss factor decreases with increase in the grade of concrete.
9. The AWLF is less in Na2SO4, when compared to HCl and H2SO4 .
10. The loss of dimension stability is more in H2SO4, when compared with HCL and Na2SO4.
11. Acid strength loss percentage is more in H2SO4, when compared with HCL and Na2SO4.
12. Compressive strength of SFRSCC is more, when compared with plain SCC

Figure 7

Figure 8

Figure 9

Figure 7,8,9. Sample cubes After Immersion of Specimens in Acids and Sulphate

E-ISSN 2581 – 7957
P-ISSN 2277 – 3916

CVR Journal of Science and Technology, Volume 17, December 2019
DOI: 10.32377/cvrjst1701

TABLE I.
QUANTITIES PER 1 CUM OF SELF COMPACTING CONCRETES

Grade of Concrete	Cement (kg/m^3)	Fine aggregate (kg/m^3)	Coarse Aggregate (kg/m^3)	Fly ash (kg/m^3)	Water (kg/m^3)	SP % Bwcf	VMA % Bwcf	Glass Fibre % Volume	Designation
M 20	260	910	690	310	240	1	0.05	-	SCCP
	260	910	690	310	240	1	0.05	0.024	SFRSCC
M 30	355	890	720	350	210	1.5	0.05	-	SCCP
	355	890	720	350	210	1.5	0.05	0.024	SFRSCC
M 40	470	883	720	355	240	1.5	0.05	-	SCCP
	470	883	720	355	240	1.5	0.05	0.024	SFRSCC
M 60	655	860	740	320	260	1	-	-	SCCP
	655	860	740	320	260	1		0.024	SFRSCC

TABLE II.
HARDENED PROPERTIES OF SCC AND SFRSCC AT 7 AND 28 DAYS

S.No.	Grade	Designation	Cube Compressive Strength (Mpa)	
			7 Days	28 Days
1	20	SCCP	17.85	26.8
2		SFRSCC	19.16	29.6
3	30	SCCP	24.7	38.8
4		SFRSCC	27.4	42.4
5	40	SCCP	33.5	51.1
6		SFRSCC	35.2	53.6
7	60	SCCP	41.9	66.8
8		SFRSCC	45.03	68.4

TABLE III.
ACID DURABILITY LOSS FACTORS OF SELF COMPACTING CONCRETE MIXES

Type of Concrete	Grade of Concrete	Acid Durability Loss Factors					
		Na_2SO_4		HCL		H_2SO_4	
		28 Days	56 Days	28 Days	56 Days	28 Days	56 Days
SCCP	20	66.01	549.36	635.45	7120.45	2521.25	13645.2
	30	41.19	359.96	658.05	4239.58	2045.83	15842.1
	40	68.01	495.25	1230.55	7989.65	2539.15	11348.0
	60	49.01	298.01	901.28	5770.25	3430.54	12299.9
SFRSCC	20	41.01	273.11	496.12	5019.99	2472.95	13456.2
	30	20.36	159.99	295.14	2759.99	2389.51	15975.2
	40	34.01	219.58	359.16	2475.69	3081.25	10910.7
	60	11.97	145.35	379.99	2850.95	2580.64	10810.2
SCCP	Average ALDF	55.96	427.68	856.58	6279.66	2611.24	13310.7
SFRSCC		26.29	189.96	390.52	3269.74	2567.5	12311.8

E-ISSN 2581 – 7957
P-ISSN 2277 – 3916

DOI: 10.32377/cvrjst1701

TABLE IV.
SORPTIVITY FOR SCCP AND SFRSCC

Time ($min^{1/2}$)	Absorption (i) kg/m^2							
	SCCP M20	SFRSCC M20	SCCP M30	SFRSCC M30	SCCP M40	SFRSCC M40	SCCP M60	SFRSCC M60
0	0	0	0	0	0	0	0	0
1	0	0.1	0	0.1	0	0.1	0	0
2.23	0.1	0.2	0	0.2	0	0.1	0	0.1
3.16	0.2	0.3	0.1	0.2	0	0.2	0	0.1
3.87	0.3	0.3	0.2	0.3	0.1	0.2	0.1	0.2
5.47	0.4	0.4	0.2	0.3	0.1	0.3	0.1	0.2
7.74	0.4	0.4	0.3	0.4	0.2	0.3	0.1	0.2
10.95	0.5	0.5	0.5	0.6	0.2	0.4	0.1	0.3
13.41	0.5	0.6	0.3	0.5	0.3	0.4	0.2	0.3
15.49	0.5	0.6	0.4	0.5	0.3	0.5	0.2	0.4
17.32	0.8	0.9	0.5	0.6	0.4	0.5	0.3	0.4
18.97	0.6	0.7	0.5	0.6	0.4	0.5	0.3	0.4
37.94	0.7	0.8	0.6	0.7	0.5	0.6	0.4	0.5
53.66	0.7	0.8	0.6	0.7	0.5	0.6	0.4	0.5
65.72	0.7	0.8	0.6	0.7	0.5	0.6	0.4	0.5

REFERENCES

[1] Chandrasekhar M, Seshagiri Rao M V, Janardhana Maganti "Structural Behavour of Steel Fibre Reinforced Self Compacting Concrete Wall Panels" BEFIB2012-8th RILEM Symposium on Fibre Reinforced Concrete Guimaraes, September 2012.

[2] W V.M.C.F. Cunha, J.A.O. Barros and J.M. Sena- Cruz "An Integrated Approach for Modelling the Tensile Behaviour of Steel Fibre Reinforced Self- compacting Concrete"-Cement and concrete research 41(2011) pp64-76.

[3] V Karthik and G Baskar (2015) "Study on Durability Properties Of Self Compacting Concrete With Copper Slag Partially Replaced For Fine Aggregate" International Journal Of Civil Engineering And Technology (Ijciet)Volume 6, Issue 9, Sep 2015, pp. 20-30, Article ID: IJCIET_06_09_003.

[4] S Venkateswara Rao, M V Seshagiri Rao, D Ramaseshu, P Rathish Kumar "Durability performance of selfcompacting Concrete" Magazine of Concrete ResearchVolume 64 Issue 11 2012.

[5] S Venkateswara Rao, M V Seshagiri Rao, D Ramaseshu, P Rathish Kumar "A Rational Mix Design Procedure for Self Compacting Concrete" 2010.

[6] Ouchi M. and Okamura H. "Effect of Super Plasticizer on Self- Compactability of Fresh Concrete", Journal of the Transportation Research Board, 1997, pp37-40.

[7] Miao Liu "Wider Application of Additions in Self-Compacting Concrete" Ph.D Thesis, University of London, July 2009.

[8] N Venkat Rao, M Rajasekhar, Mohd Mujeebuddin ahmed "An Experimental study on Durability of High strength self compacting concrete" 2013.

[9] S Shrihari and Seshgiri Rao M V "Strength and Durability properties of SCC with GBFS and MetaKaolin" Journal of Chemical and Pharmaceutical Sciences ISSN: 0974-2115, JCHPS Special Issue 2: August 2016.

[10] W Zhu J Quinn & P.J.M Bartos "Aspects od Durability of Self Compacting Concrete" 2002.

[11] EFNARC, "Specifications and guidelines for self compacting concrete", www.efnarc.org

E-ISSN 2581 – 7957
P-ISSN 2277 – 3916

CVR Journal of Science and Technology, Volume 17, December 2019
DOI: 10.32377/cvrjst1702

Self-Cured High Strength Concrete-An Experimental Study

Dr. T. Muralidhara Rao
Professor, CVR College of Engineering/Civil Engg. Department, Hyderabad, India.
Email: tmuralidhararao@gmail.com

Abstract: **The effect of elevated temperature and durability studies is studied on fifty-four numbers of self-cured high strength concrete cubes of 100mm size with ultrafine mineral admixture, Alccofine 1203. Optimum dosage of internal curing compound and Alccofine used is 0.25% and 10% respectively. Non-destructive, elevated temperature, and durability studies are conducted on the specimens. Between the temperatures 100^0C to 900^0C, the percentage of loss in weight is found to be decreased. But, compressive strength is increased at 300^0C and decreased at higher temperatures. The weight and compressive strength are increased for the cube specimens due to the specimens immersion in Sulphate, Chloride and Alkali solutions and Sea water respectively.**

Index Terms: Elevated temperature, non-destructive tests, **Durability tests, Weight, Compressive strength.**

I. INTRODUCTION

A.Self- Curing

In conventional curing, curing happens 'from external to internal'. In self-curing, curing happens 'from internal to external' through the internal reservoirs. Internal curing reduces the water evaporation from concrete and increases the water retaining capacity of the concrete. The difference between conventional and internal curing is presented in Fig.1.

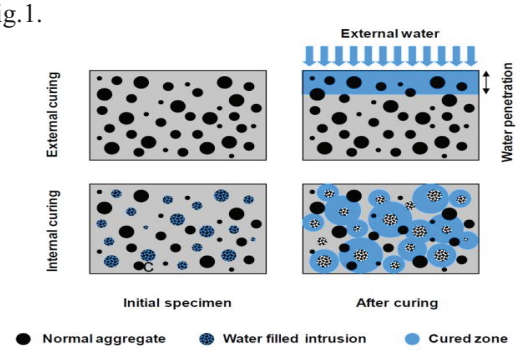

Figure 1. Conventional (external) curing and internal curing

As per ACI-308-2013, "Internal curing refers to the process by which the hydration of cement occurs because of the availability of additional internal water
that is not part of the mixing water".

B.Necessity of self curing

- In high strength concrete, the depth that the external water can penetrates is limited due to the low water-cement ratio of concrete. In such a case, Self-curing (SC) of concrete solves the problem of degree of cement hydration because self-curing enables the water to distribute more equally throughout the cross-section.
- SC is a good solution where there is an acute shortage of water.
- SC is a good solution for curing vertical members, inclined members, extreme corner locations, top-most members/areas where normal curing is difficult.
- SC is a right choice for curing of high-rise structures.
- SC is an appropriate alternative when the dependency on unskilled labour for conventional curing is high.
- SC is preferable in hot weather regions where large quantity of water is required for curing owing to the evaporation losses.
- SC is advisable when the cost of obtaining water with the desired quality is expensive.
- SC is desirable when it is required to reduce the cost of operations, quicker turn-around time in precast plants.

C. Significance of present study

Now-a-days, the foremost challenge in construction field is the lack of availability of water. Construction industry must switch over to alternate curing methods like self-curing method for the sustainable development of the environment. Self-cured concrete does not require water for curing hence, there will be no excess usage of water. Therefore, an attempt is made in the present paper to achieve the required strength and durability of high strength concrete by internal curing with suitable admixtures and the effect of elevated temperatures on self-cured high strength concrete and conventionally cured high strength concrete.

II. LITERATURE REVIEW

The water movement from internal curing agents into hydrating cement paste with a low water-cement ratio was studied and observed that the amount of water first received by the paste in the proximity of the Super-absorbent Polymer can be redistributed later to a large volume of hardening paste when the permeability becomes very low[1]. Characterization of a super-absorbent polymer was studied by determining compressive strength, split tensile strength and flexural strength of the concrete containing SAP and compared with conventionally cured concrete[2]. Three different curing techniques were used and the variation of compressive strength of medium strength and self-compacted concrete was studied. Immersion curing method gave maximum compressive strength. Internal curing with Polyethylene Glycol (PEG) gave only 5% lesser compressive strength than immersion curing[3]. Workability and strength characteristics of Normal Strength and High

E-ISSN 2581 – 7957
P-ISSN 2277 – 3916

DOI: 10.32377/cvrjst1702

Strength Concrete with Polyethylene Glycol and S orbital were studied and compared with the conventionally cured concrete of M20, M30 and M40, M60, M70 and M80 grades [4]. The variation of weight, compressive strength, flexural strength and split tensile strengths of concrete cubes was investigated with the use of PEG4000 and PEG200 at 0.1%, 0.5%, 1% in M70 grade concrete. Durability tests were also conducted [5]. Strength characteristics of M20 concrete with PEG400 were compared with the conventionally cured concrete at 3days, 7days, 14 days and 28 days [6]. Strength and workability tests were conducted on M20 and M25 grade concrete using PEG600 at 0.5%, 1%, 1.5%, and 2% [7]. Strength properties of M20 grade concrete were studied using PEG400 at different percentages [8]. Effect of solid Paraffin wax on the strength properties of concrete was studied and compared with the properties concrete made with Master Rheo-build [9].

III. EXPERIMENTAL PROGRAMME

A. Materials Used

The specific gravity of ordinary Portland Cement (53 grade) used is 3.10.The specific gravity of sand (fine aggregate) used is2.65. The specific gravity of coarse aggregate used is2.70. Potable water is used for making the concrete. The Superplasticizer used is Master Glenium ACE30JP(at 1.2% by weight of binder). The supplementary cementitious material used is Alccofine1203.The internal curing compound used is Polyethylene Glycol 8000.The mix proportions used for the preparation of high strength concrete are1:0.556:1.629:0.25.

B. Elevated Temperature Studies

Influence of temperature on Compressive strength, Weight loss and Durability properties of cubes is studied in this paper. Duration of temperature is 02 hours and varied from 100^{0}C to 900^{0}C at an interval of 100^{0}C as presented in Fig.4.

Air-cooled cubes Ultrasonic pulse velocity is measured using Portable Ultrasonic Non-destructive Digital Indicating Tester [10] and the quality of concrete is studied.

C. Ultrasonic Pulse Velocity (UPV)

For cubes with high density, homogeneity and uniformity, higher velocities values are observed. In case of poor quality cubes, lower velocities are observed. The test results of Ultrasonic pulse velocity are presented in Fig. 2.

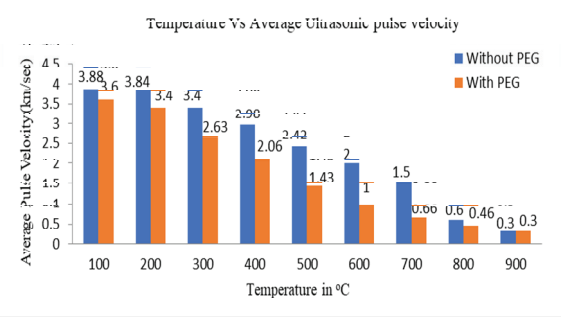

Figure 2 .Ultrasonic pulse velocity of cubes

D. Percentage loss in weight

The percentage loss in weight of cubes without PEG8000is calculated at different temperatures and presented in the Fig.3. The percentage loss in weight of cubes is found to be increased up to 900^{0}C.

Similarly, the percentage loss in weight of cubes with PEG8000 is calculated at different temperatures and presented in the Fig.3. The percentage loss in weight of cubes is found to be increased up to 900^{0}C.

The comparison of percentage weight loss of cubes without and with PEG8000 at different temperatures is presented in Fig.3.

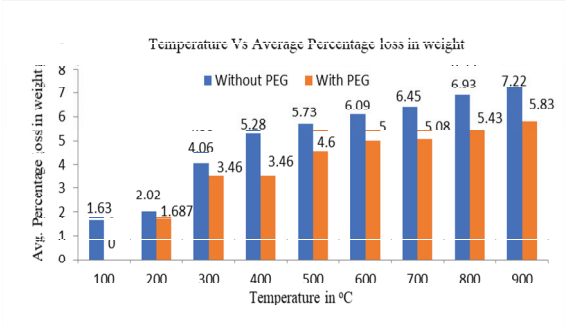

Figure 3.Weight loss of cubes without and with PEG8000

E. Compressive Strength

Compressive strength of 100mm cubes with different dosages of PEG8000 is presented in Fig.4. Total cubes cast (with different dosages of PEG8000 from 0.1% to 2.25%)are thirty-four. From Fig.3, the optimum dosage of PEG8000 is found to be 0.25%.

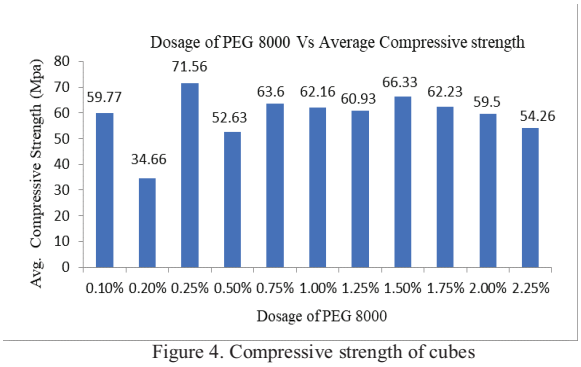

Figure 4. Compressive strength of cubes

Twenty-seven 100mm cubes are cast for studying the weight loss and compressive strength at room temperature. Twenty-seven more cubes of 100mm size are tested to study the variation in the weight loss and compressive strength cubes before and after subjecting to the elevated temperatures. After 28 days of conventional curing, cubes without PEG8000 are air dried and tested to 100^{0}C, 200^{0}C, 300^{0}C, 400^{0}C, 500^{0}C, 600^{0}C, 700^{0}C, 800^{0}C and 900^{0}C temperature for 02 hours in a high Temperature Furnace of 1000^{0}C capacity. No visible cracks are observed up to 300^{0}C. Cracks are observed in the specimens when tested to 400^{0}C and 500^{0}C. Pronounced cracks are seen on the surface of the cubes at 600^{0}C, 700^{0}C, 800^{0}C and 900^{0}C respectively. Upto 600^{0}C, no change in the colour of cubes is observed. At 700^{0}C, the color of cubes changed to pink/red. Beyond

E-ISSN 2581 – 7957
P-ISSN 2277 – 3916

CVR Journal of Science and Technology, Volume 17, December 2019
DOI: 10.32377/cvrjst1702

700^{0}C, the color of cubes changed to grey. Cubes are tested for residual compressive strength under Automatic Compression Testing Machine.

Residual compressive strength of cubes without PEG8000 is shown in Fig.5. The Compressive strength of concrete is decreased, when the cube specimens are exposed to a temperature from 100^{0}C to 200^{0}C. The Compressive strength is found to be increased at 300^{0}C. From 400^{0}C to 500^{0}C, there is a nominal decrease in the compressive strength. From 600^{0}C to 900^{0}C, an increase in the percentage decrease is observed in the compressive strength. At 600^{0}C, the average percentage decrease in compressive strength is 26.81%. At 700^{0}C, the average percentage decrease in compressive strength is 32.15%. At 800^{0}C, the average percentage decrease in compressive strength is 52.08%. At 900^{0}C, the average percentage decrease in compressive strength is 69.83%. The decrease in compressive strength between 600^{0}C and 800 may be due to the decomposition of C-S-H gel and dehydration of calcium hydroxide (CH) into free lime. Decomposition of calcium carbonate and the loss of free water may be the reason for the decrease in compressive strength of concrete at 900^{0}C.

Comparison of residual compressive strength of cubes without and with PEG8000 is presented in Fig.5.Compressive strength of concrete is decreased, when the cubes are exposed to a temperature from 100^{0}C to 200^{0}C. The Compressive strength is found to be increased at 300^{0}C. The increase in strength at 300^{0}C may be due to the increase in the surface forces among the gel particles. From 400^{0}C to 500^{0}C, an increase in the decrease of compressive strength is observed. From 600^{0}C to 900^{0}C, the compressive strength is decreased.

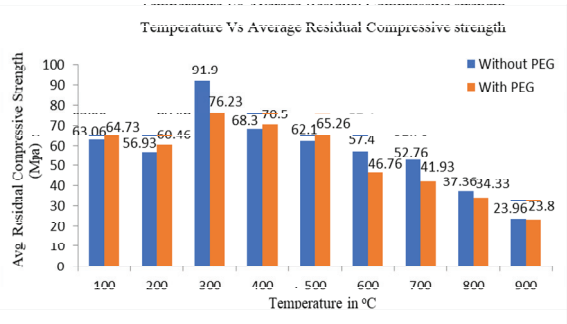

Figure 5.Average residual compressive strength of Cubes without and with Polyethylene Glycol 8000

F. Sulphate Test

Three cubes of 100mm size are cured in water for 28 days. Then the cubes are dried at 50^{0}C for 24 hours and weights are taken before placing in the Sulphate solution (2.5% Na_2SO_4 and 2.5% $MgSO_4$ by weight of water).After the prescribed period, the average percentage loss in weight of cubes is calculated at 7, 14, 28 and 56 days and shown in Fig.6.

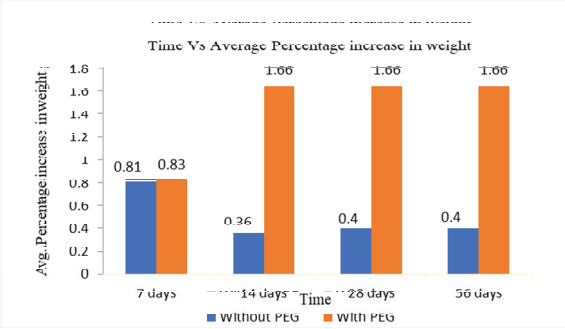

Figure 6. Average percentage increase in weight of cubes tested for Sulphate attack

G. Chloride Test

Three cubes of 100mm size are cured in water for 28 days. Then the cubes are dried at 50^{0}C for 24 hours and weights are taken before placing in the Sodium chloride solution (5% of Nacl by weight of water).After the prescribed period, the average percentage loss in weight of cubes is calculated at 7, 14, 28 and 56 days and shown in Fig.7.

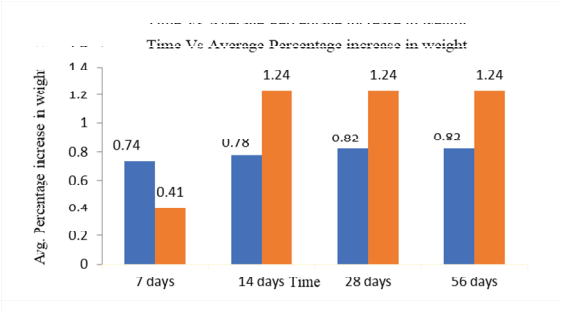

Figure 7. Average percentage increase in weight of cubes tested for Chloride attack

H. Alkali Test

Three cubes of 100mm size are cured in water for 28 days. Then the cubes are dried at 50^{0}C for 24 hours and weights are taken before placing in the Sodium hydroxide solution (5% of sodium hydroxide solution by weight of water).After the prescribed period, the average percentage loss in weight of cubes is calculated at 7, 14, 28 and 56 days and shown in Fig.8.

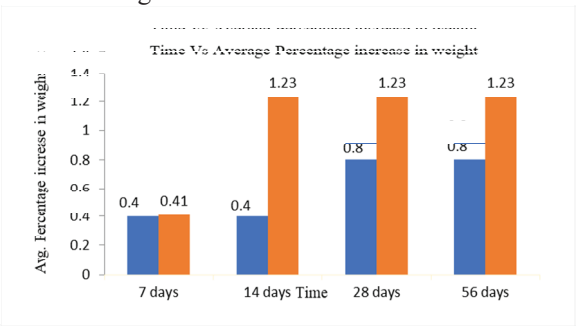

Figure 8. Average percentage increase in weight of cubes tested for NaoH attack

I. Sea Water Test

Three cubes of 100mm size are cured in water for 28 days. Then the cubes are dried at 50^{0}C for 24 hours and

E-ISSN 2581 – 7957
P-ISSN 2277 – 3916

DOI: 10.32377/cvrjst1702

weights are taken before placing in the sea water (5% of Sea water solution).After the prescribed period, the average percentage loss in weight of cubes is calculated at 7, 14, 28 and 56 days and shown in Fig.9.

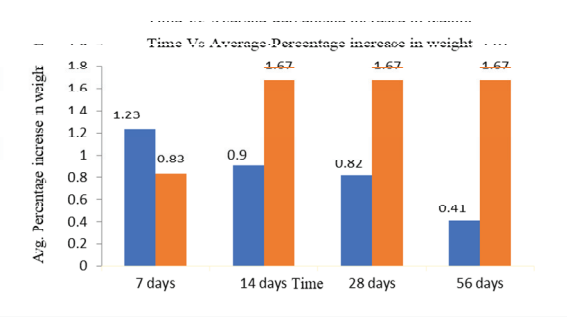

Figure 9. Average percentage increase in weight of cubes tested for Sea Water attack

J. Pulse Velocity

The average pulse velocity of cubes without and with PEG8000 is presented in Fig.10.

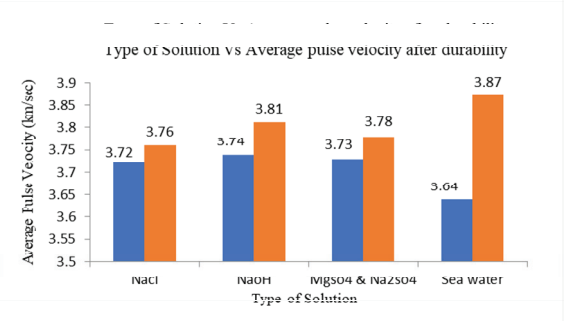

Figure 10. Average pulse velocity cubes

The interfacial transition zone thickness variation and the decrease in the voids ratio of hardened concrete may be attributed to the increase in weight and compressive strength of the cubes.

K. Sorptivity Test

100mm concrete cubes are placed in the oven at a temperature of 50^0C for 03 days, before placing cubes in contact with water[11]. Sorptivity coefficient is calculated as $1.5873x10^{-4}$ mm/min$^{0.5}$.Sorptivity values are presented in Fig.11.

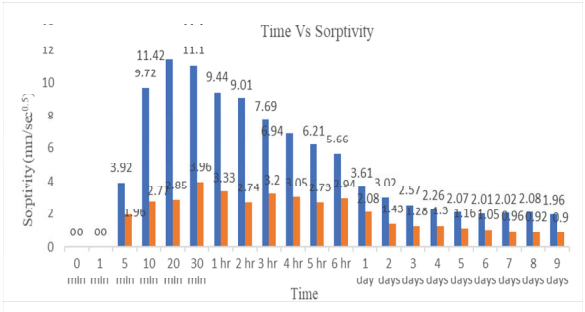

Figure11.Sorptivity of concrete cubes without and with PEG8000

IV. Discussions and Conclusions

Self-curing of concrete using PEG8000 is found to be a good alternative for conventional curing of concrete. Discussions and conclusions are presented below.

1. 10% replacement of cement replacement by Alccofine1203 is found be an optimum percentage forobtaining an average compressive strength of 79.93MPa without PEG8000.
2. Optimum dosage of PEG8000 is found to be 0.25% by weight of binder forobtaining an average compressive strength of 71.56MPa. The percentage of difference between the compressive strengths achieved without and with PEG8000 was 10.47%.
3. Without PEG8000, the average Compressive Strength of concrete cubes at 56 days of curing in Nacl, NaoH, $MgSO_4$ plus Na_2SO_4 solutions and Sea water is found to be 91.83 MPa, 94.6 MPa, 86.93 MPa and 89.10 MPa respectively. Without PEG8000, the average Compressive Strength of concrete cubes before 56 days of curing was 69.71MPa, 79.93 MPa, 63.55MPa and 78.40MPa.The percentage increase in compressive strength is found to be 31.73, 18.35,36.78 and 13.64.The increase in compressive strength may be due to the increase in density of concrete cubes.
4. Compressive Strength of concrete cubes with PEG8000 after 56 days of curing in Nacl, NaoH, $MgSO_4$ plus Na_2SO_4 solutions and Sea water is found to be 75 MPa, 77 MPa, 72.56 MPa and 73.33 MPa respectively. The average Compressive Strength of high strength concrete cubes without PEG8000 before 56 days was 71.3MPa, 71.2 MPa, 69.2MPa and 70.73MPa.The percentage increase in compressive strength was found to be 5.18, 3.77, 4.85 and 3.67.
5. Initial rate of water absorption of high strength concrete cubes without and with PEG8000 is not linear due to the increase in water absorption whereas the secondary rate of absorption is linear due to less water absorption. More water absorption may be attributed to the precondition of the concrete cube specimens at a temperature of 100^0C for 24 hours. Less water absorption during 1day-7days may be attributed to the less pore space available after the initial absorption period of 1min-6hour.
6. Compressive strength of 100mm cubes after two hours at 300^0C is found to be increased by 18.55%. The increase in compressive strength at 300^0C may be due to the increase in surface forces between gel particles because of the removal of moisture content. After critical temperature of 300^0C, the compressive strength of cubes is decreased considerably upto 900^0C. Similar trend is observed for concrete cubes with PEG8000.

As per the discussions, the use of PEG8000is recommended for the preparation of high strength concrete in the water scarce areas or where potable water is not available for the preparation of concrete.

CVR Journal of Science and Technology, Volume 17, December 2019
DOI: 10.32377/cvrjst1702

REFERENCES

[1] Mateusz Wyrzykowski, PietroLura, Francesco Pesavento, DariuszGawin, 'Modeling of water migration during internal curing with Superabsorbent Polymers', Journal of Materials in Civil Engineering,vol. 24, Issue 08, August2012.

[2] Amal Francis k, Jino John, 'Experimental investigation on mechanical properties of self-curing concrete', International Journal of Emerging Trends in Engineering and Development, vol.2, Issue 3, March 2013.

[3]] Nanak, J., Pamnani, Verma, A.K., Bhatt, D.R.,' comparison of compressive strength of medium strength self-compacted concrete by different curing techniques', International Journal of Engineering Trends and Technology,vol. 4,Issue 5, May2013.

[4] Vedhasakthi, K., Saravanan, M.,' Development of normal strength and high strength self-curing concrete using Super Absorbing Polymers and comparison of strength characteristics', International Journal of Research in Engineering and Technology, vol. 03, Issue 10, October 2014.

[5] Bala, K., Subramanian, Siva, A., Swaminathan, S.,Arul, M.G., Ajin,' Development of high strength self-curing concrete using Super Absorbing Polymer', International Journal of Civil, Environmental, Structural, Construction and Architectural Engineering,vol. 09, Issue 12, 2015.

[6] Siddiqui Mohammed Junaid, 'An experimental investigation on internally cured concrete', International Journal on Recent and Innovation Trends in Computing and Communication,vol. 04, Issue 4, April 2016.

[7] Mohammed, V., Shafeeque, Sanofar, P.B., Praveen, K.P., Jithin Raj, Nikhil,V.P., Gopikrishna, P.M., 'Strength comparison of self-curing concrete and normal curing concrete', SSRG International Journal of Civil Engineering, vol. 3 Issue 3, March 2016.

[8] Basil, M., Joseph, 'Studies on properties of self-curing concrete using Polyethylene Glycol', IOSR Journal of Mechanical and Civil Engineering, December-2017.

[9] Mohammed Bilal, Ambikapathi, 'Experimental study on internal curing of high strength concrete', International Journal of Engineering Sciences & Research Technology, January-2017.

[10] IS:13311(Part-1)-1992, "Non-Destructive Testing of Concrete-Methods of Test".

[11] ASTM:C1585-04, "Standard Test Method for measurement of rate of absorption of water by hydraulic cement concretes", PP 1-5.

E-ISSN 2581 – 7957
P-ISSN 2277 – 3916

CVR Journal of Science and Technology, Volume 17, December 2019
DOI: 10.32377/cvrjst1703

Role of Liquid Tuned Mass Dampers in Improving Torsional Competence of Asymmetric Buildings

A Shruthi[1] and Dr. N. Murali Krishna[2]
[1]Asst. Professor, CVR College of Engineering/Civil Engg. Department, Hyderabad, India
Email: shruthiarikeri95@gmail.com
[2]Professor, CVR College of Engineering/Civil Engg. Department, Hyderabad, India
Email: nmuralikrishna1956@gmail.com

Abstract: **The development of urban environment is reflected by the increase in tall structures. These structures are highly vulnerable of lateral forces caused by different kinds of natural calamities. To counter their effect on structures, many types of structural elements like shear walls, infill frames etc., are tried over a period of time. But, their inclusion is often unacceptable, besides the cost escalation. In this backdrop, tuned mass dampers are tried as the most viable the alternatives to shear walls. Many types of tuned mass damper systems are explored as on date. Currently, the concept of liquid tuned mass dampers as TMDs is attracting wide research interest as it is an integral part of structural system, go well with the architectural features of the building and do not cause much cost escalation. Modelling the overhead water tank in a building as liquid tuned mass dampers would significantly reduce the amplitude of vibration and the maximum base shear in a building when subjected lateral disturbances.**

A Tuned Mass Damper (TMD) is a device consisting of a mass and spring that is attached to a structure in order to reduce the dynamic response of the structure. The frequency of the damper is tuned to a particular structural frequency so that when that frequency is excited, the damper will resonate out of phase with the structural motion. The Tuned Liquid Mass Damper (TLMD) is modeled with the help of overhead water tanks which form an integral part of the building. These tanks while serving the purpose of storing water, would also meet the requirements desirable of a tuned mass damper. The structural effectiveness of building with and without TLMD is presented by carrying-out the structural analysis using both Response Spectrum Method and Linear Time History Analysis. The performance of the tuned liquid mass dampers is demonstrated by comparing the values of Maximum Story Deflection and the magnitudes of Base shear of the building for different tank capacities. The study is proposed to be carried out on an RC building with plan asymmetry, located in a highly seismic active region using ETABS.

Index Terms: **Tall structures, Tuned Mass Damper (TMD), Tuned Liquid Mass Damper (TLMD), Base shear, Water tank, Seismic vibrations.**

I. Introduction

Urbanization of a metropolis is in general reflected by tall buildings all around and improvised infrastructure. For a structural designer, tall structures pose design challenges as they are highly vulnerable to natural calamities like Cyclones and Earthquakes. Even the man induced causes like blasts may pose severe threat to the high raised structures. On seismic front, the threat to structures is caused due to huge amount of lateral forces and lateral displacements. The above two reasons necessitate the provision of large sizes of column elements and very stiff structural configuration, which is not always acceptable.

To avert the undesirable effects caused by the lateral forces on structures, the shear walls are introduced in some of the bays of the building structures. Excessive use of shear walls in buildings is also not always acceptable as their placement infringes with the vehicular movement and the architectural features of the building. As the next alternative, the base isolators are tried at to reduce both base shear and the lateral displacements of the buildings. Though the idea appears to be acceptable, it is a costly proposition, hence it is not a desirable alternative. In this backdrop, introduction of Tuned Mass Dampers is considered the most effective alternative. The TMDs are both economical and are effective in reducing both base shear and amplitude of vibrations of the building subjected to dynamic causes. Amongst the Tuned Mass Dampers, the usage of Liquid Tuned Mass Dampers are more encouraged. Studies on Liquid Tuned Mass Dampers are the prime area of the present-day research activity. Since the overhead water tanks are integral part of a structure, they can serve as Tuned Liquid Mass Dampers and are considered a very cost-effective solution in seismic design.

In the present study, the mass of water in the tank plus the mass of the water tank constitute the total mass of the Tuned Mass Damper. The stiffness of the columns of the water tank serves as stiffener of the Tuned Mass Damper. The structural damping due to the concrete structure constitutes the damping of the Tuned Mass Damper. By suitably altering the mass of liquid in the water tank, the size of the water tank and the number and size of the columns supporting the water tank, the mass, the damping and the stiffness of the Tuned Liquid Damper are tuned.

A. Objective of the study

The objective of the present study is to propose a suitable method to choose the size of the water tank and mass of the water tank with water to arrive at an optimal configuration of the Liquid Tuned Mass Damper. Such an arrangement should result in the lowest possible base shear and lateral displacement in the event of seismic disturbance to the building.

CVR Journal of Science and Technology, Volume 17, December 2019
DOI: 10.32377/cvrjst1703

B. Procedure Adapted

In the present study, a high-raised RCC building subjected to seismic activity is analyzed using Response Spectrum Method and Linear Time History analysis method using ETABS. For the purpose of this study, a G+10 storied building with asymmetric configuration located in Zone-III and Zone-IV of seismic disturbance is considered. The analysis is carried out with and without considering the effects of Liquid Tuned Mass Dampers. The study is carried-out on Rectangular, L-shaped, T-shaped and U-shaped buildings. The studies are repeated by varying the water level in tanks as empty, one-third full, two-third full and full water tank conditions.

II. LITERATURE REVIEW

Mudabbir Imran and B. K. Raghu Prasad had examined the effectiveness of both single and multiple Tuned Mass Dampers (TMDs) when subjected to various earthquake ground accelerations using ETABS. It was seen that MTMD with Non-uniform mass ratio was more efficient than MTMD with uniform mass ratio, but it cannot be economical [1].

Lucchini et al proposed a method for designing a TMD system for the seismic protection of a multi-storied buildings. It was found that with the increase of the total mass of the TMD system, its performance tends to improve, the building response reduces and becomes less sensitive to the uncertain parameter variations. Uncertainty in the properties of the ground excitation reduces robustness of the TMD system by increasing the variation of its performance. With the increase of the uncertainty level, it has been observed that period and damping of the TMD units increases [2].

S.M. Zahrai and A. Ghannadi-Asl had discussed the effectiveness of Tuned Mass Dampers (TMDs) to control the structures under earthquake excitations using tuned mass dampers for buildings with different number of storeys and heights. The results of time-history analysis were compared with those of a response spectrum analysis for the structures with and without TMD in order to judge its effectiveness. It was observed that TMD is effective in reducing maximum displacement in MRF buildings of Tabas earthquake and El Centro earthquake [3].

Ashish A. Mohite et. al. had carried out the analysis of the seismic behavior of different storeys of a building with tuned mass damper and without tuned mass damper by using ETABS. It was found that the TMDs can be successfully used to control vibration of the structure. For the regular building frame, TMD was found to effectively reduce top storey displacement. The reduction was found to be decreasing in a descending order from bottom storey to top storeys. With these results it was concluded that the TMD should be placed at top floor for the best control [4].

Saurabh Chalke and P.V. Muley had discussed the vibration control of the framed structure using tuned mass damper by using ETABS 2015 by analyzing a G+51 storied structure without damper and with tuned mass damper and compared the displacement and drift values under the dynamic condition. It was concluded that the values of displacement and drift were found to be more on structure when acted upon by dynamic conditions without damper. By assigning Tuned Mass Damper to the structure, it was found to be more stable as the values of displacement and drift were reduced and the acceleration also been reduced significantly using tuned mass damper [5].

Rajashekhar S. Talikoti et. al. had studied the effectiveness of TMD in controlling the vibrations of structure. A building structure was modelled with and without TMD and Response spectrum analysis was carried-out. From the study, it was found that TMD was more effective when it is attached at the top floor of building and the presence of TMD resulted in gradual decrement of the displacement, the storey drift and the fundamental period of the structure [6].

Manjusha M had carried out the analytical investigation to study the feasibility of implementing water tank as a passive Tuned Mass Damper (TMD) using ETABS 2015. Multi-storey concrete building structure was taken for the study and a water tank was placed on the roof. The mass and frequency of both were tuned to the optimized values. The behavior of the tank under full and empty tank condition subjected to earthquake data was studied. It was concluded that TMD had effectively reduced the overall behavior of the structure resulting in economic and safe design and can successfully be used to control the response of the structure [7].

M.J Tait et. al. investigated the performance of unidirectional and bidirectional Tuned Liquid Dampers (TLDs) under random excitation. A series of experiments were carried-out on scale model structure-tuned liquid damper systems to evaluate their performance. The results are compared with that of a well-known tuned mass damper. This study has resulted in the development of performance charts for a tuned liquid damper. These charts allowed the efficiency of a tuned liquid damper to be examined for a number of varying parameters, which included the excitation amplitude, water depth and building frequency. It was concluded that a TLD is efficient and robust to reduce dynamic structural motions that occur as a result of random excitation [8].

Chidige Anil Kumar and E Arunakanthi analyzed the feasibility of implementing water tank as passive TMD and found the optimum level of water which would reduce peak response of the structure subjected to seismic forces using SAP2000 by considering a three and seven storeyed building designed for gravity and seismic using 1893:2002. Influence of TLD was found to be effective and the model study showed encouraging results for Bhuj earth quake data. It was found that the roof displacements, story drifts, time period and base shear have been reduced for 2/3 level of water tank model compared to other levels concluding 2/3rd

E-ISSN 2581 – 7957
P-ISSN 2277 – 3916

DOI: 10.32377/cvrjst1703

level as the optimum level of water to be maintained for effective results. It was concluded by them that if the level of water in the tank is maintained between half full to two thirds full (having mass ratio 25%) there is a tendency to mitigate the vibrations of RC frame structures under seismic excitations [9].

III. METHODOLOGY

The dynamic analysis of the building is carried out using Response Spectrum method and Linear Time History method corresponding to seismic Zone-III and IV of seismic activities.

Modelling of structure using TLD is as follows:

1. A three-dimensional model of G+10 storied building structure is created using ETABS.
2. Creating and assigning Material properties.
3. Creating and assigning Section properties.
4. Response spectrum and Time history functions are defined for the desired zones considered in the study.
5. Assigning the external and internal wall loads acting on the structure wherever necessary.
6. Assigning the floor finish load and live load acting on slab panels.
7. A water tank is created at the desired location on the topmost floor of the existing building structure.
8. The water tank with desired length, width and height are created and the beam, column and slab properties are assigned.
9. The next step is modelling a Tuned Liquid Damper which is attached to the water tank of the same building.
10. A TLD is modelled in ETABS using a combination of 'Linear link type' and a 'Point spring' attached in series.
11. From Define→Section properties→Link/support properties, add a new link property by selecting the 'Linear link type'. The directional properties U1, U2, and U3 are selected in which U3 type is fixed.
12. From Properties option→modify/show all→the stiffness and damping values for U1, U2 directions are entered.
13. Mass and weight of the TLD (the water) is entered, which is the load acting on the water tank or the weight of water present in the water tank. In this step, the water level is varied to effect the changes in the values of mass and weight of TLD and changes are affected in the stiffness and damping as well.
14. Define →Spring properties→Point springs→Add new spring, select the 'User specified/link properties option'.
15. From the 'single joint links at point' dialogue box, add the previously defined link property and the axial direction '+z' selected.
16. Links are drawn using 'draw link' option.
17. The links are connected to the columns in '+z' direction (upward), along which the water tank is standing.
18. The point spring which is defined earlier is assigned to the joints at the base of the water tank by using 'Draw springs' option.
19. The mass of the TLD is assigned towards the free end of the link by selecting the joints of water tank, where springs and links are connected.
20. From the command Assign→Joint loads, the load value is assigned in downward or '-z' direction. The total load acting on the water tank is divided equally on to the number of columns on which it is standing as shown in Figure 1.

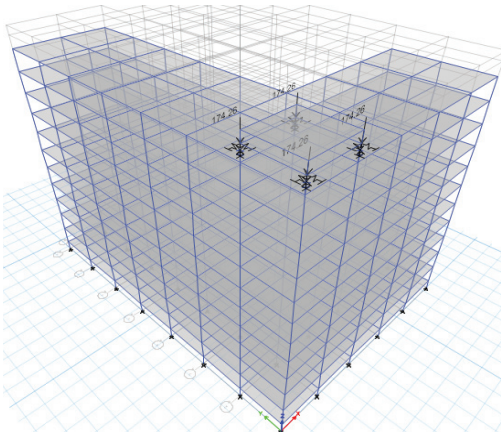

Figure 1. Plan with Joint loads in ETABS

The buildings considered for the study are RC ordinary moment resisting space frames of G+10 storied located in Zone III and Zone IV of seismic disturbances. The analysis is carried-out on a rectangular shaped building and three different asymmetric shaped buildings of plan shapes L, T and U. The layout plan is such that each one of the bays is 6m long. The study is conducted by varying the water level in water tank by considering 1. Empty water tank, 2. One-third full, 3. Two-third's full and 4. Full water tank conditions using ETABS.

The Plan configuration consists of

1. Model 1 - L-shaped Building plan (Figure 2),
2. Model 2 - T-shaped Building plan (Figure 3),
3. Model 3 - U-shaped Building plan (Figure 4),
4. Model 4 - Rectangular Building plan (Figure 5),

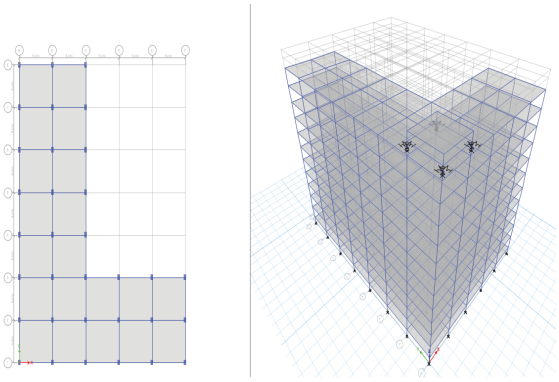

Figure 2. Plan and Isometric view of Model-1 with TLD

E-ISSN 2581 – 7957
P-ISSN 2277 – 3916

DOI: 10.32377/cvrjst1703

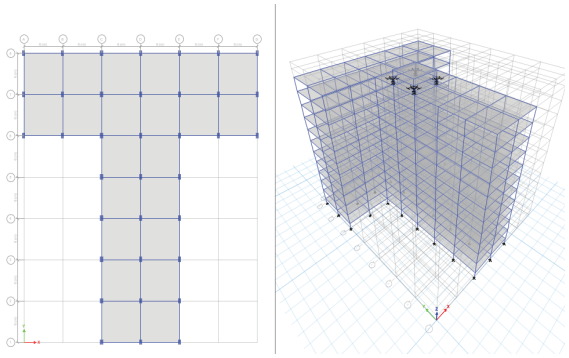

Figure 3. Plan and Isometric view of Model-2 with TLD

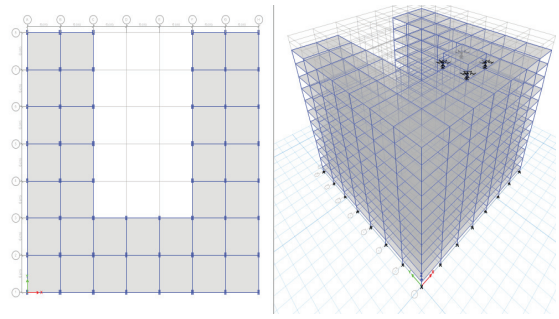

Figure 4. Plan and Isometric view of Model-3 with TLD

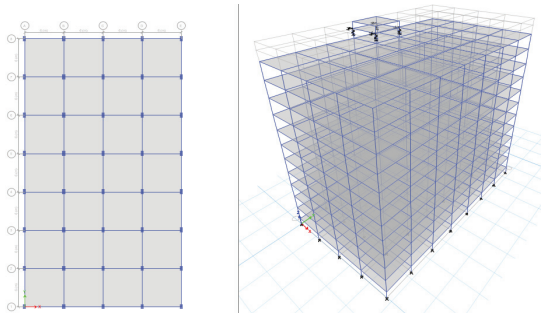

Figure 5. Plan and Isometric view of Model-4 with TLD

IV. Specimen Calculations

The Preliminary data for the Analysis of the frame in ETABS is considered as per the prevailing construction practices which is presented below.

1. Type of structure - Moment Resisting Frame
2. Materials - M30, Fe-500
3. Size of Beams - 300x450 mm
4. Size of Columns - 450x750 mm
5. Depth of slab - 150 mm
6. External Wall load - 11.14KN/m (IS 875 Part-1)
7. Internal Wall load - 5.57KN/m (IS 875 Part-1)
8. Seismic zone factor - 0.16 & 0.24 (IS 1893:2016)
9. Response Reduction Factor - 5 (IS 1893:2016)

A. Calculations of watertank for Model-1

Total mass of the structure = 70209.18KN
Water required for single person= 135 liters
No. of persons in each flat =5
No. of flats in the building =25
Total no of persons =125
Water required =16875Litres

Water tank height = 0.75 m
Volume of tank = LxBxH
Area of tank (LxB) = 22.5 m^2
L = 6 m
B = 6 m
H = 0.75 m
Total dead load = 530.82KN
Live Load (Water Required) = 165.48 KN
Total water tank load = 697.05KN

B. Calculations of the Tuned Liquid Damper for Model-1

$$\text{Mass ratio } (\gamma) = \frac{\text{Mass of the water tank}}{\text{Mass of the structure}}$$

Natural frequency (ω_n) = 1.874rad/sec

Time period (Tn) = 3.351 sec

$$\text{Tuning ratio } (f_{opt}) = \frac{1}{1+\gamma}$$

$$\text{Optimum damping ratio } (\xi_{dopt}) = \sqrt{\frac{3\gamma}{8(1+\gamma)}}$$

Optimum stiffness $K_{opt} = \gamma k f_{opt}^2$
Optimum Damping $C_{opt} = 2\omega m \xi_{dopt} \gamma$
The above calculations are listed below in Table 1

TABLE I.

Calculations Of TLMD Parameters For Varying Water Level In The Tank

	Empty Water tank	One-third level Water	Two-third level water	Full water tank
Mass ratio	0	0.003	0.006	0.0099
Tuning ratio	1	0.996	0.993	0.9901
Optimum damping ratio	0	0.035	0.049	0.0613
Optimum stiffness (KN/m)	0	82.72	164.37	244.94
Optimum Damping (KN-s/m)	0	30.74	87.09	160.26

E-ISSN 2581 – 7957
P-ISSN 2277 – 3916

DOI: 10.32377/cvrjst1703

Responses Of Structure For Model-1 (L-Shape)

Base shear in Zone-III

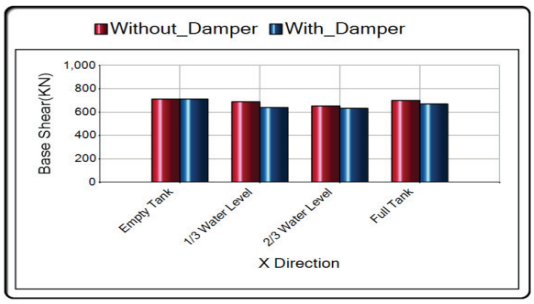

Figure 6. Base shear in Time History Analysis along X direction

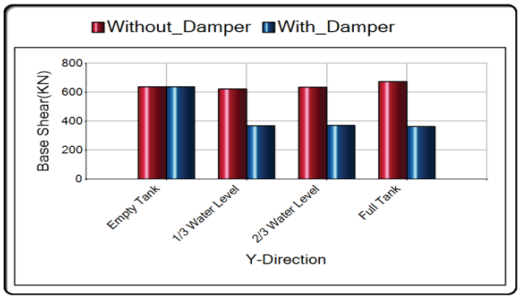

Figure 7. Base shear in Time History Analysis along Y direction

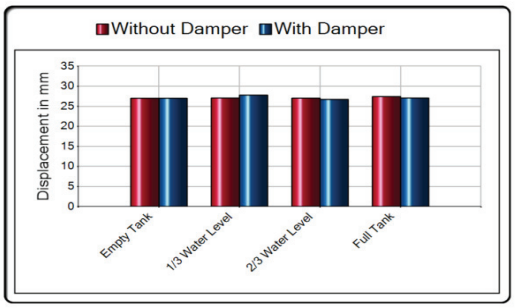

Figure 8. Maximum Storey Displacement in Time History Analysis along X direction

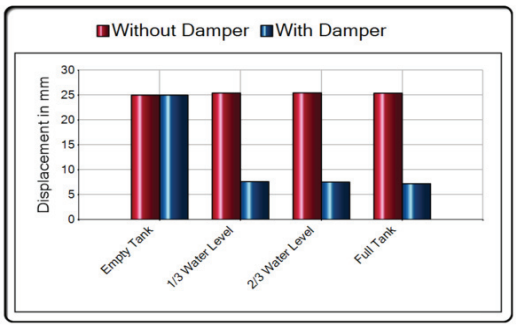

Figure 9. Maximum Storey Displacement in Time History Analysis along Y direction

Responses Of Structure For Model-2 (T-Shape)

Base shear in Zone-III

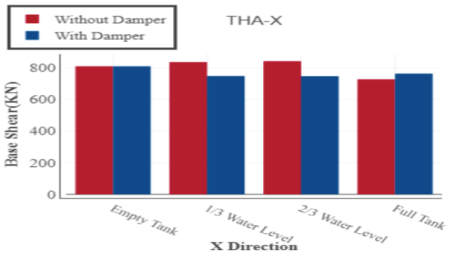

Figure 10. Base shear in Time History Analysis along X direction

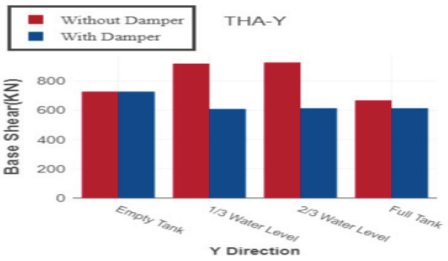

Figure 11. Base shear in Time History Analysis along Y direction

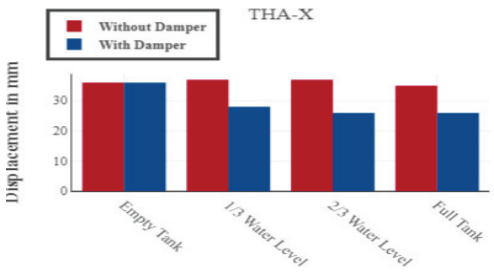

Figure 12. Maximum Storey Displacement in Time History Analysis along X direction

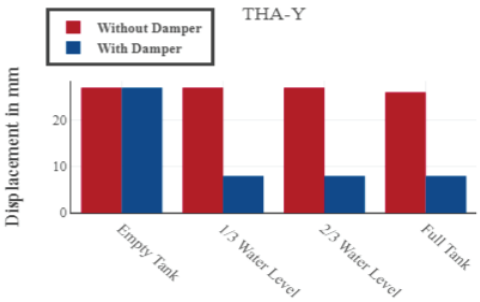

Figure 13. Maximum Storey Displacement in Time History Analysis along Y direction

E-ISSN 2581 – 7957
P-ISSN 2277 – 3916

CVR Journal of Science and Technology, Volume 17, December 2019
DOI: 10.32377/cvrjst1703

V. Results and Discussions

The studies are carried-out for water tanks empty, one-third full, two-third full and full tank conditions.The information furnished in Table 2 listed below clearly shows the percentage reduction in the magnitudes of base shear and maximum storey displacements with the utility of the TLD approach. The list of observations reported seperately for zone-3 and zone-4 of seismic intensities are as shown below in Table 2.

TABLE II.

Percentage Reduction In The Magnitudes Of Base Shear And Max Displacements From Linear Time History Analysis Using Tld Approach

	Zone-III		Zone-IV	
PLAN	Base shear	Displace ments	Base shear	Displac ements
L-shaped building	46%	71%	66%	83%
T-shaped building	8%	67%	34%	68%
U-shaped building	40%	73%	41%	74%
Rectangular shaped building	41%	35%	41%	65%

Zone-III

1. The magnitude of base shear is found to be reduced by 46% in Y-direction for L-shaped building with the action of Tuned Liquid Mass Damper using Time History method (Figure 7).
2. The Max Storey displacement for Y-direction is found to be reduced by 71% for L-shaped building with the action of Tuned Liquid Mass Damper using Time History method (Figure 9).
3. The magnitude of base shear is found to be reduced by 8% for full tank condition in Y-direction for T-shaped building with the action of Tuned Liquid Mass Damper using Time History method (Figure 11).
4. The Max Storey displacement for X and Y direction is found to be reduced by 28% and 67% respectively for T-shaped building with the action of Tuned Liquid Mass Damper using Time History method (Figure 13).
5. The magnitude of base shear is found to be reduced by 40% corresponding to with TLD condition in Y direction from for U-shaped building with the action of Tuned Liquid Mass Damper using Time History method
6. The Max Storey displacement for Y-direction is found to be reduced by 73% for U-shaped building with the action of Tuned Liquid Mass Damper using Time History method.
7. The magnitude of base shear is found to be reduced by 41% in Y-direction for Rectangular-shaped building with the action of Tuned Liquid Mass Damper using Time History method.
8. The Max Storey displacement for Y-direction is found to be reduced by 35% for Rectangular shaped building with the action of Tuned Liquid Mass Damper using Time History method.

Zone-IV

9. The magnitude of base shear is found to be reduced by 66% in Y-direction for L-shaped building with the action of Tuned Liquid Mass Damper using Time History method.
10. The Max Storey displacement for Y-direction is found to be reduced by 83% for L-shaped building with the action of Tuned Liquid Mass Damper using Time History method.
11. The magnitude of base shear is found to be reduced by 33.4% for full tank condition in Y-direction for T-shaped building with the action of Tuned Liquid Mass Damper using Time History method.
12. The Max Storey displacement for X and Y direction is found to be reduced by 30% and 68% respectively for T-shaped building with the action of Tuned Liquid Mass Damper using Time History method.
13. The magnitude of base shear is found to be reduced by 40.8% in Y direction for U-shaped building with the action of Tuned Liquid Mass Damper using Time History method.
14. The Max Storey displacement for X and Y direction is found to be reduced by 13.6% and 73.57% respectively for U-shaped building with the action of Tuned Liquid Mass Damper using Time History method.
15. The magnitude of base shear is found to be reduced by 41% in Y-direction for Rectangular-shaped building with the action of Tuned Liquid Mass Damper using Time History method.
16. The Max Storey displacement for Y-direction is found to be reduced by 64.8% for Rectangular shaped building with the action of Tuned Liquid Mass Damper using Time History method.

VI. Conclusions

The objective of the study is completely achieved by the present study as it can be seen from the list of conclusions. The size of the water tank for the complex is fixed as per the norms of relevant Indian Standards. The quantum of water requirement for each dwelling unit is fixed based on the per capita water requirements as fixed by the local standards.

Based on the studies carried out on different shapes of buildings in different seismic zones, the following conclusions are made:

1. With the introduction of the Tuned Liquid Damper for L-shaped building, the magnitude of base shear and Max storey displacement are found to reduce in about 46% and 71% (Figure 7 and Figure 9) respectively in Y-direction (in the direction of weak axis) whereas no

CVR Journal of Science and Technology, Volume 17, December 2019
DOI: 10.32377/cvrjst1703

change is observed in X-direction (Figure 6 and Figure 8).

2. The magnitude of base shear and Max storey displacement is found to reduce in about 10% and 34% (Figure 10 and Figure 12) respectively in X-direction and 30% and 68% (Figure 11 and Figure 13) respectively in Y-direction (in the direction of weak axis) for T-shaped building when equipped with Tuned Liquid Mass dampers.
3. The magnitude of base shear and Max storey displacement is found to reduce in about 40% and 73% respectively in Y-direction (in the direction of weak axis) for U-shaped building when equipped with Tuned Liquid Mass dampers.
4. The magnitude of base shear and Max storey displacement is found to reduce in about 41% and 65% respectively in Y-direction (in the direction of weak axis) for Rectangular shaped building when equipped with Tuned Liquid Mass dampers.
5. It is observed that a structure equipped with Tuned Liquid Mass Damper (TLMD) is effective in controlling the the base shear and Maximum storey displacements of the structure when compared to a structure without Tuned Liquid Mass Damper.

Based on the conclusions, the present study clearly demonstrates that there is a substantial reduction of base shear and amplitude of vibration in tall buildings especially in the direction of weak axis, when the overhead water tanks are modelled as Tuned Liquid Mass Dampers.

REFERENCES

[1] Mudabbir Imran, Dr. B. K. Raghu prasad “Seismic Response of Tall Structures Using Tuned Mass Dampers”, IJREAS (2017)
[2] A. Lucchini, R. Greco, G. C. Marano and G. Monti “Robust Design of Tuned Mass Damper Systems for Seismic Protection of Multi-storey Buildings”, ASCE (2014)
[3] S.M.Zahrai, A. Ghannadi-Asl “Seismic Performance of TMDs in Improving the Response of MRF Buildings”, Scientia Iranica (2008)
[4] Ashish A. Mohite, G.R. Patil “Earthquake Analysis of Tall Building with Tuned Mass Damper”, IOSR (2015)
[5] Saurabh Chalke, P.V. Muley “Vibration Control of Framed Structure Using Tuned Mass Damper” International Journal of Engineering Development and Research (2017)
[6] Khemraj S. Deore, Dr. Rajashekhar S. Talikoti, Kanhaiya K. Tolani “Vibration Analysis of Structure using Tuned Mass Damper”, International Research Journal of Engineering and Technology (2017)
[7] Manjusha M, Dr.Vra Saathappan “Analytical Investigation of Water Tank as Tuned Mass Damper Using Etabs”, International Research Journal of Engineering and Technology (2017)
[8] M. J. Tait, N. Isyumov, A. El Damatty “Performance of Tuned Liquid Dampers”, ASCE 2008)
[9] Chidige Anil Kumar, E Arunakanthi “A Seismic Study on Effect of Water Tank modelled as TMD”, International

E-ISSN 2581 – 7957
P-ISSN 2277 – 3916

CVR Journal of Science and Technology, Volume 17, December 2019
DOI: 10.32377/cvrjst1704

How Sustainable is a Conventional Building?

Yashwanth Pamu
Assoc. Professor, CVR College of Engineering/Civil Engg. Department, Hyderabad, India
Email: yashwanthpamu@gmail.com

Abstract: **India is one of the largest energy utilizing countries, China and United States of America being the first and the second respectively. Developed countries have already adopted mandatory reduction in energy utilization per GDP. But India has not fixed any such targets though the target of achieving 175 GW of clean energy is in the process. Building or construction industry is a major consumer of energy and therefore there is a scope for reduction in energy consumption by adopting green building policies by new and existing buildings. In India, IGBC and GRIHA are the organizations which certify buildings whether green or not, based on many parameters. These parameters aim at reducing the load on the environment. One such important parameter is energy, including energy consumption, alternate ways of producing energy. Every building can be close to a green building to a little extent. This paper attempts to assess how close a conventional building is to a green building based on IGBC standards.**

Index Terms: Alternative materials, Environmental load, Rating systems, Energy, IGBC, GRIHA

I. Introduction

The building foot print in our country is increasing at a faster rate than expected. This is a positive sign for the country in terms of economic growth. But at the same time, the CO_2 emissions are also increasing at the same rate. Abanda and Byers have investigated that the buildings utilized 32 % of global energy and responsible for 19 % energy related greenhouse gases [1]. There is an immediate need to introduce the concepts of green buildings which can help in the growth of the country in a sustainable way.

Green measures in existing buildings can help to address international issues like reduction in CO_2 emissions, reduction in usage of natural resources, usage of renewable energy, recycling of waste, recycling and reuse of water and water efficiency. Waidyasekara et al., highlighted the significance of addressing the environmental pollution caused by waste water because of construction activities [12]. Gupta and Kumar have mentioned that the building construction industry utilizes 40 % of stone, sand and gravel internationally [5]. Implementation of green measures can enhance a person's health and reduce the stress. Attom, Abed, Elemam, Nazal and ElMessalami have stressed that buildings consume 16 % of water worldwide [2]. Guggemos and Horvath have specified that the construction sector is one of the largest users of water and energy [4].

Green measures can be systematically implemented in existing buildings with the help of green building rating systems. Vierra cited that there are about 600 rating systems globally [11]. The two rating systems widely used in India are GRIHA and IGBC. Pamu et al., summarized that IGBC rating system has many advantages over GRIHA rating system as IGBC is easy to understand and analyze. GRIHA rating system is complicated and difficult to understand for a common man [9]. With the increase in awareness among the people, it is easy to motivate them to practice sustainable measures in our everyday life. Sev documented that the building environmental assessment tools have become popular in recent times and fascinated the construction industry [10]. Pamu and Kona stated that a green building is the one, which minimizes the negative impacts of construction right from its stages of design to its operation and maintenance stage [8]. Hikmat et al., stated that green building assessment tools offer a means to demonstrate that the building is successful in meeting n expected level of performance [6]. This paper gives a basic idea on how easy it is to transform an existing traditional building into a green building.

II. Green Building Certification

Boonstra and Petterson highlighted the necessity of environmental assessment methods which respond to environmental issues and define sustainable levels [3]. IGBC green existing buildings O&M certification system is the first program developed in India for existing buildings. The rating system will be reviewed periodically and updated based on the innovations and market requirements. The stakeholders will play an important role in updating the rating systems. The certification system encourages the use of Indian building standards and codes in order to avoid deviation from Indian standards.

The IGBC flow chart for green building certification is shown in figure 1[7]. The figure shows the process of certification right from registration to award of rating.

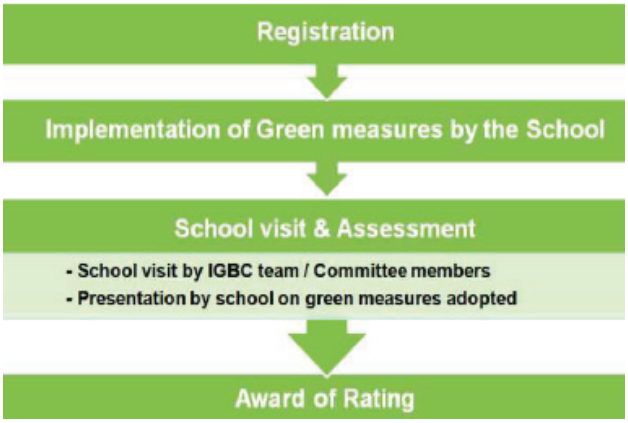

Figure 1. IGBC certification flow chart

E-ISSN 2581 – 7957
P-ISSN 2277 – 3916

DOI: 10.32377/cvrjst1704

TABLE I.
GREEN FEATURES AND THEIR WEIGHTAGE

S.no.	Green Feature	Weightage (Points)
1	Site & Facility Management	18
2	Water Efficiency	26
3	Energy Efficiency	30
4	Health & Comfort	14
5	Innovation	12
TOTAL		100

Apart from the green features mentioned in the table I, there are two mandatory requirements which have to be fulfilled are very basic requirements. These can be satisfied effortlessly. Table II shows the levels of certification based on points earned.

TABLE II.
LEVELS OF CERTIFICATION BASED ON POINTS EARNED

S.No	Points Achieved	Rating
1	50-59	Best Practices
2	60-69	Outstanding Performance
3	70-79	National Excellence
4	80-100	Global Leadership

III. METHODOLOGY

In this paper, an attempt is made to assess a conventional building at CVR College of Engineering i.e. P.G. block based on the green features of the building. By this, it can be checked how close a conventional building is to a green building. The evaluation of green features is done based on I.G.B.C. recommendations which are provided in their manual for certification of existing schools. The manual is called IGBC green EB O&M manual for schools provided in IGBC website.

A. Site and Facility Management (Maximum 18 points)

i) Eco-friendly Commuting Practices. (Max. 4 points)

Figure 2. Parking area of the campus

Figure 2 shows the parking facility in the campus for the vehicles of the college.

TABLE III.
POINTS FOR ECO-FRIENDLY COMMUTING PRACTICES

S.No	Percentage of occupants served with bus / pool service	Points
1	25%	2
2	50%	4

The points scored in this sub-criterion are 4 as per table III. There are 60 dedicated buses for the college.

ii). Eco-friendly landscaping practices. (Max. 2 points)

Figure 3. Landscape around the building

TABLE IV.
POINTS FOR ECO-FRIENDLY LANDSCAPING PRACTICES.

S.No	Percentage of organic fertilizers used or use of locally adaptive plants	Points
1	50%	1
2	75%	2

All the plants in the campus are locally adaptive which require less amount of water for their growth. The points scored in this sub-criterion are 2 as per table IV. The landscape is shown in figure 3.

iii). Heat Island Reduction. (Max. 4 points)

TABLE V.
POINTS FOR HEAT ISLAND REDUCTION, NON-ROOF

S.No	Percentage of shaded non-roof hardscape areas	Points
1	50%	2
2	75%	4

Figure 4. Solar panels on the building

The points scored in this sub-criterion are zero as there are hardscape areas covered with tree canopy/open grid pavers/ solar panels.

iv). Heat Island Reduction, roof. (Max. 4 points)

E-ISSN 2581 – 7957
P-ISSN 2277 – 3916

CVR Journal of Science and Technology, Volume 17, December 2019
DOI: 10.32377/cvrjst1704

TABLE VI.
POINTS FOR HEAT ISLAND REDUCTION, ROOF

S.No	Percentage of roof area with high reflective materials.	Points
1	50%	2
2	75%	4

The points scored in this sub-criterion are 2 as more than 50% of the roof is covered with solar panels as shown in figure 4.

v). Outdoor Light Pollution Reduction. (Max. 2 points)

The points scored in this sub-criterion are 2 as the college functions only during day time.

f) Building Operation & Maintenance. (Max. 2 points)

The points scored in this sub-criterion are zero as scoring credit points in this sub-criterion requires HVAC systems, Lighting systems, etc. which are not provided in the college.

B. Water Efficiency (Maximum 26 points)

i). Water efficient fixtures. (Max. points 6)

The points scored in this sub-criterion are zero as there are no water efficient fixtures in the building.

ii). Rain Water Harvesting. (Max. points 6)

TABLE VII.
POINTS FOR WATER EFFICIENT FIXTURES

S.No	Percentage of rain water harvested on site from roof and non-roof areas	Points
1	25%	2
2	50%	4

The points scored in this sub-criterion are zero as there are no rain water harvesting pits.

iii). Waste Water Treatment. (Max. points 4)

The points scored in this sub-criterion are 4 as there is a Sewage Treatment Plant. 100 % of waste water generated in the campus is treated on-site and safely disposed.

iv).Waste Water Reuse. (Max. points 4)

TABLE VIII.
POINTS FOR WASTE WATER REUSE

S.No	Percentage of treated water reused	Points
1	75%	2
2	100%	4

The points scored in this sub-criterion are 2 as the treated waste water is used for watering plants.

v). Water Metering. (Max. points 4)

Figure 5. Water meter in the building

The points scored in this sub-criterion are 4. The meters used can be seen in figure 5.

vi). Turf Area. (Max. points 4)

The points scored in this sub-criterion are zero as the turf area is very high. In order to score points in this sub-criterion, there should be less turf area.

C. Energy Efficiency (Maximum 30 points)

i). Improved Energy Performance (Max. points 14)

The main intent of this sub-criterion is to reduce the ill-effects on environment by enhancing the energy efficiency of the building. The points are given as 2, 4, 6, 8, 10, 12 and 14 based on the Energy Performance Index (EPI) for different climates. The annual energy consumption of the building under study doesn't achieve the limits mentioned in the IGBC manual.

The points scored in this sub-criterion are zero.

ii). On Site Renewable Energy. (Max. points 6)

TABLE IX.
POINTS FOR ON SITE RENEWABLE ENERGY

S.No	Renewable energy as a percentage of total energy consumption	Points
1	2.5%	2
2	5%	4
3	7.5%	6

The points scored in this sub-criterion are 6 as more than 10% of renewable energy is generated at site.

iii). Off Site Renewable Energy. (Max. points 6)

TABLE X.
POINTS FOR OFF SITE RENEWABLE ENERGY

S.No	Percentage of annual energy consumption	Points
1	25%	2
2	50%	4
3	75%	6

The points scored in this sub-criterion are zero.

iv). Energy Metering. (Max. points 4)

This should demonstrate that the facility has energy metering and monitoring for the following applications:

E-ISSN 2581 – 7957
P-ISSN 2277 – 3916

CVR Journal of Science and Technology, Volume 17, December 2019
DOI: 10.32377/cvrjst1704

- Renewable energy generation
- Power backup systems
- Interior lighting consumption

The points scored in this sub-criterion are 4 as the building has all the mentioned requirements.

D. Health and Comfort (Maximum 14 points)

i). Carbon dioxide Monitoring and Control (Max. points 2)

The main intent of this sub-criterion is to monitor carbon dioxide levels continuously and control it. This should be provided for occupant's health and well-being.

The points scored in this sub-criterion are zero.

ii). Isolation of Pollution Equipment & Systems (Max. points 2)

The purpose is to reduce the exposure of building residents to dangerous indoor pollutants which badly affect indoor air quality and residents health.

The points scored in this sub-criterion are zero.

iii). Eco-friendly housekeeping chemicals (Max. points 2)

The intent is to encourage housekeeping chemicals which are not hazardous to health of the occupants.

The points scored in this sub-criterion are zero.

iv).Thermal comfort and indoor room temperature (Max. points 2)

The intent is to provide comfortable thermal indoor environment to promote productivity and well-being of occupants.

The points scored in this sub-criterion are 2.

v). Facilities for differently abled people (Max. points 4)

Figure 6. Ramp for differently abled people

Figure 6 shows the ramp provided for differently abled people. The points scored in this sub-criterion are 4.

vi). Occupant well-being facilities (Max. points 2)

Figure 7. Indoor sports facility for occupants

The intent is to provide amenities to improve physical fitness and emotional well-being of the occupants. Figure 7 shows the indoor games facility in the campus.

The points scored in this sub-criterion are 2.

E. Innovation Category (Maximum 10 points)

The purpose is to inspire innovation in the performance of existing buildings to reduce the negative impacts on environment. Two points can be achieved if there is at least one IGBC accredited professional in the campus.

The points scored in this sub-criterion are zero.

The sum of all the points scored in all the green features is 48. Figure 8 shows the points scored under different green features against maximum points.

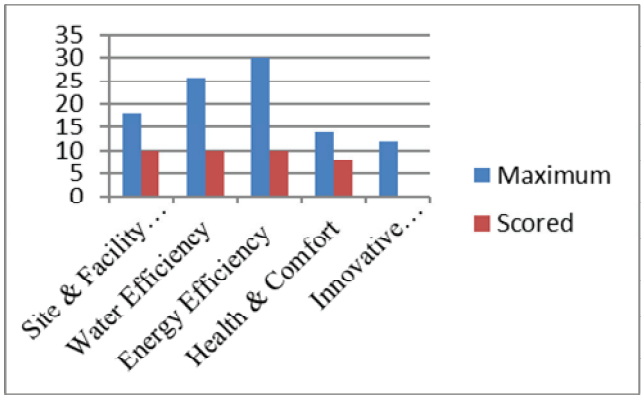

Figure 8. Maximum points VS Scored points

IV. Discussions & Conclusions

Sustainable or green buildings provide many tangible and intangible benefits to the occupants. The building rating/assessment systems are also very much useful in planning. The building assessment tools play an important role in planning by helping the planners manage the built environment and also in providing incentives for sustainable or green building.

After analyzing a conventional building based on its green features, a conventional building can easily be transformed into a green building by adapting simple sustainable principles. The first green feature or criteria as per IGBC certification system is site and facility management, which has a maximum score of 18. The points scored by the building in this criteria are 10. The sub-criterion such as eco-friendly commuting practices, eco-friendly landscaping practices, heat island reduction of roof and outdoor light pollution reduction. But the sub-criterion such as heat island reduction of non-roof and building operation and maintenance could not score points. This aspect of the building can be improved by surface parking, open grid pavers or by planting trees so as to get the shade from the canopies. The building operation and maintenance performance can be improved by providing HVAC systems such as chillers and cooling towers.

The second green feature or criteria is water efficiency. The total points scored in this criterion are 10 out of 26. This shows that the building the score not even 50% of the maximum score and there is a lot of scope for improvement. Analyzing the first sub-criterion, ordinary water fixtures can be replaced with water efficient fixtures to save a lot of

water. By doing so, 6 points can be scored in the first sub-criteria. There is also a long term benefit of saving water from being wasted. The second sub-criterion is rain water harvesting. The main intent of this is to capture at least 25% of runoff volumes from non-roof and roof areas. This can also be done at less cost, thereby improving the score and thereby moving still closer to a green building. The other sub-criterion where no points are scored is the last one i.e. reducing the area of turf in the landscaping to reduce the water consumption. This can be done by placing potted plants in place of turf and increasing landscape areas on basements, roofs, etc.

The third green feature or criteria is Energy efficiency which carries 30 points, i.e. 30% of the total points. But the points scored are only 10. In the first sub-criterion, the points scored are zero out of 14 as the annual energy consumption of the building under study doesn't achieve the limits mentioned in the IGBC manual. At least minimum points can be achieved by placing automatic sensors for switching on and off for lights, fans and air conditioners in the building. Studies show a greater improvement in energy efficiency after installing automatic sensors in the building. The other sub-criterion where there is a scope for improvement is the third one i.e. offsite renewable energy. This reduces the use of energy generation through fossil fuels. At least 2 points can be achieved by utilizing 25% of annual energy from offsite renewable energy sources. The other sub-criterions have scored well.

The fourth green feature is health and comfort. The total points scored are only 4 out of 8. The first sub-criterion, carbon di-oxide monitoring and control weigh 2 marks. These points can be easily achieved by placing carbon dioxide sensors and maintain CO_2 level of less than 530 ppm within the building. The next sub-criterion is isolation of polluting equipment and systems, weighing 2 points. This can be obtained by isolating the areas and room such as janitor rooms, printer/Xerox rooms. These areas should be provided with exhaust systems. The third sub-criterion is eco-friendly housekeeping chemicals. This requirement can be met by using housekeeping chemicals which meet GS-37 or other Indian standards and two points can be achieved.

The last green feature is Innovation. The total weightage is 12. By using some innovative methods which are not mentioned in the manual to reduce the load on the environment, a few points can be achieved. Having an IGBC accredited professional can fetch 2 points. This can be done by encouraging the occupants of the building to take IGBC accreditation test. This test can be cleared after undergoing a two-day training program at IGBC office.

It can be concluded that by following some basic standards, mentioned in this paper, a conventional existing building can be transformed into a green building. It has to be noted that this evaluation of green features is done based on the assumption that the building under study has followed all the mandatory requirements mentioned in the manual.

REFERENCES

[1] Abanda., F and Byers, L. (2016). "An investigation of the impact of the building orientation on energy consumption in a domestic building using emerging Building Information Modeling (BIM)." Energy 97., 10.1016/j.energy.2015.12.135

[2] Attom., M, Abed., F, Elemam., M, Nazal., M, and ElMessalami, N. (2016). "The effect of treated waste water on compaction and compression of fine soil" World Academy of Science, Engineering and Technology, International Journal of Civil, Environmental, Structural, Construction and Architectural Engineering.

[3] Boonstra., C. and Petterson, T.D. (2003) "Tools for environmental assessment of existing buildings" (online) Sustainable Building and Construction", UNEP Industry and Environment, April 2003

[4] Guggemos., A.A. and Horvath, A. (2006). "Decision support tool for assessing the environmental effects of constructing commercial buildings", Journal of Architectural Engineering, 2006, pp. 187-195.

[5] Gupta, A., and Kumar, A. (2010). "Composite materials: addressing the climate change." Asia Pacific Business review., 10.1177/097324701000600107

[6] Hikmat., H. Ali and Saba, F. Al Nsairat. (2008). "Developing a green building assessment tool for developing countries – case of Jourdan". Built and Environment 44, pp. 1053-1064

[7] Indian Green Buildings Council (IGBC) – "Green existing buildings operation and maintenance" abridged reference guide, April 2013.

[8] Pamu Yashwanth and Kona Mahesh (2019). "A comparative study on green building rating systems in India in terms of energy and water". CVR Journal of Science and Technology. pp. 21-25

[9] Pamu Yashwanth, VSS Kumar, M.R. Rajagopal and Kona Mahesh (2019). "A comparative study on green building rating systems in India for existing schools, National Conference on Innovations in Civil Engineering through Sustainable Technologies, September 2019.

[10] Sev, A. (2009a). "A comparative analysis of building environmental assessment tools and suggestions for regional adaptations". Civil Engineering and Environmental Systems, Vol. 28, No. 3, September 2011, pp. 231-235

[11] Viera, S.(2011). "Green building standards and certification systems". Washington DC: Steve Winter Associates.

[12] Waidyasekara., K.G.A.S, De silva., M.L, and Rameezdeen, R. (2012) Value of sustainable use of water in construction industry, 2nd International Conference on Sustainable Built Environment, 14-16 December 2012 at Kandy, Sri Lanka.

E-ISSN 2581 – 7957
P-ISSN 2277 – 3916

CVR Journal of Science and Technology, Volume 17, December 2019
DOI: 10.32377/cvrjst1705

Seismic Analysis of RC Elevated Rectangular Water Tank using Various Staging Patterns

M. Sai Ramya[1] and J. Sandhya Rani[2]
[1] PG Scholar, CVR College of Engineering/Civil Engg. Department, Hyderabad, India.
Email: medisettysairamya950@gmail.com
[2] Asst. Professor, CVR College of Engineering/ Civil Engg. Department, Hyderabad, India.
Email: sandhyajaligama25@gmail.com

Abstract: **Elevated water tanks are the structures of greater importance which are considered as the main lifeline elements. Many displeasing experiences have taken place earlier due to the damage and collapse of elevated water tanks due to the occurrence of earthquakes. The reason behind the damage is lack of providing proper supporting system to the water tank to withstand the dynamic loads and also due to improper selection of staging. The main objective of the present study is to evaluate the seismic response of elevated rectangular water tank with different staging patterns and different water level conditions (full, half and empty). Four types of bracing systems of elevated water tank such as normal bracing, diagonal bracing, V bracing, and cross bracing are considered for the analysis with various water level conditions. A total of 12 combinations were analysed and base shear, base moment and roof displacement for the fixed models were calculated with SAP2000 v 20.0.0 software using Response Spectrum Method (RSM) and results are presented.**

Index Terms: **Elevated rectangular water tank, Staging patterns, Water level conditions, SAP2000 version20, RSM.**

I. Introduction

Water is a very important source like food and air for the existence of life. To make it available for common public, Government of India provided a substantial amount to the water supply project. Elevated water tank is a structure used to store water, which is supported by a tower. The crest of the tower provides required pressure to supply water. Therefore, it is constructed at an elevation to accommodate useful storage and also maintain sufficient pressure for the water distribution system [6]. During the high peak hours of the water system, the static potential reserved in the tank is used to provide the pressure in the water pipes and helps the pumping systems by maintaining the necessary water pressure without increasing pumping capacity. They also present enough water pressure for fire-fighting when the pumping systems are not sufficient to provide large amount of water needed for fire extinguishing.

During an earthquake, sudden release of energy from the Earth's crust takes place, due to which seismic waves propagates. Earthquakes causes shaking or displacement of the structures constructed on the surface of the earth, which leads to destruction of the property and can also cause loss of life. Industrial liquid storage tanks may contain highly poisonous and inflammable liquids. Therefore, it is very important to consider the safety of liquid storage tanks and these tanks should be made leak proof and there is a chance of leakage of these poisonous liquids during an earthquake.

Liquid storage tanks are primarily classified into two types:

a) Ground supported tanks and
b) Elevated tanks.

Elevated tanks depend on hydrostatic pressure induced by the altitude of water enabling the supply of water even during power interruptions. This feature of elevated water tanks proves more efficient during power interruption after the occurrence of severe earthquakes and also in the situations where pumping systems are unable to work which depend on electrical power.

Elevated water tanks are generally supported on reinforced concrete frame, steel frame, masonry pedestal or reinforced concrete pedestal. In the present study, the elevated water tank is supported on reinforced concrete pedestals.

A. Scope of present study

In the present work models of elevated rectangular water tank set in seismic zone-II with medium soil, the soil is analysed by a linear dynamic methodology using SAP2000. The scope of present study aims at analysis of elevated storage tank with different water level conditions and includes displacement, base shear, base moments for a given structure, and to seek out the variation of relative results.

B. Objectives of present study

The objectives of present study are as follows:

a) The main objective of this study is to evaluate the seismic response of elevated water tank with different staging patterns and water level conditions (full, half and empty) by using response spectrum method
b) To study numerous responses like roof displacement, base shear, base moment etc.

II. Types of Bracing Patterns

In this study four types of bracing patterns are considered. They are normal, diagonal, cross, and V bracings [9] as shown in Figure 1, Figure 2, Figure 3 and Figure 4.

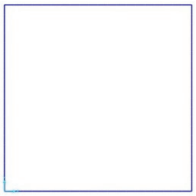

Figure 1. Normal bracing

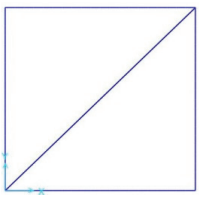

Figure 2. Diagonal bracing

E-ISSN 2581 – 7957
P-ISSN 2277 – 3916

CVR Journal of Science and Technology, Volume 17, December 2019
DOI: 10.32377/cvrjst1705

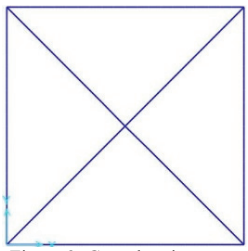

Figure 3. Cross bracing

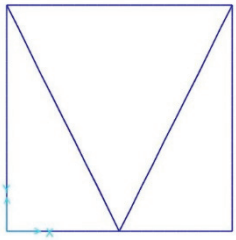

Figure 4. V bracing

III. Literature Review

Some of the research works carried out since 2013 are presented below:

Pavan.S. Ekbote, Prof. Dr. Jagadish.G. Kori had discussed the Seismic behavior of RC Elevated Water Tank under different types of staging patterns. The main aim of this study is to understand the behaviour of supporting system which is more effective under different response spectrum method with SAP 2000 software. In this paper different supporting systems such as radial bracing and cross bracing have been taken and the Base shear, Over-turning moment, Bending Moment, Story displacement had been calculated and the results are stated. [1]

Varun Suchak, Assistant Professor Dipak Jivani (May 2014) had discussed the Seismic Performance of Elevated Tank Staging Patterns under Different Ground Motions. An attempt has been made in this paper to understand the behavior of supporting system which is more effective under different earthquake recorded ground motions. In this paper time history analysis is carried out for elevated tank with three types of staging pattern under different five earthquake ground motion records. [2]

Ankush N. Asati, Prof. Dr. Mahendra S.Kadu (Aug 2014) had discussed the Seismic Investigation of RC Elevated Water Tank for Different Types of Staging Patterns. The seismic behavioural effect of elevated circular water tank is studied for constant capacity and constant number of columns; for various types of staging arrangement in plan, and variation in number of stages in elevation by using finite element method-based software SAP2000. [3]

Miss. Sonali M. Maidankar, Prof. G.D. Dhawale, Prof. S.G. Makarande (Jan.- 2015) had discussed the Seismic Analysis of Elevated Circular Water Tank using various Bracing Systems. The main aim of this study is to understand the behavior of different staging, under different loading conditions and strengthening the conventional type of staging, to give better performance during earthquake. For three different types of bracing systems, applied to the staging of elevated circular water tank for earthquake zones. Analysis is carried out using SAP2000 v15. [4]

Sudip Jha M.Tech, Cherukupally Rajesh, Associate proff. P. Srilakshmi (November 2015) had discussed the Behaviour of an Elevated Water Tank for Different Staging Patterns and Different Staging Heights. In this paper an extensive computational study has been conducted to find out the performance of elevated water tank under wind force. [5]

Sonali M. Pole, Asst. Professor. Amey R. Khedikar had done the Seismic Investigation of RC Elevated Water Tank for different Types of Staging Systems. The aim of this study is to understand the behaviour of different staging, under different loading conditions and strengthening the conventional type of staging, to give better performance during earthquake. This paper presents seismic analysis of elevated water tanks supported on different staging pattern with different tank storage capacities. [6]

J Visuvasam, J Simon, J S Packiaraj, R Agarwal, L Goyal and V Dhingra (2017) had discussed the Seismic response of elevated rectangular water tanks considering soil structure interaction. In this paper, the flexible base was provided as spring stiffness in order to consider the effect of soil properties on the seismic behaviour of water tanks. A linear time history earthquake analysis was performed using SAP2000. [7]

Mayank Gopal Manwani, Deepa P. Telang (May 2017) had discussed a Review on Seismic Analysis of Elevated Water Tank with Variations of H/D Ratio and Container Shape. In this study, Seismic forces acting on an Elevated water tank e.g. circular Tank and rectangular tank are studied with constant stagging height. [8]

IV. Methodology

Earthquakes are caused due to ground vibration which imparts a non-linear lateral load on structure for a period of time. These seismic vibrations are unpredictable and are destructive events for the structures. Exact estimation of the seismic forces for the design of the seismic proof structure is practically impossible. When the natural frequency of the lateral load coincides with the natural frequency of the sloshing water inside the tank, it results in severe damage or failure of the structure. Seismic analysis is a group of structural analysis which describes the response of the structure to the earthquake. Seismic analysis is also applicable in structural design where earthquakes are extensive. The seismic analysis of a structure involves assessment of the earthquake forces acting at various levels of the structure during an earthquake and the effect of such forces on the behavior of the overall structure is also determined. The analysis is classified as static and dynamic in approach as per the code provisions.

Further, Structural analysis methods can be categorized into the following categories-

- Equivalent static analysis or Linear static analysis
- Response spectrum analysis or Linear dynamic analysis
- Pushover analysis or Non-linear static analysis
- Time history analysis or Non-linear dynamic analysis.

In the present study, response spectrum method of analysis is carried out.

A.Response Spectrum Method

Response spectrum method is considered as a linear dynamic analysis. This method allows the multiple modes of response of a building to be taken into consideration (in the frequency domain) the considerable effect of any mode

E-ISSN 2581 – 7957
P-ISSN 2277 – 3916

DOI: 10.32377/cvrjst1705

except the fundamental mode on the response of the structure is considered. In this methodology, the response of Multi Degree of Freedom (MDOF) is expressed as the superposition of every Single Degree of Freedom (SDOF) system, that is then combined to calculate the whole response. This can be needed in many building codes for all apart from terribly simple or terribly complicated structures. Computer analysis is used to confirm these modes for a structure. For each mode, a response is read from the planning spectrum, based on the model frequency and also the model mass and they are then combined to produce an estimate of the overall response of the structure.

V. Problem Description

In the present study four types of arrangements have been considered i.e. normal, diagonal, cross and V bracings for fixed base models. An elevated rectangular water tank of 1,08,000 liters capacity is supported on RC staging of 9 columns with horizontal bracings of 200 x 200 mm at three levels. Grade of concrete and steel are M30 and Fe415, respectively. Density of concrete is 25 kN/m^3. The structural software SAP 2000 v20 is used to model the elevated rectangular water tank using response spectrum method and models are shown in Figure 5. Other dimensions of the elevated tanks are illustrated in the Table-I.

TABLE I.
PARAMETERS OF E.W.T

Parameters	Values
Capacity of tank	108000 lit
Density of concrete	25 kN/m^3
Grade of steel	Fe 415
Grade of concrete	M30
No. of columns	8
Height of staging	20
Staging levels	3
Size of beam	300 mmx450 mm
Size of braces	200 mmx200 mm
Size of columns	600 mmx600 mm
Slab size	150 mm
Wall size	200 mm
Height of tank	3 m
Response reduction factor	5
Zone	V
Seismic zone factor	0.36
Importance factor	1

VI. Elevated Water Tank Models

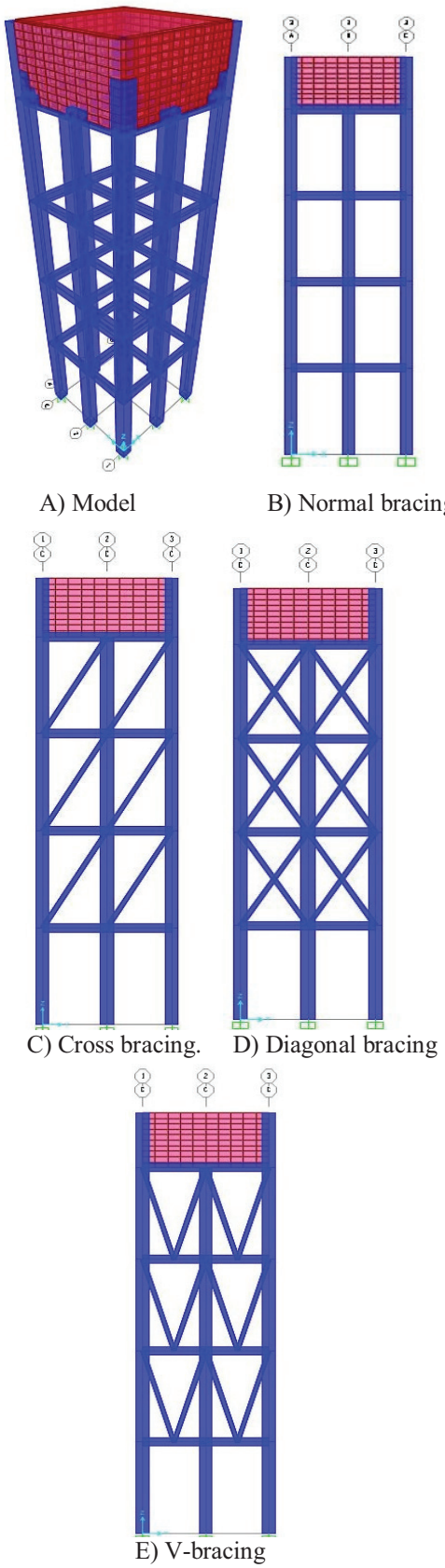

Figure 5. Models of E.W.T

E-ISSN 2581 – 7957
P-ISSN 2277 – 3916

CVR Journal of Science and Technology, Volume 17, December 2019
DOI: 10.32377/cvrjst1705

VII. RESULTS

Response spectrum analysis is carried out using SAP 2000 for fixed base models. The results obtained for elevated water tank with different water level conditions and various staging patterns are Roof displacement (Figure 6), Base shear (Figure 7) and Base moment (Figure 8). Subsequent discussions are made about the results obtained.

TABLE II.
ROOF DISPLACEMENT FOR DIFFERENT STAGING PATTERNS

Fluid level Conditions	ROOF DISPLACEMENT (mm)			
	Bracing types			
	Normal bracing	V bracing	Diagonal bracing	Cross bracing
Empty	9.9095	5.7987	3.2869	3.9202
Half Full	12.166	4.4822	2.651	2.6283
Full	25.187	5.6618	3.6243	3.3199

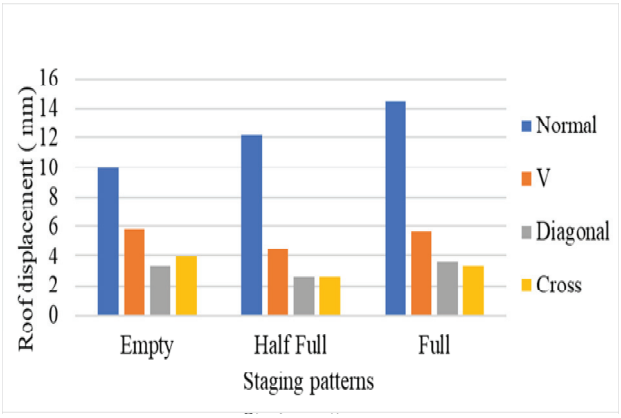

Figure 6. Roof displacement (in mm) for different staging patterns

TABLE III.
BASE SHEAR FOR DIFFERENT STAGING PATTERNS

Fluid level	BASE MOMENT My (kN-m)			
	Bracing types			
	Normal	V	Diagonal	Cross
Empty	175.136	233.239	160.264	224.898
Half Full	263.879	242.427	165.399	233.751
Full	318.406	281.257	196.331	244.758

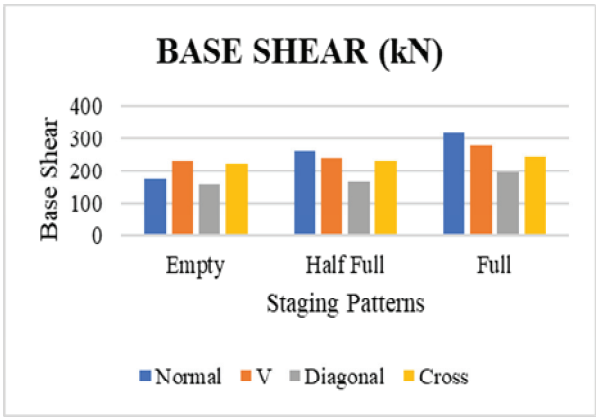

Figure 7. Base shear (in KN) for different staging patterns

TABLE IV.
BASE MOMENT FOR DIFFERENT STAGING PATTERNS

Fluid Level condition	BASE MOMENT Mx (kN-m)			
	Bracing types			
	Normal	V	Diagonal	Cross
Empty	2976.95	3027.82	2184.54	2772.63
Half Full	3709.19	3828.75	2629.38	3502.29
Full	4403.86	3828.83	2759.6	3923.9

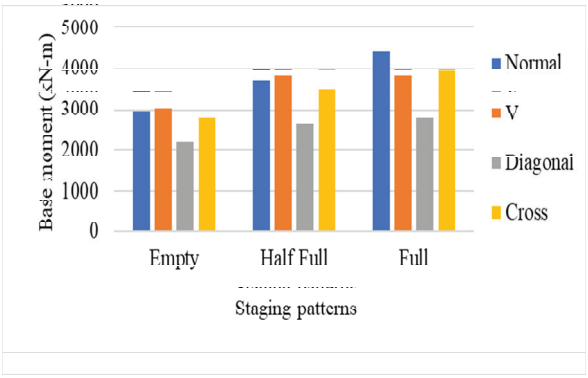

Figure 8. Base moment (kN-m) for different staging patterns

VIII. CONCLUSIONS

a) It is observed that diagonal bracing provide minimum value of lateral displacement for empty tank, half tank and full tank condition.
b) The diagonal bracings are more effective compared to the other type of bracings of bracings for empty, half and full tank conditions.
c) As the water level with the elevated tank increases from empty to half and full, the displacement of water tank also increases gradually from 9.1mm to 14mm.
d) Base shear will increase as the capacity of water increases. It is observed that the capacity of water

CVR Journal of Science and Technology, Volume 17, December 2019
DOI: 10.32377/cvrjst1705

tank will increase from empty tank to full tank, then the Base shear will also increase from 175kN to 318KN.

e) It is observed that diagonal bracing provides minimum value of Base shear for empty, half and full tank condition.
f) Base moment will increase as the capacity of water increases. It is observed that as the capacity of water increases from empty tank to full tank the Base moment will also increase from 525kN-m to 955kN-m.
g) Its observed that diagonal bracing provide minimum value of Base moment for empty, half and full tank condition.

IX. Scope For Further Work

a) The further scope of the work is to consider water tanks with varying capacities and shaft geometries in order to verify the effects of these parameters on the nonlinear response of such structures.
b) The application of seismic isolators or energy dissipaters can be investigated in controlling the seismic response of RC shafts.

References

[1] Pavan.S.Ekbote, Jagadish.G.Kori, "Seismic Behaviour of RC Elevated Water Tank under Different Types of Staging Patterns" Journal of E ngineering, Computers & Applied Sciences (JEC&AS), Volume-2, No.8, August 2013.
[2] Varun Suchak, Dipak Jivani, "Seismic Performance of Elevated Tank Staging Patterns under Different Ground Motions", Volume- 1, Issue -6, May 2014.
[3] Ankush.N.Asati, Mahendra.S.Kadu,"Seismic investigation of RC Elevated Water Tank for Different Types of Staging Patterns", (IJETT) -Volume 14 Number 1 – Aug 2014.
[4] Ms.Sonali. M.Maidankar, G.D. Dhawale,S.G. Makarande, "Seismic Analysis of Elevated Circular Water Tank using various Bracing Systems", (IJAERS) - Volume-2, Issue-1, Jan.- 2015.
[5] Sudip Jha, Cherukupally Rajesh, Sri Lakshmi, "Behaviour of an Elevated Water Tank for Different Staging Patterns and Different Staging Heights", IJMETMR, August 2015.
[6] Sonali.M.Pole, Amey.R.Khedikar, "Seismic Investigation of RC Elevated Water Tank for different Types of Staging Systems", Volume- 6, Issue 7, July 2017.
[7] J Visuvasam, J Simon, J S Packiaraj, R Agarwal, L Goyal and V Dhingra, "Seismic response of elevated rectangular water tanks considering soil structure interaction", IOP Conf. Series: Materials Science and Engineering 263 (2017).
[8] Mayank Gopal Manwani, Deepa P. Telang , "Review on Seismic Analysis of Elevated Water Tank with Variations of H/D Ratio and Container Shape", IJCSMC, Vol. 6, Issue. 5, May 2017, pg.202 – 208.
[9] Prashant A Bansode, V. P. Datye, "Seismic Analysis of Elevated Water Tank with Different Staging", Journal of Geotechnical Studies Volume- 3 Issue 1.

E-ISSN 2581 – 7957
P-ISSN 2277 – 3916

CVR Journal of Science and Technology, Volume 17, December 2019
DOI: 10.32377/cvrjst1706

Implementation of Automatic Aircraft Tracking with RTL-SDR

Dr. Yedukondalu Kamatham[1] and Sushmitha Pollamoni [2]
[1]Professor, CVR College of Engineering/ECE Department, Hyderabad, India
Email: kyedukondalu@gamil.com
[2]PG Scholar, CVR College of Engineering/ECE Department, Hyderabad, India
Email: spullamoni@gmail.com

Abstract: **To improve the efficiency, safety, and capacity of air space system, an Automatic Dependent Surveillance-Broadcast (ADS-B) is one of the popular technologies used in air traffic surveillance. The ADS-B uses 1090 MHz band. ADS-B is complemented by existing radar-based technologies to locate aircraft. The coexistence of radar systems and ADS-B is a key system to detect and resolve conflicts in the Next Generation Air Transportation System (NGATS). But, the major disadvantage of ADS-B is its implementation complexity and increase in cost without user-friendly. This paper focuses to reduce the complexity and cost of ADS-B system implementation in MATLAB with the help of Software Defined Radio (SDR). SDR is user-friendly and easy to handle aircraft information without increasing the cost. The ADS-B system implemented with SDR can receive the multiple numbers of aircraft information such as altitude, latitude, longitude, speed, and direction in real-time. Usage of SDR maximizes the information coverage with reliability and can achieve timely communication in Air Traffic Control (ATC) networks.**

Index Terms: **SDR, ADS-B, ATC, NGATS**

I. INTRODUCTION

Nowadays, with the increase in demand of National Air Space Systems (NAS), Federal Aviation Administration (FAA) faces number of challenges due to fundamental limitations of current radar systems. The air transportation systems are modernized by research and development programs of growth in air traffic levels of NAS. The main objective of an air transportation system is to provide safety and efficiency. Airspace is divided into two sectors in which each sector has Air Traffic Controller (ATC) responsible for managing air traffic. Sector in an aircraft is centrally controlled by corresponding ATC [1]. In U.S., Next Generation Air Transportation System (NGATS) is referred as a future system.

In airspace, the most congested region of air traffic (information flow) is controlled by centralization results in most efficient operations. Nevertheless, the implementation of such centralization on large scale is most expensive which requires all aircraft information to be relayed to the central facility through surveillance. This problem is aggravated as traffic demand increases. Similarly, in low traffic density, the aircraft interactions are less, and centralization efficiency is more as a distributed control strategy (aircraft unilaterally resolves in skirmish). The multiple aircraft in distributed system, that cooperate for the safety and efficiency of air traffic management.

To provide centralized surveillance, current systems depend on ground-based radar systems. Deployment of ground radar systems is very expensive and complex to maintain [2]. In areas, the system without line of sight, cannot provide coverage and subjected to terrain blockage. Instead of using expensive ground radar systems, NGATS aircraft will have wireless communication platform with enhanced onboard sensing capabilities [3]. The system in an area with line of sight constraints, the wireless systems can operate and enable cooperative techniques.

The primary target of FAA's NGATS plan is to transform the air transportation system into an adaptive, flexible and highly automated system capable of handling the expected increase in air traffic. The Cyber-Physical Systems (CPS) primary example is NGATS in which computations for monitoring, optimization, and sensing are tightly coupled with the actions of the aircraft themselves [4].

According to the NGATS plan, the design of Automatic Dependent Surveillance-Broadcast (ADS-B) is to increase the capacity, safety, and efficiency of NAS by sharing enhanced information between aircraft and Air Traffic Control (ATC) facilities [5]. ADS-B frequently transmits aircraft information such as aircraft number, position, altitude, speed and directions are determined by using satellite-based navigation systems. ADS-B shares frequency band 1090 MHz, which is same as current radar systems. ADS-B is less expensive when compared to conventional radar systems [6].

This paper deals with a low-cost solution for automatic aircraft tracking with Software Defined Radio (SDR). The SDR is used for ADS-B implementation of a real-time air traffic monitoring system. SDR is used to provide rapidly prototyping high-performance wireless communication systems with integrated software solutions [7]. SDR is a Universal Serial Bus (USB) device with low cost which receives RF radio signals. This device is designed for DVB-T (Digital Video Broadcast-Terrestrial) receivers. By handling SDR in different modes, to receive any kind of signal in the range of frequency tuner operates. This device is designed to receive not only Digital Television (DTV) signals but also receive all radio frequency signals in specified frequency range [8], [9]. The range of SDR is different from device to device depending on the components mostly used. However, SDR operates in the frequency range of 25 MHz to 1.75 GHz. The RTL-SDR front-end receives RF signals live off the air, down converted to form baseband signal, digitizes them and the output is the samples of baseband signal [10].

E-ISSN 2581 – 7957
P-ISSN 2277 – 3916

DOI: 10.32377/cvrjst1706

The rest of this paper is organized as follows: Section II deals with functionality of ADS-B and Section III presents implementation of ADS-B with RTL-SDR. Section IV represents results and discussions and the conclusion of this paper is presented in section V.

II. ADS-B WITH ATC

The air traffic controller (ATC) provides advisory service to aircraft from ground in non-controlled airspace. The main aim of ATC is to prevent collisions, expedite the flow of air traffic. ATC provides security to defensive role, operated by military in some countries. In many countries, depending on the operating range of airspace, the services are provided to all private, military aircraft, which depends upon the class of airspace and type of aircraft, ATC releases instructions that pilot should obey.

ADS-B is defined as an Automatic Dependent Surveillance-Broadcast which periodically broadcasts signals for tracking aircraft to determine its position by satellite navigation. The ATC on ground stations receives the information and ADS-B is a second surveillance radar. By providing the situational awareness of air traffic, the information is received by other aircraft which lead to self-separation. ADS-B is 'automatic' and does not require external input or pilot. It is dependent on aircraft navigation system data.

ADS-B consists of two services, they are "ADS-B Out and ADS-B In" for controlling the aircraft worldwide as replacing the radar with the primary surveillance method. For upgrading and enhancing aviation infrastructure and operation of NGATS national airspace ADS-B is used. ADS-B is an integral part of NGATS national airspace. With Traffic Information Services-Broadcast (TIS-B) and Flight Information Services-Broadcast (FIS-B) applications, the ADS-B system provides weather information in United States. To provide the information to ATC about the aircraft's visibility and enhances safety in real-time, ADS-B transmits the position and velocity data every second. For inexpensive aircraft tracking, planning and dispatch of data infrastructure are provided by ADS-B. Air Traffic Control is used as primary surveillance radar and secondary surveillance radar is used to know the location and identify the aircraft. Mode S transponder is an aircraft's equipment that is used to provide information to ATC about aircraft. Air Traffic Control Radar Beacon System (ATCRBS) is a secondary radar system currently used by aircraft, to achieve the compatibility between ATCRBS and Mode-S.

The avionics is an electronic system, which is used in aircraft, artificial satellites, and spacecraft. This system includes communication, navigation, display, management of multiple systems and hundreds of systems are fitted to aircraft to perform individual functions. This can be as simple as searchlight for police helicopter. By mode-S transponder, ADS-B, multichannel Distance Measuring Equipment (DME) minimizes size of avionics used in Aeronautical Radio Navigation Services (ARNS).

III. IMPLEMENTATION OF ADS-B WITH RTL-SDR

ADS-B receives signals with the help of Mode-S signal scheme. Mode-S is an aviation transponder interrogation mode type. When the interrogation request is received by an aircraft, the request is sent back to squawk code of transponder. Mode-S is designed with following properties as given in Table 1. ADS-B messages contain information about Altitude, Aircraft ID (24-bit Sequence).

TABLE I.
INPUT PARAMETERS

Transmit frequency	1090 MHz
Modulation	Pulse Code Modulation
Data rate	1 Mbps
Short Squitter Length	59 µsec
Extended Squitter Length	112 µsec

In Figure 1, at a physical layer, RTL-SDR is designed and it acts as a source. SDR samples the received signal at a rate of 2.4 MHz with interpolation factor of 5 to a practical sampling rate of 12 MHz with data rate of 1 Mbps. The packet synchronizer and Mode-S transponder are in a physical layer, work on sub-frames of data equivalent to squitter packets. The synchronizer first correlates the received signal with 8-µsec preamble and then a peak value is determined. The validation synchronization point is obtained by checking the preamble sequence either matches or not. The Mode-S data format is shown in Table II. The received messages of shown on a Graphical User Interface (GUI) by Data viewer. According to received messages, the time gets updated. if received signal time (t) is less than delay time (t_{end}) then signal gets processed to the physical layer and displays the experimental view of ADS-B as shown in Figure 2. With the help of NooElec software, the SDR drivers are installed in MATLAB. The SDR with range of 75 MHz to 1.25 GHz is used in this work for tracking the information of aircraft. Figure 3 shows the NooElec RTL-SDR, procured at a price of Rs 4000 is used for this experimental work.

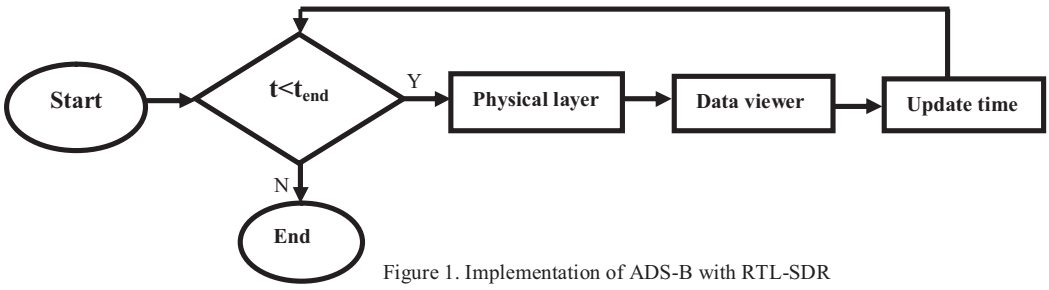

Figure 1. Implementation of ADS-B with RTL-SDR

E-ISSN 2581 – 7957
P-ISSN 2277 – 3916

CVR Journal of Science and Technology, Volume 17, December 2019
DOI: 10.32377/cvrjst1706

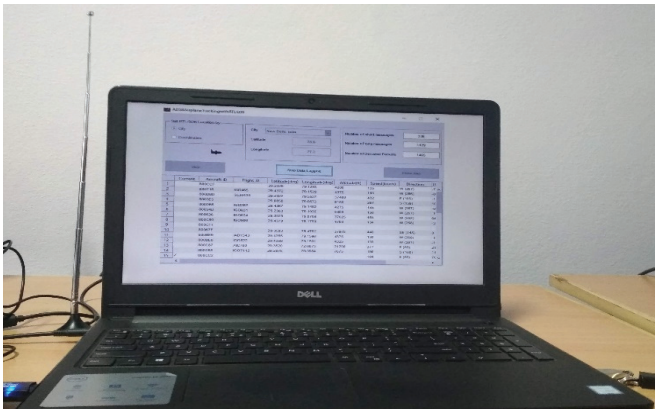

Figure 2. Experimental Setup of ADS-B

Figure 3. RTL-SDR diagram

TABLE II.
SQUITTER LENGTH INFORMATION

S.No.	Bit size	Bits	Name
1	5	1-5	Downlink Format
2	3	6-8	Capability
3	24	9-32	ICAO Aircraft Address
4	5	33-37	Type Code
5	51	38-88	Data
6	24	89-112	Parity ID

Mode-S signal format with sync pulse i.e. 8 µsec long followed for both 56 and 112 µsec. The data representation is shown in Figure 4.

A. Decoding Technique

The decoding process of ADS-B is shown in Table 2 has 5 parts with 112 bits long: Downlink format (DF) (5 bits) - Capability (CA) (3 bits) - ICAO (24 bits) – Data (56 bits) – Parity Identity (PI) (24 bits).

B. ADS-B Message types

The basic relationship between each type of code and information contained in the DATA segment is given in Table 3. For calculating Latitude, Longitude and Altitude values of an aircraft following expressions are used with Compact Position Reporting (CPR).

TABLE III.
INFORMATION ABOUT CODES

S.No.	TC	Content
1	1-4	Aircraft Identification
2	5-8	Surface Position
3	9-18	Airborne Position (w/Baro Altitude)
3	19	Airborne Velocities
4	20-22	Airborne Positions (w/GNSS Height)
5	23-31	Reserved for other uses

C. Calculation of Latitude

$$j = floor\left(59 + Lat_{cpreven} - 60 + Lat_{cpreven} + \frac{1}{2}\right) \quad (1)$$

First, two constants will be used

$$dLat_{even} = \frac{360}{4 * NZ} \quad (2)$$

$$dLat_{odd} = \frac{360}{4 * NZ - 1} \quad (3)$$

Where NZ is a present latitude value. For computing latitude values the following expressions are considered:

$$Lat_{even} = dLat_{even} * \left(\mathrm{mod}(j.60) + Lat_{cpr\,Even}\right) \quad (4)$$

$$Lat_{odd} = dLat_{odd} * \left(\mathrm{mod}(j.59) + Lat_{cpr\,odd}\right) \quad (5)$$

Final latitude is chosen depending on the timestamp of the frames:

$$Lat_{odd} = \begin{cases} Lat_{even} & if\ (T_{even} \geq T_{odd}) \\ Lat_{odd} & else \end{cases} \quad (6)$$

D. Calculation of Longitude

For an Even frame:

$$ni = \max\left(NL\left(Lat_{even}\right), 1\right) \quad (7)$$

$$dLon = \frac{360}{ni} \quad (8)$$

$$m = floor\left(\begin{matrix} Lon_{epr\,even} * \left[NL\left(Lat_{even}\right) - 1\right] - \\ Lon_{epr\ odd} * NL\left(Lat_{odd}\right) + \frac{1}{2} \end{matrix}\right) \quad (9)$$

$$Lon = dlon * \left(\mathrm{mod}\left(m, ni\right) + Lon_{cpr\,even}\right) \quad (10)$$

For an Odd frame: $ni = \max\left(NL\left(Lat_{Odd}\right) - 1, 1\right)$ (11)

$$dLon = \frac{360}{ni} \quad (12)$$

E-ISSN 2581 – 7957
P-ISSN 2277 – 3916

CVR Journal of Science and Technology, Volume 17, December 2019
DOI: 10.32377/cvrjst1706

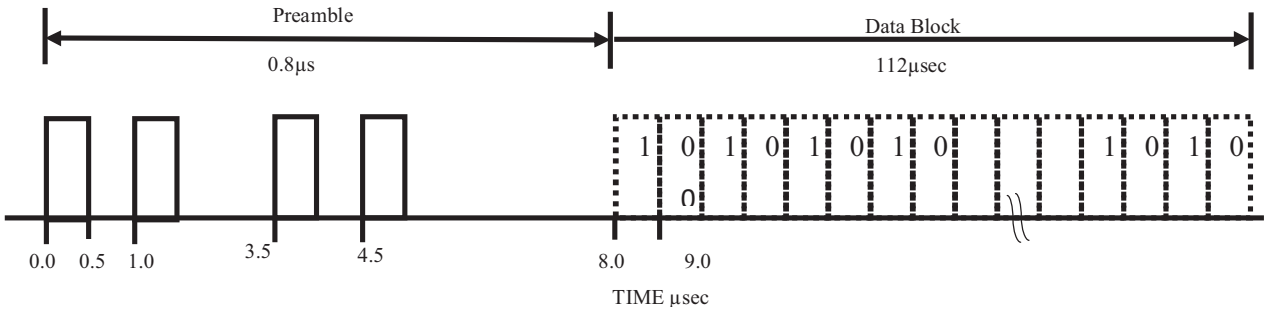

Figure 4. Mode-S data representation

$$m = floor\left(\begin{array}{l} Lon_{epr\,even} * \left[NL\left(Lat_{even}\right) - 1 \right] - \\ Lon_{epr\,odd} * NL\left(Lat_{odd}\right) + \frac{1}{2} \end{array} \right) \quad (13)$$

$$Lon = dlon * \left(\bmod\left(m, ni\right) + Lon_{cpr\,even} \right) \quad (14)$$

E. Calculation of Altitude

From the data frame, the altitude of aircraft is calculated. This Q-bit (bit 48) indicates whether the altitude is encoded in multiples of 25 or 100 ft and NQ denotes the N number of times of Q bits in multiple signals. The final altitude value will be:

$$Alt = NQ25 - 1000\left(ft\right) \quad (15)$$

Finally, for tracking of aircraft Latitude, Longitude, and Altitude are obtained.

IV. Results and Discussions

The RTL SDR receives the radio frequency signals of ADS-B. To display the information, the ADS-B Airplane Tracking Window is displayed. To track the exact location with SDR, depending on the requirements the city or coordinates are selected. If city is selected, then latitude and longitude values will be displayed automatically i.e. for example: in Figure 5, New Delhi is selected as the city; latitude and longitude values are displayed as Latitude – 28.5 and Longitude – 77.2. The SDR starts receiving the tracking the Aircraft information. From the aircraft the short messages and long messages are received and displayed. Here short messages are displayed as 336 and long messages are displayed as 1129. The received short and long messages are decoded and displayed as 1465.

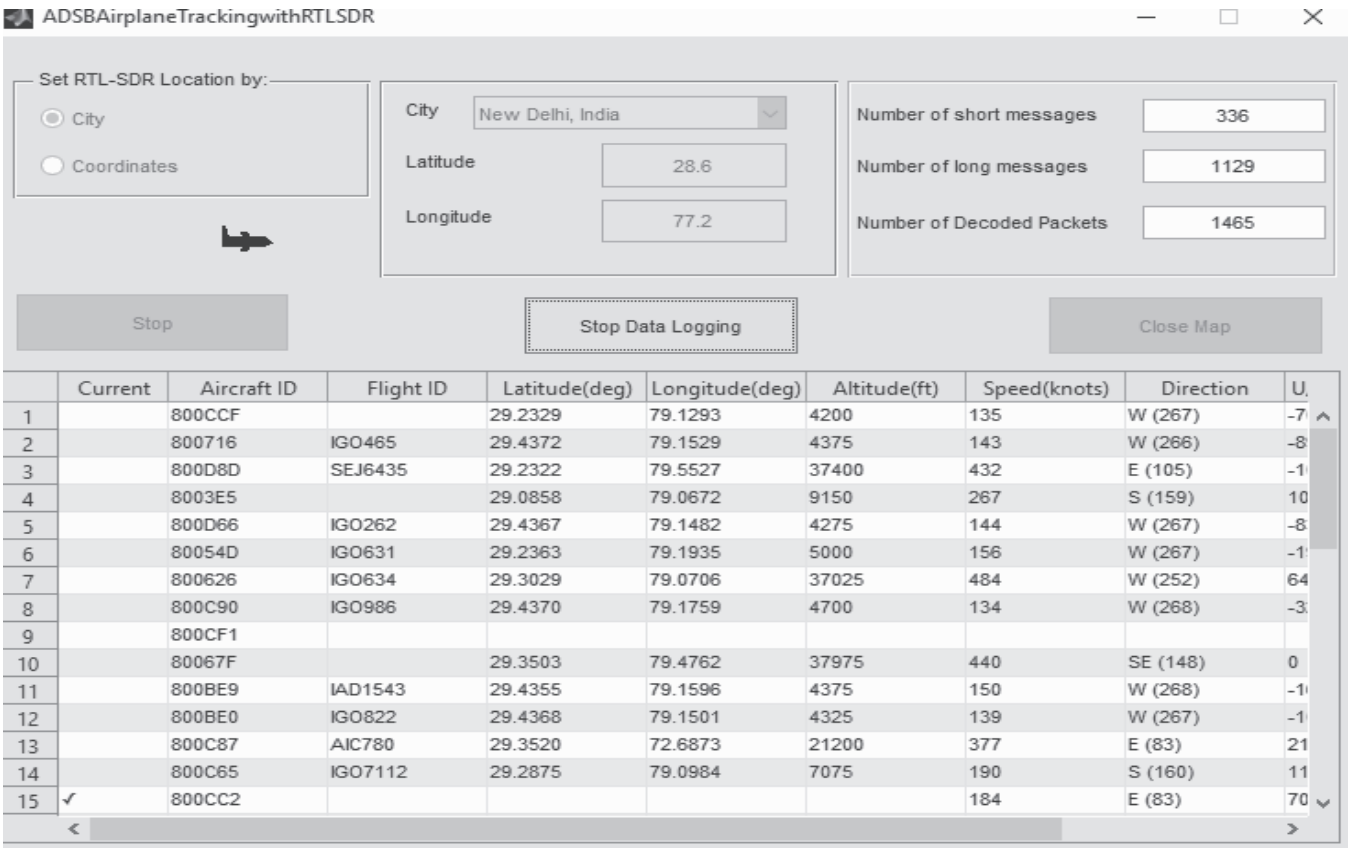

	Current	Aircraft ID	Flight ID	Latitude(deg)	Longitude(deg)	Altitude(ft)	Speed(knots)	Direction	U
1		800CCF		29.2329	79.1293	4200	135	W (267)	-7
2		800716	IGO465	29.4372	79.1529	4375	143	W (266)	-8
3		800D8D	SEJ6435	29.2322	79.5527	37400	432	E (105)	-1
4		8003E5		29.0858	79.0672	9150	267	S (159)	10
5		800D66	IGO262	29.4367	79.1482	4275	144	W (267)	-8
6		80054D	IGO631	29.2363	79.1935	5000	156	W (267)	-1
7		800626	IGO634	29.3029	79.0706	37025	484	W (252)	64
8		800C90	IGO986	29.4370	79.1759	4700	134	W (268)	-3
9		800CF1							
10		80067F		29.3503	79.4762	37975	440	SE (148)	0
11		800BE9	IAD1543	29.4355	79.1596	4375	150	W (268)	-1
12		800BE0	IGO822	29.4368	79.1501	4325	139	W (267)	-1
13		800C87	AIC780	29.3520	72.6873	21200	377	E (83)	21
14		800C65	IGO7112	29.2875	79.0984	7075	190	S (160)	11
15	✓	800CC2					184	E (83)	70

Figure 5. Aircraft tracking information

E-ISSN 2581 – 7957
P-ISSN 2277 – 3916

CVR Journal of Science and Technology, Volume 17, December 2019
DOI: 10.32377/cvrjst1706

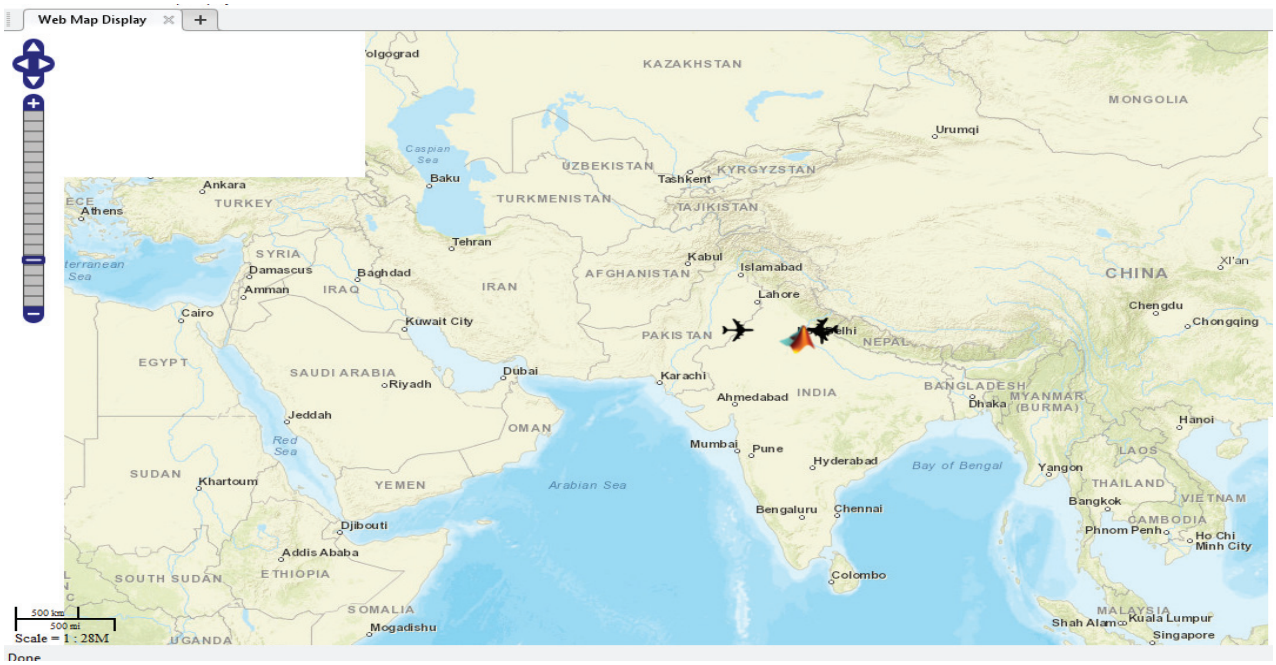

Figure 6. Geographical map of Airplanes tracking

With the selection of city of the specified latitude and longitude, the aircraft are tracked and displayed with Aircraft ID, Flight ID, Latitude (deg), Longitude (deg), Altitude (ft), Speed (knots), Direction. The current aircraft information is displayed with √ (tick) mark. For example, current aircraft tracking is displayed with the Aircraft ID-800716, Aircraft ID-IGO465, Latitude-29.4372, Longitude-79.1529, Altitude-4375 feet, Speed-143 knots, Direction-West (266°).

The aircraft is displayed in the world map shown in Figure 6 according to data tracked like time, altitude, direction. To display all aircrafts in this map to and fro to New Delhi, this city latitude and longitude values should be selected from the Figure 5. The background of map can also change according to requirement of either local map or geographical map. If we point cursor on aircraft image in Figure. 6, it displays the timing of aircraft and altitude, latitude and longitude of aircraft. If coordinates selected, according to requirements latitude and longitude values should be entered, and same process is repeated for this procedure. If this RTL-SDR is used for tracking of an aircraft, bulky equipment (used in conventional tracking systems) is not required so that complexity, cost of system is drastically reduced.

V. Conclusions

In this paper, ATC becomes the most prominent technology in surveillance system. ADS-B is also most important part of ATC for aircraft tracking systems in ATC because it provides aircraft information. To reduce the cost and complexity of ADS-B system, the system is implemented with help of RTL-SDR. The RTL-SDR is user friendly and easy for tracking. SDR receives the aircraft information with altitude, longitude, latitude and tracked aircraft are displayed. According to the aircraft gets tracked, the information is shown in map. The ADS-B system is used in many surveillance applications for tracking aircraft.

References

[1] Next generation implementation plan, Flight Attendant, 2011.
[2] Edward A Lester and R. John. Hansman, “Benefits and Incentives for ADS-B Equipage in the National Airspace System”, Mass Institute of Technology, ICAT-2007.
[3] RTCA (firm), SC-186, “Minimum Aviation Performance Standards for Automatic Dependent Surveillance Broadcast (ADS-B)”, Washington, DC: RTCA, ©1998.
[4] Krishna Sampigethaya, Radha Poovendran, Sudhakar Shetty, Terry Davis and Chuck Roy, “Future E-Enabled Aircraft Communications and Security: The Next 20 Years and Beyond”, Proceeding of IEEE, Volume: 99, Issue: 11, pp: 2040-2055, November 2011.
[5] RTCA DO-242, “Minimum Aviation System Performance Standard for Automatic Dependent Surveillance Broadcast (ADS-B)”, December 2006.
[6] Magaly Varga, Zsolt Alfred Polgar, Horia Hedesiu, “ADS-B Based Real-Time Air Traffic Monitoring System”, 2015 38th International Conference on Telecommunications and Signal Processing (TSP), pp: 215-219, 2015.
[7] Akshay N, Shruthi R, Sushmitha K N, Vanitha R and Dr. Rekha K R, “Live Aircraft Detection with Mode-S Transponder Using RTL-SDR”, International Journal of Advanced Research in Computer Science and Software Engineering, Volume: 7, Issue: 5, pp: 490-496, May 2017.
[8] D. Poirier-Quinot, P. Duvaut, L.Girardeau, B.F.G. Katz, “3D Head-Mounted Antenna Array Architecture Optimization based on the Fisher Information Matrix”, IV International Congress on Ultra-Modern Telecommunication and Control Systems 2012, pp:135-142, 2012.
[9] J. Mitola, “The Software Radio Architecture”, IEEE Communication Magazine, Volume: 33, Issue: 5, pp: 26-38, May 1995.
[10] G. Gilbert, “Historical Development of the Air Traffic Control System”, IEEE Transaction on Communications, Volume: 21, Issue: 5, pp: 364-375, May 1973.

E-ISSN 2581 – 7957
P-ISSN 2277 – 3916

CVR Journal of Science and Technology, Volume 17, December 2019
DOI: 10.32377/cvrjst1707

Brain Image Registration using Evolve Contourlet Transform: An Efficient Way to Register the Monomodal MRI-T2 Images

Abhinav Kumar[1] and Dr D. Sasikala[2]
[1]PG Scholar, Indian Institute of Technology (BHU)/ ECE Department, Varanasi, India
Email: abhinavk.ece17@iitbhu.ac.in
[2] Former Professor, CVR College of Engineering/CSE Department, Hyderabad, India
Email: anjansasikala@cvr.ac.in

Abstract: **There are subsequently several image registration methods and they ensure excessive impact in the medical world. It is applied in the data examining in medicine, investigating in remote sensing, satellite imaging, etc., In this paper the algorithm is put forward registers' images of the identical modalities MRI T2 to MRI T2. There are some disadvantages of wavelet transform that have to be operated with the contourlet transform, but then that is now subsequently undertaking specific preprocessing after employing the contourlet transform harnessing the image enhancement technique using their low-subband that was got by the Laplacian pyramid as a part of decomposition and then reconstructing the image by using the reverse contourlet transform and then registering the reconstructed image with the targeted image by utilizing the geometrical transformations. The investigational outcome demonstrates that the Evolve Contourlet Transform imparts advantageous conclusions than the wavelet and also the traditional contourlet transform.**

Index Terms: **Registration, Wavelet Transform, Contourlet Transform, Evolve Contourlet Transform, Mutual Information, Correlation Coefficient**

I. INTRODUCTION

The brain image registration is originating in the sector of medical image analysis in image processing. The research scope is very prominent in this unit as the more high-tech. Evolution in medical image analysis simpler remedy by the doctor. Medical science is professionally using the medical imaging in medicine and the major extents where it could toil out in terms of modalities would be on X-rays, Ultrasounds (US), Computed Tomography's (CT), Magnetic Resonance (MR) and Nuclear imaging as well. Subsequently, now in this exploration work, monomodal brain images are considered especially MRI T2 brain images are experimented. In so many areas, this will work as a key factor like in pharmaceutical industries, research labs in terms of medical imaging devices, research labs in terms of drug trials, research labs in terms of evaluating the quality of health care. [1]

Image registration is a process by which the pixels in two images just coincide to the matching points in the scene. So, by registration what it is inevitable is that if there are two imageries existing for example image A and image B or more images of identical entity in distinct time slot or selected from diverse devices placed at numerous spots. So, in these types of cases, if it is found that total unique image that will state more on the data contrast to additional image [1, 2].

Image registration is castoff for countless usages apart from that of the medical science, for illustration - in remote sensing, in satellite images, etc., In view of image registration, in a detailed manner in medical image analysis, for consideration of it clearly, a sample regarding a patient is procured. He goes for CT scan that day, the same day a patient goes for a CT scan after six months, but the location is altered, the CT scan center is reformed and that center after having a different CT machine with different resolutions, it is identified to all that the body is amending with time. For example, weight loss or weight gain. So, the CT scan must be unrelated with minor modification. Now the doctor requires in fact to relate amongst what occurred six months ago and what ensues that day for diverse points, like this registration is operated for orientation amid what comes about at what site before six months. At that flash moment the registration is sorted out point to point and predicts and displays that six months ago that point looked like that. The main criterion of registration is to blend the series of data with the discrepancies, if any or with their parallels into a solitary data. These collections of data are attained by appraising the equivalent scene or an entity apprehended at dissimilar point of time or from distinct viewpoints, in diverse coordinate systems. This research has been executed with two types of images; one is MR images and the other CT scan images.

Heaps of transforms or loads of techniques are readily available for performing the registration of images. Discussing the nature of the transformation, then there are chiefly two categories in general: Geometric transformations and Affine transformations. This is for the reason that aligning of images to intersect the universal aspects and add the variances if every, are to be highlighted for instantaneous perceptibility to the bare eye. This method can be grouped on four diverse facets similar to 1) the feature selection means extracting features from an image using their similarity measures and a correspondence basis, 2) the transformation function, 3) the optimization procedure, and 4) the model for processing by interpolation. So various algorithms are made known in distinctive research papers for image registration in which some are exceptional.

Image registration is categorized as intensity based and

E-ISSN 2581 – 7957
P-ISSN 2277 – 3916

DOI: 10.32377/cvrjst1707

feature based image registration techniques. Further are categorized based on linear and nonlinear transformations.

The task accomplished in this artefact benefits contourlet transform in an evolved fashion for image registration. At this juncture roughly, pre-processing is accomplished formerly then the registration that alters the predictable procedure of contourlet transforms to accomplish image registration. Similarly, this article task stretches with the virtual investigation and relative analysis of wavelet transform and Evolve Contourlet Transform in medical image registration. The balance out of the paper or this work is systematically well-ordered as the following ensues. Section 2 provides an overview of the related works of image registration by deliberating some highlights of divergent techniques. Section 3 explicates the wavelet transforms and this elementary prevailing contourlet transform in image registration. Section 4 describes the steps forward for contourlet transform i.e., Evolve Contourlet Transform image registration. Section 5 exemplifies the investigational outcomes to verify the efficiency of this anticipated method in image registration and Section 6 accomplishes the article with a treatise.

II. Related Works

This research is executed to deliver an extensive investigation of the current resources available on Image registration methods [3].Consequently, there are countless techniques - to suggest a trivial number of image registrations using various transforms namely, Hough transform [4], Finite Fourier transform [5], Walsh and Fast Walsh Hadamard transform [6, 7, 8], Shift Invariant Feature Transform [9], Scale Invariant Feature Transform [10], Translation-Invariant Feature Transform [11, 12], Adaptive Polar and Modified Adaptive Polar transforms [8, 13], Wang Landau Adaptive Monte Carlo approach [14], Discrete Cosine transform [15], and thus various works were completed on Image Registration. This sector familiarizes approximately specific significant labels of research papers in image registration.

An appraisal of image registration techniques [1, 16, 17] and medical image registration techniques [1, 18, 19] are achieved. A computerized parallel image registration technique based on the Correlation of Wavelet facets [2] and Wavelet transforms [16, 18, 20, 21, 22, 23, 24]. Use of Multiresolution Wavelet Attribute Pyramids for Mechanized Registration of Multi-sensor Imagery [25]. Edge sensor assessment using pragmatic ROC curves [26], an association amongst edge detection and the nonlinear multiresolution depictions [27], Image coding using wavelet transform [24,28]. The nonsubsampled contourlet transform concept, blueprint, and usages [29]. Contourlets in Beyond Wavelets [30]. Image Registration by Contour Matching using Tangent Angle Histogram [31]. Medical image harmonizing – an analysis with categorization [32]. Approaches for registration, interpolation and interpretation of three-dimensional medical image data for utility in 3-D display, 3-D modeling and therapy planning [33].

III. Discrete Wavelet Transform and Inverse Discrete Wavelet Transform

As soon as a familiarization on digital communications ascends, for instance, an audio signal, the gorgeous smooth audio pattern is being renewed into an extremely sporadic stream of bits. The meaning here for sporadic is, when diffusing that flow of bits, on a communiqué network, in reality, initiating incoherence each time a bit alters over. So subsequently, for every single bit interval, there is a variation of waveform and hence, disjointedness at various levels, still if not in the function, in its derivative or in a second derivative whatsoever exist. the notion of signifying constant functions in terms of sporadic ones has its status in hands-on communiqué and thus, what Haar wavelet ensured is as follows. Owing to these origins of their virtuous aspects in [34], it can be emphasized that when associated with the traditional approaches, the Haar wavelet technique is extensively further sophisticated in concept, added appropriate in mathematical scheming and, furthermost of the whole lot, it is immeasurably expeditious in information handling .Equations (1), (2) and (3) are associated with Haar Wavelet Transforms.

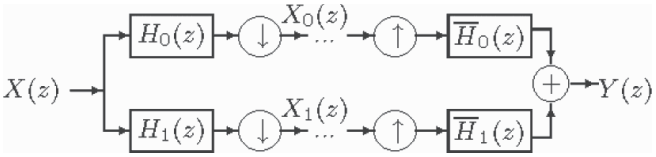

Figure 1. The low-pass and high-pass decomposition filters of Conjugate Quadrature Filter (CQF)bank of Discrete Wavelet Transform (DWT)

By means of Figure. 1 arithmetical lookout: Say H_0 and H_1 are the low-pass and high-pass categorization filters of Conjugate Quadrature Filter (CQF) bank of Discrete Wavelet Transform (DWT), correspondingly. H_0 and H_1 can be put up to make certain concerning the Prefect Reconstruction (PR) necessities, i.e.,

$$Y(z) = X(z)\, z^{k} \quad (1)$$

where $X(z)$ and $Y(z)$ reveal the input and output signals, $k \in Z$. Yet, the aliasing in the output of disintegrated subband ,$X_0(z)$and $X_1(z)$, arise for the reason that of downsampling procedure that can be suggested by the subsequent investigations.

$$X_0(z) = [X(z)H_0(z)] \downarrow 2 = X'_0(z) = [z^{-1}X(z)H_0(z)] \downarrow 2 \quad (2)$$

where "↓2" is a representation of the downsampling technique by the factor of "2". If X(z) is deferred by one sample, i.e., X′(z)=z^{-1}X(z), the output $X'0(z)$ becomes

$$\begin{aligned} X'_0(z) &= [z^{-1}X(z)H_0(z)] \downarrow 2 \\ &= X\left(-z^{\frac{1}{2}}\right)H_0\left(z^{\frac{1}{2}}\right) + X\left(-z^{\frac{1}{2}}\right)H_0\left(-z^{\frac{1}{2}}\right) \\ &= z^{(-1/2)}[X(z^{(1/2)})H_0(z^{(1/2)}) - X(-z^{(1/2)})H_0(-z^{(1/2)}) \\ &= z^{(-1/2)}[X_0(z)] \downarrow 2 \end{aligned} \quad (3)$$

This transform embraces the filtering and down-sampling functions. As implied in Figure. 2, at each level of the wavelet categorization, four innovative images are fabricated from the exemplar image. The new-fangled images are named conferring to the filter (low-pass or high-pass) that is put in to the real image in horizontal and vertical directions. For illustration, the LH image is an

E-ISSN 2581 – 7957
P-ISSN 2277 – 3916

CVR Journal of Science and Technology, Volume 17, December 2019
DOI: 10.32377/cvrjst1707

outcome of the gain of the low-pass filter in horizontal direction and highpass filter in vertical direction. Consequently, the four images shaped from each breakdown level are LL, LH, HL, and HH. The LL image is measured as a reduced version of the previous image as it holds utmost particulars. The LH image comprehends horizontal edge facets, still the HL comprises vertical edge facets. The HH encompasses high frequency data only and is stereotypically noisy and is, so, not beneficial for the registration [30]. In wavelet categorization only, the LL image is employed to yield the next level of breakdown.

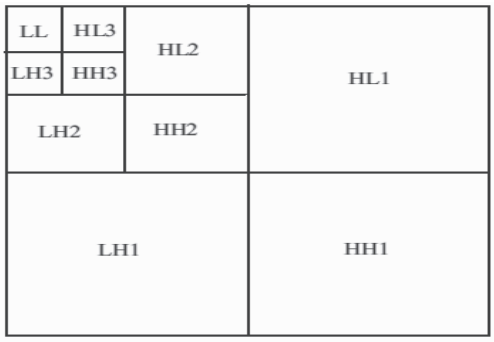

Figure 2. Image Compression Levels -1st level, 2nd level and 3rd level.

But then again, this system is unsuccessful in capturing the resourceful observable facts in imageries in the targets other than the horizontal and vertical directions. Do and Vetterli anticipated a proficient indicator multiresolution image exemplification termed the contourlet transform [30].

IV. Contourlet Transform

The Contourlet Transform (CNT) offers a multi-resolution and directional categorization; meanwhile it consents for a diverse quantity of targets at every calibration. First, a Laplacian pyramid is applied to gain control over the spot incoherence, formerly it is trailed by a Directional filter bank to associate spot incoherence into linear structures.

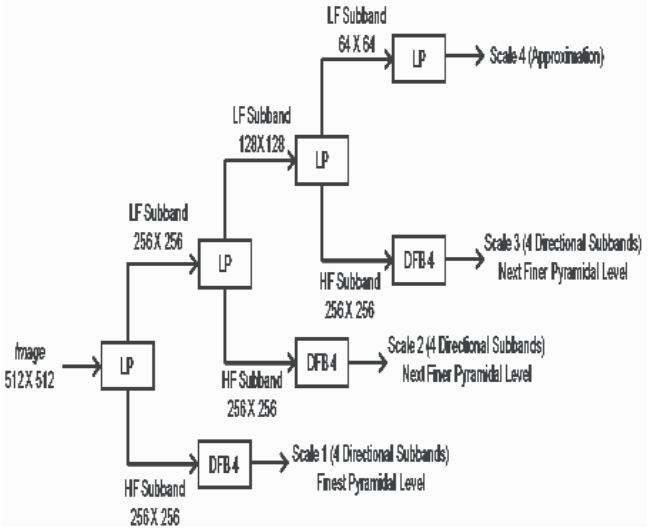

Figure 3. The flowchart of CNT for a 512 x 512 image

Owing to downsampling and upsampling, the contourlet transform is shift-variant, translation-invariant and scale-invariant. Yet, shift-invariance is vital in image analysis functions such as edge detection, contour characterization, and image enhancement [35, 36]. This aspect is just the reverse in the contourlet transform. Translation-invariant feature is essential for denoising [11, 12] and Scale-invariant feature is utilized for renormalizing signals [10]. These aspects are synchronized in the contourlet transform.

Contourlet transform is a resourceful indicator, targets multiresolution expansion that is digital friendly. Contourlet approximates multiscale, local and directional contour segments. The notion of contourlet transform emanated by means of the curvelet transforms that hinges on curvelet production that is the blend of numerous concepts [29, 37].

For achieving the contourlet categorization of an image, it is essentially obligated to have applied two transforms to it, the very first one is the Laplacian Pyramid (LP) and the second one is Directional Filter Bank (DFB) to yield orientation edge constituents of a segment in the interior of an image.

Contourlet Transform contributes a multiresolution, local and directional expansion of the image using Pyramidal Directional Filter Bank (PDFB). The PDFB fuses Laplacian Pyramid (LP) that depicts the spot incoherence, with a DFB that associates these incoherences into linear constructions.

Figure. 3, shows the flowchart of CNT for a 512 x 512 image. As shown in Figure 3, first stage of CNT is LP decomposition and DFB are in the second stage. LP scheme is shown in the following Figure 4. Here, the input image x is the first lowpass filtered by analysis filter H and then downsampled to give off a coarse approximation a. It is then interpolated and disseminated owing to the synthesis filter G. The resultant image is deducted from the previous existing image x to get hold of the bandpass image b. This system can be recapitulated.

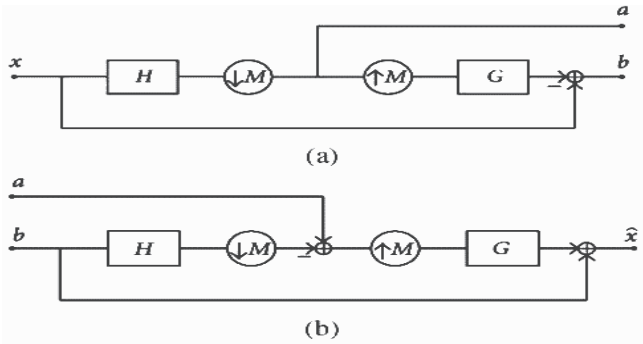

Figure 4. Laplacian pyramid. (a) One level of decomposition (b) The new reconstruction scheme

Equations (4), (5) (6) and (7) are associated with rigid transformation application. A rigid transformation applying on any vector v engenders an altered vector $T(v)$ in term of

$$T(v) = R\,v + t \quad (4)$$

where $R^T = R^{-1}$, R= orthogonal transformation and t = vector forwarding the translation of the derivation.

An apt rigid transformation has the following determinant,

E-ISSN 2581 – 7957
P-ISSN 2277 – 3916

CVR Journal of Science and Technology, Volume 17, December 2019
DOI: 10.32377/cvrjst1707

$$det(R) = 1 \quad (5)$$

i.e., the R doesn't churn out a reflection, and stay alive in for a rotation. When an orthogonal transformation matrix begets a reflection, its determinant is -1[38].

V. Anticipated Approach: Evolve Contourlet Transform

The aim of image registration using Evolve Contourlet Transform is to assimilate complementary and redundant data from multiple images to generate a single image that encompasses of better-detailed data of the image than any of the specific source images. Here, both wavelets transform and Evolve Contourlet Transform registrations are implemented. Initially apply wavelet transform on an image and then perform reverse wavelet transform and by using this recreated image, registration is harnessed. In Evolve Contourlet Transform, first, apply the conventional contourlet transform, then rebuild the image by putting on the inverse contourlet transform. But, before the reformation, whatsoever image is acquired the lowpass and high pass sub-band or sub-images playing with that low sub-band and fundamentally, enhancing of the pixel values is resolved by applying fractional scalar multiplication. As the entire entity is a matrix by carrying out this the rebuilt image augment and impart more knowledge on the image. Obtaining this renovated image, image registration is then executed with the target image by using the same procedures of the above-mentioned geometrical transformations on the wavelet transform.

A. Wavelet Transform for Monomodal Image Registration Process

Algorithm:

Step 1:Put into operation wavelet transform on an imageI_1gaining an imageI_2

Step 2:Render reverse wavelet transform of I_2 and by means of this I_4reconstructed image registration is utilized obtaining image I_5.

Step 1 description:

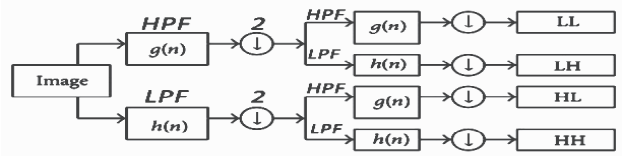

Figure 5. Discrete Wavelet Transform (DWT)

Figure 5. shows the approximation of DWT. The decimator down samples the input signal g(n), h(n) by a factor of 2.

Wavelet contexts of the Haar have remained illustrated to high-level measurement and ranking. The wavelet transforms have two types of coefficients, namely, 1. Scaling coefficients: created by manipulating the usual value of two neighboring models. They prove the approximation signal. 2. Wavelet coefficients: produced by scheming the contrast value of two neighboring examples. They explain the detailed signal. The Haar wavelet is a reasonable method and operating by the algorithmic calculation. Approximating the values of the scaling coefficients encompasses discovering the totality of two data models and distributing it by 2. Correspondingly, assessing the values of the wavelet coefficients take in resulting in the variance of two data examples and sharing it by 2.

Taking a discrete series that is signified as f(x). This signal is a direct outcome of sampling of input data signal. In this subsequent discrete order, two in line models are engaged that are labeled as X and Y. At that point, if the Haar transform is used on this order, the X and Y, will be replaced by Average and difference values that are considered,

$$\alpha = (X + Y)/2 \quad (6)$$

$$d = (Y - X) \quad (7)$$

Figure 6. indicates Haar Wavelet Transform. An order is chosen that is signified as$\lambda_{0,k}$, with number of example, such that, $0 \leq k \leq n$.

The average and difference values are calculated for every pair, where$\mathbf{X} = \lambda_{0,2k}$ and $\mathbf{Y} = \lambda_{0,2k+1}$

As the n number of models is divided into odd and even models, the order will hold n/2, pairs. The difference and average values are specified as,

$$\lambda_{-1,k} = (\lambda_{0,2k} + \lambda_{0,2k+1})/2 \quad (8)$$

$$\gamma_{-1,k} = \lambda_{0,2k+1} - \lambda_{0,2k} \quad (9)$$

Equation (8) and (12) does the average and Equation (9), (10) and (11) produces the difference of in line models.

The input data order $\lambda_{0,k}$is separated into two signal elements1.$\lambda_{-1,k}$with n/2 averages and 2. $\gamma_{-1,k}$with n/2 differences.

With the support of these average and difference values, the original signal can be improved. The average values are supposed to be the approximate signal depiction and the different values are measured as finer or complete signal depiction. In the occasion that original data order has predominant local consistency that indicates that the data discrepancy between the models is somewhat low. In such circumstances, the estimated signal depiction nearly looks a lot like the original data and the complete signal will be insignificant. Occasionally the complete signal will be near to 0, in that occasion, it can be totally constricted.

The approximate signal order, $\lambda_{-1,k}$is split more into 2 signal elements,1.$\lambda_{-2,k}$with n/4 averages and 2. $\gamma_{-2,k}$with n/4 differences and so on.

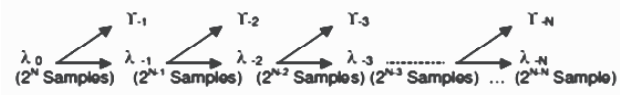

Figure 6.HaarWavelet Transform

E-ISSN 2581 – 7957
P-ISSN 2277 – 3916

CVR Journal of Science and Technology, Volume 17, December 2019
DOI: 10.32377/cvrjst1707

Save both 'a' and 'X' and same way'd' and 'Y' in the matching place.

Originate by computing'd'

Predict stage: $d = (Y - X) \rightarrow Y = d$ (10)

(Substitute for the value of Y)

Here, the difference is considered for in line models, and the outcome will be kept in odd numbered places. So, revised as $Y = Y - X$.

Updated stage: $a = X + \frac{d}{2} \rightarrow X = a$ (11)

(Substitute for the value of X)

So, revised as $X = X + \frac{d}{2} \rightarrow X = X + \frac{(Y-X)}{2} = (X + Y)/2$ (12)

(Average value in line models)

Taking an example of a sequence of n sample, denoted as $\lambda_{0,k,}$ where, $0 < k < n - 1$. Considering the approximation level as 0. At the next level that is 1, this order can be transformed into a pair of other groups. It starts with dividing the input models to odd and even parts that is stated as lazy wavelet transform. Though, this does not aid the compressed signal depiction. In the next step, the prediction and updation methods of the lifting arrangement are originated that transforms the above order a) Approximation signal, denoted as, $\lambda_{-1,k,}$ where, $0 < k < \frac{n}{2} - 1$. b) Detailed signal $\gamma_{-1,k}$, where, $0 < k \leq \frac{n}{2} - 1$.

Step 2 explanation:

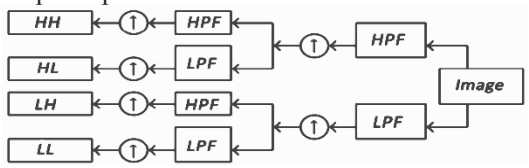

Figure 7.Inverse Discrete Wavelet Transform (IDWT)

The interpolator up samples the input signal g(n), h(n) by a factor of 2.

Also, the innovative values of X and Y can be attained by smearing inverse Haar transform,

X = a - d/2 (13)

Y = a + d/2 (14)

Figure 8.Haar Inverse Transform

$$X = X - \frac{Y}{2} = a - \frac{d}{2} = \frac{(X+Y)}{2} - \frac{(Y-X)}{2}$$

(X substitute's average value) (15)

$$Y = Y + X = d + X = (Y - X) + X$$

(Y substitutes Difference value) (16)

From Figure 7. Inverse wavelet transform is effortlessly realized from Equation (13) and (14) by merely swapping the sign in discrete wavelet transform. The Haar wavelet is well-thought-out as the modest orthogonal wavelet with minimalized provision in Figure 8. Thus, original values can be found with the aid of Equation (15) and (16).

The Inverse wavelet transformation is just performed in backward way of discrete wavelet transformation. With the support of lifting arrangement, it is no matter what but problematic to acquire inverse wavelet transform. It is straightforwardly realized by swapping the sign. Figure 7 and Figure 8 indicate the Haar Inverse Discrete Wavelet Transforms.

B. Evolve Contourlet Transform for Monomodal Image Registration Process

Algorithm:

Step 1: Put on the conventional contourlet transform on an imageI_1.

Step 2: I_2 image is acquired the lowpass and high pass sub-band or sub-images playing with that low sub-band and fundamentally, enhancing of the pixel values is resolved by applying fractional scalar multiplication.

Step 3: Provide inverse contourlet transform of I_3 and by means of this I_4 renovated image registration is employed finding image I_5.

In both the cases the Mutual information and correlation coefficient are measured, and the results are compared.

Step 1 clarification: Contourlet transforms – Multiresolution and multidirectional expansion using non-separable filter banks.

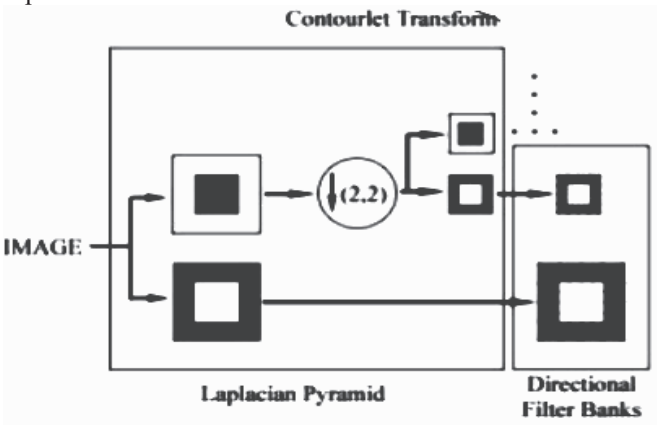

Figure 9. Contourlet Transform

From the Figure 9. Contourlet Transform the Laplacian Transform and the directional filter bank are expanded and shown in Figure 10 and Figure 11 i.e., the frequency partitioning representation of directional filter bank are shown below.

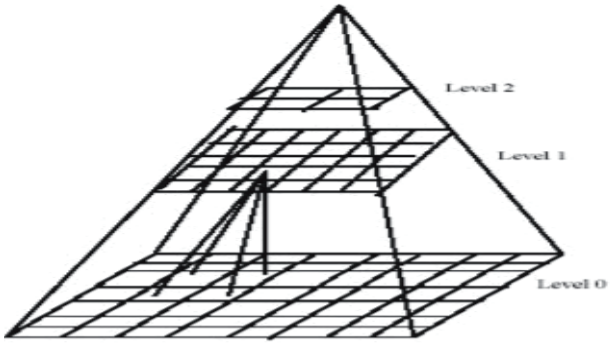

Figure 10. Laplacian Pyramid

E-ISSN 2581 – 7957
P-ISSN 2277 – 3916

DOI: 10.32377/cvrjst1707

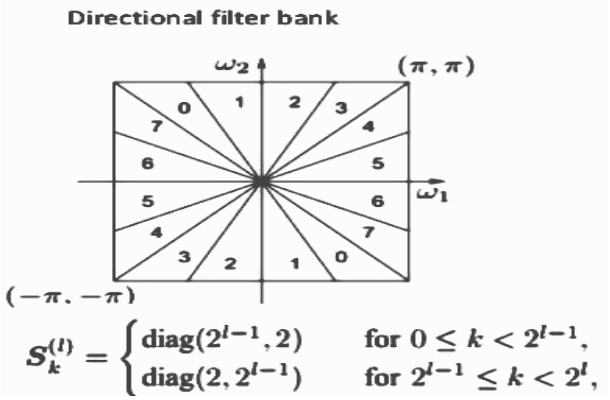

Figure 11. Frequency Partitioning

$$Y'_{i,j} = f(Y_{i,j}) \quad (17)$$

Step 2: A threshold $T_{i,j}$ is computed for each sub-band.

$$f(Y_{i,j}) = \begin{cases} W_1 Y_{i,j}(n1,n2) & if\ b_{i,j}(n1,n2) = 0 \\ W_2 Y_{i,j}(n1,n2) & if\ b_{i,j}(n1,n2) = 1 \end{cases} \quad (18)$$

Step 2 enhancement: Performs multi-scale salient features-based image enhancement by improving salient features like edges, lines, curves and contours using its anisotropy and directionality properties [35, 36].

Step 3 elucidation: The Inverse Contourlet Transform (ICT) is harnessed in Equation (18) in view of the improved directional sub-bands to acquire the ultimate improved image from Equation (17).

Denoting C and C^{-1} as the Contourlet and Inverse Contourlet transforms, correspondingly; D_T is the diagonal matrix that, with threshold value T, zeroes out irrelevant coefficients in the coefficient vector, whose total values are lesser than T. Let $\hat{X}$ the noisy high-resolution image; and $\hat{X}'$ the denoised high-resolution image. The sparseness constraint by hard thresholding can be marked as Equation (19).

$$\hat{X}' = C^{-1} D_T C \hat{X} \quad (19)$$

VI. Investigational Outcomes

Dissimilar medical image dataset used to achieve outcomes in this experiment. The dimensions of the dataset are changed. Consider the distinctive brain image acquired from the varied angle of the same patient at another time slots. The quality of the images attained after registration of images by this method has been tested using the Mutual Information and Correlation Coefficient.

A. Mutual Information

The Mutual Information (MI) between two variables deal with the volume of information that one variable comprises about another. High MI states a huge drop of ambiguity and low MI states an insignificant decrease in ambiguity and zero MI between two variables indicate that the variables are autonomous.

From Equation (20), it calculates the degree of dependence of the two images as MI, higher degree infers better quality, $I(X;Y) = \sum_{y \in Y} \sum_{x \in X} p(x,y) \log \left(\frac{p(x,y)}{p_1(x) p_2(y)} \right)$ (20)

- X and Y – Two discrete random variables
- $p(x,y)$ - Joint probability distribution function of X and Y
- $p_1(x)$ and $p_2(y)$- Marginal probability distribution function of X and Y

B. Correlation Coefficient

There are two images, the first is template image and the second one is the candidate image, or say one is target image and another one is registered image. So, correlation states about the close relation between the pixels in the template and candidate image or target and registered image.

From Equation (21), Correlation Coefficient (CC) is a computation of how the forecasted data from a prediction model fit with the realistic data.

If there is no association between the predicted data and actual data, the CC is very low. As the association is increasing, the CC will also increase. The higher value of CC states concerning the better association between both the data.

$$C(t,s;\theta) = \frac{\sum_x \sum_y \left[I_1^{new}(x,y) - \overline{I_1^{new}(x,y)} \right] \left[I_2^{new}(x\cos\theta - y\sin\theta - t, x\sin\theta + y\cos\theta - s) - \overline{I_2^{new}(x,y)} \right]}{\sqrt{\sum_x \sum_y \left[I_1^{new}(x,y) - \overline{I_1^{new}(x,y)} \right] \sum_x \sum_y \left[I_2^{new}(x\cos\theta - y\sin\theta - t, x\sin\theta + y\cos\theta - s) - \overline{I_2^{new}(x,y)} \right]^2}} \quad (21)$$

$I_1^{new}(x,y), I_2^{new}(x,y)$ – Two new images that differ from each other by rotation and translation only.

t, s – Shifting parameters between the two images.

θ – Rotation angle

$\overline{I_1^{new}(x,y)}, \overline{I_2^{new}(x,y)}$- Average structure value of the pixels in the overlapping parts of images $I_1^{new}(x,y), I_2^{new}(x,y)$

Tools- for the experimentations Matlab2017 R2017a were utilized.

For study Monomodal MRI T2 images are taken into account and the results are conferred and are instituted and are made known as below.

C. Output I

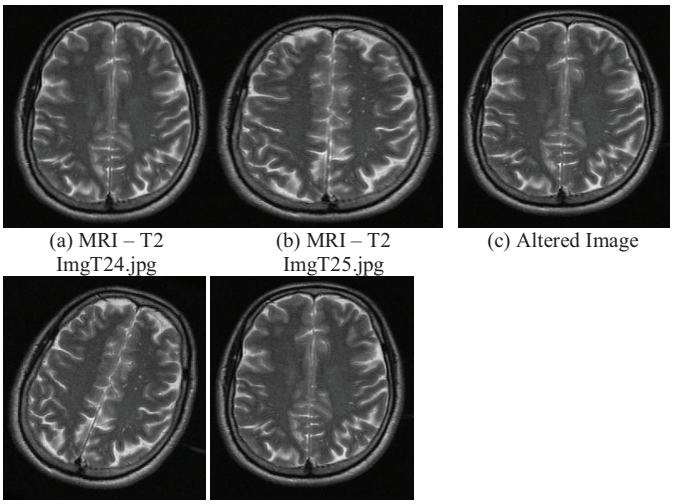

(a) MRI – T2 ImgT24.jpg | (b) MRI – T2 ImgT25.jpg | (c) Altered Image

(d) Angle (theta) change in transformation = 18 degrees | (e) Registered Image using Contourlet Transform

Figure 12. Registration using Wavelet Transforms for 18 degrees

E-ISSN 2581 – 7957
P-ISSN 2277 – 3916

DOI: 10.32377/cvrjst1707

From Figure 12. ImgT24.jpg and ImgT25.jpg, both after having the same modality MRI-T2 are registered using Wavelet Transforms with 18 degrees rotation to get the following output. Mutual Information = 1.4051, Correlation Coefficient =0.8640 and Computation Time = 4.9780

From Figure 13. the above-mentioned images are registered using Contourlet Transforms with18 degrees rotation to get the output given below. Mutual Information = 1.3680, Correlation Coefficient = 0.8646 and Computation Time = 7.0196.

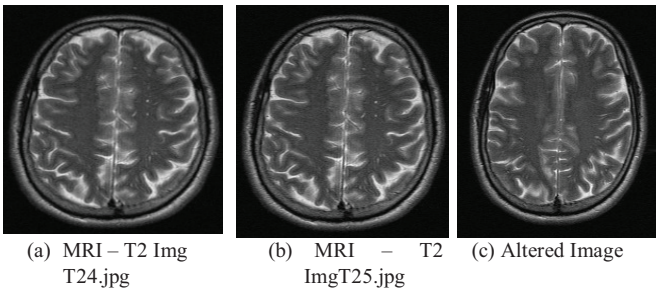

(a) MRI – T2 Img T24.jpg | (b) MRI – T2 ImgT25.jpg | (c) Altered Image

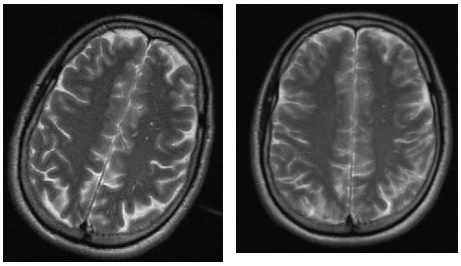

(d) Angle (theta) change in transformation = 18 degrees | (e)Registered Image using Contourlet Transform

Figure 13. Registration using Contourlet Transforms for 18 degrees

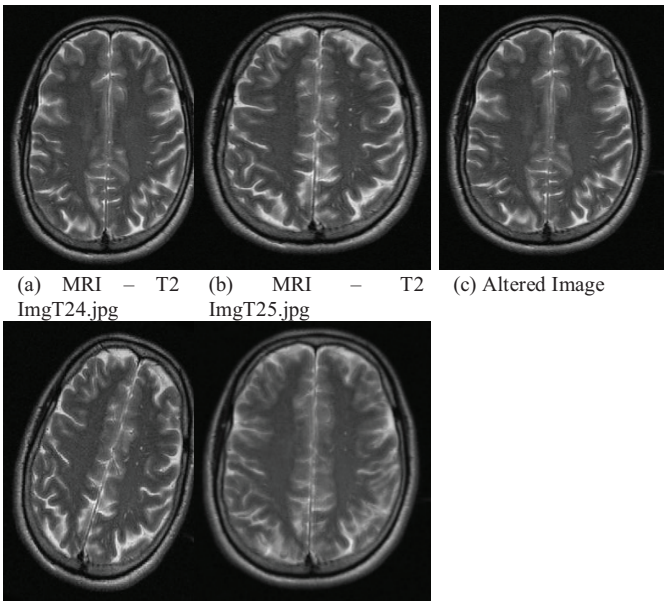

(a) MRI – T2 ImgT24.jpg | (b) MRI – T2 ImgT25.jpg | (c) Altered Image

(d) Angle (theta) change in transformation= 18 degrees | (e)Registered Image using Contourlet Transform

Figure 14. Registration using Evolve Contourlet Transforms for 18 degrees

From Figure 14. the aforesaid images are registered using Evolve Contourlet Transforms with18 degrees rotation to obtain the output given as: Mutual Information = 1.5283, Correlation Coefficient =0.8711 and Computation Time = 6.7361.

From the Output I, though the computation time of the Evolve Contourlet Transform is a little high the MI and CC measures are high when compared to both registrations using Wavelet Transforms and Contourlet Transforms.

D. Output II

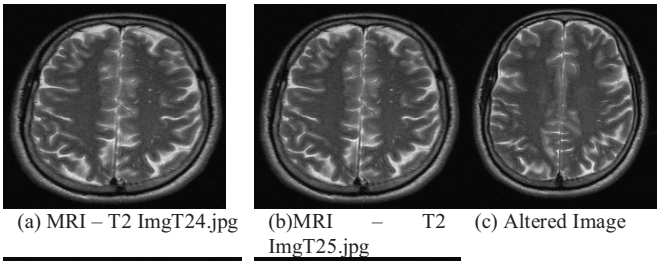

(a) MRI – T2 ImgT24.jpg | (b)MRI – T2 ImgT25.jpg | (c) Altered Image

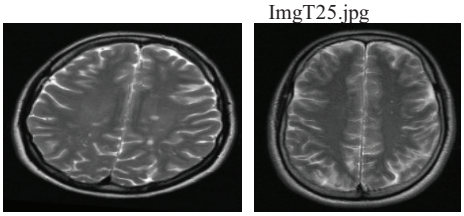

(d) Angle (theta) change in transformation = 7 degrees | (e)Registered Image using Contourlet Transform

Figure 15. Registration using Wavelet Transforms for 7 degrees

From Figure 15. the aforementioned images are registered using Evolve Contourlet Transforms with 7 degrees rotation to obtain the output given as: Mutual Information = 1.0647, Correlation Coefficient =0.6365 and Computation Time = 4.9513

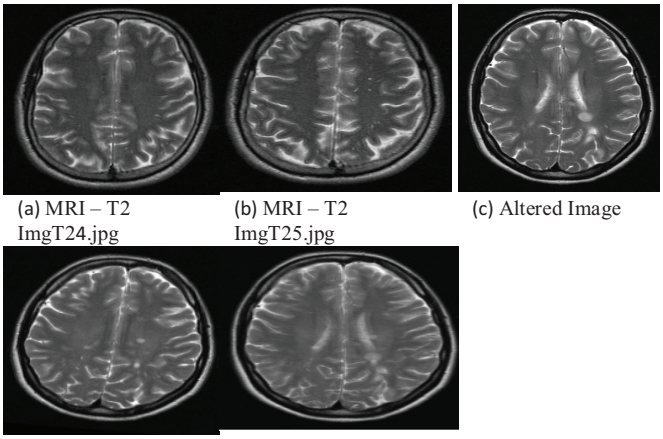

(a) MRI – T2 ImgT24.jpg | (b) MRI – T2 ImgT25.jpg | (c) Altered Image

(d) Angle (theta) change in transformation = 7 degrees | (e)Registered Image using Contourlet Transform

Figure 16. Registration using Contourlet Transforms for 7 degrees

From Figure 16. the said images are registered using Contourlet Transforms with 7 degrees rotation to obtain the output mentioned below as: Mutual Information = 1.0360, Correlation Coefficient =0.6379 and Computation Time = 5.9192.

E-ISSN 2581 – 7957
P-ISSN 2277 – 3916

DOI: 10.32377/cvrjst1707

From the Output II too despite the fact that the computation time of the Evolve Contourlet Transform is a little high but less than Contourlet Transform. The MI and CC measures are high too when compared to both the registrations using Wavelet Transforms and Contourlet Transforms.

Relating the consequences, it is evidenced that Evolve Contourlet Transform yields worthiest effects given away from amongst the three transforms.

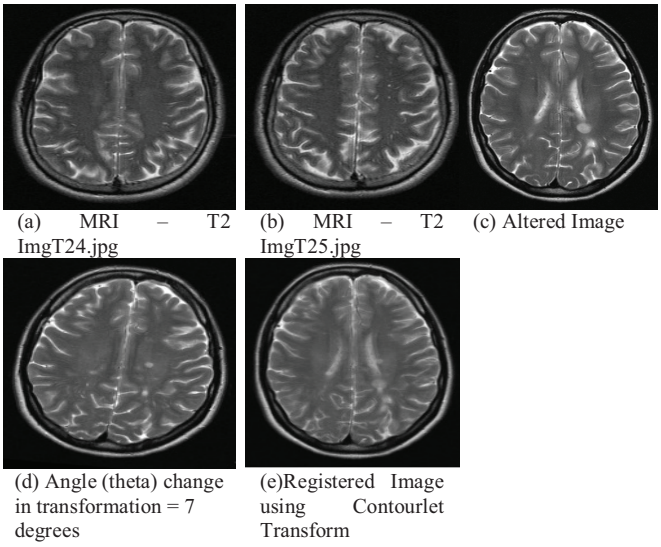

(a) MRI – T2 ImgT24.jpg (b) MRI – T2 ImgT25.jpg (c) Altered Image

(d) Angle (theta) change in transformation = 7 degrees (e)Registered Image using Contourlet Transform

Figure 17. Registration using Evolve Contourlet Transforms for 7 degrees

From Figure 17. the aforementioned images are registered using Evolve Contourlet Transforms with 7 degrees rotation to obtain the output given below as : Mutual Information = 1.6480, Correlation Coefficient = 0.8462 & Computation Time = 6.7157.

VII. Future Works and Conclusions

Rigid image registration using the existing wavelet transform - the conventional contourlet transform is performed. Furthermore, in this paper, a new algorithm for medical image registration, an Evolve Contourlet Transform is proposed. After performing the rigid image registration using contourlet transform, Evolve Contourlet Transform too was performed using MRI T2 images. The quality of the images obtained by these techniques was analyzed and verified using the Mutual Information and Correlation Coefficient measures. The experimental results were illustrated by the imageries. It proves that the applied Evolve Contourlet Transform is a better approach than the conventional contourlet transform for medical image registration. The future work is focused on the improvement on the results by using some other transforms or by further changes in the Evolve Contourlet Transform Algorithm. Correspondingly testing can be done by adding a few more metrics along with the Mutual Information and Correlation Coefficient.

References

[1] J. B. A. Maintz and M. A. Viergever, "A Survey of Medical Image Registration," Journal of Medical Image Analysis, vol. 2, no. 1, pp 1-36, 1998.

[2] J. L. Moigne, W. J. Campbell and R. F. Cromp, "An Automated Parallel Image Registration Technique Based on the Correlation of Wavelet Features," IEEE Transactions on Geoscience and Remote Sensing, vol. 40, no. 8, pp. 1849-1864, Aug 2002.

[3] Abhinav Kumar and Dr Anand Mohan, “Review of Image Registration Techniques”, Journal of Emerging Technologies and Innovative Research (JETIR), vol. 6, no. 4, pp. 24-27, April 2019.

[4] F. Zana, J.C. Klein, “A multimodal registration algorithm of eye fundus images using vessels detection and Hough transform”, IEEE Transactions on Medical Imaging, vol. 18, no.5, pp. 419-428, May 1999.

[5] E. De Castro, C. Morandi, “Registration of Translated and Rotated Images Using Finite Fourier Transforms”, IEEE Transactions on Pattern Analysis and Machine Intelligence, vol. PAMI-9, no. 5, pp. 700-703, Sept 1987.

[6] Sasikala D, and Neelaveni R, “An Analysis of Brain Images using Fast Walsh Hadamard Transform”, International Journal of Computer Applications (IJCA), 2011, Vol.13, No.1, pp 23-29.

[7] Sasikala D, and Neelaveni R, “Correlation Coefficient for Registration of Monomodal Brain Images using Fast Walsh Hadamard Transform”, Proceedings of IEEE International Conference on Communication, Control and Computing Technologies (ICCCCT 2010), Syed Ammal Engineering College, Ramanathapuram, Tamilnadu, India, 7th -9thOctober, 2010.

[8] Sasikala D, and Neelaveni R, “Performance Analysis of Brain Image Registration Technique using Fast Walsh Hadamard Transform and Modified Adaptive Polar Transform”, Journal of Scientific and Industrial Research (JSIR), 2011, Vol 70, No.2, pp 123-128.

[9] Xiaolong Dai and S. Khorram, “A Feature-based Image Registration Algorithm using Improved Chain-code Representation Combined with Invariant Moments”, IEEE Transactions on Geoscience and Remote Sensing, vol. 37, no. 5, pp. 2351-2362, Sept 1999.

[10] Sahil Suri, Peter Schwind, Peter Reinartz and Johannes Uhl, “Combining Mutual Information and Scale Invariant Feature Transform for Fast and Robust Multisensor SAR Image Registration”,75th Annual American Society for Photogrammetry and Remote Sensing ASPRS Conference, March 9-13, Baltimore, Maryland, 2009.

[11] H. S. Stone, J. L. Moigne, and M. McGuire, "The Translation Sensitivity of Wavelet-based Registration”, IEEE Transactions on Pattern Analysis and Machine Intelligence, vol. 21, pp. 1074-1081, Oct. 1999.

[12] A. Antoniadis, G. Oppenheim, *"Translation-Invariant De-noising in Wavelets and Statistics”*, New York: Springer-Verlag, 1999.

[13] Sasikala D, and Neelaveni R, “Image Registration using Modified Adaptive Polar Transform”, Procedia Computer Science, Elsevier, ScienceDirect, vol. 2, pp. 321-329, September 2010.

[14] Sasikala D, and Neelaveni R, “Brain Image Registration Techniques using Wang Landau Adaptive Monte Carlo Approach”, Journal of Scientific and Industrial Research (JSIR), 2013, Vol 72, No.2, pp 114-121.

[15] Ruhina B. Karani and Tanuja K. Sarode, “Image Registration using Discrete Cosine Transform and Normalized Cross Correlation”, Proceedings on International Conference and

workshop on Emerging Trends in Technology (ICWET 2012), Thakur College of Engineering & Technology, Mumbai, India, Feb 24-25, 2012, International Journal of Computers Applications, no.2, 2012.

[16] W. Pratt, *Digital Image Processing*, New York: Wiley, 2010.

[17] Zilnva B, Flesser J. "Image Registration Methods a Survey", Journal of Image and Vision Compute, vol.21, no.1 1, pp-977-1000, 2003.

[18] A. Aldroubi, M. Unser, "*Wavelets in Medicine and Biology*", CRC Press, Taylor and Francis Group, 1996.

[19] S. C. Strother, J. R. Anderson, X. Xu, J. Liow, D. C. Bonar, and D. A. Rottenberg, "Quantitative Comparisons of Image Registration Techniques Based on High Resolution MRI of the Brain. Journal of Computer Assisted Tomography, vol. 18, no. 6, pp 954–962, 1994.

[20] A. Cohen, C. Rabut, L. L. Schumaker, "Curvelets: A Surprisingly Effective Nonadaptive Representation for Objects with Edges in Curve and Surface Fitting", TN, Nashville: Vanderbilt Univ. Press, 1999.

[21] E. J. Candès, D. L. Donoho, " New Tight Frames of Curvelets and Optimal Representations of Objects with Piecewise C2 Singularities ", Communications on Pure and Applied Mathematics, pp. 219-266, Feb. 2004.

[22] I. Daubechies, *"Ten Lectures on Wavelets*, PA, Philadelphia: SIAM, 1992.

[23] Pavithra C and Dr. S. Bhargavi, "Fusion of Two Images Based on Wavelet Transform", International Journal of Innovative Research in Science, Engineering and Technology, vol. 2, no. 5, pp. 1814-1819, May 2013.

[24] M. Antonini, M. Barlaud, P. Mathieu, I. Daubechies, "Image Coding using Wavelet Transform", IEEE Transactions on Image Processing., vol. 1, pp. 205-220, Feb. 1992.

[25] I. Zavorin and J. L. Moigne, "Use of Multiresolution Wavelet Feature Pyramids for Automatic Registration of Multisensor Imagery, IEEE Transactions on Image Processing, vol. 14, no. 6, pp. 770-782, June 2005.

[26] K. Bowyer, C. Kranenburg, S. Dougherty, "Edge Detector Evaluation using Empirical ROC Curves", Journal of Computer Vision and Image Understanding, vol. 84, no. 1, pp. 77-103, 2001.

[27] A. Cohen, B. Matei, "Compact Representation of Images by Edge Adapted Multiscale Transforms", IEEE International Conference on Image Processing, Thessaloniki, Greece, 7-10 Oct 2001.

[28] B. N. Kingsbury, "Image Processing with Complex Wavelets", *Philosophical Transactions* of Royal Society London, pp. 2543-2560, Sep 1999.

[29] L. da. Cunha, Jianping Zhou and Minh N. Do, "The Nonsubsampled Contourlet Transform: Theory, Design, and Applications", IEEE Transactions on Image Processing, vol. 15, no. 10, pp. 3089-3101, 2006.

[30] M. N. Do and M. Vetterli, *"Contourlets, in Beyond Wavelets"*, J. Stoeckler and G. V. Welland, (Eds), San Diego, CA: Academic Press, New York, 2003.

[31] Xiangyu Yu, Lihua Guo. "Image Registration by Contour Matching using Tangent Angle Histogram", IEEE Congress on Image and Signal Processing, Sanya, Hainan, China, 27-30 May 2008.

[32] P. A. Vanden Elsen, E. J. D. Pol, and M. A. Viergever, "Medical Image Matching– a Review with Classification". IEEE Engineering in medicine and biology, vol.12, no.1, pp 26–39, 1993.

[33] D. Vandermeulen. "Methods for Registration, Interpolation and Interpretation of Three-Dimensional Medical Image Data for Use in 3-D Display, 3-D Modelling and Therapy Planning", PhD thesis, University of Leuven, Belgium, 1991.

[34] ÜloLepik, and Helle Hein, "Application of the Haar wavelet method for solution the problems of mathematical calculus", Review article in Waves Wavelets Fractals Advanced Analysis, DE GRUYTER Open Access, vol. 1, pp. 1-16, January 2015.

[35] Zhi Qu, Yaqiong Xing and Yafei Song, "An Image Enhancement Method Based on Non-Subsampled Shearlet Transform and Directional Information Measurement", Information (Switzerland), vol. 9, 308, no. 12, pp. 1-15, December 2018.

[36] E.P. Simoncelli, W.T. freeman, E.H. Adelson, and D.J. Heeger, "Shiftable Multiscale Transforms", IEEE Transactions on Information Theory, vol. 38, no.2, pp. 587-607, March 1992.

[37] J. P. Zhou, et al., "Nonsubsampled Contourlet Transform: Construction and Application in Enhancement", IEEE International Conference on Image Processing, ICIP2005, Genoa, Italy, 1, 2005, pp. 469-472.

[38] O. Bottema& B. Roth,."*Theoretical Kinematics"*. Dover Publications. Reface. ISBN 0-486-66346-9, 1990.

E-ISSN 2581 – 7957
P-ISSN 2277 – 3916

CVR Journal of Science and Technology, Volume 17, December 2019
DOI: 10.32377/cvrjst1708

Semi-circular Slotted Monopole Antenna for Future Ultra-Wideband Applications

Srikanth Itapu
Asst. Professor, CVR College of Engineering/ ECE Department, Hyderabad, India
Email: sri.hydblues@cvr.ac.in

***Abstract*: Semi-circular slotted monopole antennae are investigated for IoT based ultra-wideband (UWB) applications. The studied antennae are compact and of small size (40mm x 30mm x 1.53mm) with a 50Ω co-planar waveguide (CPW) - feed line. The conventional circular disc monopole antenna impedance bandwidth is improved by introducing multiple cuts on the circular disc. Three designs are examined and compared to the classical circular monopole design: iteration 1, iteration 2 and the proposed antenna with nine semi-circular rings. The proposed antenna offers the measured impedance bandwidth from 3.5 GHz to 60 GHz and beyond, which is comparatively 6 times of normally achieved by conventional antenna. The measured radiation patterns of semi-circular rings antenna are presented in both H- and E-plane.**

***Index Terms*: Microstrip antenna, Monopole antenna, CPW-feed, UWB system.**

I. Introduction

Ultra-wideband (UWB) communication systems have the advantages of low power consumption, high-speed data rate etc [1]. UWB components such as printed microstrip antennas are proved to be a great choice for present day IoT systems due to small size, low cost, and ease of fabrication and integration in microwave circuits [2]. With Co-Planar Waveguide (CPW)- feed, parameters such as broader frequency bandwidth, greater impedance matching, minimal loss in radiation, and lower dispersion [3-4] are achieved. Over the past few years, CPW-feed UWB antenna designs [5-6] have gained a lot of attention and reported in the literature but significantly differ primarily by the conductor and the ground plane configuration and shapes.

In [7], the CPW-feed UWB antenna proposed is based on circular disc conductor, and a partial rectangular ground plane. The antenna in [8] consists of a step-typed monopole conductor with a step-slope ground plane. In [9], the antenna is designed as an open annulus strip as ground plane and an open crescent patch in the inner space of the annulus as a radiating element. In [10], the authors introduce annular slot and round corners into the ground and use a round- edged bowtie-shaped conductor. All these antennas predominantly offered an impedance bandwidth of upto 11 GHz, which satisfies the present FCC UWB requirement. For future UWB system at higher frequency beyond 11 GHz [11], there is a necessity of an ultra-compact antenna which can cover present as well as future UWB systems. From [12-14], it is evident that the antenna structure offers wide bandwidth performance.

In this paper, we present the UWB antenna with nine cuts in circular disc. The study is primarily aimed to extend the upper limit of the FCC standard to a higher level for future UWB applications. Fractal geometry has been incorporated for this use. The basic circular monopole design is compared with a fractal structure of five concentric semi-circular cuts of 0.2 mm width with an increment in the radius by 1.0 mm from 1.0 mm to 5.0 mm and another fractal structure of nine semi-circular cuts of 0.2 mm with an increment in the radius by 1.0 mm from 1.0 mm to 9.0 mm as shown in Fig. 1. The dimensions of the antennae are 40.0 mm x 30.0 mm on substrate thickness of 1.53 mm and dielectric constant (FR-4 substrate) ε_r=4.3.

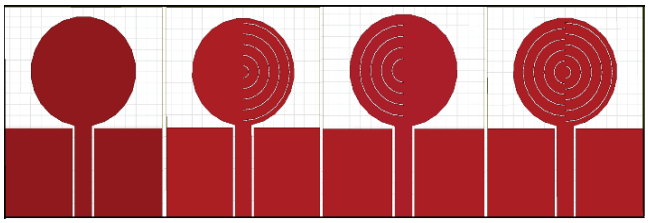

(a) (b) (c) (d)

Figure 1. Geometry of three antenna design.

II. Antenna Geometry

The proposed antenna design with concentric circular rings is derived from the classical monopole design. Fig. 1(a) is purely a circular monopole antenna with rectangular ground plane. In Fig. 1(b), semi-circular rings are incorporated with five cuts each of thickness 0.2 mm subsequent radii ranging from 1.0 mm to 5.0 mm (Iteration 1). In Fig. 1(c), four semi-circular rings with radii ranging from 1 mm to 4 mm are incorporated (Iteration 2). Such concentric turns increase the magnetic confinement of the microwave signal [15] from the source through the SMA connector. Finally, the proposed antenna design is presented in Fig. 1(d), which is a culmination of both the iterations 1 and 2.

III. Critical Design Parameters

The three designs have been simulated. The simulation results are shown in Fig. 2. It is observed from Figure 2, that the first resonance occurs at 3.5 GHz for the circular monopole, and at 3.2 GHz for both the iterative structures (i.e iteration 1 and 2). The return loss of the all four designs are compared upto 60 GHz range. It is evident that the effect of fractal geometry comes into picture for enhancing the upper frequency limit with design 2 and design 3 respectively. This

E-ISSN 2581 – 7957
P-ISSN 2277 – 3916

CVR Journal of Science and Technology, Volume 17, December 2019
DOI: 10.32377/cvrjst1708

is because each semi-circular cut adds up to the resonance frequencies, thus extending the spectrum. The asymmetrical cuts effect the higher frequency side by adding up each of the resonance frequencies resulting out of each cut. Hence, the upper limit of the spectrum is increased to 60 GHz.

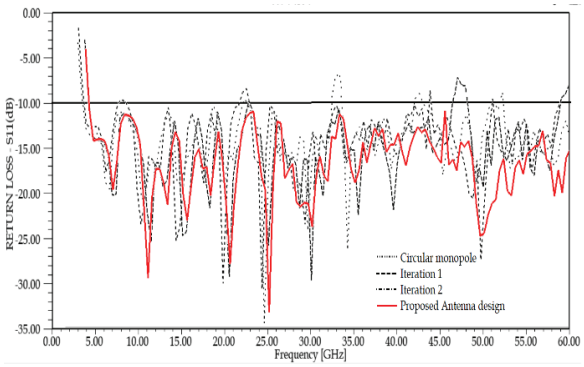

Figure 2. Simulated return loss of three antenna designs.

The proposed antenna was fabricated and the return loss was measured using a Rohde & Schwarz Vector Network Analyser with a frequency range from 100 MHz to 60 GHz. The photograph of this antenna is shown in Fig. 3. The experimental results are shown in Fig. 4 and shows a good correlation to the simulated data.

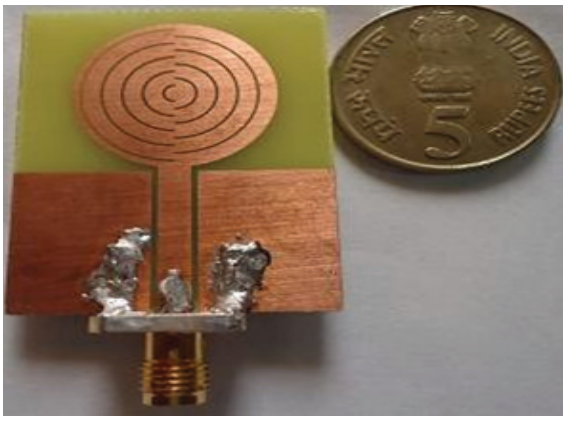

Figure 3. Photograph of fabricated antenna.

The measured impedance bandwidth of this antenna is achieved from 3.5 GHz to 40 GHz beyond the required. There is deviation of the measured and simulated results. This is because of Low quality of SMA connector used as well as fabrication constraints, uncertainty in dielectric constant, thickness of the substrate. The SMA connector has not been considered during simulation. This is because of computational time taken by HFSS software. Also, for the convenience and repetition of the measured data, we have taken enough care to present the experimental retune loss by measuring it randomly at two different times.

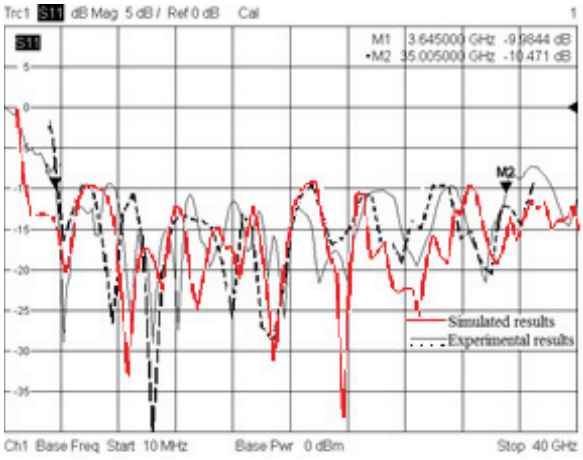

Figure 4. Measured and Simulated results of antenna with nine cut antenna.

IV. Current Distribution

The current distributions of all the four antenna designs – circular monopole, iteration 1, iteration 2 and the final proposed antenna are presented in this section at the frequencies 15GHz, 30GHz, 45GHz and 60GHz shown in Fig. 5 to 8.

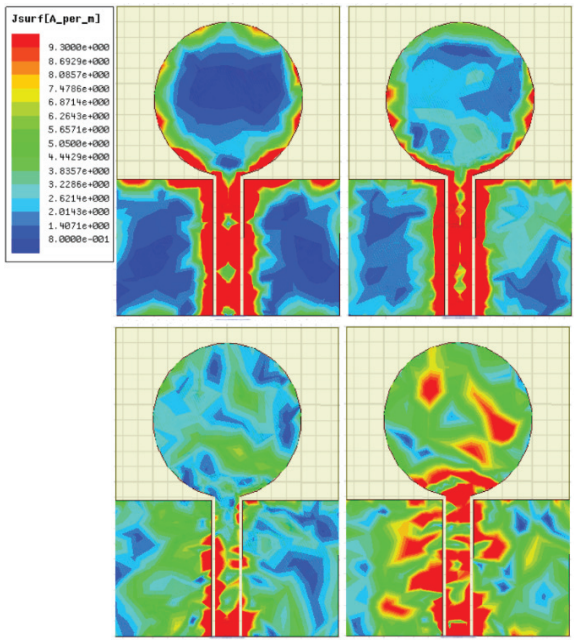

Figure 5. Current distributions of classical monopole at 15GHz, 30GHz,45GHz, and 60GHz.

For the circular monopole, three minima can be observed at 15.0 GHz which corresponds to the first three resonance frequencies of the design. The first minima (means first resonant frequency) indicates resonance mode which can be seen by current maxima over the feed line and ground plane. As the frequency is increased, the resonances merge and it becomes impossible to distinguish between number of

E-ISSN 2581 – 7957
P-ISSN 2277 – 3916

CVR Journal of Science and Technology, Volume 17, December 2019
DOI: 10.32377/cvrjst1708

minima. The current is symmetrically distributed from the feedline through the circumference of the circular patch at frequencies 15.0 GHz, 30.0 GHz, 45.0 GHz and 60 GHz. Increase in the frequency results increase in current distribution in the ground plane. It is because of the increase in the minima that the power flow to the circular patch is minimized.

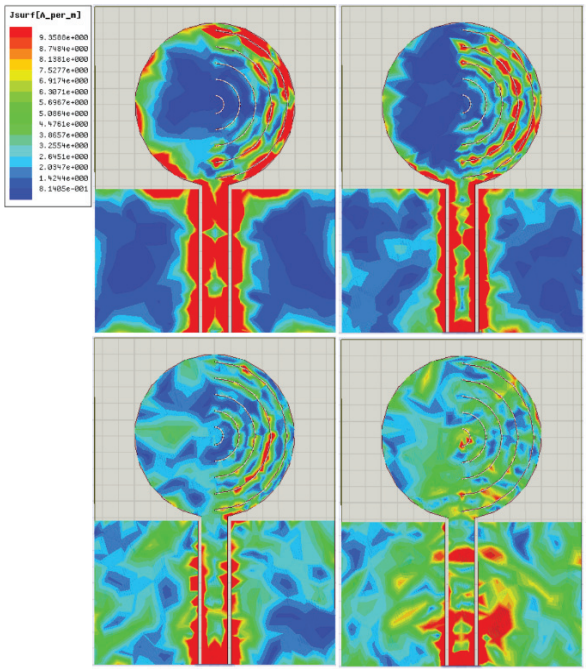

Figure 6. Current distributions of Iteration 1 design at 15GHz, 30GHz, 45GHz, and 60GHz.

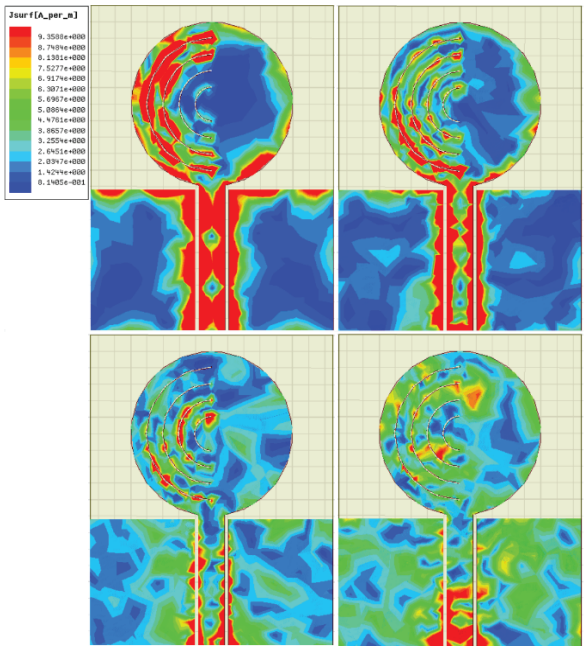

Figure 7. Current distributions of Iteration 2 design at 15GHz, 30GHz, 45GHz, and 60GHz.

For the Iterative designs 1 and 2 (Fig. 6 and 7), the first two minima can be observed at 15.0 GHz which corresponds to the first resonance frequency of the design. The current is symmetrically distributed from the feedline through the circumference of the circular patch and along the fractal cuts at frequencies 15.0 GHz, 30.0 GHz, 45.0 GHz and 60.0 GHz. The asymmetrical cuts effect the higher frequency side by adding up each of the resonance frequencies resulting out of each cut. Hence, the upper limit of the spectrum is increased to 45.0 GHz for design 2 and 63.5 GHz for design 3.

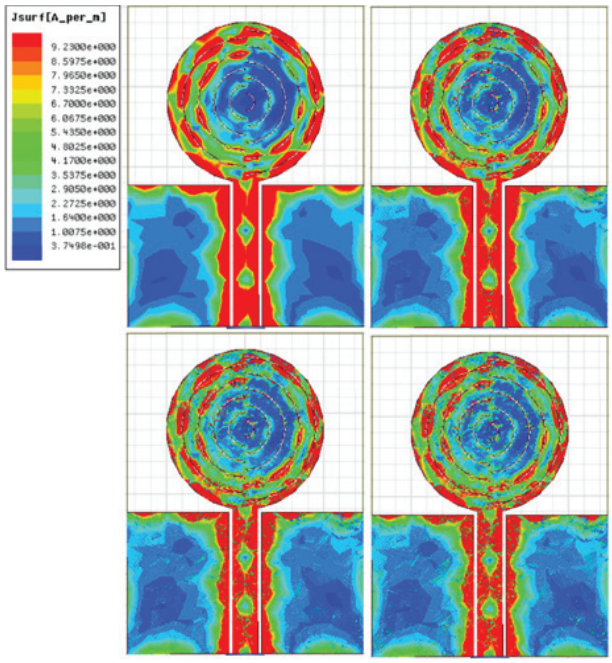

Figure 8. Current distributions of nine cuts at 15GHz, 30 GHz, 45GHz, and 60GHz.

From Fig. 8, it is evident that the circular rings indeed effect and influence the current distribution (seen in red at the edges of the rings in Fig. 8). This current accumulation results in a smooth impedance bandwidth ranging from 3.5 GHz to 60 GHz.

V. Measured Radiation Patterns

The E- plane and H-plane radiation patterns of proposed antenna have been measured at selective frequencies shown in Fig. 9 and 10. The E-plane radiations are measured in anechoic chamber at 5GHz, 10GHz, 20GHz, 30GHz, 40GHz, 50GHz, 60GHz. The E -plane radiation patterns throughout the band are bidirectional as shown in Fig. 9. Similarly, H - plane radiation patterns are also measured at various frequencies like 3.5GHz, 4.5GHz, 6GHz, 8GHz, 11GHz and 18GHz as shown in Fig. 10. The nature of H-plane patterns is nearly omni-directional. It is also observed, as the frequency increases, the radiation patterns are slightly deteriorated. It may be because of the edge reflections, FR4 lossy substrate and fractal nature of antenna and generation of higher mode at higher frequencies.

E-ISSN 2581 – 7957
P-ISSN 2277 – 3916

CVR Journal of Science and Technology, Volume 17, December 2019
DOI: 10.32377/cvrjst1708

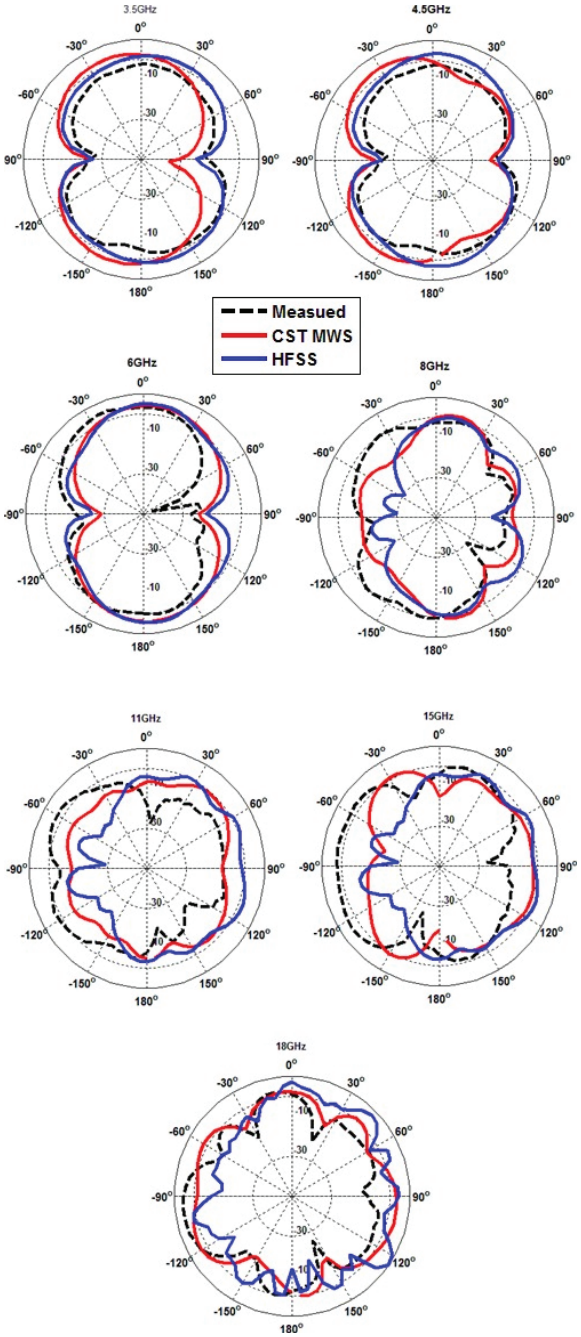

Figure 9. Measured E-plane Radiation patterns at 5, 10, 20, 30, 40, 50 and 60 GHz frequencies.

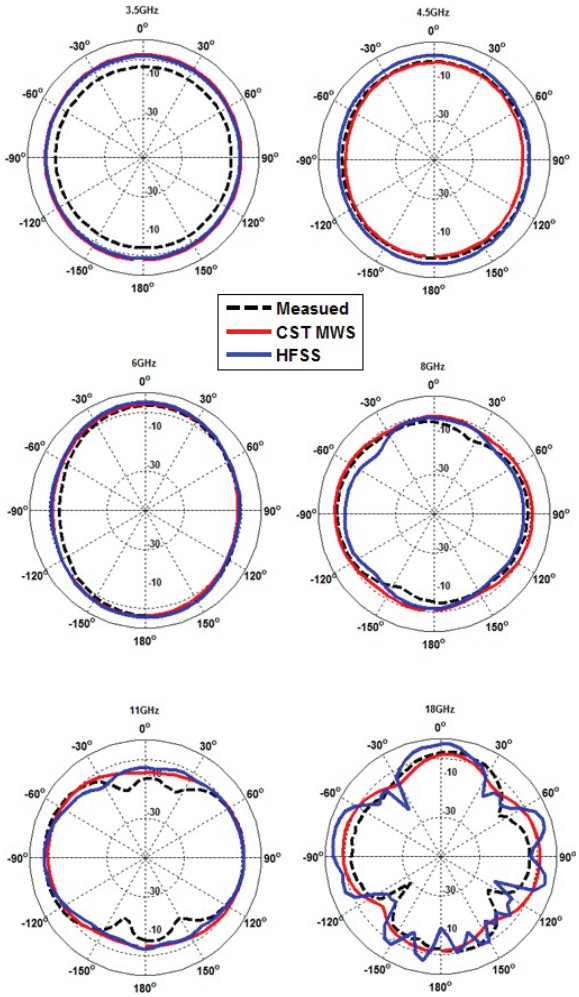

Figure 10. Measured H-plane Radiation patterns at 10, 20, 30, 40, 50 and 60 GHz frequencies.

VI. Peak Gain and Radiation Efficiency

The peak gain of the proposed antenna has been measured and compared with simulated gain using HFSS and CST MWS. The peak gain was measured upto 18 GHz because of limitation of availability of reference antenna. A good agreement found between measured and simulated peak gain as shown in Fig. 11. It is noticed from the measured and simulated results, as the frequency increases, the peak gain increases. This is because, at higher frequencies, the receiving area becomes more in comparison to short wavelength. The radiation efficiency of the proposed antenna has also been simulated using HFSS and CST MWS and compared as shown in Fig. 12. From Fig. 12, it is noticed that the radiation efficiency decreases with increase in frequency. This is because of loss increase with

CVR Journal of Science and Technology, Volume 17, December 2019
DOI: 10.32377/cvrjst1708

frequency increase due to high loss tangent of substrate used. It is noticed from Fig. 11 and 12, there is a little difference between the gain and radiation efficiency simulated using HFSS and CST MWS. This difference is because of different numerical techniques used in commercial software.

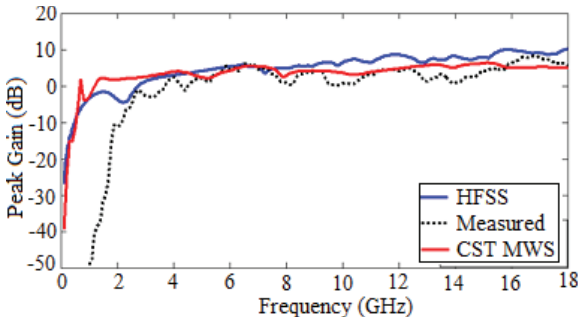

Figure 11. Simulated and measured gain.

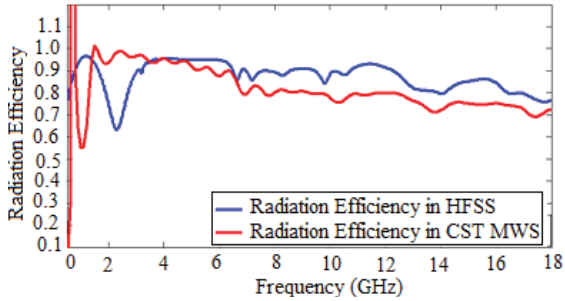

Figure 12. Simulated Radiation Efficiency of the proposed antenna.

VII. Conclusions

A compact UWB antenna with semi-circular ring structures with CPW feed have been designed and experimentally validated for ultra-wideband frequency from 3.5GHz to 60GHz. The measured radiation patterns of this antenna with circular rings are omni- directional in H-plane and bidirectional in E- plane. This antenna is simple to design, easy to fabricate, compact in size and easy to integrate with MIC/MMICs devices. Such an antenna can be used for future UWB applications, smart IoT applications and medical imaging.

References

[1] First Report and Order, “Revision of Part 15 of the Commission’s Rule Regarding Ultra-Wideband Transmission System FCC02–48,”*Federal Communications Commission,* 2002.

[2] C.A. Balanis, *Antenna Theory, Analysis and Design*, Wiley, Hoboken, USA, 2005.

[3] D.-C. Chang, B.-H. Zeng, and J.-C. Liu, "CPW- fed circular fractal slot antenna design for dual- band applications", *IEEE Trans. Antennas Propag.*, Vol. 56, No. 12, pp. 3630- 3636, Dec.2008.

[4] A. U. Bhobe, C. L. Holloway, M. Piket-May, and R. Hall, "Wide-band slot antennas with CPW feed lines: hybrid and log-periodic designs", *IEEE Trans. Antennas Propag.,* Vol. 52, No. 10, pp. 2545-2554, Oct. 2004.

[5] I. Srikanth and Raj Kumar, “On the design of apollonian packing fractal antenna for UWB applications”, Microwaves & RF, 2012.

[6] Raj Kumar and I. Srikanth, “Design of apollonian gasket ultrawideband antenna with modified plane”, Microwave and Optical Tech. Lett., vol. 54, no. 8, 2012.

[7] J. Liang, L. Guo, C.C. Chiau, X. Chen and C.G. Parini, “Study of CPW-fed circular disk monopole antenna for ultra-wideband applications”, *IEE Proc. Microwaves, Antennas & Propag.,* Vol. 152, No. 6, pp. 520-526, Dec. 2005.

[8] J.-Y. Jan, J.-C. Kao, Y.-T. Cheng, W.-S. Chen, and H. M.Chen, "CPW-fed wideband printed planar monopole antenna for ultra-wideband operation", *Proc. 2006 IEEE AP-S International Symposium and URSI National Radio Science Meeting,* Albuquerque, New Mexico, pp. 1697-1700, 9-14 July 2006

[9] M.-E. Chen and J.-H. Wang, "CPW-fed crescent patch antenna for UWB applications", *Electronics Letters*, Vol. 44, No 10, pp. 613-614, May 2008.

[10] L. Zhao, C.-L. Ruan, and S.-W. Qu, "A novel broadband slot antenna fed by CPW", *Proc. 2006 IEEE AP-S International Symposium and URSI National Radio Science Meeting*, Albuquerque, New Mexico, pp.2583-2586,9-14 July 2006.

[11] M. N. Srifi, S. k. Podilchak and Yahia M. m. Antar” Compact Disc monopole antennas for current and future ultrawideband (UWB) applications*”,IEEE Trans. on antennas and propagation*, vol. 59, No. 12, Dec. 2011, pp. 4470-4480.

[12] S. Tripathi, A. Mohan and S. Yadav, “A Compact Koch Fractal UWB MIMO Antenna with WLAN Band-Rejection”, *IEEE Trans. Antennas & Prop.*, Vol. 14, pp. 1565-68, Aug. 2015.

[13] A. Amini, H. Oraizi and M.A.C. Zadeh, “Miniaturized UWB Log-Periodic Square Fractal Antenna”, *IEEE Trans. Antennas & Prop.*, Vol. 14, pp. 1322-25, Mar. 2015.

[14] T. Ali, B.K. Subhash and R.C. Biradar, “A Miniaturized Decagonal Sierpinski UWB Fractal Antenna”, *PIERS C*, vol. 84, pp. 161-174, 2018.

[15] S. Itapu, D.G. Georgiev and V. Devabhaktuni, “Improvement in inductance and Q-factor by laser microstructuring of ferromagnetic on-chip thin film inductors*”, J. of Elec.Mag. Waves and Appl.*, vol. 29, no. 12, pp. 1547-1556, 2015.

E-ISSN 2581 – 7957
P-ISSN 2277 – 3916

CVR Journal of Science and Technology, Volume 17, December 2019
DOI: 10.32377/cvrjst1709

Experimental Verification of Object Detection using X-Band Radar

Amit Arora
Assoc. Professor, CVR College of Engineering/ECE Department, Hyderabad, India
Email: amit06arora@gmail.com

Abstract: **In this paper, experimental setup for object detection using continuous wave X-band radar (Radio Detection and Ranging) is presented. Detection of object in free space through the radar system at X-band is verified. It is observed that as the size of the object (target) is increased, the received echo will be more such that the received signal strength is high. Furthermore, as the distance between the radar and the target is increased, the received signal strength is low.**

Index Terms: **Detection, EM wave, horn antenna, microwave, radar, X-band**

I. Introduction

Radar is an electromagnetic (EM) system equipped with microwave sensor (antenna) for the detection and location of objects present on the ground, in the space, underground and undersea in situations like darkness, haze, fog, rain and snow. The range to the target is calculated from the relation,

$$R = cT_R / 2 \quad (1)$$

where c is the speed of light ($3x10^8$ m/s) and T_R is the time the radar signal takes to travel to the target and back. It is possible to obtain the range of information using continuous wave (CW) radar by modulating the carrier with frequency or phase. Depending on the application several types of radars are available. Long range ground-to-air and air-to-ground missiles employ the bistatic radar, where radar transmitter and receiver are in two separate locations. For better immunity from the interference by large, stationary / slow moving objects continuous wave radar is preferred [1]. To determine the velocity of moving object Doppler radar is utilized.

Monopulse radar is designed such that it compares the incident signal with differently polarized reflected signals and is used for tracking the targets. To find out the probability of rain and atmospheric condition weather, radar is used. It works on Doppler shift to measure the speed of wind and precipitation in clouds. For geographical planning of smart city, dams and roads, mapping-radar is preferred. For avoiding the collision of ships and marine application, navigational-radar is used. Search radar searches if any object is present in its surrounding space. It has the knowledge of all the objects around it [2]. A tracking radar tracks a continuously a particular target and predicts its future position.

After receiving signals from objects, processing is needed to reduce the noise and increase the signal strength so that the signal is properly displayed on the screen. The display is another important part of radar like A-scope, B-scope, C-scope and widely used Plan Position Indicator (PPI) in which distance from the centre indicates a range, angle around the display represents the azimuth angle to the object.

II. Theory

A radar system has a transmitter and an antenna that radiated EM in desired directions. When these waves are intercepted by an object (metallic) they are usually reflected or scattered in various directions. The radar waves that are scattered back toward the transmitter (echo) are the desirable ones that make the radar work. Radar receivers are usually, but not always (bistatic), in the same location as that of the transmitter (monostatic) [3]. The weak absorption of radio waves (in the microwave frequency range) by the medium (air/atmosphere) through which it passes is what enables radar to detect objects at relatively long distances.

The maximum distance at which an object can be detected by the radar is,

$$R_{\max} = P_t A_e^2 \sigma / 4\pi\lambda 2 S_{\min} \quad (2)$$

where P_t is the transmitter power, A_e is receiver antenna aperture area, σ is radar cross section (size) of the target, λ is the wavelength of the signal and $S_{\min}$ is minimum detectable signal strength (sensitivity) [1].

The determination of the position and motion target size and shape of the target can be done by using different parameters of receiving a signal like echo time, antenna position, Doppler frequency shift, polarization, strength of the received signal etc. [4].

In practical radar applications the echoes are monitored continuously on an electronic display, such as an A-scope or B-scope or PPI [1]. As shown in figure 1, the A-scope, shows the amplitude of the echo versus range to the reflecting object. The B-scope provides a representation of space, with the vertical axis representing range of the reflecting object and the horizontal axis azimuth angle of the object. C-scope displays azimuth vs. elevation of the target. The spot is displayed indicating the direction of the target off the centerline axis of the radar, or more specifically the aircraft or weapon it is attached to. The PPI display provides display of the airspace around a radar site. The distance out from the center of the display indicates range, and the angle around the display is the azimuth to the target [1].

E-ISSN 2581 – 7957
P-ISSN 2277 – 3916

CVR Journal of Science and Technology, Volume 17, December 2019
DOI: 10.32377/cvrjst1709

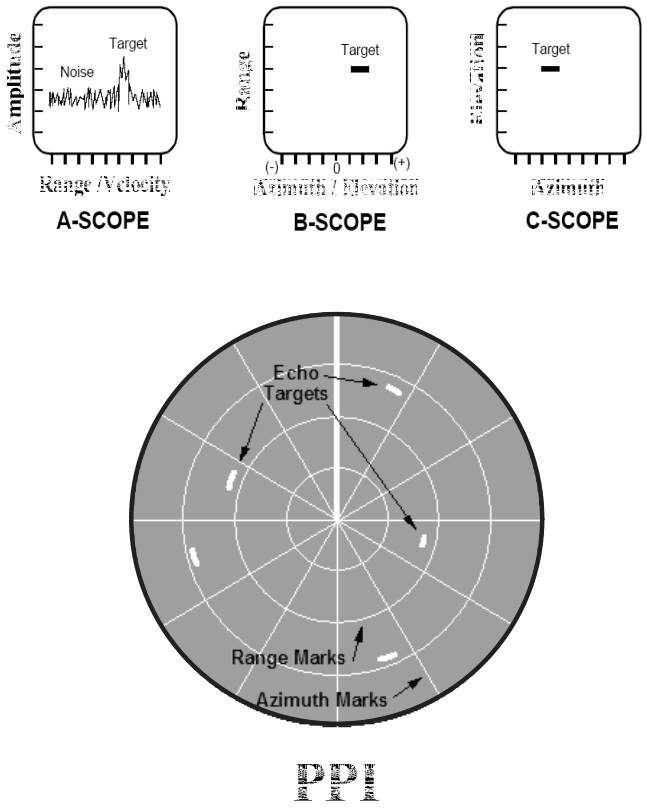

Figure 1. Standard radar displays.

III. Experimental Set Up

Components used in this experimental setup have high mechanical, electrical standards and tolerances. Waveguides are fabricated by drawing tubes of different cross sections of brass or copper plate with high extrusion quality. The specifications of X-band waveguide, frequency range 8.2-12.4 GHz, width 2.286 cm, height 1.2 cm and tolerance 7.6 μm.

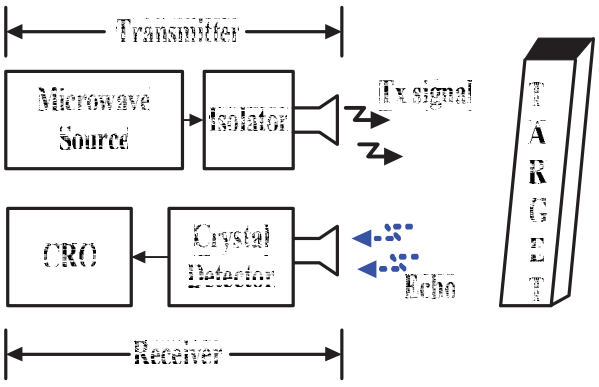

Figure 2. Experimental setup for object detection using cw X-band radar.

Figure 2 shows the block diagram of the experimental setup of X-band cw-radar including target. In the transmitter section main parts are microwave source, isolator and pyramidal horn antenna and in the receiver section pyramidal horn antenna, crystal detector and CRO.

IV. Description of Equipment

A. Microwave Source

Figure 3 shows the image of the reflex klystron tube. The reflex klystron tube oscillator has been used as microwave source. For proper working of microwave tubes, a reliable power source with very high regulation and low ripple contents is used. The klystron power supply also provides all the other d.c. voltages required for operation of the reflex klystron tube such as beam, heater anode and repeller voltages. The klystron power supply has built in modulation facilities of amplitude and frequency modulation.

Figure 3. Reflex Klystron tube.

The klystron tube is a single cavity variable frequency microwave generator of low power and low efficiency. Figure 4 shows the schematic diagram of reflex klystron tube [5]. It consists of an electron gun, a filament surrounded by cathode and a focusing electrode at a cathode potential.

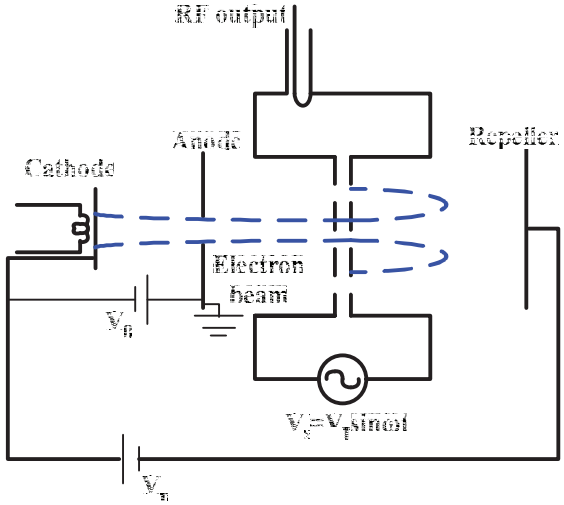

Figure 4. Schematic diagram of Reflex klystron.

Electrons are emitted from the cathode material (by heating the cathode), focused by a focusing electrode, accelerated by applying a positive potential to the

E-ISSN 2581 – 7957
P-ISSN 2277 – 3916

CVR Journal of Science and Technology, Volume 17, December 2019
DOI: 10.32377/cvrjst1709

accelerated electrode. The electron beam enters the rf cavity, interacts with the rf signal (filtered noise) in the cavity proceeds further into the repeller space, and gets reflected by the repeller electrode, gives away its energy to the anode, and finally gets collected by the anode. A magnetic field of sufficient strength is applied along the length of the tube to avoid the de-bunching of the electrons in the beam. The mechanism of velocity modulation takes place in the reflex klystron tube, and converts the unmodulated dc electron beam into the modulated rf beam.

B. *Isolator*

As shown in Figure 5, it is a two port device which provides negligible (ideally zero) attenuation for transmission in one direction and maximum (ideally infinity) attenuation for transmission in the other direction. This device is essential to avoid the reflected power from the load to reach the microwave source, thereby avoiding damage to the source.

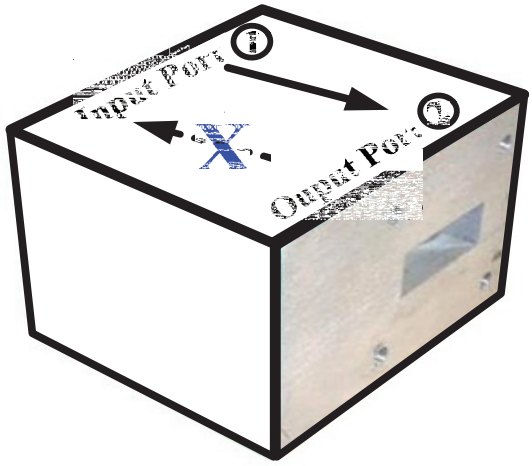

Figure 5. Isolator.

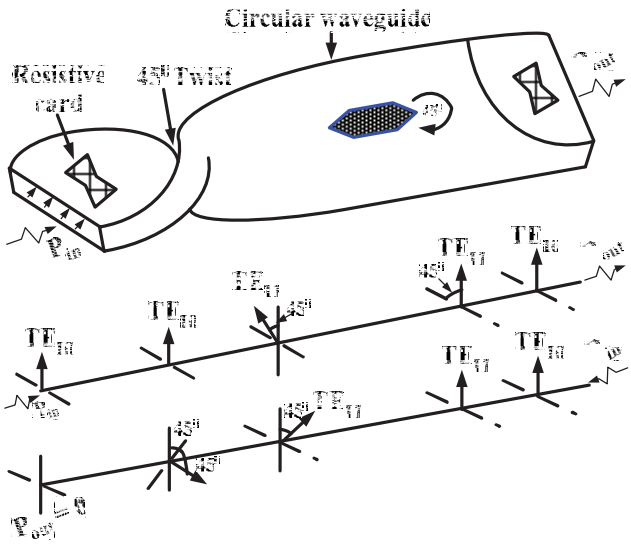

Figure 6. Working principle of Isolator.

Figure 6 depicts the working principle of isolator. An EM wave entering in the input port is perpendicular to the resistive card, hence passes through it unattenuated, but rotated 45° (CCW) due to the twist in the waveguide. As the signal progresses further the ferrite material ($MeO.Fe_2O_3$) along the path rotates the signal 45° CW. This result in cancelling each other's rotating effect, resulting in no change in orientation of the wave. Hence the signal is perpendicular to the resistive card at the output end, therefore unattenuated by it. The EM emerges from the output port without attenuation.

When an EM wave enters from the output port perpendicular to the resistive card, it is unattenuated by the resistive card, but rotated 45^0 CCW due to the ferrite material present along the path. It is further rotated 45^0 CCW due to the twist section of the waveguide resulting in a total twist of 90^0. The signal now becomes oriented parallel to the resistive card and hence completely attenuated by it.

C. *Pyramidal Horn Antenna*

The pyramidal horn antenna as shown in figure 7 is a combination of the E-plane and H-plane sectoral horns and as such is flared in both directions. Its parameters are,

$$\varphi_e = \tan^{-1} B_1 / 2L_E \quad (3)$$

and

$$\varphi_h = \tan^{-1} A_1 / 2L_H \quad (4)$$

where B_1, L_E is horn width and the slant height respectively in E-plane and A_1, L_H is horn width slant height respectively in H-plane [6]. For perfect pyramidal horn antenna both angles must be same.

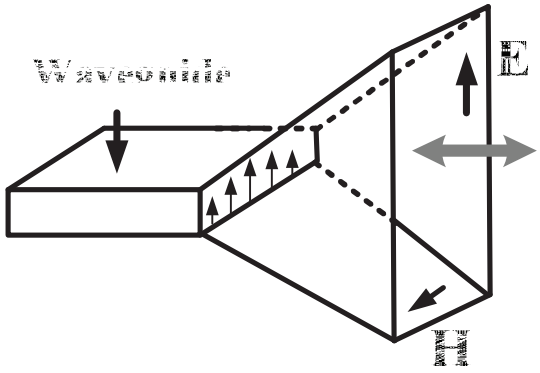

Figure 7. Pyramidal horn antenna.

An opened out waveguide also radiates, but its radiations are poor due to impedance mismatch between the waveguide and its surrounding medium (air/atmosphere). To improve impedance matching between the waveguide and the medium, the waveguide is flared out usually along its breadth and height. This becomes a pyramidal horn antenna. The flaring angle should be proportional to the axial length of the antenna so that the field at different points on the aperture of the horn is approximately in-phase. This is required to improve the directivity of the beam the horn. If the flare angle is small the resulting wave will be spherical instead of a plane wave.

E-ISSN 2581 – 7957
P-ISSN 2277 – 3916

DOI: 10.32377/cvrjst1709

The horn antenna possesses no resonant elements and therefore it is able to operate over a wide bandwidth.

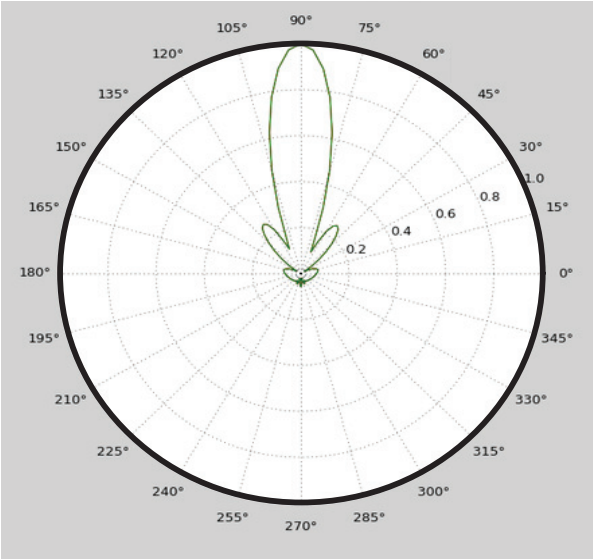

Figure 8. Radiation pattern of the horn antenna.

Figure 8 shows the typical radiation pattern of a horn antenna. It can be seen that it has a narrow beam width with negligible minor lobes. This type of antenna receives echo only from the desired object (target), and does not pick-up echoes from surrounding objects likes walls etc.

D. Crystal detector

Fixed detector (crystal detector) mount is simple and easy to use component for detecting microwave power. It consists of a detector crystal mounted in a section of a waveguide and shorting plunger for matching purposes. The output from the crystal may be fed to an indicating instrument. It is shown in figure 9.

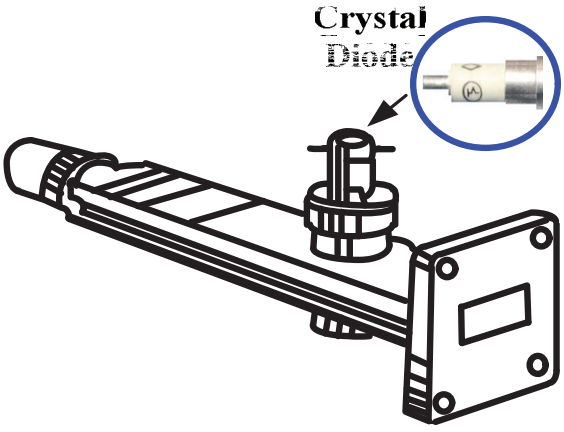

Figure 9. Fixed detector with crystal diode.

E. CRO

The oscilloscope observes the changes in the electrical signals over time, thus the voltage and time describe a shape and it is continuously graphed beside a scale. By seeing the waveform, we can analyze the properties like amplitude, frequency etc.

V. EXPERIMENTAL PROCEDURE AND RESULTS

Figure 10 shows the photograph of the setup used in the laboratory for carrying out this experiment. In the figure the target is on at the left side mounted on a stand. The radar system is placed on a bench on the right side in the photograph.

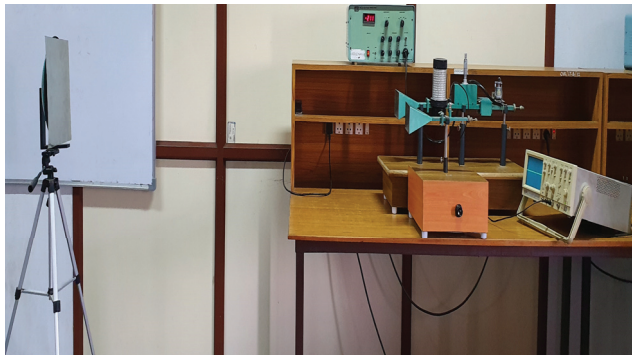

Figure 10. Photograph of experimental setup.

An Aluminum (Al) sheet of size 1ft x 1ft was placed at an initial distance of 1 foot in front of the radar system, and the received echo strength is measured. The distance of the sheet is gradually increased by 1 foot and the corresponding echo strength is measured. Later in the same procedure is repeated for the Al sheet of size 3ft x 3 ft.

TABLE I.
RECEIVED SIGNAL STRENGTH BY (1X1) FT. AND (3X3) FT OBJECT WITH DISTANCE

S. No.	Distance of object rom radar (feet)	Received voltage from (1*1) feet Al sheet (mV)	Received voltage from (3*3) feet Al sheet (mV)
1	1	12.2	26.4
2	2	8.0	25.2
3	3	5.6	13.4
4	4	3.4	4.4
5	5	2.2	3
6	6	1.11	2.6

Table 1 shows received signal strength with respect to distance for different size of Al sheet.

The variation of radar echoes strength as a function of distance is plotted in Figure 11. It can be seen that larger target results in a stronger echo as shown by the top line in the figure.

E-ISSN 2581 – 7957
P-ISSN 2277 – 3916

DOI: 10.32377/cvrjst1709

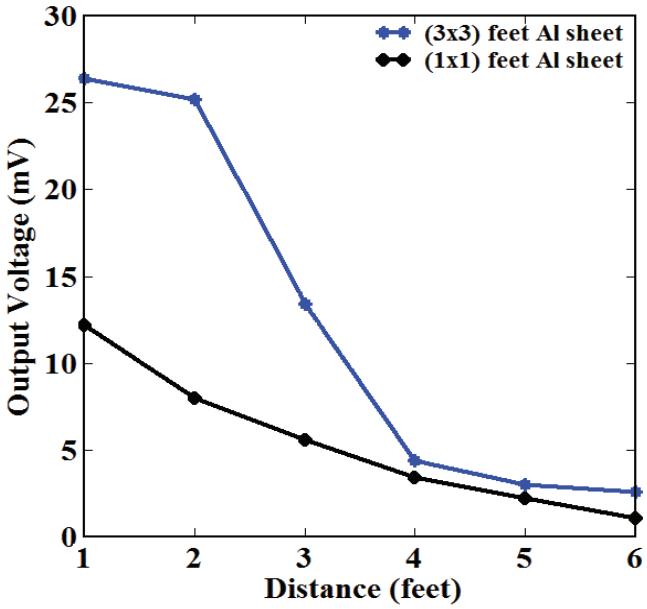

Figure 11. Variation of radar echo as a function of the object, size and distance.

VI. Conclusions

Object detection by using X-band cw-radar has been demonstrated. Experimentally it has been observed that the received signal strength is decreasing with increase the distance of a target with radar and also found that for large target aperture received echo is more and vice versa. It is possible to observe echo from the target kept on a rotating platform. With this method we can get the approximate size and shape of the target. By placing transmitter and receiver of radar at different locations, it is possible to observe the target from different directions.

References

[1] M.I. Skolnik, *Radar handbook.* Mc Graw Hill, 1962.
[2] B. Edde, *Radar*. Pearson, 2007.
[3] Wehner, R. Donald, *High resolution radar*. Norwood, MA, Artech House, Inc., 1987.
[4] Richards, A. Mark, *Fundamentals of radar signal processing*. Tata McGraw-Hill Education, 2005.
[5] Liao, Y. Samuel, *Microwave devices and circuits*. Pearson Education India, 1989.
[6] Balanis, Constantine A. *Antenna theory: analysis and design*. John wiley & sons, 2016.

E-ISSN 2581 – 7957
P-ISSN 2277 – 3916

CVR Journal of Science and Technology, Volume 17, December 2019
DOI: 10.32377/cvrjst1710

VLSI Implementation of Seed Transistor for Super Gate Design based on Grid based Transistor Network Generation

T. Subha Sri Lakshmi
Asst. Professor, CVR College of Engineering/ECE Department, Hyderabad, India
Email: rupashubha@gmail.com

Abstract: **In VLSI digital design, the Propagation Delay, Power Dissipation and Area of circuits are strongly related to the number of transistors which are present on an IC. Hence transistor optimization is special interest when designing digital integrated circuits. Therefore, efficient algorithms are used to generate optimized transistor networks, which are quite useful for designing digital integrated circuits (ICs). Several methods have been proposed for generating and optimizing transistor networks. Most Traditional solutions are based on factoring Boolean expressions in which only Chain - Parallel (CP) arrangement of transistors can be obtained from factored forms. Whereas grid-based methods are able to find CP and also non - CP (NCP) arrangements with potential reduction of transistor count. This method is an effective way of improvising VLSI circuits. In this an efficient algorithm is proposed i.e. Novel (Seed) method. It is automatically generates networks with minimal transistor count starting with irredundant sum of products (ISOPs) as inputs. Novel method is able to deliver both CP switching networks and NCP switching network arrangements, which improves VLSI circuit's performance in terms of area, power and delay. All the network circuits are implemented in ASIC Cadence by using 45nm and 90nm technology with GPDK libraries. By using Cadence Virtuoso tool, it can obtain schematics of design and its test bench, power analysis, SPICE simulation and its simulation waveform.**

Index Terms**: Transistor network, CMOS circuits, NMOS circuits, Super Gate design, Seed method, ISOP, CP and NCP.**

I. Introduction

Logic synthesis plays a major role in design automation. A logic function can be represented by a binary decision diagram (BDD). Here, a technique is proposed to construct a BDD whose nodes can be implemented by CMOS logics and Pass-Transistor Logics (PTL) in a cell library. The conventional synthesis flow needs three cell libraries: CMOS cell library, Pass Transistor Logics cell library, and CMOS remapping pattern. To simplify the synthesis flow, the logic function is decomposed into two kinds of functions and map them to Pass Transistor Logics and CMOS cells, respectively. The cell library contains high speed cells and low power cells. The experimental results in better performance and use less area than conventional CMOS technology mappings [1]. Dynamic circuits are widely used in today's high-performance microprocessors for obtaining timing goals that are not possible using static CMOS circuits. Currently, no commercial tools are able to synthesize dynamic circuits and therefore their design is either completely done by hand or aided by proprietary in-house design tools. This paper describes methodologies and tools for the design and synthesis of dynamic circuits, including general monotonic circuits, which consist of alternating low-skew and high-skew logic gates that may both contain functionality. Synthesis results show standard domino, dynamic-static domino, monotonic static CMOS, zipper CMOS, and footless domino and clock-delayed domino circuits to have average speed improvements of 1.57,1.66,1.47,1.71 and 1.60 times over static CMOS, respectively [1]. This paper is organized as follows. Section II gives an overview of existing system and its arrangements. Section III presents the Novel Method which minimizes the transistor count. Section IV presents the super gate design with few examples in different technologies. Section V presents and demonstrates the efficiency of Novel Method by providing experimental results in terms of transistor count, area minimization and power dissipation of the network. Finally the conclusion is drawn in Section VI.

II. Existing System

To generate an optimized switch network circuits various methods are designed and implemented. In which the frequent traditional way of approach to achieve Chain-Parallel (CP) associations of transistors by using factorization process and CP net can be obtained from factored form. In few more cases grid based methods are used to implement the CP and also Non-CP (NCP) arrangements [10, 6] to get least transistor count. Even with the defects of earlier literature work, there are so many improvement techniques to get an optimized switch net which gets a minimum no. of transistors [2]. The main disadvantage of earlier work is usage of more number of transistors, more power and more area.

III. Novel Method

In this an efficient algorithm is proposed i.e., Novel Method (Seed). It automatically generates networks with minimal transistor count starting with irredundant sum of products (ISOPs) as inputs. Novel method is able to deliver both CP switching networks [3] and NCP switching network arrangements, which improves VLSI circuit's performance in terms of area, power and delay. All the network circuits are implemented in ASIC Cadence by using 45nm & 90nm technology with GPDK libraries. By using Cadence Virtuoso tool, can obtain a schematics of design and its test

E-ISSN 2581 – 7957
P-ISSN 2277 – 3916

DOI: 10.32377/cvrjst1710

bench, power analysis, SPICE simulation and its simulation. This method introduces a new algorithm for Boolean factoring. The proposed approach is based on a novel synthesis paradigm, functional composition, which performs synthesis by associating simpler sub-solutions with minimum cost. The method constructively controls characteristics of final and intermediate functions, allowing the adoption of secondary criteria other than the number of literals for optimization. This multi objective factoring algorithm presents interesting features and advantages when compared to previous works [3]. For the mentioned below Boolean expression, CP network is designed using factorization method shown in Fig. 1(a) which consist of 7 switches. Active grid analysis techniques, consecutively, endow with the NCP solution shown in Fig. 1(b), and also with 7 switches. However, the finest network design consists of only 5 switches as shown in Fig.1(c), is not available by any of these techniques. [4]

Example: F = a · b + a · c + a · d + b · c · d

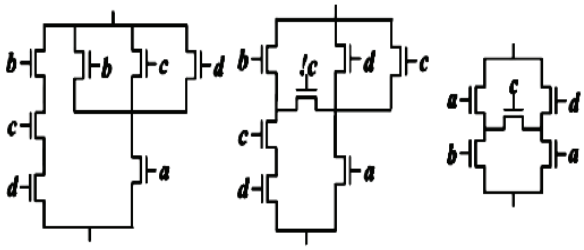

(a) (b) (c)

Figure 1. Transistor networks corresponding to (1). (a) CP solution from factored form. (b) NCP from existing graph-based generation methods (c) Optimum NCP solution.

A Switch is a component which is designed by having one control input and two contact inputs. Control input specifies the relation or connection between two contact inputs as shown in Fig. 2(a). In general switch represents an ideal MOS transistor. In this paper switch is replaced with transistor. When two transistors are connected in chain the flow of electrons is shown in Fig. 2(b), represents an AND operation, whereas parallel network seen in Fig. 2(c), which leads to OR operation. Example of CP network is shown in Fig. 2(d). An NCP transistor network cannot be designed by placing the transistors or contacts either in chain and/or in comparable. [3,4]

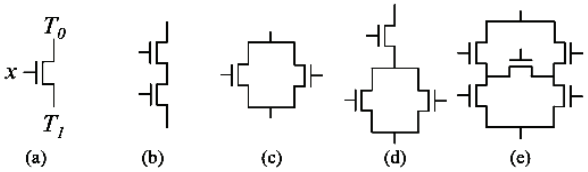

Figure 2. Represents of (a) MOS Transistor (b) chain (c) Comparable (d) CP (e) NCP.

The Novel (Seed) Method gives a reduced switch network which consists of very less number of transistors with the help of using Sum of Products technique. This method comprises 2 blocks i.e., Seed finding and Switch net circuit. Kernels are mainly used as a grid structures and they are help in designing well-organized CP and NCP transistor networks. Finally from the first block design get, inequitable nets which carry out switch sharing, and results in a solitary net which represents F. The obtained solitary net circuit consists of very less number of transistors compared to general Boolean expression. Various Boolean expression are taken into consideration and tested them to achieve few improvements towards area and power Flow chart of Novel (Seed) method is shown in Fig.3.

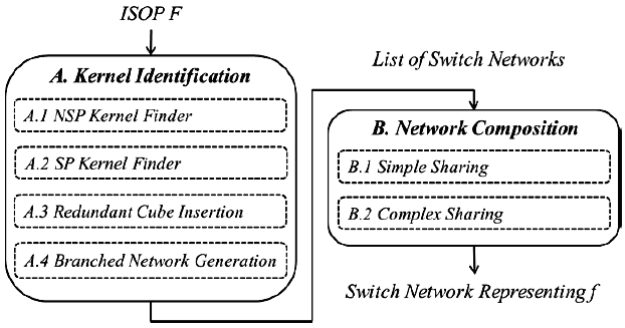

Figure 3. Execution Flow of the Proposed Method

A. Seed Identification

The identification module of Seed is divided into four steps. In the process of kernel identification module, the possible CP and NCP networks are searched by using Seed, which is known as intermediate data structure.If Ui ^ Uj_= Ø, then only existence of edge (Ui,Uj) Є G, i_ = j is possible. Here, edge g is labeled as Ui∩Uj. To perform logic sharing using Seed structure, the determination of relationship among cubes of F is possible. All steps of Seed identification module are used to extract Seeds from F because of which transistor count optimization is possible.[5]

In Seed identification module, each step is used to find transistor networks which are used to represent the sub-functions of the target function f. To obtain the optimized NCP networks from the input ISOP F, the NCP kernel finder steps are used. Depending on the availability of transistor network, the circuit is achieved which are removed from F by using cubes. This process leads to a simpler ISOP F1.In CP kernel finder step method; the CP networks can be searched by using the input F1.In the same way, CP network cubes are eliminated from F which results in F2. To generate NCP or CP networks, rest of the cubes of F2 were not useful. So, to find NCP arrangements with repeated paths, and finally the repeated paths are added into the kernels. Hence the repeated paths are eliminated from F2 which results in F3. The final step generates group of transistor networks, which consists of comparable paths corresponding to cubes from F3. The final output of the Seed identification module generates a list of transistor networks, which is treated as output. [5]

Non Chain-Comparable Seed Finder – The ISOP form of a Boolean function is assumed to be f which is given by F = c1+c2+…….+cn, where the number of dices F is denoted by n. The combinations of 4 dices are taken simultaneously

E-ISSN 2581 – 7957
P-ISSN 2277 – 3916

CVR Journal of Science and Technology, Volume 17, December 2019
DOI: 10.32377/cvrjst1710

among n dices to identify NCP Kernels. By adding those 4 dices, an ISOP L can be obtained, which is known as sub-function of f. L is used to get a Seed with 4 vertices. To make sure that the generated Seed results in NCP transistor network, [5] 2 rules need to be verify i.e.,

First Rule: The set of edges which are connected to the vertex u Є U is assumed to be G_v. The cube is also known as vertex. The literals from u should be shared through edges g Є G_v for each cube u Є U.

Second Rule: The obtained kernel from L should be isomorphic of same form as shown in Figure 4.The type of grid stencil is known as NCP Kernel. To map NCP Seed to a transistor network, the edge swapping technique can be applied over Seed 3 edges. The generic NCP Seed is assumed as shown in Fig.4. The edge is shifted to g_4 place, g_4 is shifted to g_3 place, g_3 is shifted to g_2 place in order to map the kernel into a network. In order to get the network shown in below figure 4, such type of rearrangement process is applied. This procedure is helpful to make sure that each part of the network denotes a Dice from the sub function l. [5]

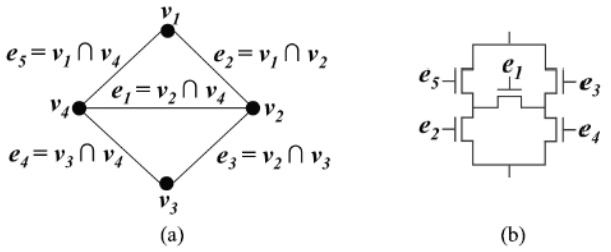

Figure 4. (a) NCP Seed template (b) Resulting Transistor network

A dice combination produces set of all possible 4 combinations of dices. Let it be'd'. Assume an ISOP which has n dices. The time complexity of get dice combinations is assumed to be O (n4). Each Seed contains one of 4 dices possible combinations. The resultant kernel sub routine's time complexity function is assumed to be O (n^2p). As 4 dices are combining simultaneously, the resultant function is assumed to be O (p). [5]

First Rule: It can be tested by using complexity of time and also it is similar to the obtained Seed subroutine. The grid with 5 edges only obeys second rule. At time O (1) this type of list will be done. The edge reordering subroutine process will be executed only if both rules are satisfied. This process should be done at a constant time to obtain transistor networks; the found NCP transistor network will be added. This process is done in constant time O (n4). As shown in Fig. 5, the Seed is going to be obtained for every combination of 4 dices. The resultant Seed sub routines time complexity function is assumed to be O (n^2p), where p is no. of variables in F. As 4 dices are taken into consideration, the complexity function can be reduced to O (p).

Chain-Comparable Seed Finder – let ISOP form F1 which is used to represent the dices, which were not used to generate transistor network in the NCP Seed finder step. The identification process of CP Seeds will be done by combining 4 n dices from F1. Then 4 vertices Seed is

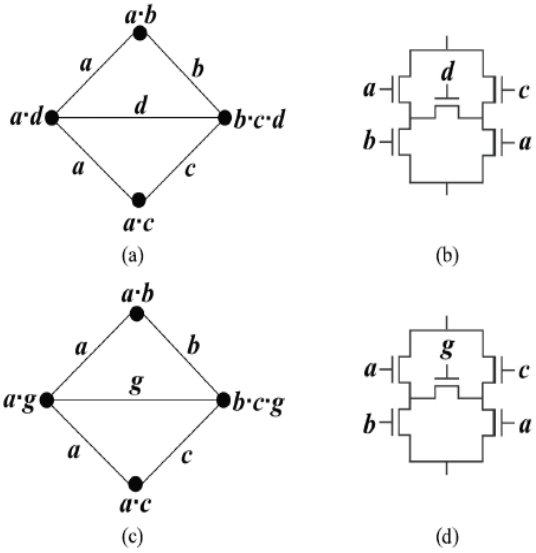

Figure 5. NCP Seeds (a) M_2 and (c) M_3, obtained from (4). Corresponding transistor networks (b) T_2 and (d) T_3

obtained. To check whether the resultant Seed is a valid CP network or not, both rules (first and third rule) must be satisfied. The resultant Seed must be same form to the grid. This type of grid stencil is termed as CP Seed. To obtain the transistor network, some changes should be performed on Seed by the CP Seed finder step. The first step includes that the kernel edges should be mapped to a supplementary template grid as shown in figure 6. Later by applying edge ordering sub routine one supplementary template grid in order to get a transistor network as shown in Fig. 6. [5]

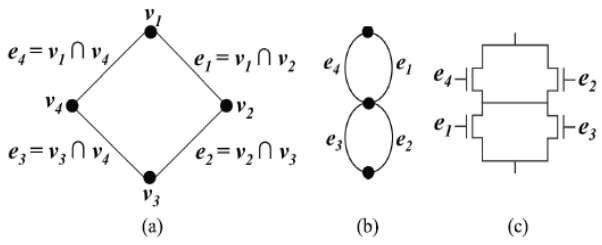

Figure 6. (a) CP Seed template (b) Supplementary Template grid (c) Resulting Transistor network.

Third Rule: Obtained Seed need to be isomorphic to the grid as shown in the Fig. 6(a). Such grid template is defined as CP Seed. To obtain the transistor network CP seed finder step should perform some transformations over the seed. Seed edges are given to supplementary template which results in transistor network by pertaining the edge reordering subroutine ended the supplementary template grid as shown in Fig. 6(c).

Superfluous dice Insertion – In most of the scenario NCP structures are arranged with the help of superfluous dice method in place of using CP structures as shown in the Fig. 7. Even dice is not present in NCP and CP networks; the

E-ISSN 2581 – 7957
P-ISSN 2277 – 3916

CVR Journal of Science and Technology, Volume 17, December 2019
DOI: 10.32377/cvrjst1710

superfluous dice insertion step tries to construct NCP Seeds by adding the left over dices. Let S be an ISOP which represents the Boolean function s. A dice d is superfluous if S + d = s. Transistor network which represents an ISOP function s is taken into the consideration [7]. Designing or Functioning of superfluous dice d in a circuit defined as superfluous path. Superfluous path gives best performance in logic sharing.

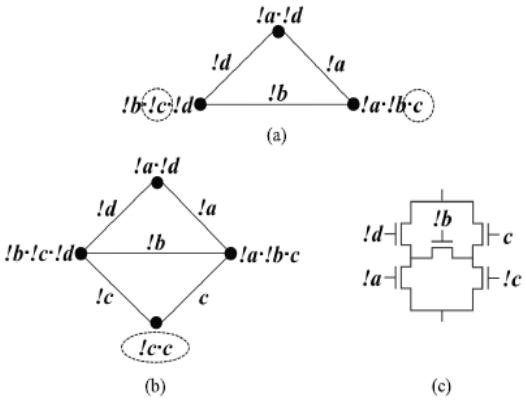

Figure 7. (a) Grid D1 (b) NCP Seed with Superfluous dice (c) Resulting Transistor network.

Stem Net Creation – During a net is created or found the dices are removed from ISOP S. Logic Sharing plays a prominent role, even though dices are not present in the designed nets. The left over dices in S3 forms as a unique transistor net [7]. Therefore stem net creation step converts each remained dice S3 into a stem of transistors which are connected in chain. Three left over dices are present to implement. Final net is shown in Fig. 8.

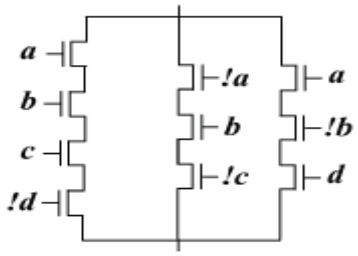

Figure 8. Stem Transistor Net

B. Network Composition

During Seed Identification module, net composition modules obtain the function F and a record of biased transistor networks S is produced. By executing logic sharing on the nets which are derived from S in a repeated and continuous process. In the target net to remove superfluous transistors, trouble-free and intricate sharing is used. The trouble-free sharing and intricate sharing are discussed in the below section.

Trouble-Free Sharing – Edge sharing technique is realized via trouble-free sharing method. Mostly the method negotiates the transistor net exploring for equivalent transistors, and all the transistors are organized with the help of literals. Net is reconstructed in which 1 universal knot is present between the corresponding transistors are available [8]. In general case, the corresponding transistors must be interchanged in the nets in order to utilise the universal knot. In this case only one transistor is utilised and used which leads to a superfluous transistors. After doing trouble-free sharing, the circuit performance of the net will be verified to make sure for a precise target function. This process is performed continuously over the net until there are no possible transistors left over for carve up the universal knot.

Intricate Sharing – Intricate sharing step gets an in-complete net which is provided by the stem net creation step and strives to do further optimizations. As explained in earlier cases i.e., trouble-free sharing step, when a universal knot [8] is available the transistor starts to enable its sharing mechanism to operate continuously with the subsequent knots. When the net is too large it will be difficult to find the universal knot which leads to further some more iterative steps. Therefore, in bid to perk up these sharing mechanisms, straightforward CP transistor compressions are used as shown in Fig. 9.

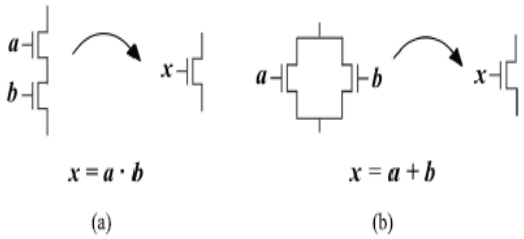

Figure 9. (a) Chain Transistor Compression (b) Comparable Transistor Compression

IV. Super Gate Design Using Seed Method

Four Boolean expressions are considered up to 6 literals. All the four Boolean expressions are designed using three different logic styles i.e., CMOS logic style, NMOS logic style and finally with Super Gate logic style by using Novel (Seed) Method. The transistor level circuits are designed and implemented using Cadence Design Suite 6.1.6 version with GPDK 45nm and 90nm technology libraries. SPICE simulations are carried out for the expressions in all the logic styles for the expression. Post-Layout Simulations are carried out during implementation phase. The below Four Boolean expressions are represented with P and N net's and only N net's.

Expression 1: F = w.x + w.y + w.z + x.y.z

This expression contains 4 literals with logic AND & logic OR operation. The expression is designed with a) CMOS style which contains both P and N net's in the circuit b) NMOS style which contains only N net's c) Super Gate Design style (using Seed Method) which contains only N net's with reduced path design & number of transistors compared to NMOS and CMOS style. Fig. 10 gives schematic structures in three styles and simulation waveform.

E-ISSN 2581 – 7957
P-ISSN 2277 – 3916

DOI: 10.32377/cvrjst1710

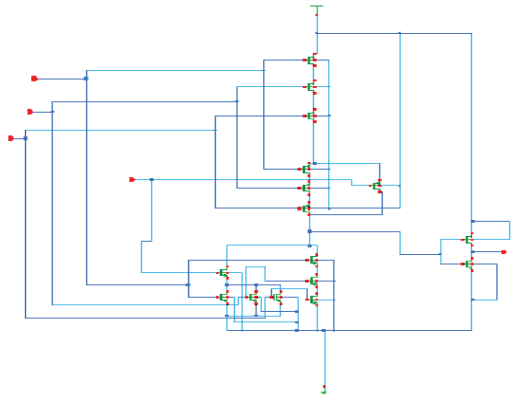

Figure 10. (a) Schematic structure of expression 1 in CMOS design style

CMOS design style of the expression 1 contains 8 nmos and pmos transistors for the reduced network by using Boolean algebra.

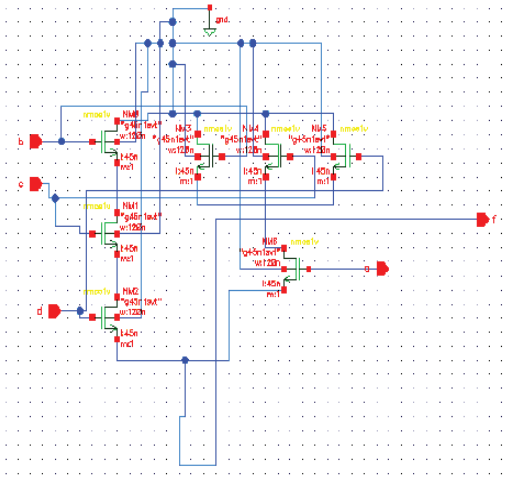

Figure 10. (b) Schematic structure of expression 1 in NMOS design style

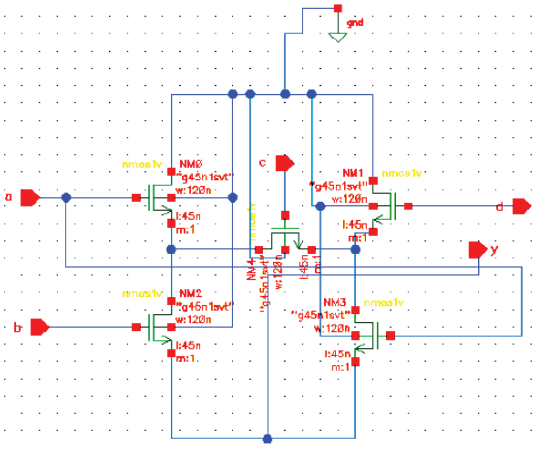

Figure 10. (c) Schematic structure of expression 1 in Super Gate style

Expression 1 by designing using Super Gate design consists very minimum number of transistors in terms of SP network.

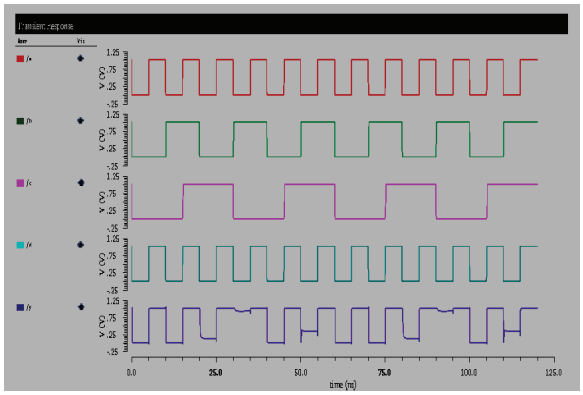

Figure 10. (d) Simulation waveform of Expression 1.

In the above simulation x-axis is defined by time in terms of nano seconds (ns) and y-axis defined by voltage in terms of volts (v).

Expression 2: F = w.x + w.y.s + z.s +x.y.z

This expression contains 5 literals namely w, x, y, z, s. Fig. 11 gives schematic structures in three styles and simulation waveform.

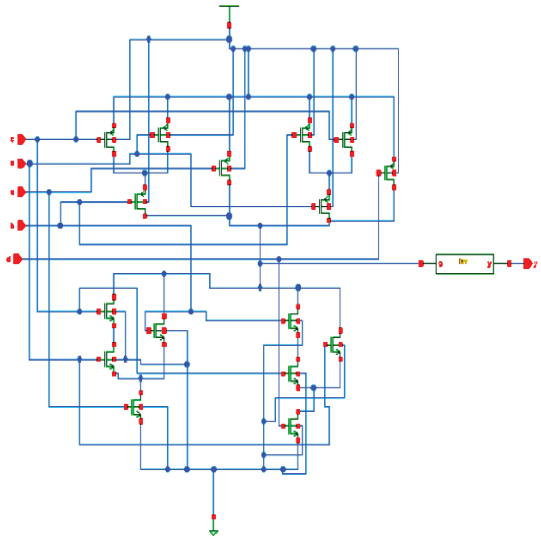

Figure 11. (a) Schematic structure of expression 1 in CMOS design style

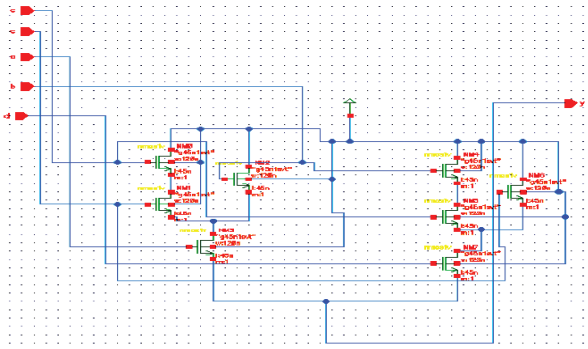

Figure 11. (b) Schematic structure of expression 1 in NMOS design style

E-ISSN 2581 – 7957
P-ISSN 2277 – 3916

CVR Journal of Science and Technology, Volume 17, December 2019
DOI: 10.32377/cvrjst1710

Expression 2 by designing using CMOS design consists of very maximum number of transistors in terms of Boolean algebra and it contains 9 nmos and pmos transistors. In NMOS design style it only consists of 7 nmos transistors.

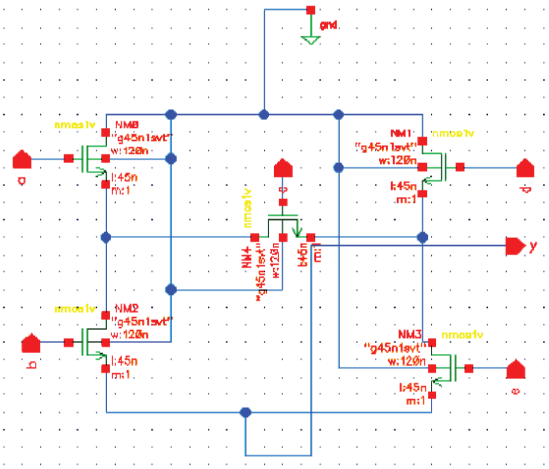

Figure 11. (c) Schematic structure of expression 2 in Super Gate design style

Expression 1 by designing using Super Gate design consists very minimum number of transistors in terms of SP network.

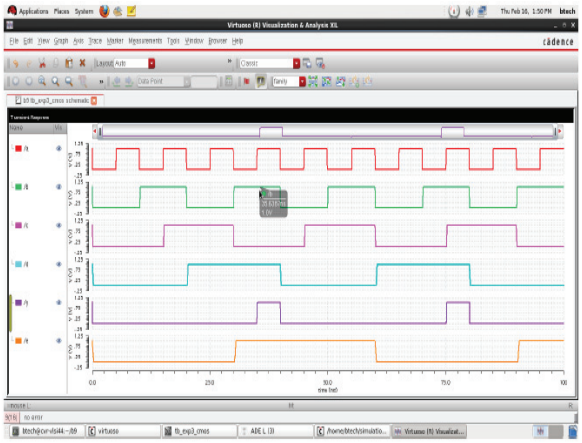

Figure 11. (d) Simulation waveform of Expression 2.

In the above simulation x-axis is defined by time in terms of nano seconds (ns) and y-axis defined by voltage in terms of volts (v).

Expression 3: F = w.'x'.y'.z' + w'.x.z + w'.x.y +w.x'.y + w.x'.z + w.x.y'.z' + x.y.z

This expression contains 4 literals namely w, x, y, z. The function is expressed in terms of its complements finally inverter is needed to be added at output side. The entire expression is minimized by using SOP or POS form, the reduced Boolean expression is designed by using various design styles. Fig. 12 gives schematic structures in three styles and simulation waveform.

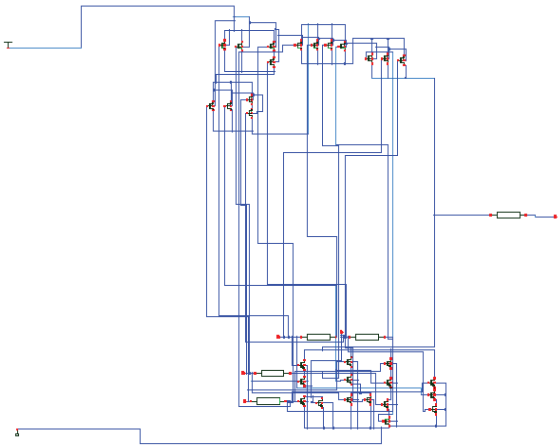

Figure 12. (a) Schematic structure of expression 3 in CMOS design style

Expression 3 CMOS design contains 5 inverters, 15 pmos and 15 nmos transistors. Complexity wise it has some difficulties to perform layout design.

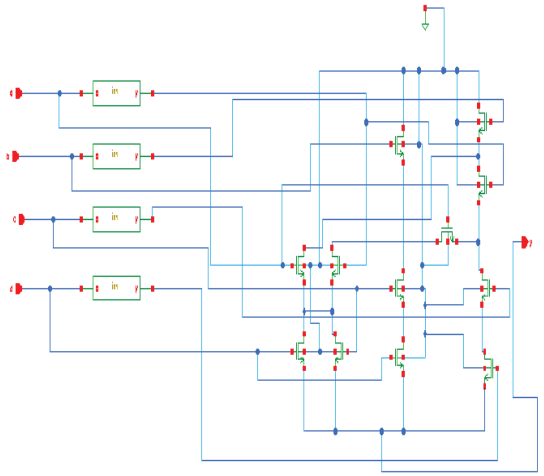

Figure 12. (b) Schematic structure of expression 3 in NMOS design style

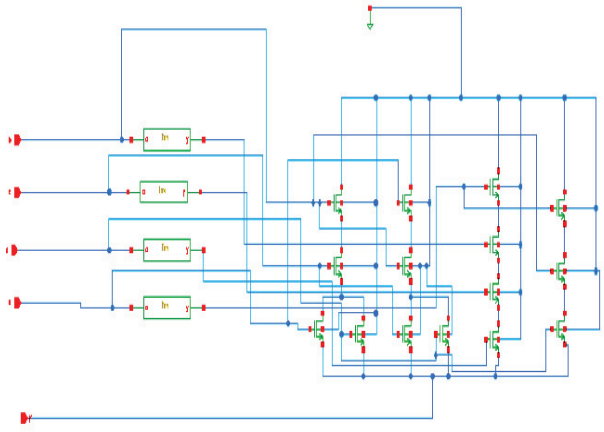

Figure 12. (c) Schematic structure of expression 3 in Super Gate design style

E-ISSN 2581 – 7957
P-ISSN 2277 – 3916

CVR Journal of Science and Technology, Volume 17, December 2019
DOI: 10.32377/cvrjst1710

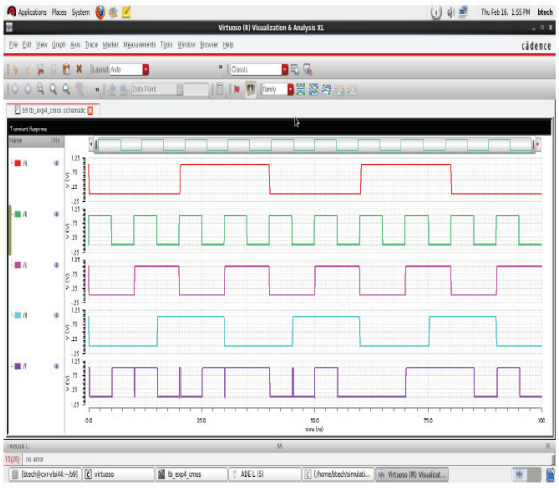

Figure 12. (d) Simulation waveform of Expression 3.

In the above simulation x-axis is defined by time in terms of nano seconds (ns) and y-axis defined by voltage in terms of volts (v).

Expression 4: F = w.x + w.y + w.z +x.y.z + x.y.v +y.s + w.v

This expression contains 6 literals namely w, x, y, z, s, v. The Fig. 13 gives schematic structures in three styles and simulation waveform. Boolean algebra (Demorgans law) is applied for the above expression so finally at the output side inverter is designed to retain the original output. CMOS design style of the expression 4 contains 11 nmos and pmos transistors and 1 inverter for the reduced network by using Boolean algebra for 6 literals i.e., w, x, y, z, s, v.

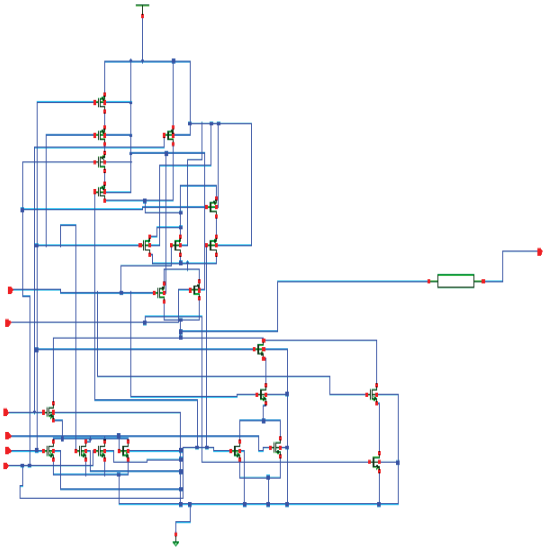

Figure 13. (a) Schematic structure of expression 4 in CMOS design style

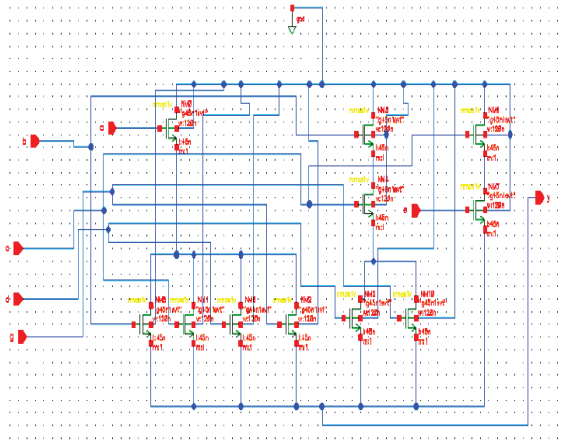

Figure 13. (b) Schematic structure of expression 4 in NMOS design style

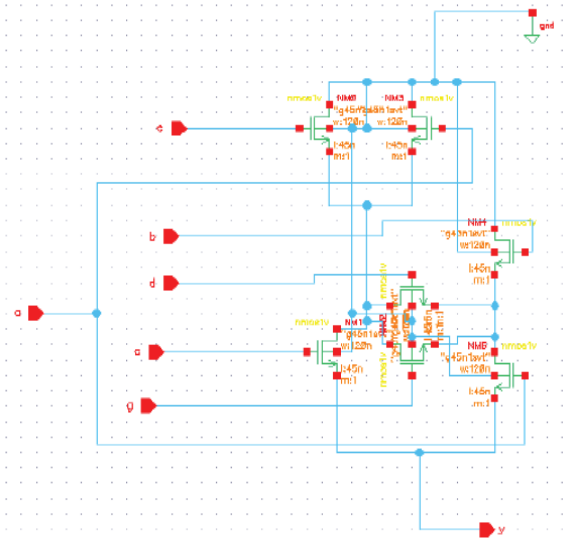

Figure 13. (c) Schematic structure of expression 4 in Super gate style

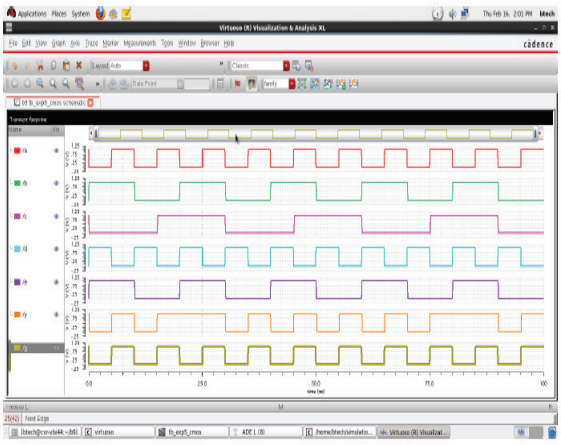

Figure 13. (d) Simulation waveform of Expression 4.

In the above simulation x-axis is defined by time in terms of nano seconds (ns) and y-axis defined by voltage in terms of volts (v).

E-ISSN 2581 – 7957
P-ISSN 2277 – 3916

DOI: 10.32377/cvrjst1710

V. Experimental Results

For evaluation and verification, the proposed Novel (Seed) Method is applied over four different Boolean expressions and compared with CMOS and NMOS logic style in three different aspects i.e., Transistor count [9] in Table I, Power Dissipated in nano watts of the network is shown in Table II and Total Area occupancy of the network in Table III.

TABLE I.
Transistor Count Minimization

	CMOS	NMOS	Super Gate
Expression 1	16	7	5
Expression 2	18	8	5
Expression 3	42	23	20
Expression 4	24	11	7

TABLE II.
Power Dissipation

	CMOS	NMOS	Super Gate
Expression 1	191.1 E-9	765.8 E-12	400.4 E-12
Expression 2	6.274 E-6	364.9 E-12	300.9 E-12
Expression 3	36.95 E-6	59.41 E-9	34.55 E-9
Expression 4	1.566 E-6	475.6 E-12	481.5 E-12

TABLE III.
Area Occupancy

	CMOS	Super Gate
Expression 1	171.797µm	18.473 µm
Expression 2	311.1797 µm	41.8914 µm
Expression 3	214.01 µm	15.30 µm
Expression 4	1072.78 µm	614.47 µm

VI. Conclusions

This paper describes an efficient super gate design method which is related on various combinations of Boolean functions in which to get a good relationship with the previous results. Four various combinations of Boolean functions were taken into consideration to get complete analysis of area, power and timing 1) deposit of four-input P-class Boolean functions 2) deposit of handcrafted arrangements that do not present transistors in CP associations 3) a given Boolean function with eleven variables a more complex type 4) the set of 5 – input transistor network is designed. A Novel (Seed) Method is designed and implemented in this paper, mainly used to generate optimized transistor networks. Novel (Seed) Method approach generates more general arrangement of network than the usual CP associations. The results give a significant and drastic change in the transistor count to implement the logic network or circuit compared to the existing approach. In CMOS technology the performance (timing), Power Dissipation and Area of Digital IC's are improved with the help of transistor count minimization concept. In general, Novel (Seed) method which is proposed in this paper reduces the power dissipated in the circuit, total Area and Number of Transistors used. These things even can be achieved by using STSCL logic and GTI Technique with few limitations.

References

[1] Y.T. Lai, Y.C.Jiang and H-M Chu, "BDD decomposition for Mixed CMOS/PTL logic circuit synthesis", in Proc. IEEE Int. Symp Circuits Syst (ISCAS), vol.6, May 2005,pp,5649-5652
[2] H.Al Hertani, D.Al Khalili and C Rozon,"Accurate total static leakage current estimation in transistor stacks," in proc. IEEE Int.Conf.Comput Syst.Appl,Mar.2006,pp.262-265
[3] D.Kagaris and T Haniotakis,"A methodology for transistor efficient super gate design," IEEE Trans. Very large Scale Integration Syst., Vol.15, no.4, pp,488-492, Apr.2007.
[4] T.J.Thorp, G.S.Yee and C.M.Sechen, "Design and synthesis of dynamic circuits,"IEEE trans. VLSI Syst., vol.11, no.1, pp, 141-149, Feb.2003.
[5] A.I.Reis and O.C.Andersen,"Library Sizing,"U.S.Patent 8015517, June 5, 2009.
[6] E.M Sentopvich et.al, "SIS: A system for sequential circuit synthesis," Dept., Elect. Eng. Comput. Sci., Univ. California, Berkley, Ca, USA, Tech. Rep, UGB/ERL M92/41, May1992.
[7] M.Rostami and K.Mohanram,"Dual-vth independent gate FinFETs for low power logic circuits," IEEE Trans.Comput-Aided Design Integration Circuit Systems., vol.30, no.3, pp. 337-349, Mar-2011.
[8] V.N.Possani,R S de Souza, J s Domingues, Jr. l V Agostini, F S Marques, and L S da Rosa, Jr. "optimizing transistor networks using a graph based network techniques", J analog Integration Circuits Signal Processing., vol. 73,no. 3,pp. 841-850, De. 2012.
[9] L S da Rosa, Jr F s Marques, F R Schneider, R P Ribas and A I Reis and "A Comparative study of cMOS gates with minimum stacks," Proc. 20th Annu., Conf. Integ. Circuit Systems Design (SBCCI), Sep.2007, pp. 93-98..
[10] M C Golumbic, A Mintz and U Rotics,"An improvement on the complexity of factoring read once Boolean functions", Discrete Appl. Math vol. 15

E-ISSN 2581 – 7957
P-ISSN 2277 – 3916

CVR Journal of Science and Technology, Volume 17, December 2019
DOI: 10.32377/cvrjst1711

Dog Breed Identification Using Convolutional Neural Networks on Android

Dr. D. Durga Bhavani[1], Mir Habeebullah Shah Quadri[2], Y. Ram Reddy[3]
[1]Professor, CVR College of Engineering/CSE Department, Hyderabad, India
Email: drddurgabhavani@gmail.com
[2]PG Scholar, CVR College of Engineering/ CSE Department, Hyderabad, India
Email: quadrishah846@gmail.com
[3]Software Engineer, Eximius Design India Pvt. Ltd., Bengaluru, India
Email: ramreddyy@eximiusdesign.com

Abstract: **Identifying the breed of a dog, is a challenging image classification problem. In this paper, we implement an android application that identifies the breed of a dog via image analysis, using a Convolutional Neural Network (CNN) and transfer learning model. The android application lets the user click or upload a picture of a dog. It then pre-processes the image and extracts the features required for testing. Prediction of dog breed is done using CNN and transfer learning. We have used Stanford's standard dog dataset for training the model and achieved an accuracy of 94% on the testing data.**

Index Terms: **Dog Breed Identification, Convolutional Neural Networks, Pre-trained Models, Android**

I. Introduction

Dogs are the most preferred among pets. Potential customers who are looking to buy a dog may do their research by scouting dogs owned by other people. It may not always be possible to approach the owner and inquire about the breed the dog belongs to. Additionally, it is possible that the owners themselves may be unaware of the breed of their dog. In this paper, we have tried to address this market requirement by automating the process of finding a dog breed via an android application that lets you know the breed of the dog, simply by snapping its picture.

Convolutional Neural Networks (CNN) works like human vision. In simple terms we can innately classify things using our vision. CNN provides a software, the ability of image identification and recognition by building a mathematical model and implementing it in the form of an algorithm.

CNN is a class of the feed forward artificial neural networks and deep learning. It is similar to regular neural networks, except that it takes every input as an image. Thus, the assumption allows us to conceal few properties to the architecture thereby making the feed forward function more efficient. CNNs are proven to be effective in analyzing the visual imagery. They use multi-layer perceptron's and usually require less preprocessing in comparison with other image classification algorithms. CNNs have at least one fully connected layer preceded by the desired number of fully convolutional layers as a standard multi-layered network. The input which is given in the structure image format is efficiently utilized by the design of the CNNs, i.e. they can be easily trained. One of the benefits of CNNs is that it is translation invariant, also referred to as shift invariant or space invariant artificial neural networks.

There are three main layers used in the CNNs, namely *convolutional layer, pooling layer and fully connected layer,* (CONV-POOL-FC). Each layer can be repeated a required number of times in order to accomplish the desired output. CNNs divide the images into smaller parts/features and match them individually.

- The input image comprises of raw pixel values represented in a matrix format (m x m x r, m rows, n columns, r channels, for an RGB image r=3).
- CONV layer computes the output of neurons connected to the local region by computing the dot product of the sub image and *k*-filters (size - n x n x q) and finding the average value to obtain *k*-filtered images.
- POOL layer performs down sampling operation along the spatial dimensions i.e., it takes the stack of filtered images and reduces the size of the image matrix to give an optimal output image.
- FC layer will compute the class scores, resulting in volume of size [1x1x a]

Thus, CNNs transform the input image, layer by layer from the original raw pixel values to the final class scores.

Transfer learning is a machine learning technique where an already trained model is used on another related task to attain better results. We have used convolutional neural networks and transfer learning in conjunction, to identify the breed of a dog. Our main aim is to build an android application, using which, a user can identify the breed of a dog. We intend to demonstrate how a hybrid model of pre-trained models for feature extraction gives better results.

II. Related Work

A. Literature review

Research has been done on depth wise separable convolutions in neural computer vision architectures and their effectiveness when used in place of *Inception modules* [1]. An architecture based on this idea was proposed, called Xception which have same parameter count as Inception V3 but are easy to use as regular convolution layers.

In another work, in order to speed up the training process, non-saturating neurons and a very efficient GPU implementation of the convolution operation are used [2]. There is a discussion on "dropout" method which is an effective and recently developed regularization method for reducing over fitting in the fully connected layers. A conclusion was reached by stating that the usage of very large and deep convolutional nets on video sequences where the temporal structure provides very helpful information that is missing or far less obvious in static images, proves to be effective.

Another method proposed, suggested several design principles to scale up convolutional networks which contribute to high performance vision networks having relatively modest computation cost compared to simpler, more monolithic architectures [3]. The study was done in the frame of reference of the Inception architecture and comparison was drawn between the error rates with the others proving the discussed method efficient. This method demonstrated that high quality results can be reached with very low receptive field resolution which might be helpful in detecting small objects in various systems.

In another study, the architectures-Inception-ResNet-v1, Inception-ResNet-v2, Inception v4 have been presented and discussed by the authors [4]. There is also a discussion regarding the variation of training speed with the introduction of residual connections for the Inception architecture.

A study demonstrated flexible and learning scalable, convolutional cells from data transfer to multiple image classification tasks [5]. The main aim in the mentioned approach is to design a search space that decouples the complexity of architecture from the depth of a network. The study concluded that we can use the demonstrated architecture to perform ImageNet classification with reduced computational budgets that outperform streamlined architectures targeted at mobile and embedded platforms.

Depth in visual representations is another methodology discussed for large scale image classification [6]. In this study, an assessment was made for very deep convolutional networks. By evaluating very deep convolutional networks, it was demonstrated that the representation depth is profitable for the classification accuracy, and that we can achieve state-of-the-art performance on the ImageNet challenge dataset using a traditional CNN architecture with considerably increased depth.

In another study, a system for automatically identifying dog breeds through images is described, implemented, and evaluated [7]. It follows a three staged system, in which all three stages will be at least briefly characterized, with more significance given to the implementation and evaluation of the breed identification network. The predictive models used in the above-mentioned stages have ultimately taken the form of convolutional neural networks retain in several important differences.

Work has been done to demonstrate that the difficulty in fine-grained classification problems can be mitigated by the fact that it is possible to establish accurate correspondences between instances from a large family of related classes [8]. The study combines features that can be effectively located using generic feature models with breed specific models of part locations. They also created a publicly obtainable dataset for dog breed identification, integrated with a practical system that attains high accuracy in real-world images.

Another study proposed a deep convolutional neural network architecture (Inception) that attains the new state of the art capacity for classification and detection in the ImageNet Large-Scale Visual Recognition Challenge 2014 (ILSVRC14) [9]. Its result yields proof that approximating the anticipated optimal sparse structure by readily present dense building blocks is a practicable method for enhancing neural networks for computer vision. The main advantage of this method is a remarkable quality gain at a modest rise of computational requirements compared to shallower and narrower architectures.

B. Challenges taken into consideration

In dog breed identification, there are a few concerning obstacles namely inter class variance, intra class variance, pose variance. Inter class variance can be explained as distinct similarities in different breeds. Many breeds of canines have similar features like color, fur etc., which are hard to distinguish for an untrained eye. In order to attain high accuracy, a vision algorithm must be able to differentiate the minor details which are distinct to each class. Another issue of dog-breed identification is Intra class variance. An English cocker-spaniel generally is available in black, brown and a few other colors. An animal, though belonging to same breed, may have variable features which makes it hard to distinguish the breed accurately for the convolutional neural networks. Another major issue is the Pose variance. The canines' pictures may not be available in same pose every time. The CNNs depend on their input which is an image. Thus, the pose of the animal and the noise in the background may result in decrease in the accuracy. So, pose normalization can be an important factor to achieve the accurate result.

III. Problem Statement

The pet industry is huge and ever growing. Dogs are the most preferred pets. Currently, the only way to find the breed of a dog, is to inquire about it from either the owner of the dog or the professionals in the industry. This can be a time consuming and confusing experience for a prospective dog owner. Finding the breed of a dog should be as easy as snapping a picture. However, currently there is a lack of an application that addresses this market need. In this paper, we have built an app for the android platform that uses Convolutional Neural Networks (CNN) and Transfer learning to identify the breed of a dog by simply snapping a picture of it.

IV. Proposed Method

We propose an android application that gives its users the ability to find the breed of a dog by either clicking or uploading its picture on the app. The app makes a prediction using Convolutional Neural Networks and pre-trained

E-ISSN 2581 – 7957
P-ISSN 2277 – 3916

CVR Journal of Science and Technology, Volume 17, December 2019
DOI: 10.32377/cvrjst1711

feature extraction models with the help of Keras and Tensorflow libraries.

A. System Architecture

The android application has 4 major activities, as shown in Fig.1, namely, *Upload, Take Photo, View*, and *Instructions*.

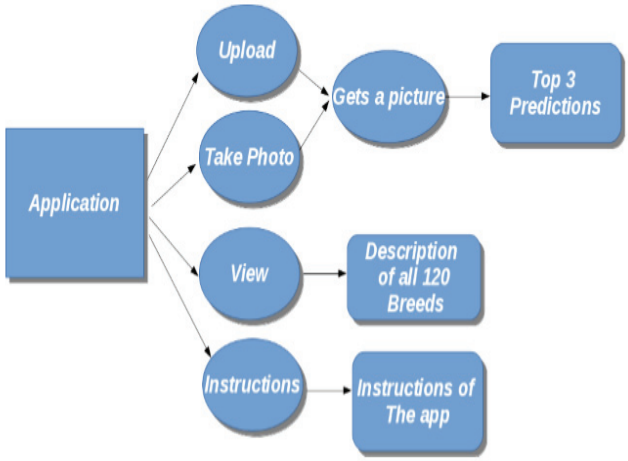

Figure 1. System Architecture

The *View* and *Instructions* activities provide the user with descriptions about different types of dog breeds and how to use this app to find the breed of a dog.

Using the *Upload* and *Take Photo* activities, the user can either upload or directly take a photo using the camera and upload it on the app. The app will then generate the top 3 predictions of the breed of the dog in the given image.

B. Dataset Used

To train the model, we have used Stanford dog's dataset. This dataset has 120 different dog breed images and each dog breed has minimum 60 images. We have divided dataset into train data, validation data and test data using stratified shuffle split where train data has 9199 images, validation data has 2000 images and test data has 9381 images.

C. Feature extraction from images

We have extracted the features of images using pre-trained models, which are trained on image-net and sent to a fully connected layer. We have used different pre-trained models such as Inception-v3, Inception-ResNet-v2, VGG16 and Xception to extract the features of the images. When Inception-v3, Inception-ResNet-v2, VGG16 and Xception are used for extraction of features from an image, accuracy percentages of 89, 94, 81, 93 are obtained respectively on the testing data.

D. Dog breed Identification on Android

To use a Keras model on an android application, we will first, run the Keras model on a server. We then convert the model into a Tensorflow protobuff (pb) file. The following steps are involved in converting a Keras model to a Tensorflow pb file:

1. Run the Keras model on the server
2. Convert the model to a Tensorflow pb file.
3. Save the latest checkpoint.
4. Freeze the graph.
5. Finally, optimize the saved model.

Steps 1 and 2 can be done using Tensorflow whereas steps 3, 4 and 5 are done using bazel. Bazel is a build and test tool. We have used it to freeze the graph and optimize the saved model which is in the format of Tensorflow protobuff.

To add TensorFlow dependencies to android, we compile *'org.tensorflow:tensorflow-android:+'* and load the protobuff file to assets folder. A Tensorflow inference interface has been created to send the uploaded image pixels to the network and get the predictions. Fig. 2 depicts how a prediction is obtained when an image is passed.

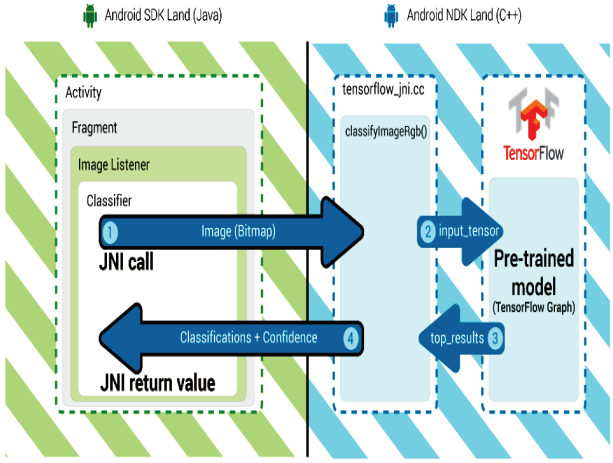

Figure 2. Android app calls from JAVA to TensorFlow

The architecture given in Fig. 2 comprises of two repositories, namely Android Standard Development Kit (android SDK) and Android Native Development Kit (android NDK.)

Android SDK is written in Java. It is designed for interfaces and useful for characteristics like activities, fragments, event listeners etc. On the other hand, android NDK is coded in C++ and is used for working with C++ files. NDK can be useful for working with Tensorflow models, as Tensorflow itself is written in C++.

Initially, the Bit-map input image is sent from SDK to NDK Tensorflow wrapper for Android (written in C++). It takes the given image and resizes it, i.e. to tensor and gives the obtained tensor to a pre-trained model (protobuff file), which is a pre-trained convolutional neural network. The model puts out a tensor (a C++ file) which is returned to the SDK.

E. Procedure

The following is the step wise procedure for deploying the model on android

1. Resize the image to (400, 400, 3).
2. Extract the features of original image from Inception-v3 (9199, 2048), Inception-ResNet-v2 (9199, 2048), Xception (9199, 1536) and

E-ISSN 2581 – 7957
P-ISSN 2277 – 3916

CVR Journal of Science and Technology, Volume 17, December 2019
DOI: 10.32377/cvrjst1711

concatenate to form the input (9199, 5632) which will be sent to a fully connected network.

3. Fully connected layer configuration is given in Fig. 3.

Dense (2048)
Activation ('elu')
Dropout (0.5)
Dense (120)
Activation('softmax')

Figure 3. Fully connected layer configuration

4. Train the model with original images and store the model as model-1.
5. Train the model with flipped version of original images and store the model as model-2.
6. Predict the breed of the dog by averaging the results of model-1 and model-2.
7. Convert Keras model to Tensorflow pb file and deploy it on android.

V. Results and Discussion

We have created a user-friendly android application that tells you the breed of dogs just by uploading an image of the dog.

Fig. 4 shows the user interface of the home screen of the android application. When the user clicks on the application, the user gets an interface showing the options: upload, Take a photo, view and instructions.

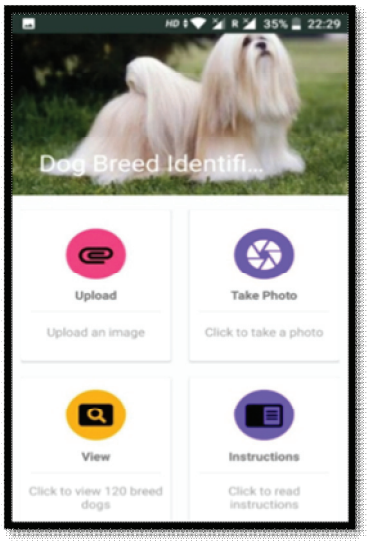

Figure 4. Home screen of the android application

When the user selects *upload*, the user will be provided with the image files on the device which user can upload to identify the breed of the dog. When *Take photo* is selected, the default camera application of the device is opened which enables the user to capture the image of the desired dog. As soon as user inputs the image (either through *Upload* or *Take photo*), the predictions of the breed and their corresponding rounded probabilities are given. As shown in Fig. 5, if the top-1 predicted class has probability above 90 percent, then only top-1 class will be displayed, else top-3 predicted classes will be displayed.

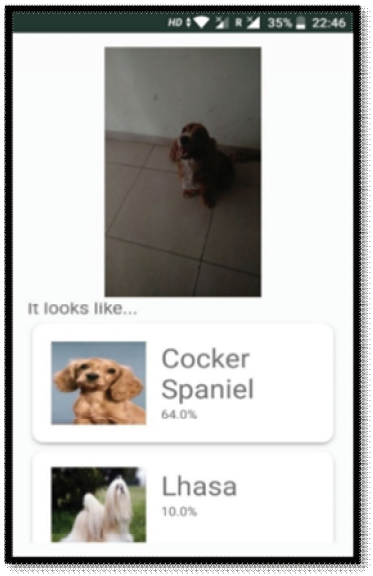

Figure 5. Prediction of uploaded image shown in recycler view

When the user clicks on *view*, 120 dog images of 120 different breeds are displayed; each image, when selected, gives the information regarding that corresponding breed. If the user selects *Instructions,* directions of uploading the image for getting better results are provided.

A. Accuracy

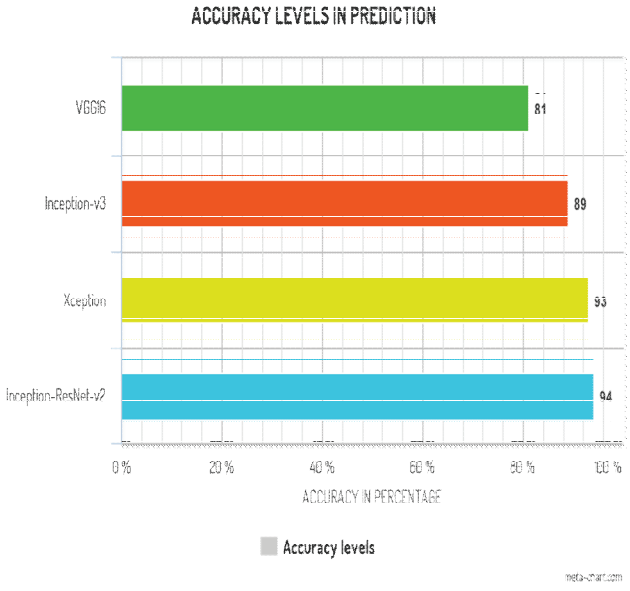

Figure 6. Accuracy levels in prediction of dog breeds with different image feature extraction tools.

Fig. 6 shows the different levels of accuracy achieved, when different pre-trained models for image extractions were used to test the model. Xception and Inception-ResNet-v2 showed the most promising results with an accuracy of 93% and 94% respectively. Inception-v3 and

CVR Journal of Science and Technology, Volume 17, December 2019
DOI: 10.32377/cvrjst1711

VGG16 achieved accuracy levels of 89% and 81% respectively. Overall, results from all the four pre-trained models have very promising accuracy levels.

B. Drawbacks and Limitations

A drawback of the application is that it works efficiently with images captured directly with the camera, but it is not efficient with images captured indirectly i.e. image captured from another image. Another drawback is its size, the application takes more memory than that of a user's convenience.

VI. Conclusion and Future Work

The proposed work is designed, implemented and tested successfully. We have created a user-friendly android application that predicts the breed of a dog by uploading or clicking an image. It works without an internet connection and gives the result instantly, thereby resulting in negligible waiting time. In this paper, we have explained how to build a dog-breed identification model using pre-trained models and deploy it on an android device. In the future, improvements can be made for reduction in the size of the application. Also, enhancements can be made to the model which gives a correct prediction for indirectly captured images as well.

References

[1] Francois Chollet, "Xception: Deep Learning with Depthwise Separable Convolutions", arXiv: 610.02357v3, Apr, 2017.
[2] Alex Krizhevsky, IlyaSutskever and GeoffreyE. Hinton, "ImageNet classification with deep convolutional neural networks", In Neural Information Processing Systems, pp.1106-1114, 2012.
[3] Christian Szegedy, Vincent Vanhoucke, Sergey Ioffe, Jonathon Shlens, ZbigniewWojna, Rethinking the Inception Architecture for Computer Vision, arXiv: 1512.00567v3
[4] Christian Szegedy, Sergey Ioffe, Vincent Vanhoucke, Alex Alemi, "Inception-v4, Inception-ResNet and the Impact of Residual Connections on Learning", arXiv: 1602.07261v2, Aug, 2016.
[5] Barret Zoph, Vijay Vasudevan, Jonathon Shlens, Quoc V.Le, "Learning Transferable Architectures for Scalable Image Recognition", arXiv: 1707.07012v3, Dec, 2017.
[6] Karen Simonyan and Andrew Zisserman, "Very Deep Convolutional Networks for Large-Scale Image Recognition", arXiv: 1409.1556v6, Apr, 2015.
[7] Dylan Rhodes, "Automatic Dog Breed Identification".
[8] J. Liu, A. Kanazawa, D. W. Jacobs, and P. N. Belhumeur, "Dog breed classification using part localization", in Proc. European Conference on Computer Vision, 2012.
[9] C Szegedy, W. Liu, Y. Jia. P. Sermanet, S. Reed, D. Anguelov, D. Erhan, V. Vanhoucke and A. Rabinovich, "Going deeper with convolutions". CoRR abs/1409.4842, 2014.

E-ISSN 2581 – 7957
P-ISSN 2277 – 3916

CVR Journal of Science and Technology, Volume 17, December 2019
DOI: 10.32377/cvrjst1712

Hooke and Jeeves Pattern Search Method and Global Optimal Solution

Dr. M. Raghava[1], B. Rambabu[2], V. Dattatreya[3]
[1]Proffesor, CVR College of Engineering/CSE Department, Hyderabad, India
Email: raghava.m@cvr.ac.in
[2]Assoc. Professor, CVR College of Engineering/CSE Department, Hyderabad, India
Email: b.rambabu@cvr.ac.in
[3]Assoc. Professor, CVR College of Engineering/CSE Department, Hyderabad, India
Email: v.dattatreya@cvr.ac.in

Abstract: **In Data Science, it is imperative to build a model that learns the parameters from the data itself to solve either predictive or prescriptive problems while ensuring improved fidelity of the solution. In this article, we propose to model the non-stationary present in the data in terms of spatial anisotropic interpolation which encapsulates the trend as polynomial regression and characterizes the associated error field as a Gaussian noise process. The fundamental emphasis of the paper lies in the minimization of anisotropic error by learning the model parameters using Hooke and Jeeve's pattern search algorithm, a gradient-free pattern search algorithm and works even in missing value scenarios. The Design and Analysis of the Computer Experiments (DACE) based metaphor are developed and the quality of results are demonstrated on benchmark functions. The proposed implementation essentially has a wide range of applications in Computer Vision, weather prediction, Ore mining, etc.**

Index Terms: **DACE, kriging, anisotropy, interpolation, regression, pattern search.**

I. Introduction

Data Engineering is a branch of Computer Science which deals with understanding the underlying process that generates data and fits a scientific or statistical model through data, analyzes it further explores the hidden patterns and uses them to prescribe a valid set of rules to resolve high-level decisions. Thus, it has changed the fundamental way in which the real-world engineering problems are addressed. The critical part is to identify the associated physical phenomenon and its realization through either statistical or mathematical model building.

Model building involves two equally important major phases namely, Design and Analysis of Data Space and selection of parameter space and it's Fine-tuning. Firstly, a selected model is fit through the data, followed by its execution and evaluation. But in real-world problems, the data generated out of a process may not fit conveniently to a closed function necessitating the application of Machine Learning algorithms [1]. In such cases, engineers alternatively try to develop a robust model that learns the underlying physical phenomenon from the data itself while ensuring certain constraints leading to optimization problems. The constraints often are confined to some standard values while building the model. Most of the times, as the parameters are not properly learned from the nature of the data, the developed models suffer from failures.

Coming to the statistical model building, it begins with collection the data under observation, classify them into dependent and independent variables and develop a function to solve classification or prediction sort of problems at hand with a minimum possible error. This aspect is addressed by answering three functional questions that constitute the data analytics pipeline: What are the variables involved in the scenarios, what kind of relationship can be modeled between the variables and finally what the external parameters are affecting these relations. The model implementation essentially requires evolving a suitable algorithm to realize the solution. Further, the model shall be translated into a computational model with the capability to handle large amounts of data.

Technologies are evolving rapidly into complete ecosystems that help to deal with Big Data. The maturity of statistical models and the latest data visualization techniques constitute the heart of this ecosystem. For example, understanding data properties in terms of moments and trend clearly help in prescriptive and predictive analytics aspects. Model building considers the division of data space into two distinct but important parts; Data Space- deals with data itself, and Parameter Space- tuning the selected parameters that can improve the performance of the solution. Initially, it is carried out by assuming the set of parameters with standard values and generates the model by following a sequence of steps. Select a domain-specific model, implement and execute the model and evaluate the correctness of the model using benchmark test beds. Very often, the model generated fails to offer the desired results reflecting its poor capabilities in capturing the latent relationship between the variables. In that case, the designer often tends to discard the model itself and work on alternatives and evaluate them. However, such a naive approach to juggle with models and flip-flop the solution set-based approach is not a good practice as the span of models available in the literature is really vast. Hence, it is imperative to shift the focus to the parameter space and learning the optimal values of parameters to yield better results from the selected model.

A very good example to illustrate this philosophy is regression. In regression we try to fit a trend surface through the points at which the responses of the system are available with least mean square error [2]. This function is then used to predict the responses at unknown locations. The quality of the results is assessed through the various cross-

E-ISSN 2581 – 7957
P-ISSN 2277 – 3916

DOI: 10.32377/cvrjst1712

validation techniques and error analysis methods. In case of high variance in the error we opt for higher-order polynomials, B-Splines, etc., as the basis functions to represent the trend. However, by its very nature regression is very sensitive to the outliers in the data space [2] and a mere change of basis functions may not result in desired quality predictions. Hence it is essential to switch the focus onto controlling the physical properties of the underlying system by incorporating few parameters and translate them into efficient implementations. One of the simpler means to work out and manipulate these parameters is to employ typical search algorithms that arrive at optimal values of the model. Literature is enriched with plenty of algorithms to predict the optimal value of the parameters. Many of these algorithms analyze the data and learn the parameters from the data itself which is widely referred to as Machine Learning. One such algorithm is Hooke and Jeeves method [3][7] which is a derivative-free method that can optimally search the parameter space and suggest ideal values of the parameters involved in the model. In the upcoming sections, we present different regression trend models and influence of values of parameters and efficient algorithms to arrive at ideal values.

II. KRIGING

Regression analysis involves taking the locations also called design sites at which the responses are available in the form of an array with location-value pairs. As there is an overwhelming amount of data, it becomes difficult to take all the data present into consideration. To alleviate this problem, we try to visualize design sites and design the experiments. While modeling the data it is not always possible to fit a sound surface through the data. This is because there are points farther away from the fit that we call them as outliers and they tend to pull the fit towards them, thus introducing high variance in the error. This error, also known as noise and can manifest in two different types depending on how we characterize it. If we try to characterize the error without a model, then it is called white noise [2]. In contrast if the same is done based on a model-driven by the spatial information then the result is called a stationary noise [3][4].

In regression models, quite often the error is considered to be white noise and disregards the correlation among the design sights across all the statistical moments. Thus, the white noise is an example of *i.i.d.* of random variables. This assumption leads the regression model to become sensitive to outliers. Stationary noise [2] is discrete signal and is similar to white noise but it is a vector that also considers the direction of the noisy data. It depicts what is the underlying shape of the change in error.

As mentioned previously, the best example to realize a prediction model is regression. Generally, there are two types of regressions, namely linear and spatial regression. In linear regression, we encounter and work on white noise whereas in spatial regression we deal with stationary noise. In real-world scenarios, spatial regression is able to solve wide varieties of problems ranging from weather prediction, ore quality assessment, epidemics, etc.

Spatial regression [2][4] deals with stationary noise which is the noise in which change in error depends on the direction. This stationary noise can be classified into three types: zeroth-order noise, first-order noise, and second-order noise. In zeroth-order assumes the trend as a constant, and first-order noise fits a general polynomial across the design space and the error feature has zero mean and in second-order stationary noise case the trend is modeled as a piecewise continuous functions value of mean is zero and variance are finite.

The second-order noise is sub-classified into isotropic and anisotropic noise [4]. Isotropic noise, as assumed to be equally distributed throughout the design space in all directions and can be modeled with relatively simpler efforts. Anisotropic noise varies not only with regard to the lag, i.e. the distance but also with the direction of the target data point. Kriging [3][5] is an implementation of spatial regression which offers a metaphor for the physical process and helps to solve the data prediction problems. The basic kriging model is well explained by the following two steps [3].

A. Model Building

Let $S=\{s_1,s_2,\ldots s_m\}$, $s_i \in \mathbb{R}^2$ contain the design sites and $Y=\{y_1\ y_2\ ,\ldots,y_m\} \in \mathbb{R}$ are associated responses. Let the trend polynomial fit through the design sites is f(s). Let $F \in \mathbb{R}^2$ is a matrix defined by $F= f(s_i)^T$ and R is the matrix representing the spatial correlation among all the design sites. The closed-form of $f(s_i)$ can be a 2-D polynomial involving the polynomial basis functions and cross-terms also. For example, the second-order polynomial is expressed as $f(s_i)= 1+ x_i + yi + x_i^2 + y_i^2 + x_iy_i$. Then the Kriging model [2] which accommodates the error is expressed as

$$F\beta + \varepsilon = Y \qquad (1)$$

For which the generalized least squares solution [2] is,

$$\beta = (F^T R^{-1} F)^{-1} F^T R^{-1} Y \qquad (2)$$

The corresponding variance estimate of the model is

$$\Sigma^2 = (Y - F\beta)^T R^{-1} (Y - F\beta)/m. \qquad (3)$$

Thus, we can observe β and σ^2 depend upon the correlation model.

B. Develop the Predictor.

The Kriging estimator at unknown design site x is given by

$$\hat{y}(x) = f(x)^T \beta + r^T R^{-1} (Y - F\beta). \qquad (5)$$

Here r stands for the vector representing the correlation between the target site and all the design sites. The estimated mean squared error is finite and depends only on the correlation kernel. We can gain control over the error model by imposing a second-order stationary field. And the stationary property is well defined through designing a spatial correlation model. The literature is enriched with the correlation models as listed in [3]. In the present study we are considering only exponential kernel which is expressed as

E-ISSN 2581 – 7957
P-ISSN 2277 – 3916

DOI: 10.32377/cvrjst1712

$$R(\Theta, d) = \exp(-\Theta|d|) \quad (6)$$

It is evident from the equation specified above the spatial correlation exponentially decreases with the lag(d) between the design sites and its behavior is further governed by the parameter Θ. If the components of the vector Θ are equal, then the spatial correlation is an instance of isotropic phenomenon whereas varying values of Θ refer to an anisotropy property. The significance of the vector Θ is it defines the shape of the error field either as a circle or an ellipse. Thus, theta influences the spatial correlation model and hence it is very essential to learn the theta value empirically from the data itself.

III. Hooke and Jeeves method and mult agent implementatio n

To optimally determine the value of Θ literature offers many algorithms such as convergence, gold-section search, Nelder-mead search, Luus–Jaakola[7] search, etc. In this work we have opted to use Hooke and Jeeves method for optimized pattern searching as it is a pattern search-based algorithm. The simplicity of this method lies in its exploratory capabilities and fast convergence. This method is a numerical procedure that is free from computation of gradients and thus avoids the operator selection policy from central, forward and backward differences. Further, if the objective function is not expressed in a closed-form but only the experimental responses are available then pattern search based algorithms are best suited to solve the unconstrained non-linear optimization problems [6]. The quality of the solution of the pattern search algorithm is dependent upon the heuristic rule selection, potentially a hybrid version and its implementation.

Hooke and Jeeves pattern search method [4] solves the optimization problem by generating the state space in explorative manner and proceeds to new state so long as the solution gets optimized. Otherwise, the algorithm retracts to the old state from the new state and proceeds in a different direction. The number of directions in which the exploration happens also can be configured. For example, in 2-D case the exploration directions can be either 4 or 8. In the case of higher-dimensional space exploration takes place sequentially along different directions.

While exploring along i^{th} dimension the optimal values along all the preceding dimensions are frozen. Once a local optimal has arrived then the algorithm anneals to new location, which we refer to as Pattern Move, along the direction in which partial optimal solution is realized. These two steps are repeated until optimal solution is realized. On the other hand, if the new pattern fails to generate further improved solution the solution backtracks to old state and explores for the optimal solution in a different direction that realizes the complete span of the search space. The algorithm strives to reach an optimal location from a random location in two types of moves Exploratory and Pattern Move as discussed below

1. Exploratory Search: A local move to seek an optimal solution. Given the current location X_c, one of the features of the location is perturbed in forward and backward directions and the feature is updated with the new value at which function evaluates to the maximum. Such a similar procedure is repeated with reference to each pattern, one at a time and new best location is configured. We characterize the exploratory move as a success if the new location is different from the initial location otherwise the move stands for failure. The outcome of the experiment is the new location.

Let X_c is the current state of the solution. Assume that the i^{th} component of X_c is perturbed by p while retaining the values of other features. Algorithm 1 lists out the behavior of Explore step for each feature X_i of the solution vector X_c. The function is evaluated at locations X_i, X_{i+} 1, and X_{i-} 1 and updates the component with the location at which the minimum value of the function is achieved. This process is repeated for all components of X_c. The algorithm returns success if new location X_n with optimal value of f is reached otherwise the Exploration returns a failure.

2. Pattern Move: Upon success from Exploration step the pattern move is taken with a leap in the direction of line joining $X_c$with X_n

A. Algorithm 1:

// Initialization $X_n := X_c$

Step 1: Calculate f:= f ($X_{c,i}$), the forward value f+ := f ($X_{c,i}$ + 1) and backward value f- := f ($X_{c,i}$, - 1).

Step 2: Find fmin := min (f, f+, f-).
Set $X_{n,i}$ that corresponds to f_{min}.

Step 3: Check i == N? If no, set i := i + 1 and go to Step 1;
Else X_n is the result and goto Step 4.

Step 4: If X_n != X_c, success; Else failure.

Step 5: Make pattern move
$X_p = X_n + \alpha(X_n - X_c)$

Step 6: Evaluate f at X_p. If it is evaluated to be better then control is transferred to Step 1. Otherwise, reduce the step size i.e. the value of α in Step 5.

Thus Hooke-Jeeves method switches between two steps Exploratory Search and Pattern Move. In the first step local optimal value is located in the vicinity and the latter step takes the solution to a new pattern in the direction of successful exploration with a long leap and repeats the Exploratory step. If the exploration at the new pattern is in vain then the quantum of leap is reduced.

In this paper, Hooke and Jeeves method is implemented to feature a parallel search mechanism by dividing the search space into disjoint regions and multiple parallel exploring agents are launched across these regions. Each agent is perceived as a random initial location in the given sub-region. The solutions generated by the exploration followed by pattern move from different agents are compared and the best solution is adapted. This parallel and divide and conquer strategy helps the empirical model to realize the global optimal solution and avoids the local optimal solution.

E-ISSN 2581 – 7957
P-ISSN 2277 – 3916

DOI: 10.32377/cvrjst1712

In the current work, a User Interface (UI)[7] had been designed by implementing a singleton pattern. The use-cases include actor being able to select a benchmark non-linear function, correlation kernel, and the number of orientations that are required by the program. Each input field is labeled with the corresponding name so that the user will find it easy to type or select the input. The other set of fields that are required are the x and y coordinates that refer to initial location of each agent, delta value, epsilon value, number of rotations and number of iterations.

The following experiments demonstrate the results of the proposed model on benchmark mathematical functions that are available in the public domain of the internet.

B. Experimental Results:

Function: Sum Square
EQUATION: $(x - 2)^2 + (y - 2)^2$ (7)
X - Value: 11
Y - Value: 13
EPSILON: 0.01
DELTA: 0.5
ITERATIONS: 150

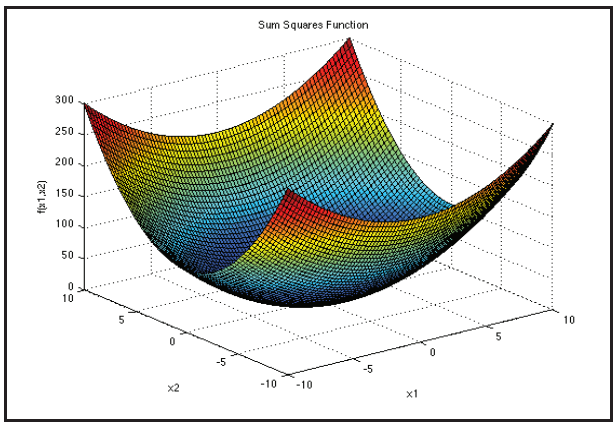

Figure1. 3-D plot

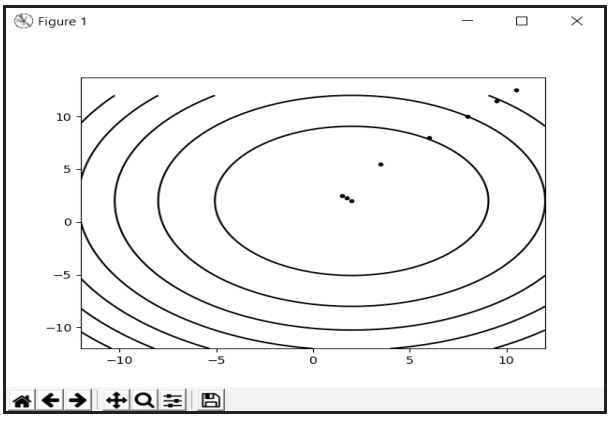

Figure 2. Contour Map

The 3D representation of the sum square function depicts the span of the function over the data space in Figure1, Figure2 presents the Contour Map to demonstrate the convergence of the algorithm in the form of traces of the solution and the benchmark function is presented in contour form. It clearly demonstrates that the solution which is started at a random location is eventually reaching the optimal value of the function by making the pattern moves. A similar analogy is applied to the subsequent benchmark function evaluations shown in Figure 4 and Figure 6.

Function: Matyas
EQUATION: $0.26(x^2 + y^2) - 0.48xy$
X - Value: 12
Y - Value: 14
EPSILON: 0.0001
DELTA: 0.5
ITERATIONS: 100

The 3D representation of the Matyas function is depicted in Figure 3 along with span of the function over the data space.

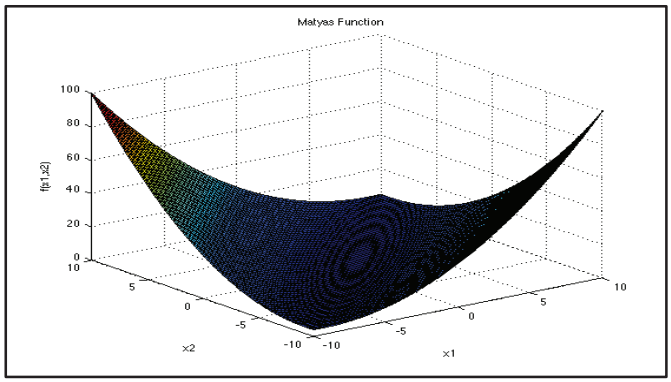

Figure 3. 3-D plot

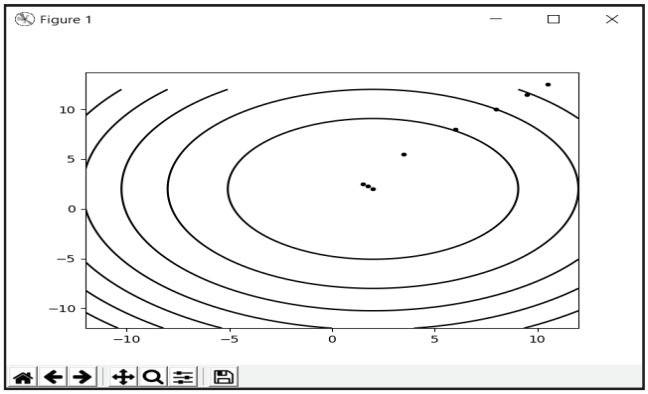

Figure 4. Contour Map.

Function: Beale
EQUATION:
$(1.5 - x + xy)^2 + (2.25 - x + xy^2)^2 + (2.625 - x + xy^3)^2$
X - Value: 5
Y - Value: 5
DELTA: 0.5
EPSILON: 0.01
ITERATIONS: 200

E-ISSN 2581 – 7957
P-ISSN 2277 – 3916

DOI: 10.32377/cvrjst1712

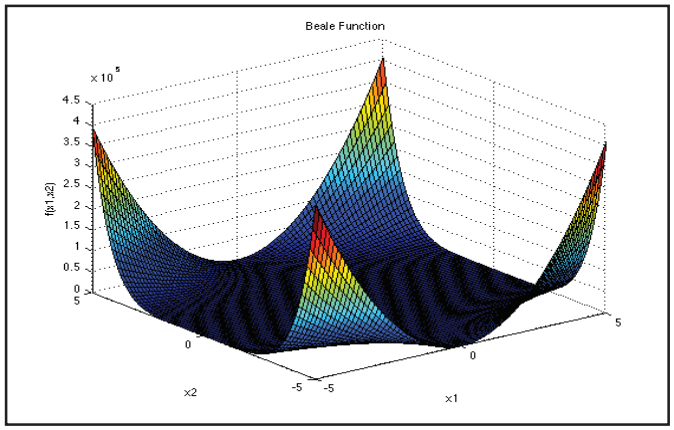

Figure 5. **3-D plot**

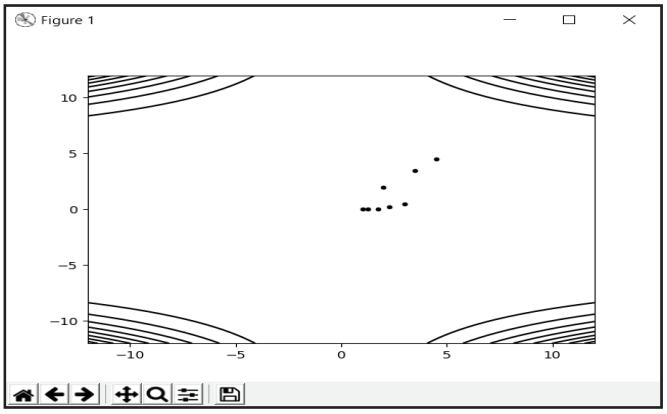

Figure 6. Contour Map.

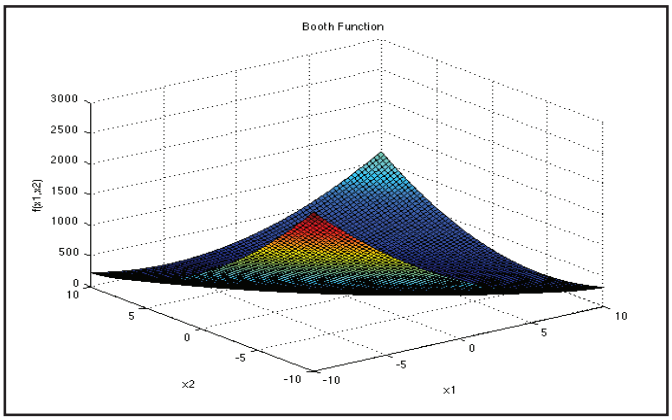

Figure 7. 3-D plot

The 3D representation of the Beale function is depicted in Figure 5. The function spans over the data space and has multiple optimal values.

In this testing process we choose a Beale function with starting coordinates as (5, 5) and having delta value 0.5 with epsilon value 0.01 with value check in eight directions.

Function: Booth

EQUATION: $(x + 2y - 7)^2 + (2x - y - 5)^2$

X - Value: 5

Y - Value: 5

DELTA: 0.5

EPSILON: 0.01

Figure 7 presents a 3D representation of the booth function and depicts the span of the function over the data space.

In this testing process, we choose a booth function with starting coordinates as (7,8) and having delta value 0.5 with epsilon value 0.001 with value check in four directions.

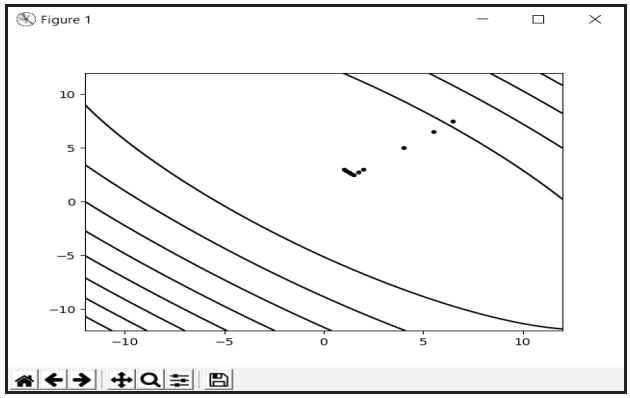

Figure 8. Contour Map.

TABLE I.
SHOWING THE CONVERGENCE OF THE PROPOSED ALGORITHM

Function	Initial Solution	Delta, Epsilon	Final Solution	Expected Solution
Circle	(11,13)	0.5, 0.01	(2,2)	(2,2)
Matyas	(12,14)	0.5, 0.0001	(0,0)	(0,0)
Beale	(5,5)	0.5,0.01	(3.0, 0.5)	(3.0,0.5)
Booth	(7,8)	0.5,0.001	(1.0, 3.0)	(1.0, 3.0)

Table 1 presents a summary of the results validating the performance of the algorithm on the benchmark functions.

IV. CONCLUSIONS OF THE PRESENT STUDY

This paper successfully validated optimization results for various benchmark functions. The analytically calculated optimum solution is best matched with closed-form solution. The paper also, demonstrated the parallel implementation of Hooke and Jeeves method that avoided the local optimal problem. The percentage error in analytical and python results depend on the number of iteration steps, length of data sets, objective function and constrained for optimization.

REFERENCES

[1]. Bishop, C. M. Pattern Recognition and Machine Learning, Springer, ISBN 978-0-387-31073-2, 2006.

[2]. Gentile, M., Frederic Courbin and Georges Meylan. "Interpolating point spread function anisotropy." Astronomy & Astrophysics manuscript, 2013.

[3]. Søren N. Lophaven, Hans Bruun Nielsen, Jacob Søndergaard, "*Correlation Models",* Aspects of the Matlab Tool DACE,Technical University of Denmark,DK-2800 Kongens Lyngby – Denmark, pg 10-39

[4]. Raghava, M., Arun, Agarwal., Raghavendra, Rao C. A Scalable Spatial Anisotropic Interpolation Approach for Object Removal from Images using Elastic Net

Regularization, MIWAI 2016, Thailand, LNCS, Vol 10053,126-140, 2016. (ISBN: 978-3-319-49396-1)

[5]. Couckuyt, I. and Forrester, A. and Gorissen, D. and De Turck, F. and Dhaene, T. Blind Kriging: Implementation and Performance Analysis, Adv. Eng. Softw.1-13, ISSN 0965-9978, 2012.

[6]. L. Armijo, Minimization of functions having Lipschitz continuous first partial derivatives, Pacic Journal of Mathematics, 16, pp. 1-3. 1966.

[7]. Hooke R & Jeeves T A. "Direct search" solution of numerical and statistical problems. J. Ass. Comput. Mach. 8:212-29, 1961.

[8]. Mark Summerfield, Rapid GUI programming with python and QT, 269 – 283, Prentice hall, ISBN-10: 0134393333, 2009.

E-ISSN 2581 – 7957
P-ISSN 2277 – 3916

CVR Journal of Science and Technology, Volume 17, December 2019
DOI: 10.32377/cvrjst1713

Analysis of Image Pre-processing in Noisy Character Recognition

Priyanka Gupta
[1]Asst. Professor, CVR College of Engineering/ CSE Department, Hyderabad, India
Email: prionnet@yahoo.com

Abstract: **This paper demonstrates the importance of various pre-processing steps for the noisy character recognition system with the help of MATLAB simulated results. Image pre-processing is one of the first and foremost steps for working with images of noisy characters among handwritten characters, printed characters, online written characters or offline written character, and it can have mixed font characters, omni-font characters, boxed discrete character, spaced discrete character or pure cursive script writing. Pre-processing of such image aims at image noise reduction, image normalization, and image compression. This paper shows that there are various steps/methods of image pre-processing. The sequence and use of a particular step/method is used based on the application requirement. The simulation result presented in this paper highlights the usability of each pre-processing steps and review the commonly used methods of each preprocessing stage.**

Index Terms: **Noisy Character, Thresholding, Noise, Character Recognition, image pre-processing**

I. Introduction

Noisy character recognition is one of the classical area of pattern recognition research for many years. Researchers have used many methods for recognizing the noisy text. Considering the significance image preprocessing, in this paper we have reviewed major methods used for various application. The main purpose of this paper is to present comprehensive literature of all image pre-processing methods at one place to serve as reference to many other researchers. The significance of each step is demonstrated with the help of simulation result as per the parameters listed in Table 1.

A. Noisy character recognition design

The stages for the noisy character recognition system from a character pixel to text recognition are as follows:

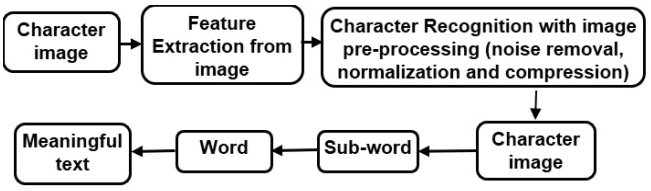

Figure 1. Various steps of the character recognition system

From the literature survey [1-4], it has been concluded that the overall neural network character recognition process can be grouped into the various stages such as: image pre-processing, image segmentation, image feature extraction, training of the network and recognition of character. Depending upon the desired system output and application, stages in the character can be combined or omitted.

B. Pre-processing

Out of the various stages in the noisy character recognition system, image pre-processing [3-4] of noisy character is foremost and necessary step to make the noisy character image appropriate for the further processing of image such as: segmentation and feature extraction algorithms. The main objective of image pre-processing step to make the task of the character recognition system easy and helps improve the overall accuracy by providing clean images. The main steps involved in the image pre-processing are: noise reduction, normalization, and compression.

Noise Reduction: Noise may get incorporated into the character image either during the process of scanning the document from optical scanning devices or during the writing of the document. The different persons have a slightly different style of writing the same character; as a result, they have varied line-disconnected segments, character-bumps, gaps between lines and filled loops, etc., Such noise can be reduced by filtering and morphological operations.

Normalization: Normalization is used to get the standardized data from the set of raw data acquired from various sources by reducing the variations that has been got during writing. The basic normalization techniques are: size normalization, slant normalization, and skew normalization.

Compression: Compression is used to improve speed of character recognition by reducing the size of the input data. To meet this image thinning and image thresholding algorithms are used apart from classical lossless image compression technique.

II. Noise Reduction

Noise reduction is the process by which we can remove noise from the acquired character image. Images may have noise from different sources such as an optical scanning device, writing instruments, etc. It is mandatory to remove the noise from these characters images in order to get a clean image for the character recognition system. Depending upon the acquired images, various types of noise removal techniques are used. In this section, it has been implemented the various commonly used noise reduction techniques and demonstrated the suitability of each technique with MATLAB simulation results.

E-ISSN 2581 – 7957
P-ISSN 2277 – 3916

DOI: 10.32377/cvrjst1713

A. Smoothing

Smoothing of the image character helps in acquiring the important pattern of data by removing the finer pattern. During image smoothing, pixel intensity levels are smoothened by modifying the data points in an image by some kind of local average intensity level of the surrounding data point pixel of. Smoothing may be used in two ways for the data analysis of the acquired characters.

In the case of smoothing assumption is correct, it will help to extract the better information. Also, help in identifying the data-points, which are flexible and robust. Image smoothing can be done with the help of various algorithms. Usually, image smoothing is done through density estimators like the histogram. Apart from these, smoothing also may be done using various filtering techniques.

Out of the various kinds of filters, Gaussian smoothing filters [5-6] are most widely used to reduce the noise. Gaussian smoothening filters are generally isotropic in nature and have the same standard deviation along with both axes. The scale of smoothing can be chosen by taking a suitable value of sigma. In [6], Gaussian mixture model Symmetric Smoothing Filter (GSF) has been designed to improve the performance of the Gaussian-smoothing filter further. Smoothed image using a normal Gaussian smoothening filter is given in Fig.3.

Figure 2. Input image of handwritten characters

Figure 3. Smoothen image of Fig. 2 using Gaussian smoothening filter with $\sigma = 2$. .

B. Sharpening

Image sharpening is used for enhancing the character's edges and other finer details. To improve the sharpness of the original image, a high pass filter version of the original image is added to the same images. Mathematically, image-sharpening operation in the spatial domain can be represented as

$$O(i,j) = I(i,j) + \lambda H\{I(i,j)\} \quad (1)$$

Where $I(i,j)$ is a spatial representation of the original image at (i,j) coordinate, H is the high-pass filter operator, λ is a sharpness tuning parameter greater than or equal to zero, and $O(i,j)$ is the output sharpened the image at the same coordinate. Depending upon the sharpness required λ value can be suitably chosen. Generally, increasing λ yields a more sharpened image.

Unsharp masking [7-8] is one of the most widely used technique for image sharpening. In this technique, image enhancement is done by subtracting a blurred version of the image from itself. Fig. 4 show the sharpen image using unsharp masking.

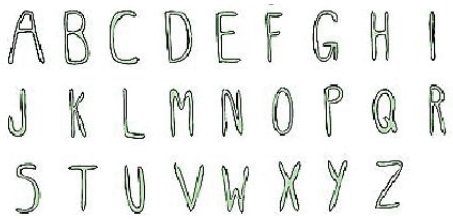

Figure 4. Sharpened image of Fig. 2 using the unsharp-masking filter.

Sharpening of the image can be further improved by the use of adaptive unsharp masking [7] or blurriness guided unsharp masking [8].

C. Thresholding

Scanned character images are represented in gray level format. In the gray level representation intensity level of each pixel of the image, varying between 0 to 255. Hence, various shades of gray are possible between these two values. To remove this ambiguity gray level image is transformed to a binary image using thresholding or binarization. During this process, the level is restricted to '1' or '0', indicating the presence or absence of the character pixel. This conversion is done by selecting a suitable threshold intensity level, above the threshold level intensity are marked as character-background '1' and below the intensity level marked as '0' character image or vice versa.

Depending on the input character image various thresholding algorithms can be: global [9] or locally adaptive methods [10]. In the case of the global adaptive thresholding algorithm, a single threshold intensity is calculated for the overall scanned characters image. While, in the case of the locally adaptive algorithm, the various threshold levels are possible on the variation of pixel level in the neighborhood of the particular character. Fig 5. and Fig. 6 shows the output image using global and locally adaptive thresholding technique respectively.

D. Contrast adjustment

Perceptivity of the particular region in the character image can be improved by contrast adjustment. During this process, contrast is improved by increasing the pixel intensity value difference between the desired region and its background. In contrast adjustment, intensity values of the images are remapped to the full display range of the data type. A good contrast image has a large difference between the intensity values of black and white representation. Contrast adjustment can be done with intensity value remapping based on various statistical parameters.

Image intensity adjustment [11], histogram equalization and adaptive histogram equalization [12-13] are a few of

E-ISSN 2581 – 7957
P-ISSN 2277 – 3916

DOI: 10.32377/cvrjst1713

popular contrast adjustment. Fig. 7, Fig. 8 and Fig. 9 show the contrast adjusted image using intensity adjusted, histogram equalization and adaptive equalization technique.

Figure 5. Binary image of Fig. 2 gray image using global thresholding

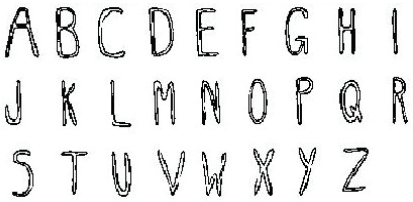

Figure 6. Binary image of Fig. 2 image using locally adaptive thresholding

Figure 7. Contrast adjusted image of Fig. 2 image using intensity adjustment

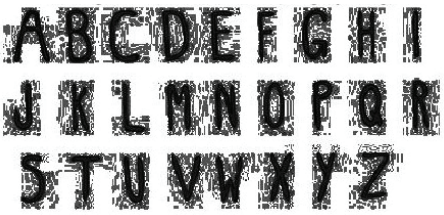

Figure 8. Contrast adjusted image of Fig. 2 gray image using histogram equalization

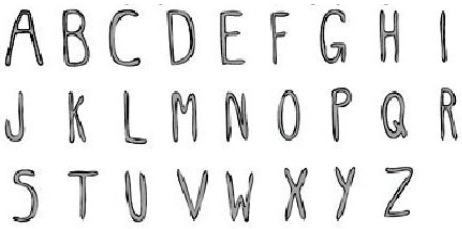

Figure 9. Contrast adjusted image of Fig. 2 gray image using adaptive histogram equalization

E. Edge detection

Edge detection is used to detect a sudden change in the intensity level. Edge is associated with the region of sudden discontinuities. There are various methods based on the threshold value of gradient [14-15] or zero crossing for edge-detection [14-15]. The most popular methods based on the threshold value of gradient are: Sobel, Prewitt, Roberts, as demonstrated in Fig. 10, Fig. 11 and Fig. 12, and zero-crossing are: zero crossings after Laplacian of Gaussian filter/any other filtering of the input image as shown in Fig. 13 and Fig. 14. However, both of these methods are likely to be fooled by noise in case of weak edges. In [16], the Canny method is using a gradient calculated from the derivative of Gaussian filter and based on two thresholding for weak and strong edges, hence it is difficult to be fooled by noise as shown in Fig. 15.

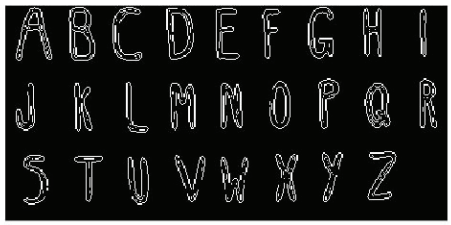

Figure 10. Edge detection of Fig. 2 gray image using the Sobel method

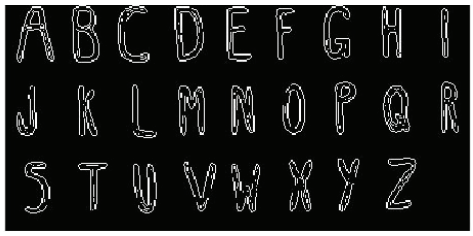

Figure 11. Edge detection of Fig. 2 gray image using Prewitt method

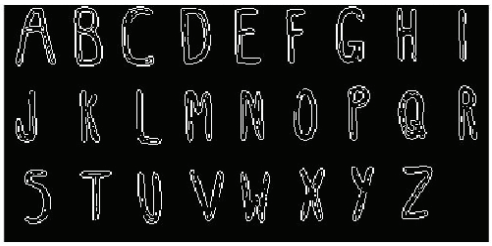

Figure 12. Edge detection of Fig. 2 gray image using the Roberts method

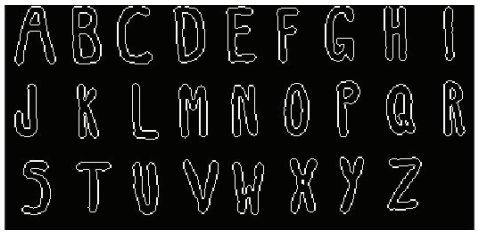

Figure 13. Edge detection of Fig. 2 gray image using the zero-cross method

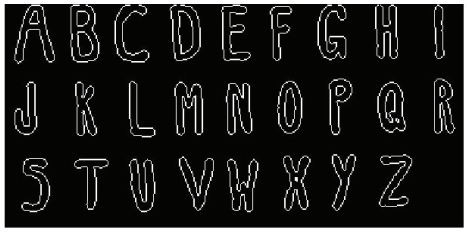

Figure 14. Edge detection of Fig. 2 gray image using zero-crossing of Laplacian of Gaussian filter

E-ISSN 2581 – 7957
P-ISSN 2277 – 3916

CVR Journal of Science and Technology, Volume 17, December 2019
DOI: 10.32377/cvrjst1713

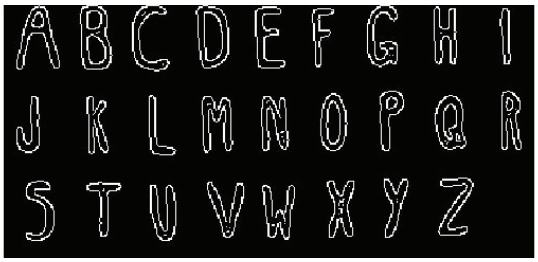

Figure 15. Edge detection of Fig. 2 gray image using Canny method

F. Erosion

Erosion is a morphological image processing technique [17] for a binary image I, erosion by a structuring element 'S', produces an output image 'O', with '1' in all the locations of (x,y) of 'S' at which 'S' fits 'I'.

I(x,y) = 1 is 'S' fits 'I' and 'O' otherwise, repeating for all pixel coordinates (x,y). Dilation removes a layer of pixels to both the inner and outer boundaries of the region. Fig. 16 demonstrates the erosion of the input gray image with 'holes' as structure element.

$$O = I \Theta S \tag{2}$$

Figure 16. Eroded image of Fig. 2 gray image

G. Dilation

Dilation is a morphological image processing technique [18], for a binary image 'I', erosion by a structuring element 'S', produces an output image 'O', with '1' in all the locations of (x,y) of 'S' at which 'S' hits 'I'.

I(x,y) = 1 is 'S' hits 'I' and '0' otherwise, repeating for all pixel coordinates (x,y). Dilation adds a layer of pixels to both the inner and outer boundaries of the region. Fig. 17 shows the erosion of the input gray image with 'square' structure element of size '2'.

$$O = I \oplus S \tag{3}$$

Figure 17. Dilation image of Fig. 2 gray image

TABLE I.
SUMMARY OF VARIOUS SIMULATION PARAMETER

S. No.	Pre-processing step	Parameter value
1.	Smoothening	$\sigma = 2$
2.	Adaptative thresholding	sensitivity=0.4
3.	Erosion	square of size 2
4.	Dilation	square of size 2

III. NORMALIZATION

Normalization [19-20] refers to operations such as the estimation and correction of a character's slant, scaling the character to a uniform size and also possibly reducing the character to a skeleton so that the line width is uniform, one unit wide. Depending upon the variation among the character image, various types of normalization methods can be used such as:

- Skew Normalization
- Slant Normalization
- Size normalization
- Curve Smoothing

IV. COMPRESSION

Compression of input data is desired, to improve the speed of character recognition. In addition to classical lossless image compression technique, thresholding and thinning [21-23] are the most popular techniques in the character recognition system.

Thresholding: It dramatically reduces the size of input grayscale image by representing it using only two intensity i.e., '0' and '1'. Because of the reduction size, it improves the processing speed of character recognition system [21].

Thinning: During this process similar value intensity level represented by a single value. Hence, during this process, there is a possibility of reducing compression. It helps in extracting desired information from the shape of the stroke. Thinning can be done pixel-wise or non-pixel wise [22-23]. Pixel level thinning is done using erosion and iterative contour pealing until one-pixel wide skeleton remained. This type of thinning is sensitive to noise and may lead to deformation of the character shape. In the case of non-pixel thinning global information of the character used for thinning. Fig. 18 represents, thinning of edge detected image Fig. 15 after image filling.

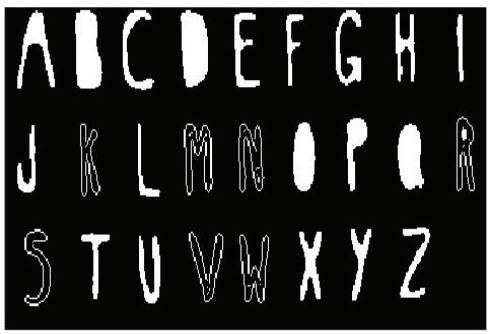

Figure 18. Thin image of the edge detected image Fig. 15 after image filling

V. Conclusion and Discussion

Image pre-processing is one of the most significant steps of character recognition. It is a multi-step process and the use of a particular step or not depending on the quality of input image. This paper shows the stage-by-stage analysis of each image-preprocessing stage with-respect to character recognition with the simulation result. The simulation parameters used in each stage such as smoothening, sharpening, normalization etc., can be further tuned based on the application requirement. Further work can be done by using the preprocessed image for a character recognition system that may be statistical ACR (Automatic Character Recognition) technique, Syntactic ACR technique or character recognition using neural networks.

References

[1] Y, Shi, W. Fan, G. Shi, "The research of printed character recognition based on neural network", *IEEE 4th International symposium on parallel architectures, algorithm and Programming*, pp. 119 – 122, 2011.

[2] H. Fujisawa, "Forty Year of research in character and document recognition an industrial perspective", *Elsevier-Patten Recognition*, vol. 41, no. 8, pp. 2435-2446, 2008.

[3] M. Cheriet, N. Kharma, C. L. Liu, C. Y. Suen, "Character Recognition System –A guide for students and Practioners ", *Wiley-Interscience Press*, 2007.

[4] W. Bieniecki, S. Grabowski, and W. Rosenberg, "Image pre-processing for improving OCR accuracy," *IEEE Int. Conf. on Perspective Technologies in MEMS Design*, pp. 75-80, 2007.

[5] L. Sorba, J. Grman, R. Ravas, "Impact of Gaussian noise and image filtering to detected corner points positions stability", *MEASUREMENT 2017,* Proceedings of the 11th International Conference, Smolenice, Slovakia, pp. 123-126.

[6] Stanley H. Chan, Todd Zickler, Yue M. Lu, "Understanding Symmetric Smoothing Filters: A Gaussian Mixture Model Perspective", *IEEE Trans. On Image processing*, pp. 5107 – 5121, Vol. 26(11), 2017.

[7] A. Polesel, G. Ramponi, V.J. Mathews, "Image enhancement via adaptive unsharp masking", *IEEE Trans. On Image processing*, pp. 505 - 510, Vol. 9(3), 2000.

[8] Wei Ye, Kai-Kuang Ma, "Blurriness-Guided Unsharp Masking", *IEEE Trans. On Image processing*, pp. 4465 - 4477, Vol. 27(9), 2018.

[9] Otsu, N., "A Threshold Selection Method from Gray-Level Histograms," *IEEE Transactions on Systems, Man, and Cybernetics*, Vol. 9, No. 1, 1979, pp. 62-66.

[10] Bradley, D., G. Roth, "Adapting Thresholding Using the Integral Image," *Journal of Graphics Tools*. Vol. 12, No. 2, 2007, pp.13-21

[11] A. Nandal, V. Bhaskar, A. Dhaka, "Contrast-based image enhancement algorithm using grey-scale and colour space", IET signal processing, Vol. 12(4), 2018, pp. 514 – 521.

[12] Yi-Chong Zeng, "Automatic local contrast enhancement using adaptive histogram adjustment", *IEEE International Conference on Multimedia and Expo 2009*, New York, NY, USA, pp. 1318-1321.

[13] Y. Wang, Q. Huang, J. Hu, "Adaptive Enhancement for Low-Contrast Color Images via Histogram Modification and Saturation Adjustment", *IEEE 3rd International Conference on Image, Vision and Computing (ICIVC) 2018*, Chongqing, China, pp. 405-409.

[14] S. J. Lim, Two-Dimensional Signal and Image Processing, *Englewood Cliffs*, NJ, Prentice Hall, 1990, pp. 478-488.

[15] J. R. Parker, Algorithms for Image Processing and Computer Vision, New York, John Wiley & Sons, Inc., 1997, pp. 23-29.

[16] J. Canny, "A Computational Approach to Edge Detection," *IEEE Transactions on Pattern Analysis and Machine Intelligence*, Vol. PAMI-8, No. 6, 1986, pp. 679-698.

[17] J. M. C. Brown, J. E. Gillam, D. M. Paganin, M. R. Dimmock, "Laplacian Erosion: An Image Deblurring Technique for Multi-Plane Gamma-Cameras", *IEEE Transactions on Nuclear Science*, Vol. 60(5), 2013, pp. 3333 – 3342.

[18] A. N. Rahman, O. Heriana, P. Putranto, et. al., "Morphological dilation for radar image enhancement", *International Conference on Radar, Antenna, Microwave, Electronics, and Telecommunications* (ICRAMET), 2017, pp. 68-71.

[19] M. Kozielski, J. Forster, and H. Ney, "Moment-based image normalization for handwritten text recognition," in *International Conference on Frontiers in Handwriting Recognition*, Bari, Italy, Sep. 2012, pp. 256-261.

[20] W. Guerfaii and R. Plamondon, "Normalizing and Restoring On-line Handwriting", *Elsevier-Patten Recognition*, vol. 26, no. 3, pp. 418-431. 1993.

[21] H. Sung, "A Skip-line with Threshold Technique for Binary Image Compression," Master Thesis, Fu Jen Catholic University, Taipei, Taiwan 106, R.O.C, Jul. 2008

[22] T. Abu-Ain, S. N. H. S. Abdullah, B. Bataineh, K. Omar, "A fast and efficient thinning algorithm for binary images", *J. ICT Res. Appl.*, vol. 7, no. 3, pp. 205-216, 2013

[23] H.K. Anasuya Devi, "Thinning: A Pre-processing Technique for an OCR System for the Brahmi Script", *Ancient Asia*, vol.1, pp 167-172, 2006.

E-ISSN 2581 – 7957
P-ISSN 2277 – 3916

CVR Journal of Science and Technology, Volume 17, December 2019
DOI: 10.32377/cvrjst1714

Imbalanced Big Data Classification using Feature Selection Under-Sampling

Ch. Sarada[1] and M. Sathya Devi[2]
[1] Asst. Professor, CVR College of Engineering/CSE Department, Hyderabad, India.
Email: sharada.ch@gmail.com
[2] Asst. Professor, CVR College of Engineering/CSE Department, Hyderabad, India.
Email: satyamaranganti@gmail.com

Abstract: **Imbalanced learning is the classification problem where the number of observations of one class, far surpasses the number of observations of another class. Different sampling approaches are proposed for paired and Multi-Class imbalanced classification. Paired Imbalanced classification encompasses two classes: one of them is majority, while the other one is a minority class. Multi-Class imbalanced classification contains more than two classes for classification. Under-sampling technique is the better sampling technique among conventional approaches. However, existing approaches may not work in the Big Data environment, as considering all the features might compromise the performance of the system. In this work, a novel method is presented which takes into account only the essential features, as well as, deals with massive data as in Big Data environment. In the proposed system, Feature Selection Under-Sampling technique is used for resampling the data. Feature selection is the vital step because it not only decreases the dimensionality of data but also helps classifier to run faster, and accuracy can also be improved. Over that, SVM learning classifier is adopted to construct the model and test the data. The proposed system is implemented using MapReduce framework by integrating statistical analytical tool R.**

Index Terms: **Big Data, Imbalanced learning, Sampling technique, MapReduce, SVM.**

I. Introduction

Imbalanced classification is the situation where the number of specimens with one class label is outstandingly lower than the specimens with other class label. In imbalanced dataset, the class with a relatively high number of specimens is called the majority class while the other one with less number of specimens is called the minority class [1][2]. This issue is prevalent in situations where an abnormal condition is vital, for eg., power pilferage, fake exchanges in banks, rare disease detection etc. In these situations, the traditional classification techniques might not give accurate results and in some cases the results can be predicted wrongly. This happens on the grounds that the traditional classification algorithms are normally intended to enhance accuracy by decreasing the error. This is because machine learning algorithms are designed to improve accuracy by reducing the error. Therefore, traditional classification models will not take imbalance ratio into consideration.

The class imbalance problem was handled at various stages like data level and algorithm level [22]. At the data level, solutions consist of different kinds of re-sampling techniques. At the algorithm level, we have cost learning algorithms which would incur more cost for misclassified minority (positive) samples and less cost for misclassified majority (negative) samples. Some of the Sampling approaches proposed are Random Over-Sampling [12][21], Random Under-Sampling [7][21] and SMOTE [4]. Popular cost learning approaches include SVM [17], k-Nearest Neighbour (kNN)[18], neural networks, genetic programming and rough set based algorithms. Under-sampling is better technique out of different traditional sampling techniques [28]. However, the existing imbalanced classification approaches cannot be adapted to the Big Data environment as the Map Reduce approach does not support these algorithms directly. Hence, a novel approach is proposed to handle the imbalanced classification problem on the massive amount of data by considering only essential features which would optimize the execution speed of the classifier and also improves its accuracy.

In this paper, the "Recursive Feature Elimination Under-Sampling" scheme is used to address the binary class imbalanced classification on the massive data. MapReduce framework with integration of statistical tool R is used for implementation. It is developed with a two-phase MapReduce. In the first phase, Feature Selection [2] is applied at every mapper to detect prominent attributes, then under-sampling is applied on the resultant dataset partition to balance it. On the resultant partitioned balanced dataset, SVM classification algorithm is applied to construct a model. Models generated by all mappers are saved for future use. In the second stage, saved models are tested with three UCI repository datasets [23]. UCI is the renowned Repository for real databases that are being used by various research communities for experimental analysis. It is observed that the accuracy of the new system is better when compared to a conventional SVM approach.

The rest of the work is organized as follows: Section 2 presents related work in imbalanced classification using sampling techniques. Section 3 describes Proposed architecture. Section 4 is about Experimental analysis and finally, Section 5 summarizes the conclusions and future scope.

II. Related Work

This section reviews the Binary Imbalanced learning as well as MapReduce Framework.

E-ISSN 2581 – 7957
P-ISSN 2277 – 3916

CVR Journal of Science and Technology, Volume 17, December 2019
DOI: 10.32377/cvrjst1714

A. Binary Imbalance Classification Problem

Binary imbalance classification is a two-class imbalanced learning problem where the total specimens in one class is extremely higher than the total specimens in other class.

B. Existing Solutions of Binary Imbalance Classification Problem:

Adequate number of solutions have been proposed previously to handle the binary class imbalance classification issue. They are data pre-processing approach and algorithm approach. In data pre-processing approach, sampling technique is used to equalize the number of specimens in both the classes. Sampling techniques include Random Under-Sampling [7] [21], Random Over-Sampling [12][21] and SMOTE[4].

Sampling strategies focus on altering the distribution of training data either randomly, or by scaling existing specimens. This scaling can be done by either adding or removing existing specimens. Adding or removing of specimens depends on sampling technique used. In Random over-sampling, duplicate specimens are added randomly. In SMOTE over-sampling approach, k-Nearest neighbour specimens are added. In Random under-sampling, specimens that do not bring any improvement are removed.

i) Random Oversampling

Random Oversampling is a sampling technique where in a number of minority specimens are increased to balance the dataset. Random Over-Sampling [12][21] is simple to implement because minority specimens are increased just by duplicating existing specimens. However, it causes an overfitting because of the repetition of minority class instances. Random Over-Sampling is shown in the figure 1.

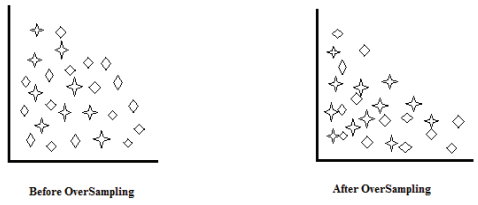

Figure 1.Random Oversampling

ii)Random Undersampling

It is the sampling technique wherein majority specimens are eliminated randomly [7] [21]. It randomly removes the majority class information to balance the dataset. However, it may discard the crucial specimens. In order to attack the issue of potential information loss, "near neighbor" method and its variations have been proposed. The basic algorithms of the near neighbor family are this: first, the method calculates the distances between all instances of the majority class and the instances of the minority class. Then k instances of the majority class that have the smallest distances to those in the minority class are selected. If there are n instances in the minority class, the "nearest" will result in k*n instances of the majority class.

"NearMiss-1" selects samples of the majority class that their average distances to three closest instances of the minority class are the smallest. "NearMiss-2" uses three farthest samples of the minority class. "NearMiss-3" selects a given number of the closest samples of the majority class for each sample of the minority class. Random Under-Sampling is shown in the figure 2.

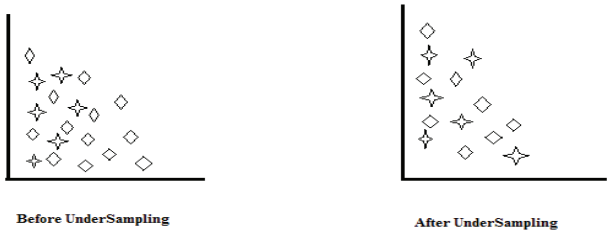

Figure 2.Random Undersampling

iii) SMOTE: Synthetic Minority Oversampling

SMOTE is an over-sampling approach proposed by Chawla et al [16],[4]. In SMOTE, *"synthetic"* specimens are created to increase the size of minority class. Unlike Random Over-Sampling that duplicates the specimens, SMOTE produce synthetic minority class specimens using k-Nearest neighbours, augmented with randomized interpolation. However, noise might be included in synthetic minority class examples.

C. MapReduce Framework

The MapReduce framework [3] is used to process huge amounts of data in parallel. In Hadoop environment, data gets distributed among all nodes and it is processed in parallel.

The MapReduce framework [3] uses three phases like Map, Shuffle, Sort, and Reduce. Map is the first phase in MapReduce that divides input data into smaller and manageable sub-tasks to execute them in parallel. Then perform the required computation tasks. The output of the map is set of key, value pairs as <key, value>. Shuffle and Sort takes the output coming from Maps and perform the sub-steps on each (key, value) pair. It also returns <Key, List<Value>> output, but with sorted key-value pairs. Reduce is the final phase in the MapReduce framework. It takes a list of <Key, List<Value>> sorted pairs from shuffle function and performs reduce operation.

III. PROPOSED SYSTEM ARCHITECTURE

In this section, architecture of the proposed system is designed as shown in Figure 3. Recursive Feature Elimination along with under-sampling is used to balance the data. The Support Vector Machine (SVM) is used for building binary classifiers.

E-ISSN 2581 – 7957
P-ISSN 2277 – 3916

CVR Journal of Science and Technology, Volume 17, December 2019
DOI: 10.32377/cvrjst1714

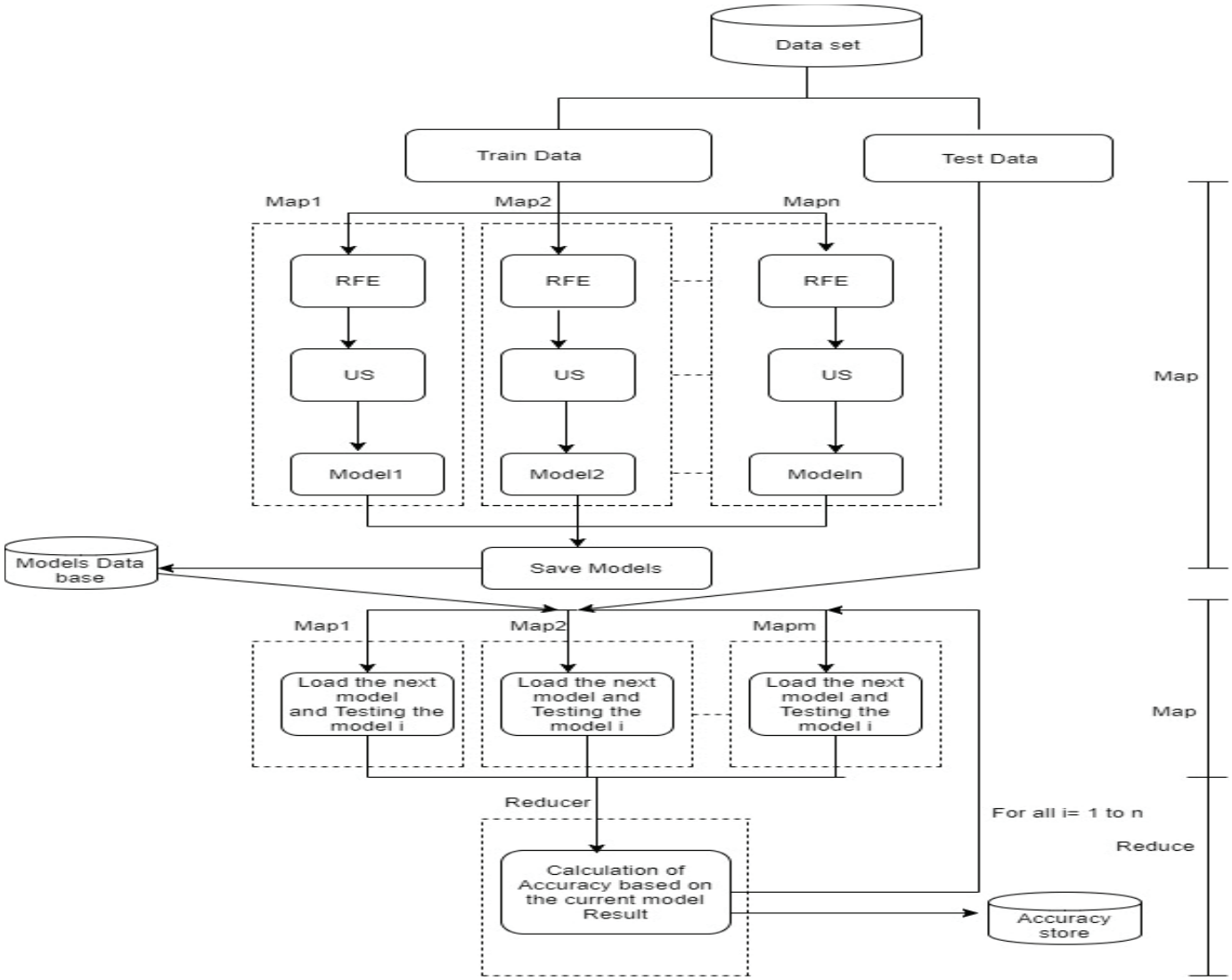

Figure 3..Proposed System Architecture

. The proposed system is developed in MapReduce paradigm. The Two-phase MapReduce scheme is used to develop the system. In the first phase of this scheme, training data splits among mappers, pre-processing is done at every mapper and then models are constructed and saved. In the second phase of MapReduce, the models are tested by dividing the test data among the mappers. Then the models are tested one by one iteratively. At the end of each iteration, reducer calculates model accuracy. The model which gives a better accuracy is considered as the resultant accuracy of the proposed system.

In the proposed system, models are saved for future use so that it supports "write once, use anywhere Principle" as long as the data to be tested is of the same domain.

A. Recursive Feature Elimination (RFE)

Recursive Feature Elimination [19], recursively eliminates the non-essential features, the remaining attributes are used to build a model, and calculate the accuracy of the model. RFE can work on the combination of attributes that contribute to the prediction of the target variable. Finally, the subset based on error rate is obtained which is low. Algorithm for Recursive Feature Elimination is presented as below.

Algorithm 1: *Recursive Feature Elimination*

Input: Dataset with a set of attributes
Output: Subset of the data of attributes

1. *Define a list of features in order of dataset. like $f_1,f_2...f_n$*
2. *Resample the sample set by Random Forest, and method by cross validation.*
3. *For all the values of f_i where i= 1 to n repeat*
   3.i. Recursive Feature Selection for f_i

E-ISSN 2581 – 7957
P-ISSN 2277 – 3916

CVR Journal of Science and Technology, Volume 17, December 2019
DOI: 10.32377/cvrjst1714

3.ii. Calculate the error rate at each f_i Level

4. Optimal feature number f: the level with minimal cross validation error rate*

5. Selected top features: the top feature f highest-frequency feature.*

B. Under- sampling (US)

The output of RFE would be the data with essential features. In under-examining, specimens of the lion's share class are chosen arbitrarily and the span of the greater part class is decreased closer to the measure of the minority class. The output of under-sampling is a balanced dataset. The yield of under-testing is adjusted dataset.

C. Support-Vector-Machine(SVM)

Support Vector Machine (SVM)[17] is the supervised machine learning algorithm which can be used for both classification and regression problems. Kernel trick technique is followed in SVM to transform the data. The optimal boundary is found between possible outputs based on these transformations. In the proposed system, SVM is used to construct the model because it gives optimum classification result.

D. Model Save

In the first phase of MapReduce, the model generated at the mapper is saved so that in the second phase of MapReduce this model is used for testing the data.

E. Model Load

Models are tested in the second phase of MapReduce. For this, test data gets split among mappers, and then models are tested iteratively like the first model in the first iteration, the second model in the second iteration and so on. In each iteration, a model is tested in each mapper with the corresponding data partition. Output of each mapper is the confusion matrix of the corresponding data partition. A confusion matrix [27] is a table that is used to portray the performance of a classification model (or "classifier").

Reducer Work

In each iteration, output of mapper is given as the input to the Reducer. The Reducer does the calculations for accuracy by aggregating the output of each mapper. Whichever model gives an accurate result is considered to be the final accurate model of the proposed system.

IV. Experimental Evaluation

In this section, the details of real-world problems having Binary-class imbalanced data are written, performance measures are explained and experimental study results are shown.

A. R-Hadoop integration

The programming language used to implement the proposed system is statistical tool R [24] in integration with MapReduce, R is an open source programming dialect and gives programming condition to factual examination, designs portrayal and detailing. R is an open source tool that provides plenty of APIs to do statistical analysis, graphics representations.

B. Datasets and Parameters

The datasets are taken from the UCI repository [23]. Table1 summarizes the details of selected datasets including a number of attributes and the Imbalance Ratio.

TABLE I.
Description About Datasets

Datasets	Attributes Before RFE	Attributes After RFE	Imbalance Ratio
Breast Cancer Wisconsin (original)(Wobc)	10	10	1.8
Breast Cancer Wisconsin (Diagnostic)(Wdbc)	32	16	1.6
Breast Cancer Wisconsin (Prognostic)(Wpbc)	34	20	3.2
Page blocks0	10	10	8.79

C. Performance Measures

Performance Measure evaluates how well an algorithm is performing on a given dataset. There are several performance measures exist in imbalanced classification like Precision/Specificity, Recall/Sensitivity, G-mean, F-measure, and AUC. However, for this study, accuracy is found using F-measure.

$$\text{Specificity} = TN/(TN+FP) \quad \text{.....(1)}$$

$$\text{Sensitivity} = TP/(TP+FN) \quad \text{.....(2)}$$

$$F\text{-measure} = 2X(\text{specificity } X \text{ sensitivity}) / (\text{specificity} + \text{sensitivity}) \quad \text{.....(3)}$$

D. Experimental Analysis

We experiment on the datasets described in Table, UCI is the renowned Repository for real databases that are being used by various research communities for experimental analysis. The dataset of breast cancer samples are taken from the same repository. In this application 75% of the dataset is taken as training data to generate the models, and the rest 25% of the dataset is taken as the testing data.

The results of testing for all datasets described in Table I are summarized in Table II. From Table II, it can be analysed that the imbalanced classification accuracy is improved when SVM is combined with Under-Sampling and Recursive Feature Elimination. The improvements are highlighted.

CVR Journal of Science and Technology, Volume 17, December 2019
DOI: 10.32377/cvrjst1714

TABLE II.
THE RESULTS OF TESTING DATA

Data Set	Accuracy of SVM	Accuracy of SVM + US	Accuracy of SVM + US + RFE
WOBC	0.964271	0.960572	**0.964271**
WDBC	0.9785	0.9785	**0.97995**
WPBC	0.898305	0.898305	**0.913792**
Page-blocks0	0.918760	0.918760	**0.885168**

It has been proved that the proposed algorithm works well to improve accuracy in case of Breast cancer dataset. At the same time, its performance is questioned for page blocks dataset. This is one possible area which has to be explored further and find out how the algorithm is actually working.

V. CONCLUSIONS AND FUTURE WORK

In this paper, the parallelization scheme with Recursive Feature Elimination based on Under-Sampling is proposed for binary imbalanced classification using MapReduce. There is an improvement in the accuracy of the proposed system compared with the conventional SVM classification with Big Data. As part of future work, we would like to test the proposed system on various large datasets to study the consistency of the model.

REFERENCES

[1] Nitesh V. Chawla, Nathalie Japkowicz, Aleksander Kolcz "Special Issue on Learning from Imbalanced Data Sets" Volume 6, Issue 1 - Page 1-6.
[2] Nitesh V. Chawla, Nathalie Japkowicz, Aleksander Kolcz ―Editorial: Special Issue on Learning from Imbalanced Data Sets‖ Sigkdd Explorations. Volume 6, Issue 1.
[3] A. H. The project, "Apache Hadoop," 2013. [Online]. Available: http://hadoop.apache.org/
[4] N. Chawla, K. Bowyer, L. Hall, and W. Kegelmeyer, "SMOTE: synthetic minority over-sampling technique," arXiv preprintarXiv:1106.1813, 2011.
[5] Triguero, D. Peralta, J. Bacardit, S. Garcia, and F. Herrera, "MRPR: MapReduce solution for prototype reduction in big data classification," Neurocomputing, vol. 150, pp. 331–345, 2015.
[6] Triguero et al., "Evolutionary undersampling for imbalanced big data classification," 2015 IEEE Congress on Evolutionary Computation (CEC), Sendai, 2015, pp. 715-722.doi: 10.1109/CEC.2015.7256961
[7] L. J. Eshelman, "The CHC adaptive search algorithm: How to have safe search when engaging in nontraditional genetic recombination," in Foundations of Genetic Algorithms, G. J. E. Rawlins, Ed. San Francisco, CA: Morgan Kaufmann, 1991, pp. 265–283.
[8] Feature selection using Genetic algorithm is online: http://topepo.github.io/caret/feature-selection-using-genetic-algorithms.html
[9] W.-Y. Chen, Y. Song, H. Bai, C.-J. Lin, and E. Chang, "Parallel spectral clustering in distributed systems," Pattern Analysis and Machine Intelligence, IEEE Transactions on, vol. 33, no. 3, pp. 568–586, 2011. J. R. Cano, S. Garcia, and F. Herrera, "Subgroup discover in large size.
[10] T. Menzies, J. Greenwald, and A. Frank, "Data Mining Static Code Attributes to Learn Defect Predictors," IEEE Trans. Software Eng., vol. 33, no. 1, pp. 2-13, Jan. 2007.
[11] G. M. Weiss, "Mining with ararity: A unifying framework," SIGKDD Explorer, vol. 6, no. 1, pp. 7–19, 2004.
[12] J. Wang, M. Xu, H. Wang, and J. Zhang, ''Classification of imbalanced data by using the smote algorithm and locally linear embedding,'' in Proc. 8th Int. Conf. Signal Process., vol. 3. 2006, pp. 1–4
[13] C. S. Ertekin, ''Adaptive oversampling for imbalanced data classification,'' in Proc. 28th Int. Symp. Comput. Inf. Sci., vol. 264. Sep. 2013, pp. 261–269.
[14] H. He, Y. Bai, E. A. Garcia, and S. Li, ''ADASYN: Adaptive synthetic sampling approach for imbalanced learning,'' in Proc. IEEE Int. Joint Conf. Neural Netw., IEEE World Congr. Comput. Intell., Jun. 2008, pp. 1322–1328.
[15] I. Triguero, M. Galar, S. Vluymans, C. Cornelis, H. Bustince, F. Herrera and Y. Saeys, ''Evolutionary Undersampling for Imbalanced Big Data Classification,'' IEEE Trans.978-1-4799-7492-4/15/$31.00@ 2015 IEEE
[16] N.V. Chawla, N.Japkowicz, A.kolcz, Editorial:special issue on learning from imbalanced data sets, SIGKDD Ex[lor. Newsl.6(1)(2004)1-6.
[17] Ch.Sarada, M.Sathya Devi, "OVO Weighted Voting for Multi-Class Imbalanced Classification Having Distance as Weight", International Journal of Science & Engineering Research Volume 8, Issue 7,July-2017.
[18] KNN Classification is online at "http://www.math.le.ac.uk/people/ag153/homepage/KNN/OliverKNN_Talk.pdf".
[19] Xue-wen Chen,JongCheolJeong, "Enhanced recursive feature elimination", Machine Learning and Applications, 2007.
[20] Prediction matrix on online. "https://classeval.word press.com /introduction/basic-evaluation-measures/".
[21] G. Batista, R. Prati, and M. Monard, "A study of the behavior of several methods for balancing machine learning training data," ACM Sigkdd Explorations Newsletter, vol. 6, no. 1, pp. 20–29, 2004.
[22] Aida Ali, Siti MariyamShamsuddin and Anca L. Ralescu, "Classification with class imbalance problem: A Review" , Int. J. Advance Soft Compu. Appl, Vol. 7, No. 3, November 2015 ISSN2074-8523.
[23] UCI repository database at online, "https://archive.ics.uci.edu /ml/datasets.html".
[24] R description at online, "https://libguides.library.kent.edu/ statconsulting/r".
[25] R and Hadoop integration in online, "http://www.rdata-mining.com/big-data/r-hadoop-setup-guide".
[26] R Studio information at online, "http://dss.princeton.edu/train-ing/RStudio101.pdf".
[27] Confusion Matrix information in, "Simple guide to confusion matrix terminology", March 25, 2014
[28] Nadeem Qazi, Kamran Raza, "Effect Of Feature Selection, Synthetic Minority Over-sampling (SMOTE) And Under-sampling On Class imbalance Classification" 2012 14th International Conference on Modelling and Simulation, 978-0-7695-4682-7/12 $26.00 © 2012 IEEE

E-ISSN 2581 – 7957
P-ISSN 2277 – 3916

CVR Journal of Science and Technology, Volume 17, December 2019
DOI: 10.32377/cvrjst1715

Optimal Design and Power Management in Shipboard System

Teja Sree Mummadi[1] and Dr.R.Vijay[2]
[1]PG Scholar, CVR College of Engineering/ EEE Department, Hyderabad, India
Email: tejamummadi54@gmail.com
[2]Assoc. Professor, CVR College of Engineering/ EEE Department, Hyderabad, India
Email: vijai.mtp@gmail.com

Abstract: **This paper deals with controlling DC power in shipboard power. Shipboard Power System (SPS) experiences disturbance due to variations in load. A DC bus distribution system developed for the U.S. Coast Guard's 270-ft Medium Endurance Cutter is simulated using MATLAB in this paper. Whenever a fault occurs in load, the system power varies. In this paper, the DC power system is controlled automatically by detecting disturbances. The proposed method includes self-governing fault detection and controlling DC power. The shipboard power system consists of a challenge related to restoration. The reliability and flexibility of the system are improved with effective integrated Energy Storage Devices (ESD) and Solar power. A maiden attempt is made in the paper with a solar panel for the cost-effective operation of the SPS. Also, the SPS with and without the solar panel is tested for optimal operation. Furthermore, this shipboard management system may be implemented in the Indian shipboard system for optimal power management.**

Index Terms: Optimal power management, DC bus distribution system, shipboard power system, energy storage system, solar power, fault detection, energy storage device.

I. INTRODUCTION

The ships which are used for both military and commercial purposes which works based on electricity are enabled by Integrated Power Systems (IPS). This IPS is now used to meet increasing demand. In critical conditions, i.e., when there is a change in load or IPS component failure, they provide real-time management for dynamic configuration to support system.

Recently, there has been much advancement in controlling and managing DC microgrid. These advancements have been implemented in applications such as traction, smart buildings, shipboard power systems and many more. The drastic development in semiconductor devices and power electronic devices over the last two decades made a way for advanced electrical networks, which are useful in automotive, space, and marine applications. These systems deliver with high efficiency and reliability [1], [2]. Because of the advancement in power electronics, DC distribution systems have gained more attraction than AC.

Though there are many advantages to the DC-based integrated power system, it is difficult to maintain optimal performance without interruption with a dynamic load. The protection schemes can detect faults and isolate them, but they do not consider the optimization constraints or balance the power after fault isolation. To meet the increasing DC shipboard power demand, all the electric ships are implementing the integrated power system [3]. They have to manage the power for the dynamic profile to support the system critical operations when there is a change in dynamic load or IPS failure.

In the IPS architecture, all the loads are supplied by a common electrical power bus, which enables the handling of the loads and generation sources more optimal and efficiently. It is able to deliver direct power to vital loads on demand [4].

A new method is introduced which controls and optimally reform a DC power system, while automatically detecting system disturbances. A dynamic approach is proposed using time scale separation. The aim is to provide coordination between system protections to ensure that the system remains stable at all stages of operation even when there is a disturbance.

To implement the approach called DC-based shipboard power system is employed. The reliability of electrical power plays a major role in this modern world. As the demand for electrical power is increased there should be an alternative for restoration and recovery after an outage or fault on the system [5]. In this case, if the power system is provided with storage devices, it can provide back-up power or power during the transition [6]. In this paper, DC Shipboard Power System (SPS) is integrated with the Energy Storage System, which acts as a feedback path.

An Energy Storage Device Subsystem is very necessary for the shipboard power system and for terrestrial electrical systems. This element helps in storing a large amount of energy, which can be used as a back-up. During any fault conditions, the electrical system can be fed by ESDs. The outage of electrical equipment and other parts or operational issue may occur if ESDs fail to provide energy during faults [7-8].

Recent developments of SPSs include integrated circuits and which are trending nowadays. Due to the advantages of DC over AC, the DC shipboard came into existence. Generally, there are two types of distribution system that includes radial type and ring type distribution system. Convectional SPSs are of radial type distribution systems.

The radial type system has a generating station at the center of the loads. The power flow is in only one direction. In radial type, if any fault occurs then it would result in loss of supply to many units until the fault is located and cleared.

E-ISSN 2581 – 7957
P-ISSN 2277 – 3916

DOI: 10.32377/cvrjst1715

When there is a change in a generation it seriously affects the load side which results in voltage fluctuations, due to this reliability and stability decrease. But recently to overcome radial distribution problems zonal distribution system is implemented. The researchers proposed a new technology that includes both radial distribution architecture and zonal approach. The zonal approach [9] employs a Starboard Bus (SB) and a Port Bus (PB), and thus dividing the ship into a few electric zones.

In this paper, the DC SPS is integrated with the Energy Storage System (ESS) where the battery is used as Energy Storage Device. By integrating the ESS with the DC SPS the system efficiency is improved. The ESS acts as a backup of the system.

ESS technologies are technologically viable nowadays. A few of them are Flywheels, the Superconducting Magnetic Energy Storage (SMES), Battery Energy Storage System (BESS), the Compressed Air Energy Storage (CAES), Super Capacitors and Pumped Hydro Storage (PHS). Either AC or DC system, for charging and discharging purposes the ESS requires power converters. Mostly used ESS is an Uninterruptible Power Supply (UPS). In this paper, the battery is used for Energy Storage Device.

This paper deals with the modeling of DC SPS with solar resources for power generation. Solar panel technology requires a power converter to boost the output power. In this paper boost converter is used as a converter for a solar panel. The buck-boost converter is integrated with ESS as a power converter.

The remaining of this paper is outlined as follows: Section II introduces about SPS configuration. Section III is about SPS power control. The modeling and simulation circuit and results are shown in Section IV. Conclusions are presented in Section V.

II. Shipboard Power System

A.Shipboard Configuration

An Electrical power distribution system for the ship must be able to provide power generation and distribution, control and some basic power electronics operations. Space and weight parameters limit the amount of discharge in the system for restoration purposes. The resistive losses in SPS are nearly negligible because of the tightly coupled distribution network.

The system characteristic of electrically integrated SPS is very similar to island microgrid except the fact that it is not automated. It will have a relatively weak power balance since the generator capacity is closely sized to the load demand [16]. In order to maintain shipboard power system reliability, it has to be automated. It is also proved that automation gives better results than manual control. In this process, multiple power generation capabilities abode throughout the ship.

B. DC Shipboard Power System

The first DC shipboard was in the 1880s but due to lack of power electronic devices, this system failed [11]. With recent advancements in power electronics devices and storage technologies, the DC SPSs have gained attention. The main motivations for the development of DC SPS are fuel economy and other advantages include:

- Implementation of parallel connection or disconnection for DC power sources will be simple.
- Dispensation from reactive power flow.
- Eliminating harmonic and imbalance problems.
- Unlike variable frequency drives, AC SPS in DC SPS regenerative energy may be easily absorbed in other loads across the DC bus.
- Due to the absence of a power factor in DC distribution, resistive loss in cables is reduced.

There is no need for phase and voltage synchronization in DC SPS. As a result, the generators are quickly brought online and connected to the DC system.

The fuel efficiency of the system operation can be improved by using DC networks by achieving the integration of advanced high speed and high-efficiency diesel generation. Hence, DC Shipboard Power Systems (DCSPSs) keep gaining an increase in research interests. The concept of Onboard DC Grid has two configurations. The first is a multi-drive approach and the second one is a fully distributed system [12]. Another new approach includes components like AC generators, inverter modules, AC motors, etc., but AC switchboard is excluded [13]. Fuel-saving is nearly 20% with the integration of variable speed diesel generator operating at the optimal speed [14-15].

III. Proposed DC Shipboard Power System Management

A.System Fault Monitoring

During steady-state operation systems, fault monitoring and protection are within the limits of healthy operations. Whenever there is any disturbance or sudden change in load, then power varies. The fluctuation in voltage/current has to be detected and cleared immediately in order to maintain reliability. In this paper, the modeled power system includes measuring devices to maintain and continuously monitor the voltage and current parameters. The measuring devices are installed at the terminals of generator, loads and in DC bus. Current, voltage and power thresholds (e.g., a certain percentage of steady-state values) are set in each of the measuring devices to detect a disturbance at a specific location and give signals.

B.Coordinated Control

In this paper, for DC SPS for power generation, the diesel generators are used. DC SPS follows the HVDC working principle, where the generated AC is converted into DC through converters (i.e., Rectifiers) and given to the load. The load combination is taken with resistance and inductance for nonlinearity. The basic block diagram of the DC shipboard power system is shown in Fig. 1.

E-ISSN 2581 – 7957
P-ISSN 2277 – 3916

CVR Journal of Science and Technology, Volume 17, December 2019
DOI: 10.32377/cvrjst1715

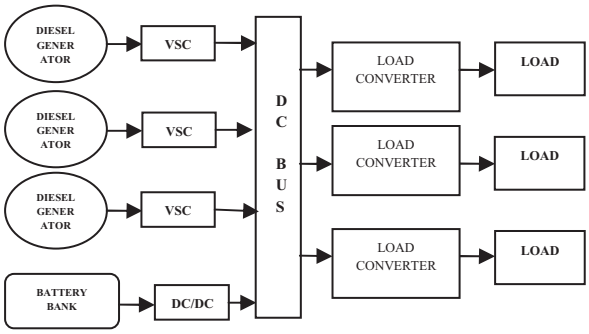

Figure 1. Basic block diagram of DC SPS

The DC bus power is again converted into AC near loads via the inverter. The battery is used as backup i.e., as Energy Storage Device. Power is supplied by three generators with diesel generators prime movers. The basic principle behind the DC ship power system and configuration is like the extension of multiple DC-links. But for these drives, electrical power consumption is more than 80%. In this regard, all DC-links are united in a common DC bus. This approach includes components like AC generators, inverter modules, AC motors, etc., but the AC switchboard is excluded. In AC SPS to control the speed of the motor, a frequency converter consisting of a rectifier and an inverter is used. The AC voltage is first converted to DC in the rectifier and then inverted back to AC. DC/DC converters are lighter than power transformers, but have a greater efficiency (> 98 %), require less maintenance and their price range is much lower. There are several ways of configuring a DC ship power network. The generators are connected on MV1 Switchboards and the energy is transformed via transformers to the converters. In the multi-drive configuration, all converters are placed in the main switchboard. That simply means that the power cables from generators to the DC bus carry AC current.

IV. Simulation Results And Discussions

A. DC Shipboard Power System Without Solar Panel

The proposed method is implemented and modeled in MATLAB version 2016a with Intel Quad-core 7th generation as shown in Fig. 2. Two-level Pulse Width Modulated (PWM) voltage source converters are used to convert the AC (3ϕ, 440V, 60Hz) power produced by the three-phase generators which are again stepped down using transformers. The DC bus reference voltage is set to 750 V. As the feedback path, Energy Storage System is used with the battery of 650V, 400Ah and connected to the DC bus through a bi-directional DC/DC converter. In MATLAB for DC/DC converter, the half-bridge converter is used. Pulse width modulation has been supplied to it.

Two disturbances are created which occur commonly in the system to validate the feasibility of the proposed approach. Two disturbances are generator loss and load start. The three generator's output power and battery power waveforms are shown in Fig. 3.

Whenever there is a fault in the generation the protecting device, i.e., a circuit breaker isolates the faulted part with the non-faulted path. At generator 3 a fault is generated at 4sec gets isolated and doesn't generate power. In MATLAB, to produce fault the circuit breaker is set to trip at 4 sec.

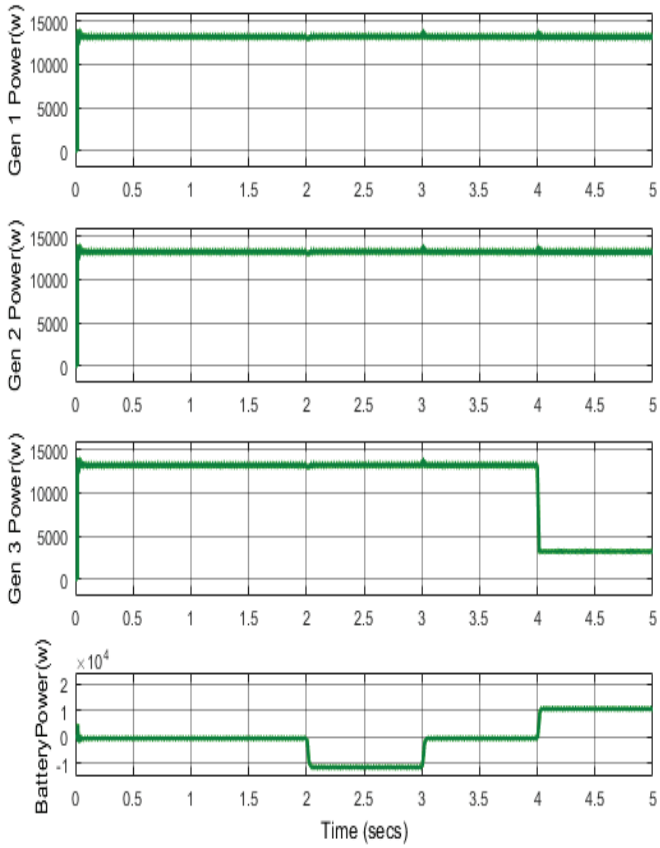

Figure 3. Three generators output power along with the battery power output

Whenever the disturbances occurred in generators and if power generation is lost, the battery supplies the power to the load. In Fig. 3 it is observed that the third generator power is lost for 4 seconds due to generation fault, i.e., power doesn't get supplied to the load. But in this concept, all the bus bars are tied together, and a reference value is set at 750V and ESS is set as feedback. Subsequently, whenever there is any fault occurred in power generation, the load gets supplies through the feedback path. Whenever there is a need for power, then the battery in the ESS injects the voltage into the system through a converter. However, the battery injects the power into the system, then the converter acts as a boost converter.

E-ISSN 2581 – 7957
P-ISSN 2277 – 3916

CVR Journal of Science and Technology, Volume 17, December 2019
DOI: 10.32377/cvrjst1715

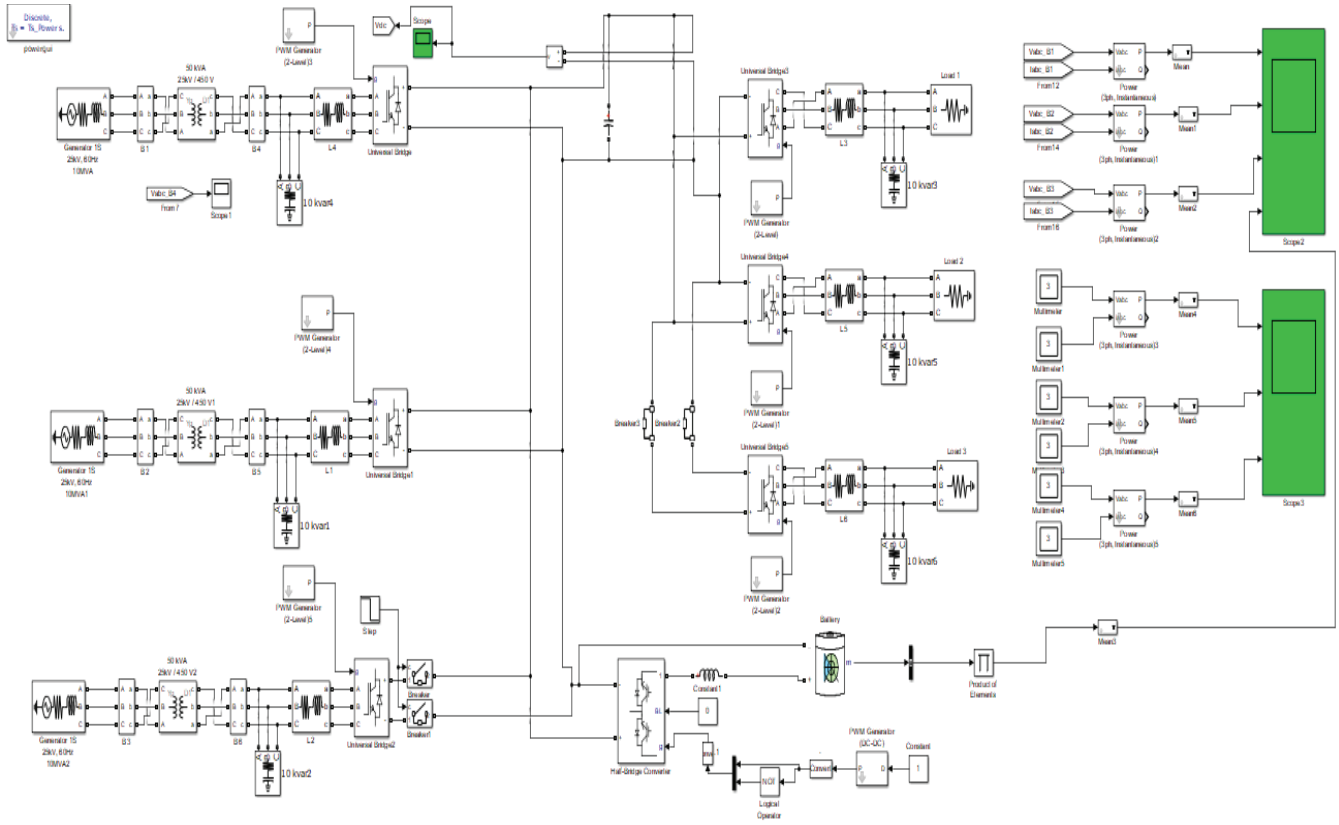

Figure 2. DC shipboard power system model

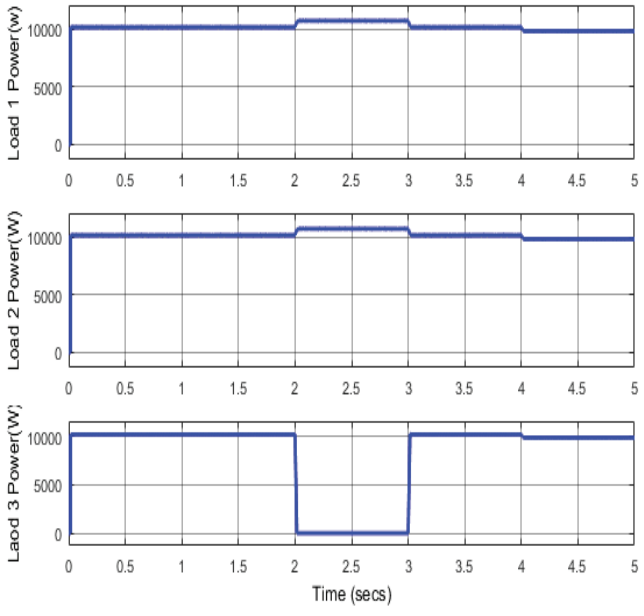

Figure 4. The output power of three connected load

In Fig.4 it is realized that the load is disconnected at 2-3 seconds, thus during that period, the excess generated power is wasted. Without ESS this power gets wasted. i.e., whenever there are disturbances at load, then the circuit breaker isolates the faulted path with the non-faulted path. At this instant, the power generated is not supplied to load. In order not to waste the excess power the feedback path absorbs the excess power. When extra power is generated, then the ESS device's battery absorbs it through DC/DC converter which acts as a buck converter and absorbs the power. The battery waveform is observed in Fig. 7 that whenever it is observing the excess power generated the battery power. The battery uses extra power to charge itself. The battery is charged whenever there is excess power. The power is balanced by injecting and absorbing. The DC voltage waveform from the 750V capacitor is observed in Fig. 5.

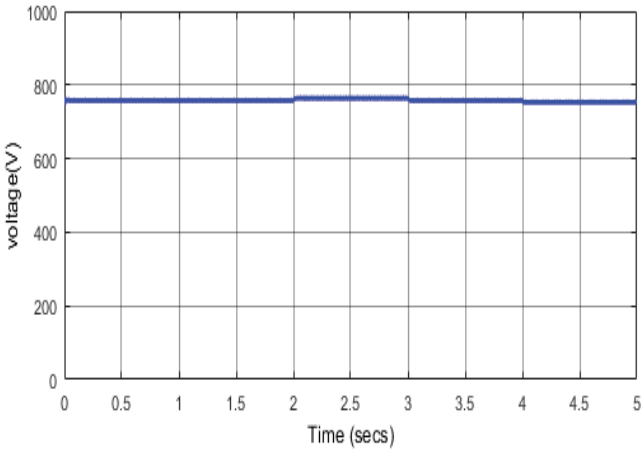

Figure 5. DC voltage from capacitor

Though there are some overshoots when disturbances occurred, it is comprehended that the DC bus voltage kept

E-ISSN 2581 – 7957
P-ISSN 2277 – 3916

CVR Journal of Science and Technology, Volume 17, December 2019
DOI: 10.32377/cvrjst1715

regulated at all points of the disturbance. The power electronics converters quickly recover the voltage regulation as depicted.

B. Shipboard Power System With Solar Panels

Solar panels are used for power generation in place of generators. The method of using solar panels is modeled and implemented in Matlab is shown in Fig. 6.

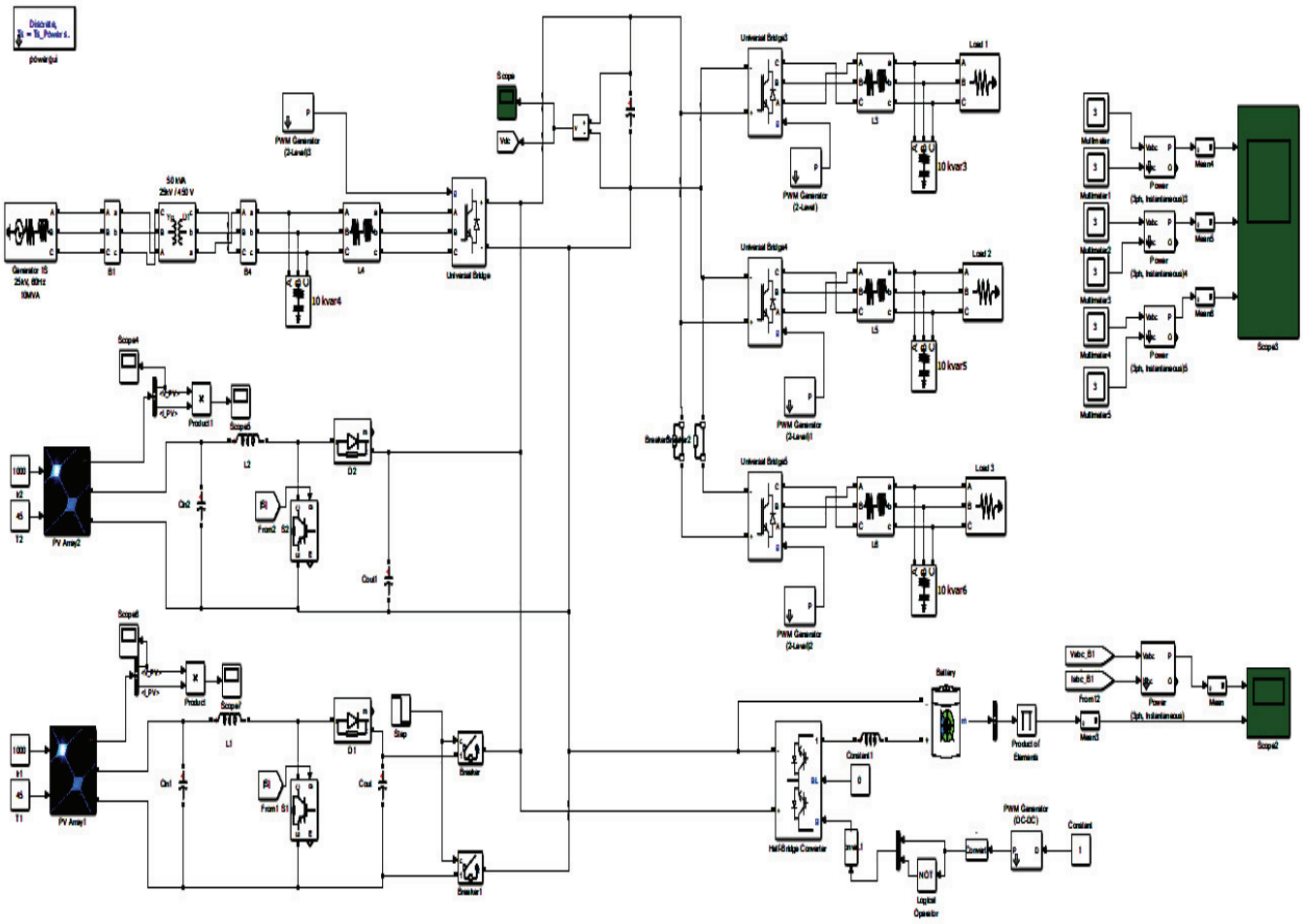

Figure 6. DC SPS using the solar panel

By using solar panels, the battery and electric motors get charged and then the usage of fossil fuels can be reduced. Solar panels directly convert sunlight to electricity. These panels produce reliable electricity without using fossil fuels. The generator 1 output power and battery waveforms are shown in Fig. 7. Only one three-phase generator and two solar panels are used which generates 9kW each. The generator 1 produces nearly 13kW of power. The battery is used as backup and support and the same relates to a DC/DC converter.

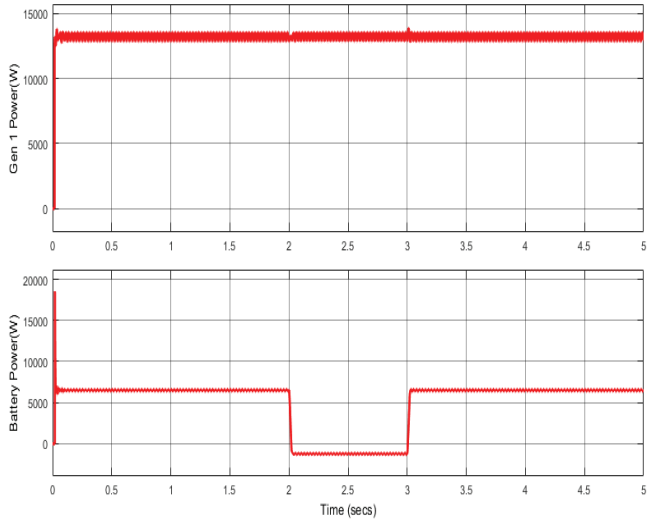

Figure 7. Generator 1 and battery waveform

E-ISSN 2581 – 7957
P-ISSN 2277 – 3916

DOI: 10.32377/cvrjst1715

The solar panel output power is simulated in Fig. 8. The ship needs approximately 10kW of power for a load. Each panel produces 8kW of output power.

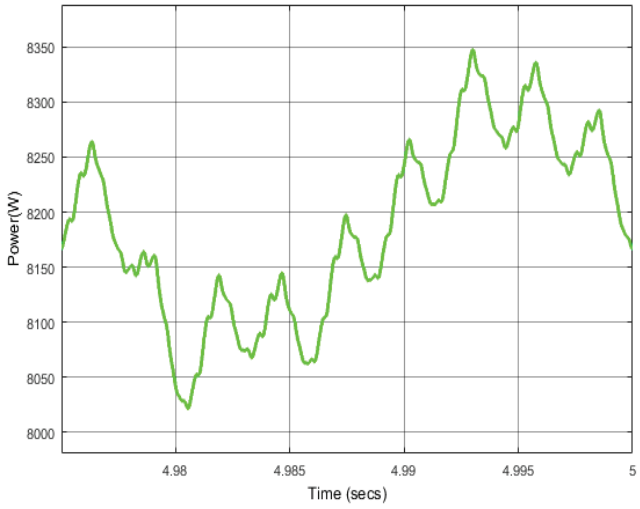

Figure 8. Solar panel output power waveform

The output power of loads is nearly 10kW each. The three-load output power is observed in Fig. 9. Whenever there is any interruption in power supply the battery provides power to the loads. If there is any fault at load and if it is isolated, then the generated power is absorbed by the battery.

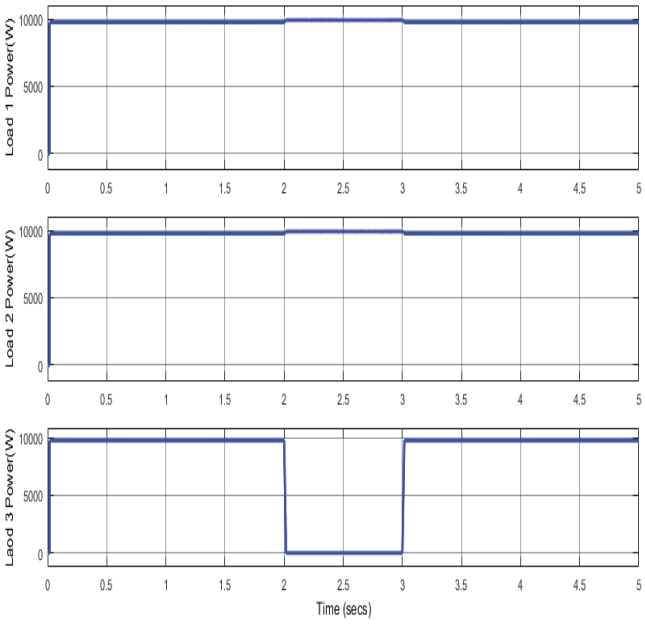

Figure 9. Load output power waveform

The usage of solar panels in this system is because of their benefits. Solar panels are very reliable and require less maintenance. These are static devices so there are no rotational losses. The solar panel system produces power in all types of weather conditions. They produce nearly 80% of their potential energy on partly cloudy days. Even in the worst cases like extremely cloudy days, they produce 25% of their total potential.

V. Conclusions

This paper proposes the controlling of DC power in the shipboard power system. The proposed method is applied to DC shipboard using solar panels and outcomes are presented. The usage of solar power reduces fuel cost and power generation losses. Moreover, solar power is eco-friendly and a cheaper energy resource. The proposed Energy storage system can produce quality results in terms of controlling DC power in the shipboard. The results indicate that the system remains stable at every instance of time of disturbances, which are introduced at specific intervals of time. Furthermore, the disturbances and faults at generators for the Indian DC shipboard can be investigated.

References

[1] R. G. Blakey, "Power electronics in warships," Power Engineering Journal, vol. 7, no. 2, pp. 65-70, 1993.

[2] Webstar, "Naval experience of power electronics maintenance," IEE Colloquium on Power Electronics Reliability, no. 202, 1998.

[3] Z. Jin, G. Sulligoi, R. Cuzner, L. Meng, J. C. Vasquez, and J. M. Guerrero, "Next-generation shipboard DC power system: introduction smart grid and dc microgrid technologies into maritime electrical networks," IEEE Electrif. Mag., vol. 4, no. 2, pp. 45–57, 2016.

[4] N.Doerry, H.Robey, J.Amy and C.Petry, Powering the future with the integrated power system. Naval Engineers Journal, 108(3), pp.267-282, 1996.

[5] R.Vijay, "Transmission Line Outage Detection and Identification by Communal Spider Optimization Algorithm", CVR Journal of Science and Technology, vol.14, pp.38-42, 2018.

[6] R.Vijay, "Quorum sensing driven bacterial swarm optimization to solve practical dynamic power ecological emission economic dispatch," *International Journal of Computational Methods*, vol. *15,* no. 03, pp.1850089-24, 2018.

[7] G. Seenumani, J. Sun, and H. Peng, "Real-time power management of integrated power systems in all electric ships leveraging multi time scale property," IEEE Transactions on Control Systems Technology, vol. 20, no. 1, pp. 232–240, 2012.

[8] S. Kim, S. Choe, S. Ko, and S. Sul, "A naval integrated power system with a battery energy storage system: Fuel efficiency, reliability, and quality of power," IEEE Electrification Magazine, vol. 3, no. 2, pp. 22–33, 2015.

[9] C.R. Petry and J.W. Rumburg, "Zonal electrical distribution systems: An affordable architecture for the future," Naval Engineers Journal, vol.105, no. 3, pp.45-51, 1993.

[10] F. Shariatzadeh, N. Kumar, and A. K. Srivastava, "Optimal control algorithms for reconfiguration of shipboard microgrid distribution system using intelligent techniques," IEEE Transactions on Industry Applications, vol. 53, no. 1, pp. 474–482, 2017.

[11] Skjong, E. Rodskar, M. Molinas, T. Johansen, and J. Cunningham, "The marine vessel's electrical power system: From its birth to present day," Proceedings of the IEEE, vol. 103, pp. 2410–2424, 2015.

CVR Journal of Science and Technology, Volume 17, December 2019
DOI: 10.32377/cvrjst1715

[12] J. F. Hansen, J. O. Lindtjorn, U.U. Odegaard, T.A. Myklebust, "Increased operational performance of OSVs by Onboard DC Grid," 4th International Conference on Technology and Operation of Offshore Support Vessels, Singapore, 2011.
[13] ABB, "Onboard DC Grid. The step forward in Power Generation and Propulsion," Tech. rep., 2015.
[14] ABB, "The step forward onboard dc grid," Tech. rep., 2014.
[15] W. Koczara and G. Iwanski, "Power Electronics for Renewable and Distributed Energy Systems Variable-Speed Power Generation" Springer, 2013.
[16] K. Hutton, B. Babaiahgari, and J.-D. Park, "A comparative study on electrical distribution systems for the US coast guard's 270-ft medium endurance cutter," North American Power Symposium (NAPS), IEEE, pp. 1–6, 2016.

E-ISSN 2581 – 7957
P-ISSN 2277 – 3916

CVR Journal of Science and Technology, Volume 17, December 2019
DOI: 10.32377/cvrjst1716

Dynamic Performance of a Stand-Alone Self-Excited Induction Generator for a Variable Speed Wind Turbine

Dr. M. Lakhsmiswarupa[1] and. R. Naveena Bhargavi[2]
[1]Professor, CVR college of Engineering/ EEE Department, Hyderabad, India
Email: swarupamalladi@gmail.com
[2]Assoc. Professor, CVR college of Engineering/ EEE Department, Hyderabad, India
Email: bhargavi.rn5@gmail.com

Abstract: **Induction generators are more appropriate machines for wind energy conversion. Induction generators generally can be operated in two modes i.e. grid or self-excited mode. Among the two, later is of improving importance due to its capability of wind energy conversion (primary) into electrical energy (secondary) for wide range of variations in the operating speed. Poor voltage regulation is observed in machine analysis. Steady-state and transient analysis of self-excited induction generator surveys that such generators are not efficient enough to maintain the frequency and terminal voltage in the absence of conventional controllers but are only used for stator and rotor currents variations. In this paper modeling of self-excited induction generator for wind energy conversion systems is designed and simulated in MATLAB environment. The system is studied for dynamic period simulation during the starting period, and load variation.**

Index Terms: **Modeling, Dynamic response, Self-Excited Induction Generator, Wind Energy Generation**.

I. Introduction

The primary energy sources also known as conventional sources are thermal power generation and nuclear power generation etc. The efficiency of these conventional methods is poor and rather they pollute the environment. Hence, much attentiveness and concentration are necessarily made towards the best usage of nonconventional energy sources such as Wind Energy, Fuel Cell, and Solar Energy etc. Among all of these, Wind Power [4] is economically cheap. Hence nowadays, it is considered as the fastest growing and the most challenging non-conventional energy.

An induction generator is also known as asynchronous generator. Induction generator is an alternating current (AC) generator which works on the principle of induction motor to generate electrical power. Induction generators generally run at speeds above the synchronous speed. Without any internal modifications, a regular AC induction motor can be used as a generator. In applications where high-pressure gas streams to lower pressure, for e.g. Mini hydro power plants and wind turbines usually Induction generators are preferred [13], because simple controls are sufficient in recovering energy.

An induction generator is usually supplied with the required excitation power from an electrical grid. Because of this, induction generators cannot usually "black start" a de-energized distribution system. However, they are often self-excited by using phase-correcting capacitors [14].

To develop the airgap magnetic flux in induction generators, reactive power is required. In case of a standalone system, reactive power is provided by connecting a capacitor bank to the machine. In case of grid connection, reactive power is drawn from the grid to maintain the air gap flux[19, 20 & 21]. Frequency and voltage are complex functions of machine parameters for stand-alone systems. Frequency and voltage at the machine will be dictated by the electric grid for a grid tied system, as it is considerably small when compared to the entire system [5].

Due to the ability to produce useful power at various rotor speeds, Induction generators are often used in wind turbines and also in micro hydro installations [8]. Compared to other generators Induction generators are simpler in electrical and mechanical aspects. They do not need any brushes and commutators hence rugged in construction.

An induction generator can operate independently and can generate sufficient reactive power when connected to a capacitor system. The generator will be ceased immediately when the load current of the generator exceeds the capability to supply both load power and reactive power. In such case, the load has to be removed, and the machine has to be restarted either with a DC excitation or with a residual magnetism present in the core. Hence, for wind power generation where speed is always a variable factor, Induction generators are best fit [12]. Induction generators cannot be used alone for grid frequency control as they are load dependent.

Electrical generators which are driven by the wind turbines by using the wind power are mostly used to reproduce electricity [3]. The rotation of blades changes according to the wind direction. These blades as they are connected to the shaft, using the gear box principles, the speed can be improved. The wind Energy is thus converted into electrical energy at the generator and the output of generator will be given to a Step up Transformer (700V/33KV). As the speed of wind changes continuously, the energy produced from the wind is also not constant. It varies continuously and gives energy in sudden bursts. About 50% of the entire energy is given out in just 15% of the operating time. [1]. The self-excited induction generator (SEIG) is best suited to generate electric power from various nonconventional energy sources [9, 11, & 13].

E-ISSN 2581 – 7957
P-ISSN 2277 – 3916

CVR Journal of Science and Technology, Volume 17, December 2019
DOI: 10.32377/cvrjst1716

An induction machine has to be provided with magnetizing energy to be operated as induction generator. A capacitor bank is to be connected across the stator terminals to achieve this [7]. The major problems with the SEIG are as follows: its terminal voltage and frequency are influenced by the prime mover speed, excitation capacitance, load current, and power factor of the load.

The disturbances in the induction motor load and source can be taken care by VSI by injecting the required amount of reactive or active power. The proposed control scheme helps to maintain the rated voltage and frequency of the SEIG.

The output power of the wind turbine can be computed by using the formula given below:

$$Pw=0.5\rho\pi R^2V^3Cp\ (\lambda, \beta) \qquad (1)$$

Pw = Extracted power from the wind
ρ = air density
R = blade radius (in m)
V = wind velocity (m/s)
Cp = power coefficient

Power coefficient (Cp) is defined as the ratio of the produced output power to the available wind power.

$$Cp = \frac{Pwindturbine}{Wind\ air} \qquad (2)$$

Pwindturbine = Cp x P_{ax}

Pwindturbine = $\frac{1}{2}$Cp ρ A V^3

II. Modeling Of The System

A. System Configuration

Figure 1 shows the block diagram of proposed SEIG for wind energy conversion system with the required supply circuit and control method. In SEIG conversion, the power consumption from wind to the electric grid will take place without change in frequency and RMS value of line voltage even with wide range of variations in wind. The proposed model is designed to generate power from the variable-frequency, variable-voltage by using the SEIG [3]. The regulated DC power, which is estimated, is used to charge a battery set and to supply DC loads [6].

Then DC power is estimated and delivered to the DC side of the three-phase voltage source inverter and is to be converted into a three-phase AC power for the AC loads [10] and for the grid connection. An effective and necessary control method is chosen to maintain the terminal dc voltage even with variations in wind turbine speed and with variations in load. Direct vector control strategy involves rotor flux orientation which is highly dynamic in nature. So dynamic performance is much needed for voltage frequency (v/f) control for a grid connected SEIG [12] for both DC and AC power applications. In induction generator, rotor flux is mainly controlled by the direct axis stator current control and quadratic axis stator current control which in turn deliver active stator power [2]. This method is used to control the electrical torque of the SEIG [5] driven by a variable speed wind turbine, where different forms of wind speed variation effect taken into primary consideration. The effectiveness of the scheme is demonstrated through simulation studies by considering different parameters into account.

B. Generator-Side Converter Control

The generator-side converter is implemented in such a way that the rotor flux and the machine torque both are controlled by field oriented scheme of current control loop. Figure 1 shows the block diagram of SEIG for WECS. The rotor flux can be tuned and controlled by controlling the *d*-axis rotor current with respect to time. The machine torque is independently controlled by q-axis rotor current control [8] [11].

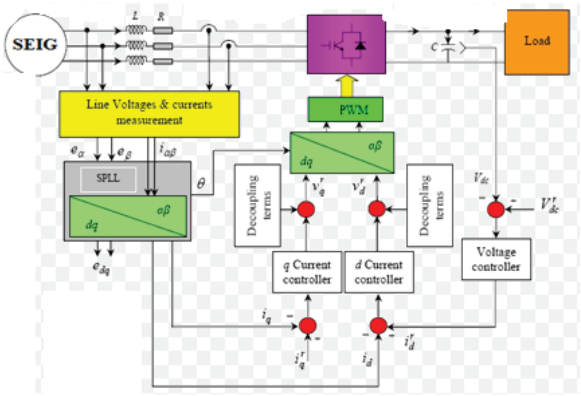

Figure 1. Block diagram of SEIG for WECS

C. Grid-Side Converter Control

The grid-side converter control involves two main control methods namely synchronous current control and direct vector control while doing the simulation. Figure 2 shows the entire control scheme of the grid-side converter [15]. The primary aim of the grid-side converter is to keep the dc –link voltage at a constant value without considering the amplitude and direction of the rotor power. The two inner loops involved in the grid side converter control are: inner loop current control through LC filter and control of Dc link voltage through dc link voltage control. The SEIG system consists of voltage insertion transformer along with an L-C filter and two PI controllers. LC filter is used to remove high-frequency components from the output voltage of VSC.

This indicates that the dc-link voltage control loop must depend upon the d-component of the grid-filter current. An outer loop DC voltage control is needed to maintain the DC link voltage constant [16]

C. Control Structure

The performance of the self-excited induction generator with variable wind speed is studied in three different modes: steady state, transient and dynamic.

The dynamic performance of SEIG is simulated in SIMULINK environment [17] without controllers and its voltage, current, active power and reactive power variation with respect to time is compared with the performance with PID controllers. There are many types of controllers, like: P, I, D, PI, PD, ID PID, controllers.

In Proportional Integral Derivative (PID) controller, only the proportional and integral actions have predominant role of action. The PI controller is advantageous and hence become much popular even when compared to PID

E-ISSN 2581 – 7957
P-ISSN 2277 – 3916

DOI: 10.32377/cvrjst1716

controller. The steady state error resulting from P controller can be eliminated using I controller. However, I-controller has drawbacks of slow response and poor overall system stability. Hence I-controller is preferred only when the speed of the response is not an issue of consideration. PI controller cannot reduce the rise time and mitigate the oscillations as PI controller has no ability to predict the future errors of the system. If applied, any amount of current, I, it guarantees certain set point overshoot.

The two methods for varying the parameters of the PID controllers are:

i) **Manual Tuning Method:** In manual tuning, the parameters are to be monitored and to be adjusted according to the system response. Ki, Kp and Kd are to be changed until the desired system response is obtained by continuous observation of the system response. Example (for no system oscillation): Initially reduce the integral and derivative gains to zero and raise the proportional gain to 100. Now slowly increase and tune integral value by monitoring the system response. As the system will be settled at some predefined value, that set point has to be modified now to verify whether the system can correct itself within tolerable period of time. If there is no quick response, proceed for lowering the integral value further. Based on the oscillatory behavior of the system, the integral value has to be recorded and to be modified accordingly (say to 100). After increasing the integral gain to 100, the proportional gain has to be tuned properly such that the oscillations are ceased. Finally, the proportional gain and integral gains are adjusted slowly to get the desired response.

Even though manual tuning method may seems simple, but it is a time consuming process which needs an experience and patience to approach fine tuning. [18]

ii) **Ziegler-Nichols Method:**

P-I controllers were popular than PID controllers almost six decades ago. Despite of its faster response and less oscillations, PID controller tends to be unstable even for little variations in the input set point or any disturbances compared to the process of PI Controllers. PID controllers are best recommended by Ziegler-Nichols Method and it is one of the most effective methods.

The basic function of controller is to make the tracking error, e (t) to maintain zero, after reaching a certain phase (wt). Conventional Controllers (PID) [7] mentioned their capability to handle various internal and external disturbances for nonlinear and time varying systems with high accuracy and robustness.

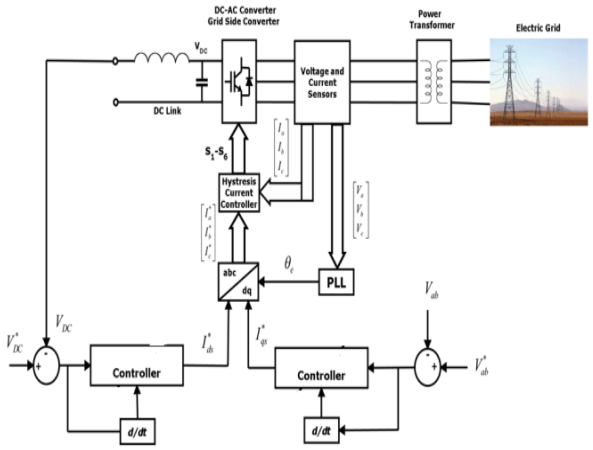

Figure 2. Control scheme of grid-side converter

III. Simulation Results

MATLAB stands for Matrix Laboratory. It is a renowned platform to solve various engineering and scientific problems. Earlier, it was a specially designed computer program to compute various matrix operations. Now it has been upgraded into the most efficient computing system which can provide solutions to many technical problems in various fields of engineering.

MATLAB possess a huge library of many predefined functions and toolboxes to make scientific programming tasks simpler and can provide more efficient solutions. It is an extensive program, with an incredibly rich variety of functions. It also has a versatile built-in function for data analysis and various tool boxes provide versatile function capability in different specializations. A performance analysis of wind-powered self-excited induction generator (SEIG) is modeled using MATLAB Simulink. The main origin of difficulties mentioned in the control of the proposed design is nonlinear in nature.

To meet the required time domain specifications for eg. Minimum overshoot, less settling time and low steady-state error, the PID current controllers (in d-q reference frame) are designed and analyzed.

Based on the dynamics of the DC link, the specifications of the inner loop voltage control are accomplished by proper design of PI voltage controller. The main merits [2] of the proposed system are: (1) Extensive control over active and reactive powers near the DC –bus (2) Unity power factor operation (3) Economically full utilization (3) disturbances due to load can be neglected and voltage compensation can also be done.

E-ISSN 2581 – 7957
P-ISSN 2277 – 3916

DOI: 10.32377/cvrjst1716

The dynamic performance of the proposed system is tested by simulating the model using MATLAB Simulink. The results were analyzed for stator and rotor reference frame. The simulation model is shown in Figure 3 and the results were shown in Figures 4-8 and are summarized in Table I.

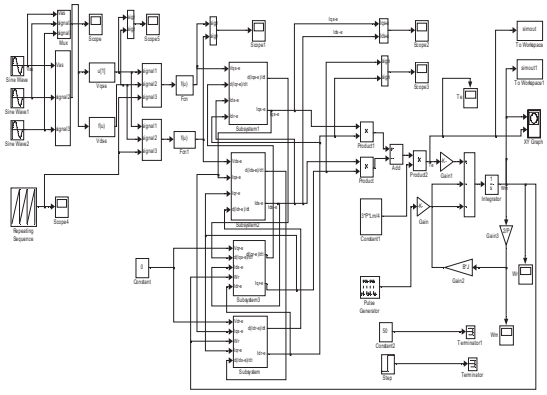

Figure 3. Simulation model of Self-excited induction generator for WECS (With PI controller)

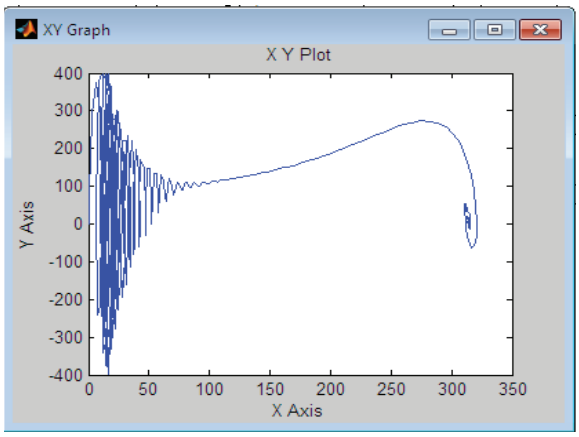

Figure 4. Speed (rpm) versus torque plot

Figure 4 shows speed versus torque plot. Speed-Torque X-Y plot is obtained in plotter for dynamic changes in load with respect to time. Here Speed variation is observed with the changes in the load torque.

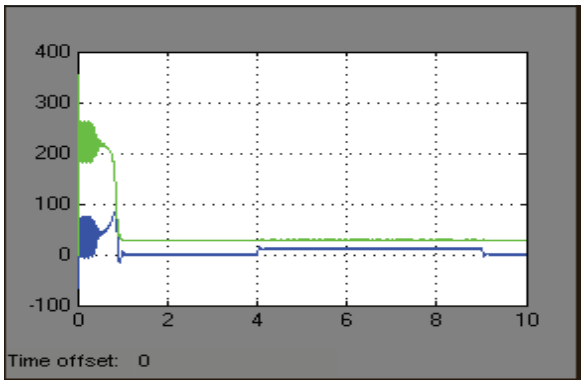

Figure 5. Stator quadrature and direct currents (Amps) versus time (secs)

Using Park transformation, the three-phase quantities are transformed to dq reference frame. Variation of Stator quadrature axis and direct axis currents with the dynamic changes in load with respect to time are shown in Fig.5.

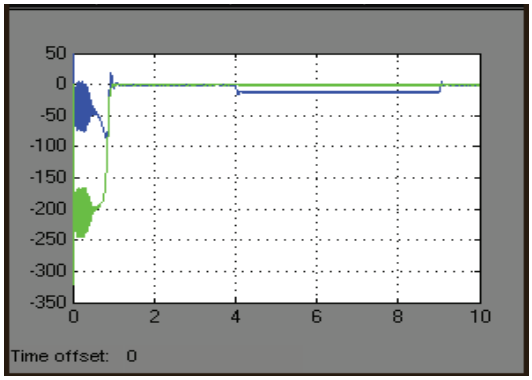

Figure 6. Rotor quadrature and direct currents (Amps) versus time (secs)

Rotor quadrature and direct currents are varied with the dynamic changes in load with respect to time and shown in Figure 6.

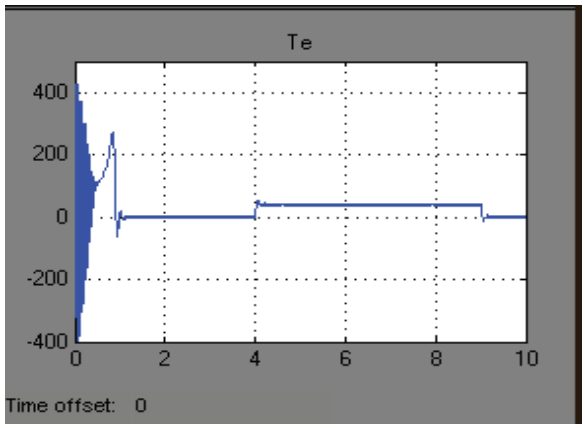

Figure 7. Electromagnetic torque (N-m) versus time (secs)

From Figure 7, Electromagnetic torque (N-m) variation is observed with the changes in the load torque for dynamic changes in load with respect to time.

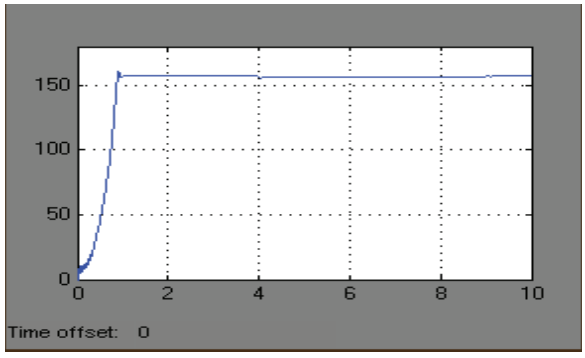

Figure 8. Speed (rpm) versus time (secs)

Figure 8 shows Variation in Speed (rpm) with the changes in the load torque for dynamic changes in load with respect to time.

E-ISSN 2581 – 7957
P-ISSN 2277 – 3916

DOI: 10.32377/cvrjst1716

IV. CONCLUSIONS

Simulation analysis of wind energy driven SEIG which supplies power to the utility grid is being presented in this paper. The controller parameters are tuned according to the tracking error by using Zeigler-Nicolas method.

TABLE I.
DYNAMIC RESPONSE OF SELF-EXCITED INDUCTION GENERATOR

		Amplitude		Time(secs)	
		Without Controller	With PID Controller	Without Controller	With PID Controller
Stator	Quadrature	90	70	Obtained at (1.2-1.8) secs	Obtained at (0.8-1) secs
	Direct	-116	-100		
Rotor	Quadrature	65	50		
	Direct	-10	-200		

The PID parameters considered in simulation are K_p =5, K_i = 0.2 and K_d = 2. The estimation of the dc link voltage to control the SEIG is done by which the desired performance of the power converter and the inverter is being achieved. Simulation studies are carried out with PID controller and the obtained results are compared with the proposed optimal tuned controller.

The simulation results verified the effectiveness and robustness of the proposed tuning technique. The results were verified with respect to the transient behavior of the wind energy system for different operating conditions. This work can be extended further by using Fuzzy Logic Controller (FLC), Artificial Neural Network (ANN) and Particle Swarm Optimization (PSO) controller which can provide a reactive power control and serve as shunt active power filter as well as a wind energy extractor.

REFERENCES

[1] H. Geng, D. Xu, B.Wu and W.Huang, "Direct Voltage Control for a Stand-Alone Wind-Driven Self-Excited Induction Generator with Improved Power Quality". *IEEE Transactions on Power Electronics*, No.26, pp.2358-2368, 2011

[2] D. Seyoum, M.F. Rahman, and C. Grantham, "Terminal Voltage Control of a Wind Turbine Driven Isolated Induction Generator Using Stator Oriented Field Control". *Proceedings of IEEE Power Electronics Conference and Exposition-APEC*, No.**2**, pp. 846-852, 2003.

[3] S. S. Murthy, O. P. Malik, and A.K. Tandon, "Analysis of self-excited induction generators," *Proc. IEE*, vol. 129, No. 6, pp. 260-265, 1982.

[4] G. Raina and O. P. Malik, "Wind energy conversion using a self-excited induction generator," *IEEE Transactions on. Power Apparatus and Systems*, vol. PAS-102, no.12, pp.3933-3936, 1983.

[5] F.M.Fayez, El-Sousy, Mohamed Orabi and Hatem Godah: "Maximum Power Point Tracking Control Scheme for Grid Connected Variable Speed Wind Driven Self-Excited Induction Generator", The Korean Institute of Power Electronics (KIPE), Journal of Power Electronics (JPE), Vol. 6, No.1, pp.52-66, January 2006.

[6] Lahcene Quazene and George McPherson: "Analysis of The Isolated Induction Generator", IEEE Trans. on Power Apparatus and Systems, Vol.PAS-102, No.8, pp.2793-2798, August 1983.

[7] R. Cárdenas, R. Peña, G. Asher, and J. Clare: "Control strategies for enhanced power smoothing in wind energy systems using a flywheel driven by a vector-controlled induction machine", IEEE Trans. Ind. Electron., vol. 48, pp. 625-635, June 2001.

[8] C. Seyoum, Grantham and M. F. Rahman: A novel analysis and modeling of an isolated self-excited induction generator taking iron loss into account, IEEE Transactions on Industrial Applications Vol. 35, No. 3, April 2003.

[9] M. Godoy Simoes, Felix A. Farrett," Alternative energy systems: design and analysis with induction generators", CRC Press, Taylor & Francis Group, Boca Raton London, New York 2008.

[10] Shakuntla Boora, "Analysis of Self-Excited Induction Generator under Balanced or Unbalanced Conditions", ACEEE International Journal on Electrical and Power Engineering, Vol. 01, Issue No. 03, December 2010.

[11] Shakuntala Boora, Gitanjali Das, "Simulink Modeling of Induction Machine Performance in Different Reference Frames", International Journal of Electronics, Electrical and Computational System IJEECS ISSN 2348-117X Volume 5, Issue 4 April 2016.

[12] H. Geng. D. Xu and B. Wuare, "Direct voltage control for a stand-alone wind-driven self-excited induction generator with improved power quality," IEEE Trans. on Power Elect., vol. 26, no. 8, pp. 632-641, August 2011.

[13] A. Karthikeyan, C. Nagamani, G. Saravana, A. Sreenivasulu, "Hybrid, open-loop excitation system for a wind turbine driven stand-alone induction generator" IET Journal on Renewable Power Generation, vol. 5, Issue no. 2, pp.184-193, August 2011.

[14] T. Burton, D. Sharpe, N. Jenkins, and E. Bossanyi, Wind Energy Handbook, John Wiley & Sons Ltd., Chichester, England, 2001.

[15] B. Singh and L. B. Shilpakar, "Analysis of a novel solid state voltage regulator for a self –excited induction generator", IEEE Proceedings on Generation, Transmission and, Distribution, vol. 145, no. 6, pp. 647-655, November 1998.

[16] N.S.Jayalakshmi and D.N.Gaonkar, ''Dynamic Modeling and Analysis of an Isolated self-excited induction generator driven by wind turbine'', *IEEE Transsactions*, pp. 1-5,2012.

[17] Avinash Kishore, G.Satish Kumar, ''A Generalized State-Space Modeling of Three Phase Self-Excited Induction Generator For Dynamic Characteristics and Analysis'', IEEE Trans.at.ICIEA 2006.

[18] Birendra Kumar Debta, Kanungo Mohanty "Analysis, Voltage Control and Experiments on a Self-Excited Induction Generator". Vol..9, Journal on Renewable Energy & Power Quali

[19] K. Trinadha, A. Kumar, K. S. Sandhu, ''Study of Wind Turbine based SEIG under Balanced/Unbalanced Loads and Excitation' 'International Journal of Electrical and Computer Engineering (IJECE) Vol.2, No.3, pp. 353-370 , , June 2012.

[20] A. Kishore, R. C. Prasad, and B. M. Karan, ''MATLAB SIMULINK Based DQ Modeling and Dynamic Characteristics of Three Phase Self Excited Induction Generator'', Progress In Electromagnetics Research Symposium, Cambridge, USA, pp. 26-29, March,2006.

[21] D. Seyoum, C. Grantham, and M.F. Rahman, "The dynamic characteristics of an isolated generator driven by a wind turbine," IEEE Trans. on Ind. Appl., vol. 39, no.4, pp. 936-944. July/ August 2003.

E-ISSN 2581 – 7957
P-ISSN 2277 – 3916

CVR Journal of Science and Technology, Volume 17, December 2019
DOI: 10.32377/cvrjst1717

Plug-in Electric Vehicle Connected to Nano-Grid without Storage System

V. Mounika[1] and Dr. S. Venkateshwarlu[2]
[1]PG Scholar, CVR College of Engineering/EEE Department, Hyderabad, India
mounikavampu94@gmail.com
[2]Professor, CVR College of Engineering/EEE Department, Hyderabad, India
svip123@gmail.com

Abstract: **Vehicle-to-Grid (V2G) describes a system in which plug-in electric vehicles, such as Battery Electric Vehicles (BEV), Plug-in Hybrid Electric Vehicles (PHEV) communicate with the power grid to sell demand response services by either returning electricity to the grid or by throttling their discharging rate.V2G storage capabilities can also enable EVs to store and discharge electricity generated from renewable energy sources such as solar and wind. When the vehicles are parked in a parking-slot, the power can be sent from Vehicle to the DC bus-bar or to the grid. From each Electric-vehicle the voltage level and State of Charge (SOC) information is uploaded to the CLOUD on a regular basis. Fuzzy-Logic shall determine the participation factor/ranking of each vehicle and is communicated to the CLOUD. The Central Controller will receive the uploaded data and depending upon the load requirement the best vehicle(s), to be connected to the grid, is/are shortlisted. The selection information is then informed to the respective electric vehicle, through cloud, so that power is sent from V2G.**

Index Terms: Electric vehicles, Fuzzy logic, Electric Storage, Internet of Things **Cloud, Frequency regulation, Nano-grid, Vehicle to Grid**

I. Introduction

The increase in population has also increased the demand for power generation. The traditional way to generate electricity is by using hydro, coal, fossil fuels, biogas etc. Depletion of these energy sources cause future generation to suffer from electricity scarcity. So, with the advancement in technology renewable energy sources like solar energy, wind energy, wave energy, etc. are being used for the generation of electricity. Release of carbon emissions into the atmosphere by burning fossil fuels from thermal plants, industries, motor vehicles cause global warming, increasing the temperature of the earth's surface and ocean causing melting of polar ice, rise in sea level, desertification. So, countries are encouraged to go for renewable resources

Penetration of renewable energies have become one of the most promising technologies. Though the renewable sources are abundant and economical, but not possible to utilize them completely for rising power demand. It causes a mismatch between the supply and the load that makes the grid unstable. So, to solve above issues a new technology has been introduced recently is the Vehicle to grid(V2G). V2G is the exchange of power between the storage of

TABLE I.
CONTROL TECHNIQUES USED IN LITERATURE

1	Charge Control and Operation of Electric Vehicles in Power Grids: A Review	Paper presented the control and optimization strategies for managing the charging/discharging EVs	-
2	Research on Vehicle-to-grid Technology	To strengthen the regulation and operation management for electric vehicles.	-
3	Integrating E-Vehicle into Power System by the execution of Vehicle-to-grid (V2G) Terminology- A Review	Survey of V2G innovation	-
4	Fuzzy Logic Control of Electric Vehicles: Design and Analysis Concepts	Nonlinear model-based analysis is performed	Fuzzy logic control
5	Load Frequency Control in Isolated Micro-Grids with Electrical Vehicles Based on Multivariable Generalized Predictive Theory	To improve the system frequency stability with complex operation situations	Multivariable Generalized Predictive Control (MGPC)
6	Vehicle-to-grid Bidirectional Energy Transfer: Grid Synchronization using Hysteresis Current Control	To achieve a flow of power between the power grid and the electric vehicle the in both the directions	Hysteresis Current Control method
7	Time of Use Price based vehicle-to-grid Scheduling of Electric Vehicle Aggregator for Improved Market Operations	To optimize EVs coordinated charging and earn monetary benefits for EV owner and System Operator	Price-based Demand Response Program (PBDRP) is proposed to enhance the value of EV owners

electric vehicles and the grid during high peak demand on the load side. Thus, contributes the clean and green environment. Electric vehicles can adjust their charging and discharging behavior based upon the load and State of Charge (SOC).

Electric vehicle is a vehicle that converts the electrical energy stored chemically in a battery to mechanical energy to move the vehicle. The types of electric vehicles available in the market are

1. Battery type electric vehicles which store energy electro-chemically in the battery like lead-acid, lithium-ion, nickel metal- hydroxide, etc. They must be plug-in to charge their battery and unplug to drive the vehicle.
2. Hybrid electric vehicles are vehicles that have more than one power source. The battery and the motor will drive the vehicle.
3. Fuel cell electric vehicles consist of two electrodes separated by electrolyte. The chemical reaction between the fuel and an oxidant directly converts the chemical energy of the fuel into electrical energy.

Electric vehicles can operate in two modes,1. Grid to Vehicle and 2. Vehicle to Grid modes of operation. In mode-1, the vehicle battery is charged from grid whereas in mode-2, the energy stored in the battery is given to the grid.

Authors of [9] Samy Faddel, Ali T. Al-Alwami has presented a review on charge control methods and operation of Electric vehicles in power grid. The objective of EV and HEV is that they help in reducing the CO_2 emission from the vehicle and help in reducing the dependency of oil in transportation. The EV as controllable load provides more flexibility to the system operator by Valley filling and peak shaving and to increase the efficiency in the demand side management system. Many strategies are introduced to control the EV charging to prevent the negative impact on the grid. They are classified into centralized, decentralized and autonomous charging controllers. Centralized EV charge control requires a good communication infrastructure. The decentralized charge controller has limited communication requirements. Whereas the autonomous charge controller is communication free. Among these strategies, the autonomous controller will reduce the communication traffic to the V2G aggregator. The different charge control strategies were overview based on real-time EV charge dispatch.

Paper [11] aim to improve the regulation and operation management of EVs. This paper explains the concept, scheme, and functioning of V2G. To reduce the greenhouse gases, an increase in oil prices of petrol or diesel and dependency on oil are the major reasons that made to develop EV. They have become more popular because of less pollution, low noise, and high efficiency. They also discussed the types of Electric Vehicles – Battery Electric Vehicle, Hybrid Electric Vehicle, and Fuel Cell Electric Vehicle available in the market. V2G will provide the peak power balancing, auxiliary storage (spinning reserve) and regulation service to balance the load frequency to the generation frequency and renewable energy sources storage and backup. The power sends to the grid in 2-ways, one way is that vehicles are joined to the distribution system at homes and the other way is vehicles are aggregated and joined to the transmission system in aggregation.

The authors of [15] Awais Hashmi and Muhammad Talha Gul have presented the survey on the latest innovation of Vehicle-to-grid. This V2G enables the two-way flow 'tween the EV and the grid. The structure of transport distribution network changes with the idea of V2G and solves the issues like filtering of current harmonics, balancing of load, control of power, etc. The vehicle will sit ideal for about 20-22 hrs. in a day and it will run for about 2-4 hrs. So, the maximum time it is at rest, at this time the vehicle can be connected to the grid to transfer its power from its battery to the grid to balance the grid storage/energy. They also explained the integrating of wind energy with EV for charging the EV battery so that the vehicle owners can save money and there will be no carbon emission from the vehicle into the atmosphere. They also explained the working principle of EV and the important sections like a storage unit, control unit, and impetus unit. Benefits and barriers for integrating V2G are also discussed briefly.

As EVs are complex electromechanical systems described by non-linear loads, so they have complex design and analysis. Jemma J Malaygiorgou and Antonio T. Alexandridis in [7] used the FLC system to control the inputs d & q components which are duty ratios of VSC, and boost converter and the external inputs are internal battery voltage and torque on car wheels. d- Component of VSC duty- ratio and boost converter duty- ratio is driven internally by fuzzy logic controllers to have optimum PMSM flux extraction and to determine battery operation and the externally driven component of a fuzzy logic controller is q- component of VSC duty-ratio input. Steady-state equilibrium is obtained when external uncontrolled inputs become constant. They proved that the EV scheme is Lyapunov stable for any bounded control inputs and the simulated results are verified with the theoretic analysis.

In a power system, deviation in frequency is one of the major reasons to cause power imbalances. The frequency changes in the system due to disturbances in load or fluctuations in renewable sources, for this reason, it is hard to maintain the desired frequency range in the system. In paper [6], Jun Yang and Zhili Zeng presented the V2G model as a solution for LFC. The EV is being used as a storage to provide energy to the grid during high load demand. Also, a controller is proposed based on Multi-Variable Generalized Predictive Control (MGPC) theory in load frequency control, to achieve Load frequency control the EV and the diesel generator are combined.

This paper [13] presents the two-way energy flow between the vehicle and grid enabling the V2G technology. EVs are used to transfer energy to the grid at peak time and extract from the grid at an off-peak time to charge the battery. Power converters like ac-to-dc and dc-to-dc converters are used to transfer power from G2V and V2G technology. The output from the inverter is synchronized by using a hysteresis current control method before feeding to the grid. Ac-to-dc converter acts as a rectifier in G2V mode and acts as an inverter in the V2G mode of operation,

E-ISSN 2581 – 7957
P-ISSN 2277 – 3916

CVR Journal of Science and Technology, Volume 17, December 2019
DOI: 10.32377/cvrjst1717

whereas the dc-dc converter acts as boost converter during battery discharge and as buck converter during the battery charging. The mode of operation either V2G or G2V is decided by the availability of SOC of the battery. If SOC is greater than the reference value, then it will be in V2G mode and if SOC is less than the reference value then it operates in G2V mode. All these observations are seen in Simulink software and the harmonics while power transfer is eliminated using LC filters. The main reason to use/develop Electric Vehicle is given here under.

Global population which is 6 Billion may increase to 10 Billion by 2050. Vehicles in use may increase from 700 Million in 2000 to 2.5 Billion by 2050.If all the vehicles are Internal Combustion Engine Vehicle (ICEV)then there will be extreme air pollution. So, sustainable transport is to be used like zero emission vehicles and that promotes public transport so that less vehicles on the roads. For charging these electric vehicles use renewable energy sources. Advantages of using Electric Vehicles with conventional vehicles are given here under.

A. Comparison of Energy sources used for transportation

- Fuels available in liquid form are petrol and diesel have similar energy content means having same specific energy. Compared to petrol, diesel has high density per unit volume, and it is economical.
- Fuels available in gaseous form are CNG - Compressed Natural Gas have low energy density compared to liquid fuels and hydrogen. Compared to liquid fuels and CNG, hydrogen has very high-power density.
- Batteries store energy in chemical form and give out energy in electrical form. With advancement in technology the size of the battery is reduced and have high capacity storage.
- Ultra-capacitors store energy in biostatic form have limited storage and ultra-flywheel store energy in mechanical form at high energy which are less reliable.

B. Pollution and Greenhouse gases

From vehicles many pollutants are released through smoke and termed as greenhouse gases that cause air pollution. They are

- Gases CO, CO_2, CH_4, NO_X (N_2O, NO and NO_2) are known as greenhouse gases. Due to the presence of these gases the infrared radiation is trapped in the atmosphere and causes greenhouse effect leads to climate change and global warming.

CO-carbon monoxide is poisonous gas that cause respiration problems in the humans and high amounts of CO2- carbon dioxide gas is released by ICE vehicles.NO_X are released into the atmosphere by diesel engines and can be minimized by using urea filters.

- $SO_X(SO_2)$- Sulphur dioxide gas is released into the atmosphere by coal based thermal power plants. When this gas reacts with the oxygen and water present in atmosphere produces sulfuric acid causes acid rains. By selecting coal with low Sulphur content for electricity production can be a solution for reducing SO_2levels.Total hydro carbons and SO_X gases will build ozone layer at the ground level which is very dangerous for human. It causes lung infections.

Therefore, emission of BEV is very less compared to ICEV and HEV lies between ICEV & BEV.

C. Energy diversification

ICEV use liquid fuels as fuel either oil or natural gas. PEV such as PHEV, BEV, FCEV uses electricity or hydrogen as energy carrier. The sources required for producing electricity can be oil, natural gas, coal or from renewable energy sources like hydro, solar, wind, tidal etc. Among all these vehicles PHEVs are most energy diversified and can run by both liquid fuels and electricity.

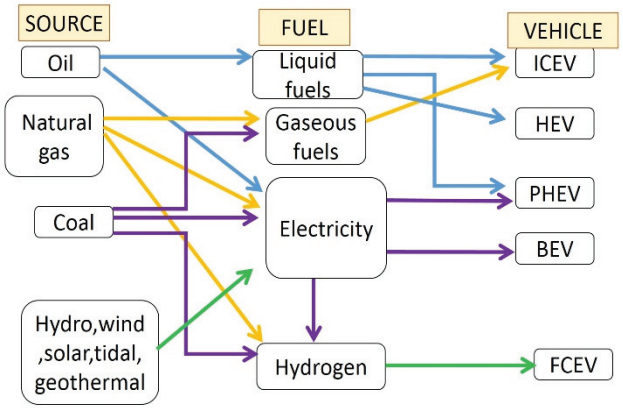

Figure 1. Energy Diversification Diagram

II. Overview of Different Electric Vehicles

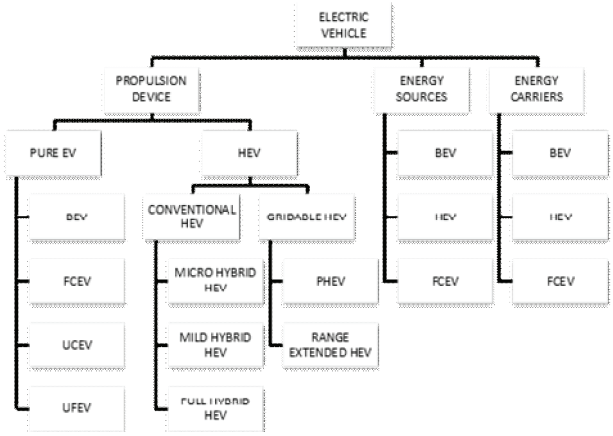

Figure 2. Electric vehicle Classification Tree

Electric vehicles based on **propulsion device** are classified into two types. They are as follows:

a) Pure electric vehicles and b) Hybrid electric vehicles

A. Pure electric vehicle

It is a vehicle that uses electric motor for propulsion. They are again classified into

1. Battery ElectricVehicle (BEV)- has battery as propulsion device.

2. Fuel Cell ElectricVehicle (FCEV)- consists of battery and fuel cell. The battery here used for absorbing regenerative power.

E-ISSN 2581 – 7957
P-ISSN 2277 – 3916

CVR Journal of Science and Technology, Volume 17, December 2019
DOI: 10.32377/cvrjst1717

3. Ultra Capacitor Electric Vehicle (UCEV)- consists of battery and ultra-capacitor. They have high specific power and stores limited energy.

4. Ultra Fflywheel Electric Vehicle (UFEV)- consists of battery and ultra-flywheel. They store energy in mechanical form at high energy and are less liable.

In above electric vehicles, battery is the common source. In FCEV, UCEV and UFEV battery is used as a hybrid source while battery in UCEV and UFEV is used for storing electrical energy since low specific energy.

B. Hybrid Electric Vehicle

It is a hybrid vehicle that uses both battery electric vehicle and IC engine as propulsion device. It offers refueling (petrol/diesel), consumes less fuel. These are classified into

(a). *Conventional hybrid electric vehicles* provide different capabilities to the system.

These are again classified into

1. Micro HEV

In this type, when the vehicle is at rest ISG supports starting and stopping of IC engine's enables recovery of regenerative energy during braking and ISG used here have low power capacity, voltage between 14-42 volts and are connected using belt-driven system.

2. Mild HEV

ISG here used has power capacity of 7-15kw and voltage between 100-150v which is slightly higher than Micro HEV type. It enables start-stop to feature, regenerative braking and power sharing during normal operation means ICE rating can be reduced.

3. Full HEV

This type offers more versatile operation and has a combination of ICE and motor to drive wheels. It requires electronic variable transmission (EVT) for 50-60kW at voltage 500-600v.It enables start-stop to feature, regenerative braking, power sharing and electric launch. Since Full HEV operates in various modes, ICE can operate in OOL (Optimum Operation Line).

Integrated Starter Generator (ISG)-is an electrical machine can be connected to IC Engine as Belt driven ISG or Crankshaft mounted ISG.

(b). Grid-able hybrid electric vehicles are vehicles that can be connected to the grid for power exchange between the vehicle and the grid during high load demand. These are again classified into

1. Plug-in hybrid electric vehicles

These vehicles are derived from Full HEV operates in blended mode. They require higher battery bank than Full HEV and battery will charge using charging probes.

2. Range extended hybrid electric vehicles

These vehicles are derived from Battery Electric Vehicle and mostly operate in Pure electric mode.

The difference between conventional HEV and grid-able HEV is, conventional HEVs can be refueled only at filling station or petrol bunk whereas, grid-able HEVs can be refueled electrically at filling stations enables direct charging of batteries by plug-in.

Electric vehicles classification based on energy sources are as follows:

a) Battery electric vehicle- In this vehicle, the battery is used as an energy source. b) Hybrid electric vehicle- In this vehicle, a combination of liquid fuels and battery is used as an energy source. c) Fuel cell electric vehicle- In this vehicle, a combination of fuel cell and the battery is used as an energy source.

Energy carrier is a medium to transfer energy from source to propulsion device. Electric vehicles classification based on energy carriers are as follows:

a) Battery electric vehicle uses electricity to transfer energy.

b) Hybrid electric vehicle uses both liquid fuels and electricity to transfer energy.

c) Fuel cell electric vehicle uses Hydrogen as energy transfer.

III. Challenges Faced by Different Electric Vehicles

A. Conventional HEV

The challenges faced by the electric vehicles are

1. They are non-zero emission vehicles.
2. Low energy diversification because oil and natural gases to be refilled after every use.
3. It has a complex system.
4. It requires variable transmission because it has its own transmission loss, creates noise and requires regular lubrication.
5. The system is quite heavy and bulky.

B. Grid-able HEV

1. These vehicles face all the challenges of conventional HEV.
2. These are high-cost vehicles as it requires high battery capacity.
3. In some vehicles they require installation of on-board charger.

C. Fuel cell EV

1. They have high initial cost since fuel cell cost is more.
2. Lack of hydrogen fuel infrastructure since it is not available.
3. Storage of hydrogen is very challenging. Hydrogen can be stored in 3 ways as
   (a). Gaseous form-compressed hydrogen gas
   (b). Liquid form- liquid nitrogen
   (c). Solid form- metal hydroxide
4. High safety concerns because of its explosive nature.

D. Ultracapacitors / Ultra flywheel EVs

1. They have a high cost.
2. They have low specific energy and cannot be used as a sole energy source as it requires a battery as HEV.
3. Ultra flywheel E Vs stores mechanical energy at high speed of flywheel often have high safety concerns.

E. Battery electric vehicle

1. They have a limited driving range.
2. High initial cost because battery size is more and limited life cycle.
3. Lack of charging infrastructure.

E-ISSN 2581 – 7957
P-ISSN 2277 – 3916

CVR Journal of Science and Technology, Volume 17, December 2019
DOI: 10.32377/cvrjst1717

IV. Fuzzy Logic Control System

Fuzzy Logic

Fuzzy logic is a multi-value system for its member elements in the range between 0 and 1. In traditional typeset we have Boolean types of answers either YES or NO, or TRUE or FALSE which is a true value logic. But in fuzzy logic we have partial cases between TRUE and FALSE.

A FLC consists of five functional blocks as indicated in fig.3. The rule base, the database, the fuzzifier, the inference engine and defuzzifier.

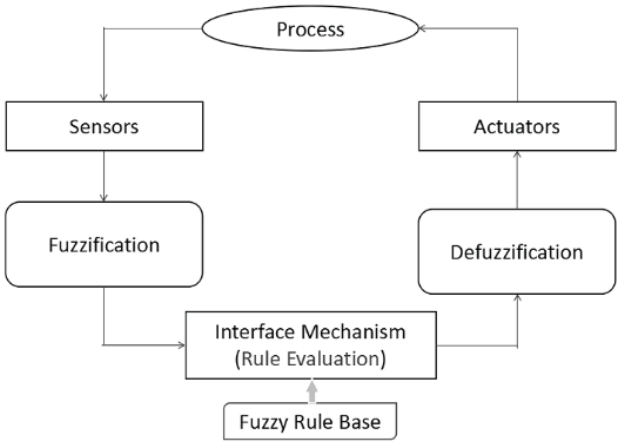

Figure 3. Fuzzy Logic Control

The fuzzy logic controller has sensors, actuators, fuzzification, inference engine and defuzzification. The input to the controller is given in word form or in sentence called as linguistic variables for example age, temperature cost.

Now a days age is defined by infant, young, old, very old and the cost is defined by very cheap, cheap, expensive these are termed as linguistic values to the given input.

Membership function represents the degree of truth in fuzzy logic and tells whether the elements present in the system are continuous or discrete. It is represented in graphical form. The Number of linguistic values is equal to the number of membership functions.

Before the inputs are given to the controller they are normalized.

1. Normalization:

Normalization is a procedure where the input values are normalized in a specific range.

2. Fuzzification:

Fuzzification is a process of converting normal values/crisp values to fuzzy values (linguistic variables). Based on membership functions apply membership function to normal values so it becomes fuzzy membership values.

(a) Fuzzy set: It defines the value between 0 and 1.

(b) Crisp set: It defines the value is either a 0 or 1.

Membership functions are selected and assigned based on the input and nature of input variable. Next fuzzy values are provided to the inference engine for controlling the further applications. This process of selecting membership functions and applying them on input is called as knowledge base. The membership functions for the input and output are given in fig. 4, 5 and 6

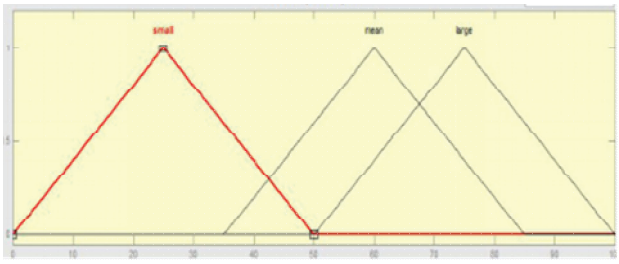

Figure 4. Membership function for SOC

It is the main part of the controller works on rules provided by the programmer. Fuzzy inputs are given to the inference engine and it selects the appropriate rules which are predefined and satisfies the fuzzy input values then applies the rule to get the fuzzy output. This process is called rule base system (it is also called as the heart of the system). The rules are written in 'IF'(antecedent) and 'THEN'(consequent) statements.

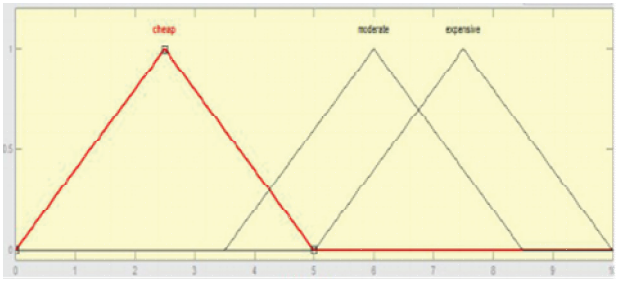

Figure 5. Membership function for COST

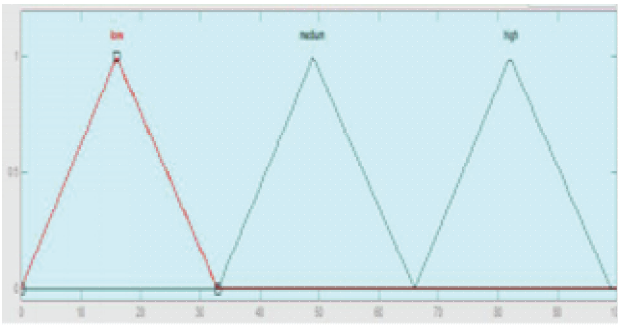

Figure 6. Membership function for EV Rating

3. Inference Engine:

It is the main part of the controller, works on rules provided by the programmer. Fuzzy inputs are given to the inference engine and it selects the appropriate rules which are predefined and satisfies the fuzzy input values then applies the rule to get the fuzzy output. This process is called rule base system (it is also called as the heart of the system). The rules are written in 'IF'(antecedent) and 'THEN'(consequent) statements.

4. Defuzzification:

E-ISSN 2581 – 7957
P-ISSN 2277 – 3916

DOI: 10.32377/cvrjst1717

Defuzzification is a process where fuzzy output values are now converted to crisp values. These values portray the actions taken by the fuzzy controller in individual control cycles. And the final output from defuzzification is given to the system. Defuzzification is also called as "rounding it off".

We have many types of inference mechanisms like Mamdani, Takagi Sugeno, etc. Among this Mamdani inference mechanism is chosen for its simplicity and easy to use. This is a direct adaptive mechanism where controllers are designed directly based on fuzzy rule base.

V. Description and Block Diagram of EV Connected to Nano Grid

The block diagram consists of 3-electric vehicles EV-1, EV-2 and EV-3 each composed of fuzzy logic controller and a battery are connected to a DC bus-bar through switches S-1,S-2 and S-3 respectively. Load is connected to the DC bus bar.

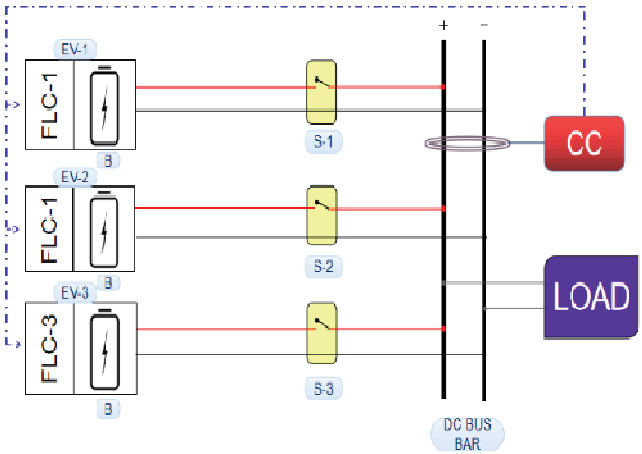

Figure 7. Block diagram of EV connected to Nano grid

The central controller will function as an information exchange between the vehicle owner and the Cloud. The information is based on the state of charge, tariff and voltage level of the battery. Cloud is a source of information storage. The voltage from the DC bus is taken as a reference voltage. If the threshold voltage is less than the reference voltage, then number of vehicles are connected to the circuit and if the threshold voltage is greater than the reference voltage then vehicles are not connected to the circuit. The fuzzy logic controller present in each vehicle will decide the ranking of the vehicle depending upon the state of charge, tariff and voltage level. The information of the vehicles with high SOC, voltage and low tariff are preferred from the central controller and this information is given to the fuzzy controller to give ranking for the vehicles. The detailed working procedure of the fuzzy controller is given in Section-IV. Once the ranking is given the vehicles are connected to the bus bar through switches. The flowchart corresponding to the implementation of the methodology is mentioned in figure 9.

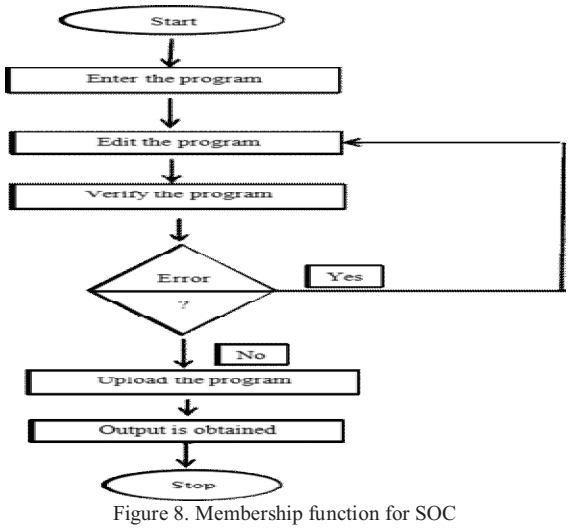

Figure 8. Membership function for SOC

VI. Results

The EVs that are parked can be connected to the power grid to send their battery power to balance the peak demand. The cost per unit and SOC of battery of each EV is given to the central controller through CLOUD.

The proposed topology is implemented and tested on a hardware kit shown in fig.9

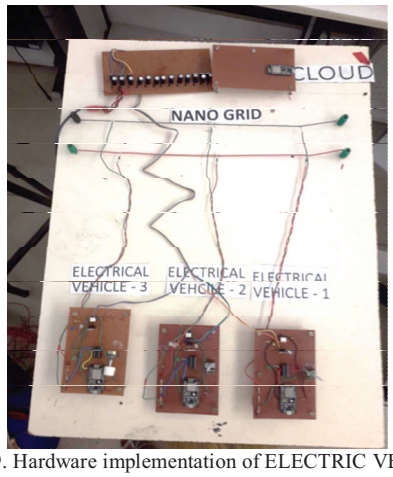

Figure 9. Hardware implementation of ELECTRIC VEHICLE

The kit is tested using fuzzy logic controller in MATLAB Software version 2015b. This fuzzy logic controller will compare the measured values from the EVs with the reference values and decide the ranking/participation factor/rating of the EV. Once the rating is obtained, it is given to the EV through central controller via CLOUD.
The output values are shown below table 2.

TABLE II.
OUTPUT VALUES OF COST, SOC AND EV RATING

COST	SOC					EVR
	50	60	70	80	90	
1	14	13	12	12	11	10
2	17	16	15	14	13	12
3	17	16	15	14	13	12
4	13	12	12	11	10	10
5	22	21	20	19	19	18
6	30	29	29	28	27	27
7	34	33	32	31	31	30
8	33	32	31	30	30	29
9	40	39	38	37	36	35
10	40	39	38	37	36	35

It can be observed from the above table when the cost is low and SOC is high, EV rating is high. The central controller will choose the EV to be connected is based on high rank i.e. low cost and high SOC of battery.

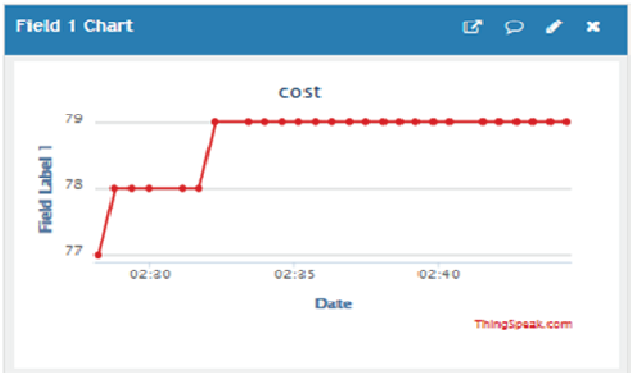

Figure a) cost

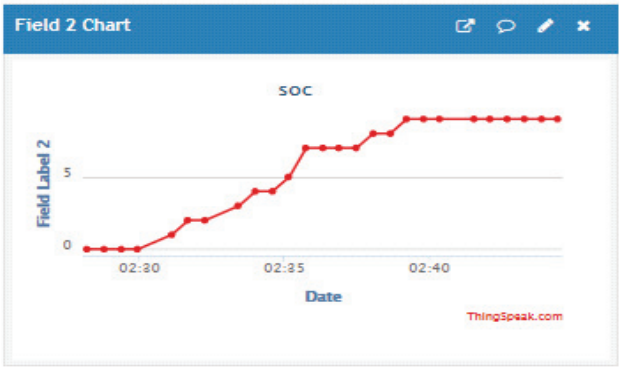

Figure b) soc

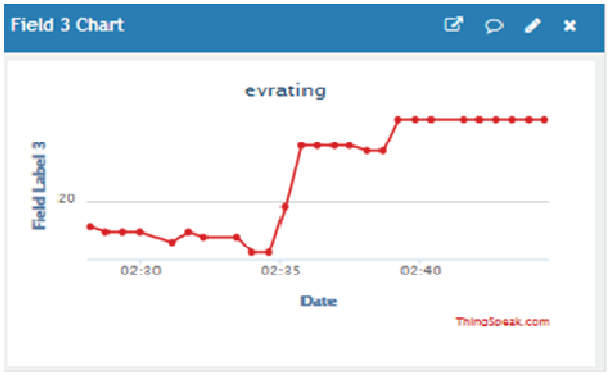

Figure c) EV rating

Figure 10. Outputs of a) COST, b)SOC and c)EV Rating in IoT

VII. CONCLUSIONS

Vehicle-to-grid (V2G) describes a system in which plug-in electric vehicles, such as battery electric vehicles (BEV), plug-in hybrids (PHEV) communicate with the power grid to sell demand response services by either returning electricity to the grid or by throttling their discharging rate.V2G provides ancillary services like reactive power support, load balancing, frequency control and enhancing renewable energy penetration to the grid. From each Electric-vehicle the voltage level and State of Charge (SOC) information is uploaded to the CLOUD on a regular basis. Fuzzy-Logic shall determine the participation factor/ranking of each vehicle and is communicated to the CLOUD. The Central Controller will receive the uploaded data and depending upon the load requirement the best vehicle(s), to be connected to the grid, is/are shortlisted and this information is given to the EV owner to connect his vehicle to the grid to transfer the power. By sending power from V2G, the EV owner will benefit economically.

In future, by connecting inverters the DC voltage from the EV can be converted to the AC voltage and the aggregate of this power could be given to the AC grid using wireless transmission.

REFERENCES

1. M. H. Hajimiri and F. R. Salmasi, “A fuzzy energy management strategy for series hybrid electric vehicle with predictive control and durability extension of the battery,” 2006 IEEE Conf. Electr. Hybrid Veh. ICEHV, pp. 1–5, 2006.
2. M. Jawad, M. B. Qureshi, A. Nadeem, S. M. Ali, N. Shabbir, and M. N. Rafiq, “Bi-Directional Nano Grid Design for Organizations with Plug-In Electric Vehicle Charging at Workplace,” IEEE Int. Conf. Electro Inf. Technol., vol. 2018-May, pp. 357–361, 2018.
3. K.S.V.Phani Kumar and S.Venkateshwarlu, “A Neuro-Fuzzy Controlled Solar Photovoltaic and PHEV based Frequency Regulation in a Microgrid without Storage System,” J. Green Eng., vol. 7, no. 1, pp. 311–332, 2017.
4. K.S.V. Phani Kumar and S.Venkateshwarlu, “Impact of distance on the harmonic active power drawn from the source and the effect on frequency of the system,” Lect. Notes Electr. Eng., vol. 436, no. 2, pp. 1–6, 2010.
5. M. T. Dai, J. H. Zheng, M. Zhang, and W. Z. Wang, “Optimization of electric vehicle charging capacity in a parking lot for reducing peak and filling valley in power grid,” APAP 2011 - Proc. 2011 Int. Conf. Adv. Power Syst. Autom. Prot., vol. 2, pp. 1501–1506, 2011.
6. J. Yang, Z. Zeng, Y. Tang, J. Yan, H. He, and Y. Wu, “Load frequency control in isolated micro-grids with electrical vehicles based on multivariable generalized predictive theory,” Energies, vol. 8, no. 3, pp. 2145–2164, 2015.
7. J. J. Makrygiorgou and A. T. Alexandridis, “Fuzzy logic control of electric vehicles: Design and analysis concepts,” 2017 12th Int. Conf. Ecol. Veh. Renew. Energies, EVER 2017, 2017
8. A. A. Ferreira, J. A. Pomilio, G. Spiazzi, and L. de Araujo Silva, “Energy management fuzzy logic supervisory for electric vehicle power supplies system,” IEEE Trans. Power Electron., vol. 23, no. 1, pp. 107–115, 2008.

9. S. Faddel, A. T. Al-Awami, and O. A. Mohammed, "Charge control and operation of electric vehicles in power grids: A review," Energies, vol. 11, no. 4, 2018.
10. T. T. Lie, K. Prasad, and N. Ding, "The electric vehicle: a review," Int. J. Electr. Hybrid Veh., vol. 9, no. 1, p. 49, 2017.
11. Y. Tu, C. Li, L. Cheng, and L. Le, "Research on vehicle-to-grid technology," Proc. - Int. Conf. Comput. Distrib. Control Intell. Environ. Monit. CDCIEM 2011, pp. 1013–1016, 2011.
12. S. Sharma, P. Jain, R. Bhakar, and P. P. Gupta, "Time of Use Price based Vehicle to Grid Scheduling of Electric Vehicle Aggregator for Improved Market Operations," Int. Conf. Innov. Smart Grid Technol. ISGT Asia 2018, pp. 1114–1119, 2018.
13. B. Rajalakshmi, U. Soumya, and A. G. Kumar, "Vehicle to grid bidirectional energy transfer: Grid synchronization using Hysteresis Current Control," Proc. IEEE Int. Conf. Circuit, Power Comput. Technol. ICCPCT 2017, 2017.
14. S. Esther, S. K. Singh, A. K. Goswami, and N. Sinha, "Recent Challenges in Vehicle to Grid Integrated Renewable Energy System: A Review," Proc. 2nd Int. Conf. Intell. Comput. Control Syst. ICICCS 2018, no. Iciccs, pp. 427–435, 2019.
15. A. Hashmi and M. T. Gul, "Integrating E-vehicle into the power system by the execution of vehicle-to-grid (V2G) terminology - A review," 2018 Int. Conf. Eng. Emerg. Technol. ICEET 2018, vol. 2018-January, pp. 1–5, 2018.
16. K. T. Chau, Z. Zhang, and F. Lin, "Chaotic modulation for vehicle-to-grid power interface," Proc. 2014 Int. Conf. Intell. Green Build. Smart Grid, IGBSG 2014, 2014.
17. B. C. Liu, M. Ieee, K. T. Chau, F. Ieee, D. Wu, and S. M. Ieee, "Opportunities and Challenges of Vehicle-to-Home, Vehicle-to-Grid Technologies," pp. 1–19, 2013.

E-ISSN 2581 – 7957
P-ISSN 2277 – 3916

CVR Journal of Science and Technology, Volume 17, December 2019
DOI: 10.32377/cvrjst1718

A Simplified Method of Improving the Power Quality in Power Electronic Circuits using a Single Pair of IGBTs

Dr. Dakka Obulesu[1], Mr. Rajashekher Koyyeda[2], Dr. T.C.Manjunath[3]
[1]Assoc. Professor, CVR College of Engineering/ EEE Department, Hyderabad, India
Email : dakkaobulesh@gmail.com
[2]Research Scholar (Part-Time), USN : 5VX17PES90, VTU RRC, Belagavi, Karnataka, India
Email: rajashekher.koyyeda@gmail.com
[3]Prof. & HOD, Dayananda sagar College of Engineering/ECE Department, Bangalore, Karnataka, India
Email : dr.manjunath.phd@ieee.org

Abstract : **This paper presents a method to reduce harmonic components in voltage-sourced circuits utilizing IGBT switches and diodes using the PWM technique and also presents a technique to improve the power quality, using a single pair of IGBTs (level-1 or stage-1). This model was developed in Simulink using the designed circuitry, which can be used for improving the power quality. The simulation results are obtained by performing the simulations in the MATLAB-Simulink environment.The simulation results demonstrate the efficacy of the method developed for harmonic suppression in power electronics-based systems, which can greatly improve the power quality.The work can also be extended to a 2-level and a 3-level inverter for an improvised versions for future works.**

Index Terms: **Elimination, Breakers, Current, Voltage, Control, Simulation, Total Harmonic Deduction, Power Semiconductor Devices, Suppression, Power Quality, Harmonics, Distortion, Level, PWM, IGBT.**

I. INTRODUCTION

The control of any device or equipment using electronic means in today's digital world finds many applications, which necessitates improvement in power quality. This world of innovations relies deeply on the seamless and continued access to electrical force or energy. Today's world is truly empowered to work at its busy pace by the availability of power commercially. Our homes and workplaces have seen the deep penetration of modern innovations and with the rise in electronic trade and commerce, the manner in which we interface with the world is constantly changing. A fundamental element in a modern and inclusively advancing nation is electric vitality. The proper quality of force, energy, or power can guarantee the ideal use of electric power. Since the power usage is relative, unwavering supply quality with flexibility of procedure is quite important [1–10].

In general, power is different from other commodities–it is created far away from where it will be used, it is transferred to the framework with the yield of many different generators, and it finally reaches the place where it is to be used through transformers in kilometers through overhead and conceivably underground cables. In privatized, commercial electrical businesses,various associations or companies own, supervise, and maintain the system resources. It is quite difficult to assure the quality and nature of the power that is transferred at the place and purpose of utilization.. Moreover, substandard power can neither be taken back from the store network nor rejected by the client or the end-user [11–20].

As mentioned, electrical power is a key element for development in any nation. Without electricity, the whole world will plunge into darkness, with the country's economy falling drastically – after all, every working device requires electricity. The world, therefore, should grateful to Thomas Alva Edison and Benjamin Franklin, Who discovered this great wonder, a thing of great importance today [21-30].

Harmonic spikes have various undesirable consequences for an appropriation framework of electrical distribution networks. They are of two types: short-term effects and long-term effects. Short-term effects are generally easily recognized, identified by over-the-top voltage mutilation. On the other hand, expanded resistive loss or voltage stress can normally identify long-term (also long-haul) effects, which frequently go undetected . Likewise, the consonant streams created by non-straight loads can associate destructively with a wide variety of electrical power equipment, mostly capacitors, transformers, engines, and generators, causing additional, overheating, loss and over-burdening [31–40].

The development of harmonic currents causes interference in telephone cables and lines. Standards to depict a practical structure for harmonic surge control have been created to offset the adverse impacts of harmonic surges on power quality. The goal is to ensure consistent – state harmonic limits that are considered acceptable by both electric utilities and their clients [41–50].

Distortion of harmonics within a power or force appropriation systems can be suppressed by implementing two methodologies: latent/passive and dynamic/passive and dynamic/active fueling. The passive type of sifting/filter by far remains the easiest and popular solution to address the problem of mutation encountered in harmonics. Since the use of detached components – which, over the years, have created an abnormal state of modernity – does not react precisely to the progression of electrical energy transmission frameworks, they have been modified to allow the

sidestepping or even by passing of certain consonant frequencies.. [1–25].

Harmonics are voltage (v) and current (i) frequency components that are embedded at the crest level of the normal sine v and i. The symphonious distortion in the waveform is mostly, because of significant increases of non-straight loads and because of innovative progresses, e.g., the use of force electronics circuits and gadgets, in AC/DC transmission connections, or burdens in the control of force frameworks using power electronics or microchip controllers. Harmonic sources are categorized into three types of loads: household load, industry load, and controlling device [25–50].

Present-day electronic gadgets, served by power circulation circuits, possess some level of symphonious frequencies. Although the surge v and i do not generally create problems, the more pronounced electrical power or energy drawn by the advanced gadgets or other non-straight loads, the more pronounced is the voltage mutilation level. Harmonic generation is related to a number of complications, such as malfunctioning of the equipment; breakers tripping suddenly; lights turning on and off suddenly; large neutral currents; heating up of conductors in the phase, loads, and transformers; UPS and transformers failing suddenly; low power factor; voltage and current surges; and depletion of system's capacity [1-50].

Hence, the question now is how to prevent harmonics. To reduce the overall harmonic content in a device, circuit, equipment, or a part of the network. One efficient method is to select a device and follow a good installation practice. If for some reason the issues cannot be detected by these elementary measures, then two fundamental steps can be taken to strengthen the distribution framework to endure voltage or current surges or introducing a gadget to mitigate or eliminate the harmonics. There are numerous methods to lower voltage or currents surges; they can range from makeshift ones to even costly and elaborate ones. Some examples include incorporating latent symphonious channels, transformers that can confine or moderate consonants, harmonics suppression networks, and dynamic channel filtering mechanisms.

The harmonic effect in a system's voltage or current is always determined in terms of the total harmonic distortion (THD) factor and high- and low-level harmonic contents. Ideally, any industry application requires the load voltage or current to be free of harmonics or at the least be < 5% of the harmonics. Most studies have shown that the THD can be lessened by a number of methodologies. There are a number of structure arrangements that can be used to resolve or reduce the impact of supply quality issues, and it is an exceptionally dynamic area of development and improvement. In such a scenario, it is advisable for clients to know about the scope of arrangements available as well as the relative merits and costs. Some important techniques used to minimize sounds/surges in voltage or current are filters that are either passive or active in nature, separation transformers,surge-reducing transformers, surge-suppression systems, and so on.

For this study, a large number of research papers were collected from various sources, studied at length, and a brief review was carried out. In-depth reviews were performed for power-quality improvement on active filters, active power filters, and active harmonic filters by Singh B., Al-Haddak, Chandra A., El-Habrouk M., Darwish M.K., Mehta P., and Akagi H. These review papers prove sufficient for first-time reviewers to understand the basic concepts of filter design, its deployment, and its further use. The principle of generation of signals for inverters and converters, which could be used in power systems for harmonic eradication, has been explained in details by D. G. Lipot A. A new concept of selective harmonic elimination scheme (SHES) for a three-phase voltage source inverter (VSI) was presented by Karthikeyan et al. based on concepts of the generation of opposite harmonic injection using the software package MATLAB.

In most of the works performed by various authors or researchers discussed in the previous paragraphs [1–50], there were certain drawbacks, disadvantages, or failures, such as they developed the algorithms only for linear loads,but higher harmonics could not be eliminated and the control algorithms were not efficient, only two to three stages of designs were used, noise was one of the important factors that could not be eliminated, the performance indices were low, very few worked on nonlinear loads, that too with respect to inductive and capacitive loadings, and so on.

In this paper,will try to address some will try to address of the above-mentioned drawbacks [1–50], and the effects of harmonics on the various types of devices will be studied in brief, a thorough analysis will be made, and new algorithms will be developed to suppress the harmonics, which will be verified through effective simulation results in the MATLAB–Simulink environment, along with the development of some hardware implementation to substantiate the research problem undertaken.

One typical issue in electrical,electronics,mechatronic, instrumentation, and computer-based systems has been maintaining the THD at below 5% level. When power sources are introduced into a circuit, it draws bended waveforms that contain some unwanted waveforms, which occurs due to the presence of direct and indirect loads. These sounds can impede the working of other electronic frameworks.

Consequently,it is important to quanity the aggregate impact of such sounds. Complete harmonic distortion provides data about the symphonious substance in a sign with respect to the key segment. Harmonic distortion levels in power systems are commonly measured as THD it can be defined as the ratio of total harmonics to the value at fundamental frequency [15].

It is mathematically represented as

$$THD = \frac{\sqrt{V_2^2 + V_3^2 + \ldots\ldots\ldots\ldots + V_n^2}}{V_1},$$

where V_n is the RMS voltage of the n^{th} harmonic and $n = 1$ is the fundamental frequency [1–25].

E-ISSN 2581 – 7957
P-ISSN 2277 – 3916

DOI: 10.32377/cvrjst1718

TABLE I.
FORMULAS FOR COMPUTING THE HARMONIC PARAMETERS

Harmonic order	$n = f_n/f_1 = GX_C/X_L$	f_1 = fundamental frequency
Quality factor	$Q = nX_L/R = X_C/(nR)$	$\omega = 2\pi f_1$ = angular frequency
Bandwidth	$B = f_n/Q$	f_n = tuning frequency
Reactive power at f_1	$Q_C = (V^2/X_C)\cdot n^2/(n^2 - 1)$	n = harmonic order = (f_n/f_1)
Active power at f_1(losses)	$P \approx (Q_C/Q)\cdot n/(n^2 - 1)$	V = nominal line–line voltage
		X_L = inductor reactance at fundamental frequency = $L\omega$
	where	X_C = capacitor reactance at fundamental frequency = $1/(C\omega)$

It is quite important to discuss the consequences of harmonics in power electrical devices, with one major effect of power system harmonics being that the current in a system which increases. This happens particularly for the third harmonic, generating a sharp increase in the zero sequence current and consequently increasing the current in the neutral conductor. This fact needs to be taken into consideration when designing an electric system that can serve nonlinear loads. Along with the increased line current, different parts of the electrical equipment can undergo damage due to the effects of harmonics on power systems. Harmonics have been experienced by electrical systems since a long time, starting from when the first AC generator went online more than a century back. Harmonics, which is very important in supplying smooth power to devices, were however very minor and had no detrimental effects back then; however, currently, with the rapid development of industrialization, it has to be given due consideration [26–50].

This study has been sectioned as follows. A background introduction with respect to the work done is presented in the Introduction section 1. Review of the single-stage inverter is presented in section 2. Development of the Simulink model is presented in section 3. Selection of the simulation parameters is presented in section 4. Running of the developed Simulink models, i.e., the process of simulation, as well as observation of the results is presented in section 5. In section 6, a discussion on the simulated results is presented, along with comments on the reduction of THD in the work considered. Conclusions are presented in section 7, followed by the acknowledgments in section 8 and a brief list of references used in the research paper in the reference section models.

II. REVIEW OF THE SINGLE-STAGE INVERTER

In this section, single-phase circuits, i.e., inverters, are designed in such a way that maximum harmonic contents can be reduced using single-stage, double-stage, or triple-stage half-bridge–full-bridge inverters so that the harmonic contents are reduced when the load is switched on and off. However, as per the context, we have used only a single-phase inverter, i.e., one stage only.

IGBTs and diode blocks are used in the construction of multistage models. IGBTs are very powerful switching devices that can be used for full harmonic suppression to obtain a smoothened output free of harmonics. After designing a proper filter and placing it at the output of the inverter, the harmonics-free waveforms can be observed. Finally, FFT analysis is carried out using the FFT commands and the "powergui" tools available in the MATLAB–Simulink window. The design is performed in one stage only, i.e., using a single pair of IGBTs.

IGBT and diodes are used to design the voltage source converter, which are controlled in the OL fashion using the discrete PWM generator. In this context, it is to be noted that the IGBT is a modified version of a gate turn-off (GTO) switch or a metal oxide silicon field effect transistor (MOSFET). In these devices, the forward voltages of the models are not considered as they do not have any role to play. The harmonic elimination system consists of only 1-ϕ models, i.e., a one is a half-bridge (single stage), and finally the performance criteria are evaluated for the single-phase case.

III. DEVELOPMENT OF THE SIMULINK MODEL

The Simulink model can be constructed using certain blocks available in the Simulink modeling library: thyristor bridges,DC sources, transformers,inductive loads,gain blocks,multiplexers,FWDs,scopes,scinks,output sources, comparators,pulse generators, and connectors Once the circuit is designed, all of the blocks have to be pulled from the Simulink library into the model and a file has to be developed. In addition, various toolboxes, such as the control system toolbox, the sim-power-systems toolbox, and signal processing toolboxes available in the Simulink, library are used. Scopes are connected at the outputs and inputs to observe the different waveforms. Note that each leg of an inverter consists of a pair of IGBTs.

Our design is used in parallel combination as it a well-known fact that when harmonic filters are connected in parallel, they yield excellent harmonic reduction in the output voltage. In the Simulink model shown, the single-phase circuit uses the same DC voltage (V_{dc} = 100V), carrier frequency (1 kHz), and modulation index (m = 0.9) for obtaining improvement in power quality. When developing the Simulink model, numerous parameters require to be set in the various blocks. In addition, to help detect voltage and currrent waveforms, scopes are connected at requisite points.

E-ISSN 2581 – 7957
P-ISSN 2277 – 3916

CVR Journal of Science and Technology, Volume 17, December 2019
DOI: 10.32377/cvrjst1718

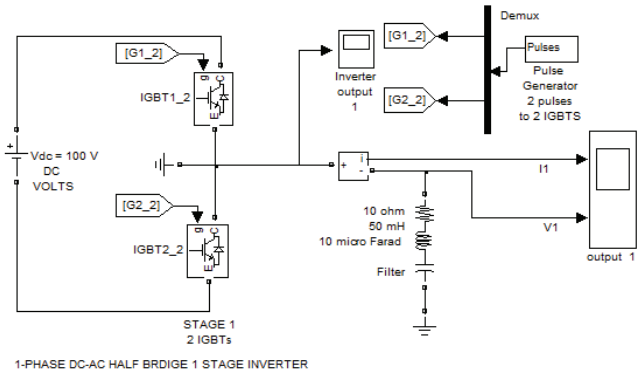

Figure 1. Simulink models for the one-stage harmonic reduction systems

The output signals are seen in the scope connected to stage-1, which shows that there is a drastic improvement in the harmonic-level suppression. An RLC filter stage is designed in such a way that its anti-harmonic signals are produced for the suppression of harmonic devices, which are produced due to the inverter actions, to obtain smooth output waveforms and to further improve the power quality. Outputs are observed for RL-, LC-, R-, and L-type filters also at the output of the load. In above Fig 1. The modeling design is performed in one stage only, viz., using a 1-ϕ, half-bridge inverter with one pair.

IV. Selection of the Simulation Parameters in Simulink

Before one can run the developed Simulink model, there are numerous parameters that need to be set in the different blocks used during its development; these parameters have been reproduced in the figures shown below. On selection of a desired block, it is double-clicked, following which the simulation parameters are entered and then saved.

V. Simulation Process Developemnt

After the Simulink model is run for the requisite simulation time, two waveforms are observed: one at the output of the inverter, which is affected by harmonic content, and the other at the output of the filter combined with the load, which is harmonic free. From the simulation results, it can be seen how the harmonics are removed to a great extent, as observed from the difference between before and after the incorporation of the harmonic filter. This shows the effectiveness of the method demonstrated in this section as to how to improve the power quality and obtain smoothened outputs at the receiving ends. Note that wherever switches come, the next immediate output will be the harmonics. Hence, this can be eliminated using multistage leg inverters; this will be further discussed in our future work. In the current research work however, only the preliminary stage, i.e., the one stage, is used for rectification of the harmonics generated as well as for improving the power quality.

VI. 1-ϕ, Half Bridge Inverter With One Pair (With Simulink Diagram and Results)

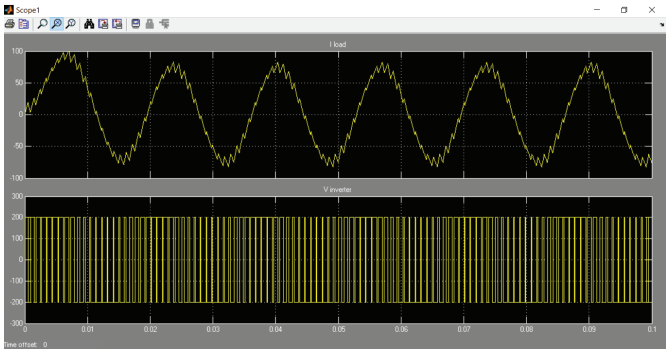

Figure 2. Simulink output display of the harmonic components waveform of the stage-1 inverter.

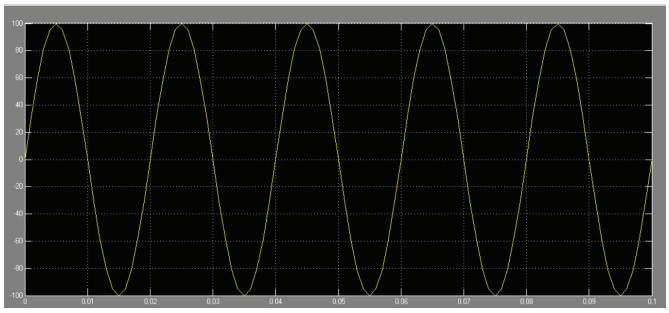

Figure 3. Simulink output display of the harmonic components waveform of the stage-1 inverter, after the output is filtered.

A 1-ϕ, half-bridge inverter consists of only a pair of IGBTs in series, to which the inputs are given from the PWM generators (supplying pulses) and the V_{dc} voltage. In turn, the output of the 1-ϕ half-bridge is connected to an RLC filter bank, which suppresses the harmonic contents in the output supply voltage, as can be seen from scope 1. Since there are two IGBTs in series in a line, the output of the pulse generator is multiplied and given to two devices.

Once the model is developed, the simulation is run for a specific period of time, which can be specified in the simulation time parameter section. The FFT analysis or the frequency spectrum can be demonstrated once the simulation is completed for the set specific simulation period. In the first case, the 1-ϕ, single-stage half-bridge inverter generates a bipolar voltage (–100 V or +100 V), and the harmonics occurs around the carrier frequency of f_c = 1 kHz with a maximum of 90% at f_c. An FFT on the first-stage load output waveform is performed next, and it appears that the THD of the load current is around 10% for the half-bridge inverter.

Fig. 2 shows that before the introduction of the harmonic filter, as seen from the waveform, there were numerous harmonic contents (3, 5, 7….). Fig. 3 shows the pulse width modulated scheme for controlling the harmonics. Once the harmonic filter is implemented, the Simulink output display of the harmonic components' waveform of the stage-1 inverter, after the output is filtered, is shown in Fig.3. The figure shows that the design is perfect as most of the

harmonic contents are removed, the output is smoothened, and the power quality is improved tremendously, which can be proved by comparing the different parameters with respect to the IGBT designed circuit for the case considered.

TABLE II.
COMPARISON OF DIFFERENT PARAMETERS WITH RESPECT TO THE IGBT DESIGNED CIRCUIT FOR THE CASE CONSIDERED

Type of harmonic elimination method	3-ϕ, 1-level inverter
THD before harmonic suppression (load v)	0.1515 15.2 %
THD after harmonic suppression (load *v*)	0.0175 1.75 %
THD before harmonic suppression (load *i*)	0.1468 14.68 %
THD after harmonic suppression (load *i*)	0.0123 1.23 %
Power factor (before)	0.85
Power factor (after)	0.9

VII. CONCLUSIONS

This paper presented a simplified method of improving the power quality in power electronic circuits using a single pair of IGBTs. Models, which were developed in the Simulink environment, were run, and the results obtained were observed. Using the total harmonic deduction formulae, the THD for the output waveforms for the current and voltage was calculated, and the results obtained were tabulated in the form of a THD reduction table. These quantitative results proved that the PWM scheme worked successfully because the THD, which had 15.2% harmonic contents before the introduction of the harmonic filter, saw a substantial reduction in its harmonic contents of load voltage down to 1.75% after the introduction of the harmonic filter. Similarly, once the proposed algorithm was implemented, the THD of 14.68% harmonic contents of the load current before the introduction of the filter substantially reduced to 1.23% after the introduction of the filter. The results obtained from the MATLAB output THD waveform evidence this fact. The net power factor too improved from 0.75 to 0.8.

REFERENCES

[1] Zainal Salam, Tan Perng Cheng and Awang Jusoh, "Harmonics mitigation using active power filter : A technical review", Elektrika, Vol. 8, No. 2, pp. 17–26, 2006.
[2] Fanghua Zhang & Yangguang, "Selective harmonic elimination PWM control scheme on a 3-ϕ 4 – leg voltage source inverter", IEEE Transaction on Power electronics, Vol. 24, No. 7, pp. 1682–1689, Jul. 2009.
[3] Mahesh A. Patel, Ankit R. Patel, Dhaval R. Vyas & Ketul M. Patel, "Use of PWM techniques for power quality improvement", International Journal of Recent Trends in Engineering, Vol. 1, No. 4, pp. 99–102, May 2009.
[4] Ming-Yin Chan, Ken KF Lee & Michael WK Fung, "A case study survey of harmonic currents generated from a computer center in an office building", Architecture Science Review, Vol. 50, No. 3, pp. 274–280, 2007.
[5] G.N.C. Fergusson, "Power quality improvement in a harmonic environment", International Electrical Testing Association (NETA) Annual Technical Conference – A reprint version, Mar. 1997.
[6] Thomas S. Key & Jih-Sheng Lai, "Costs and benefits of harmonic current reduction for switch mode power supply in commercial office building", IEEE Trans. on Industry Applications, Vol. 32, No. 5, Sep.–Oct. 1996.
[7] V. Suresh Kumar, Ahmed F. Zobaa, R. Dinesh Kannan, & K. Kalaiselvi, "Power Quality and Stability Improvement in Wind Power System using STATCOM", International Conference and Exhibition on Green Energy and Sustainability for Aride regions & Mediterranean Countries, 2009.
[8] Alexander Kusko & Mart C. Thomson, "Power quality in electrical systems", Tata Mc. Graw Hill., New Delhi, 2010.
[9] Gregory N.C. Ferguson "The cost and benefits of harmonic current reduction in low voltage distribution systems", Int. Jr. of Power Quality, Vol. 3, No. 5, pp. 45–51, May 2013.
[10] Jonathan K. Piel & Daniel J. Carnovale, "Economic and electrical benefits of harmonic reduction methods in commercial facilities", Proc. Cutler Hammer, USA, Jul. 2004.
[11] M. Aredes, J. Hafner, and K. Heumann, "3-phase four-wire shunt active filter control strategies," IEEE Trans. Power Electron., Vol. 12, No. 2, pp. 311–318, Mar. 1997.
[12] C. J. Zhan, A. Arulampalam, and N. Jenkins, "4-wire dynamic voltage restorer based on a 3-dimensional voltage space vector PWM algorithm," IEEE. Trans. Power Electron., Vol. 18, No. 4, pp. 1093–1102, Jul. 2003.
[13] N.Y. Dai, M.-C.Wong, andY.-D. Han, "A FPGA-based generalized pulse width modulator for 3-leg center-split and 4-leg voltage source inverter," IEEE Trans. Power Electron., Vol. 23, No. 3, pp. 1472–1484, May 2008.
[14] H.L. Jou, J.C. Wu, K.D. Wu, W.J. Chiang, and Y.H. Chen, "Analysis of zig-zag transformer applying in the three-phase four-wire distribution power system," IEEE Trans. Power Del., Vol. 20, No. 2, pp. 1168–1173, Apr. 2005.
[15] P. Sanchis, A. Ursua, E. Gubia, J. Lopez, and L. Marroyo, "Control of three-phase stand-alone photovoltaic systems with unbalanced loads," Proc. IEEE ISIE, pp. 633–638, 2005.
[16] G. Kamath, N. Mohan, and V.D. Albertson, "Hardware implementation of a novel, reduced rating active filter for 3-phase, 4-wire loads," Proc. IEEE APEC, pp. 984–989, 1995.
[17] S. Choi and M. Jang, "Analysis and control of a 1-ϕ inverter zigzag-transformer hybrid neutral-current suppressor in 3-ϕ 4-wire systems," IEEE Trans. Ind. Electron., Vol. 54, No. 4, pp. 2201–2208, Aug. 2007.
[18] S. Kim and P.N. Enjeti, "A new hybrid active power filter (APF) topology," IEEE Trans. Power Electron., Vol. 17, No. 1, pp. 48–54, Jan. 2002.
[19] G. Casaravilla, G. Eirea, G. Barbat, J. Inda, and F. Chiaramello, "Selective active filtering for 4-wire loads: Control and balance of split capacitor voltages," Proc. IEEE PESC, pp. 4636–4642, 2008.
[20] N.Y. Dai, M.C. Wong, and Y.D. Han, "Application of a 3-level NPC inverter as a 3-phase 4-wire power quality compensator by generalized 3D SVM," IEEE Trans. Power Electron., Vol. 21, No. 2, pp. 440–449, Mar. 2006.
[21] IEEE 100, The Authoritative Dictionary of IEEE Standard Terms, 7th edition, pp. 234, 2000.
[22] S.Khalid & Bharti Dwivedi, "Power quality issues, problems, standards & their effects in industry with corrective means", Int. Journal of Advances in Engg. & Tech., IJAET, ISSN: 2231–1963, Vol. 1, Issue 2, pp.1–11, May 2011.
[23] Rajesh Maharudra Patil, Dr. M.S. Nagaraj, Dr. P.S.Venkataramu, "A review of the effect of harmonics due to switching devices in the field of power electronics & its applications", Int. Jr. of Emerging Tech. & Research (IJETR), ISSN (E) : 23475900 ISSN (P) : 23476079, IF : 0.997, Vol. 2, No. 2, Mar–Apr. 2015, pp. 44–50
[24] http://www.ijetr.org/index.php?p=pi&volume=V2&issue=I2

[25] Narain G. Hingorani and Laszlo Gyugyi, "Understanding FACTS : Concepts and technology of flexible AC transmission systems", Wiley-IEEE Press, 452 pages, 1999.
[26] Suvas Vora, Dipak Bhatt, "A comprehensive review of harmonics effects on electrical power quality", Int. Journal of Engg. Development & Research, Paper id IJEDR1303003, ISSN: 2321–9939, pp. 15–21, 2013.
[27] Chandrasekar, T., Justus Rabi and A. Kannan, "Harmonics reduction in front end rectifier of uninterruptible power supplies with active current injection", American Journal of Applied Sciences - Science Publication., Vol. 11, No. 4, pp. 564-569, ISSN: 1546-9239, pp. 564–569, doi:10.3844/ajassp.2014.564.569, 2014.
[28] Harish Kumar S., Vengatesh V., Bhuvaneswaran E., "Power quality management in commercial buildings", Int. Journal for Research & Development in Engg. (IJRDE), ISSN: 2279-0500, Special Issue, pp. 157–165, 2014.
[29] Alireza Hoseinpour and Reza Ghazi, "Modified PWM technique for harmonic reduction", Int. Scholarly Research Network ISRN Electronics, Vol. 2012, Article ID 917897, 8 pages, doi:10.5402/2012/917897.
[30] K.L. Lian, Brian K. Perkins, and P.W. Lehn, "Harmonic analysis of a 3ϕ diode bridge rectifier based on sampled data", IEEE Transactions on Power Delivery, Vol. 23, No. 2, pp. 1088–1096, Apr. 2008.
[31] M.H. Shwehdi, F.S. AL-Ismail, "Investigating University Personnel Computers (PC) Produced Harmonics Effect on line Currents", Int. Conf. on Renewable Energies & Power Quality (ICREPQ'12), Santiago de Compostela (Spain), 28–30 Mar. 2012.
[32] Sagayaraj R., Thangavel S., "Implementation of intelligent control strategies on current ripple reduction and harmonic analysis at the converter side of the industrial inverters & trade off analysis", Jour. of Theoretical & Applied Info. Tech. (JATIT), ISSN: 1992-8645, Vol. 65 No. 2, pp. 344–351, Jul. 2014.
[33] Alham, M.H., Hassan M.A.M., El-Zahab, "Control of the shunt active power filter using artificial intelligence techniques", IEEE Int. Conf. on Control, Decision & Info. Tech. (CoDIT), Hammamert, pp. 202–207, 2013.
[34] Sam Abdel-Rahman, Franz Stückler, Ken Siu, "PFC boost converter design guide, Infineon", Application notes.
[35] Satheeswaran K., Nepolean C., Vikash M., "Harmonic elimination using boost converter", International Journal of Scientific Engineering and Applied Science (IJSEAS), ISSN: 2395-3470, Vol. 1, Issue 9, Dec. 2015, pp. 431– 434.
[36] P. Suresh Kumar, S. Sridhar, T. Ravi Kumar, "Design & simulation of boost converter for power factor correction and THD reduction", Int. Jr. of Scientific Engg. & Tech. Res. IJSETR, ISSN 2319-8885 Vol. 3, Issue 42, pp. 8462–8466, Nov. 2014.
[37] Mohammad Junaid & Bhim Singh "Analysis & design of buck-boost converter for power quality improvement in high frequency on/off-line UPS system", IEEE International Conference on Power Electronics, Drives and Energy Systems (PEDES), Mumbai, Print ISBN: 978-1-4799-6372-0, pp. 1–7, 16–19 Dec. 2014.
[38] K.S.V.Phani Kumar, S.Venkateshwarlu , "A Review on Power Quality in Grid Connected Renewable Energy System", CVR Journal of Science and Technology, Volume 5, pp.84-89, December 2013.
[39] G.Sree lakshmi,"Diode Clamped Multilevel Inverter Fed SPMSM", CVR Journal of Science and Technology ,Vol.13, pp. 56–60, December 2017.
[40] Singh B., Al-Haddak, Chandra A., "A review of active filters for power quality improvement", IEEE Transactions on Industry Electronics, Vol. 46, No. 5, pp. 960–971, 1999.
[41] El-Habrouk M., Darwish M.K., Mehta P., "Active power filters : A review", Electric Power Applications, IEE Proc., Vol.147, Issue 5, pp. 403–413, 2000.
[42] Akagi H., "Active harmonic filters", Proc. of the IEEE, Vol. 93, Issue 12, pp. 2128–2141, Dec. 2005
[43] Holmes D.G., Lipot A., "Pulse width modulation for power converters: Principles and practice", IEEE Press Series on Power Engineering, Wiley-IEEE Press, Edition 1, Oct. 2003.
[44] V. Karthikeyan, V.J. Vijayalakshmi, P. Jeyakumar, "Selective Harmonic Elimination (SHE) for 3-Phase Voltage Source Inverter (VSI)", American Journal of Electrical and Electronic Engineering, Science and Education Publishing, DOI:10.12691/ajeee-2-1-4.
[45] Ray R.N., Chatterjee & Goswami S.K, "Reduction of voltage harmonic using optimization – based combined approach", Proc. on IET Power Electronics, Vol. 3, Issue 3, pp. 334 – 344, 2008.
[46] Mohamed S.A., Dahidah and Vassilios G. Agelidis, "Selective harmonic elimination PWM control for cascaded multilevel voltage source converters: A generalized formula" IEEE Trans on power electronics, Vol. 23, Issue 4, pp. 1620–1630, Jul. 2008.
[47] Wells, Jason R., Xin Geng, Chapman, Patrick L. & Krein, Philip T. "Modulation based harmonic elimination" IEEE Transactions on Power Electronics, Vol. 22, Issue 1, 2007.
[48] G.Manohar,Dr.S.Venkateshwarlu "Performance Analysis of three level diode clamped Inverter fed Induction machine using Multicarrier PWM Techniques",CVR Journal of Science and Technology, Vol. 16,pp.59-65,June 2019.
[49] Hadji S. Touhami O. and C.J. Goodman, "Vector- optimized harmonic elimination for single phase pulse width modulation inverters / converters", IET Electrical Power Appl., Vol. 3, pp. 423–432, 2007.
[50] Agllidis V.G., Balouktsis A. & Cosar C., "Multiple sets of solutions for harmonic elimination PWM bipolar waveforms: Analysis & experimental verification", IEEE Trans. Power Electron., Vol. 22, No. 1, pp. 491–499. 2007.

E-ISSN 2581 – 7957
P-ISSN 2277 – 3916

CVR Journal of Science and Technology, Volume 17, December 2019
DOI: 10.32377/cvrjst1719

Detection and Mitigation of Faults in 13–Level Cascaded H-bridge Converter STATCOM

Podupuganti Anusha [1] and R.Harsha Vardhan [2]
[1]PG Scholar, CVR College of Engineering/EEE Department, Hyderabad, India
Email: anushapodupuganti@gmail.com
[2]Asst.Professor, CVR College of Engineering/EEE Department, Hyderabad, India
Email: 83.harsha@gmail.com

Abstract: **This paper deals with the detection and mitigation of faults in 13-level converter STATCOM. The FACTS device used is flexible in reactive power compensation, voltage regulation, to reduce harmonics of the grid that must be protected from faults in the switches. Due to frequency switching of the STATCOM, the possibility of the switch malfunction such as open circuit and short circuit faults are predominant. Many static synchronous compensators use multilevel converters to lower the switching faults. The pulse width modulation techniques applied to a proposed cascaded 13-level to detect the faulty switch and mitigate it. In this paper the performance analysis of PWM techniques are computed with dynamic fault conditions.**

Index Terms: **STATCOM, Detection of Faults, Pulse Width Modulation Techniques, Multi-level Converter**

I. Introduction

These days the demand for power has been increasing year after year. Practically when the unpredictable loads that are coupled to the grid system are of unbalanced in nature electrically, the quality of the voltage and current reduces. In order to maintain the quality of the grid system STATCOM is used. With the utilization of STATCOM, reactive power is able to compensate, voltage regulation can be improved.

The control techniques incorporated in STATCOM [1] are generally of two level or three level conventional PWM topologies. With the decrease in the level of the modulated waveform of the Voltage Source Converter, the change in the form of electrical signal is relatively high. So, reactive power will be injected along with harmonics into the grid system with the utilization of STATCOM [2]. The harmonics in the voltage creates large damages to the loads, thereby reducing system efficiency. To overcome this issue a cascaded H-bridge with multilevel is connected. The reason for compelling a multilevel converter topology to the STATCOM is to create an harmonic insertion into the power system. The level of H-Bridge used is a cascaded 13th level STATCOM [3]-[4]. Formulation of the levels of the PWM given as m=2n+1, where m=no of H-bridges. Simplified model of 13-level cascaded H-bridge STATCOM is shown in figure 1. Each phase consists of 6 full bridges and each H-bridge has 4 Insulate Gate Bipolar Transistors (IGBTs) with anti-parallel diode to avoid circulating currents.

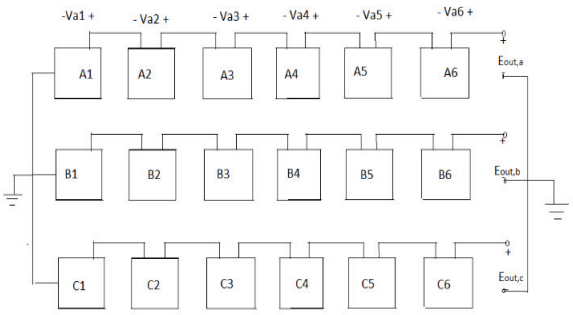

Figure 1. Simplified 13-level cascaded H-bridge STATCOM

As the level of converters used is more, the no of switching devices used also will be more. So it is important fault-lenient STATCOM. The malfunction of power unit in a proposed system will result in the blow up of switch modules which in turn lead to short circuit or open circuit of the respective bridges. These kinds of transient conditions on the power system cause insipient damages like disruptions in the voltages of the grid system and also may create severe dip due to switching. So it is significant to identify the location of faulty bridge and remove it. Early detection of these faults helps to avoid abnormal event progression. With the comparison of capacitor DC voltage to a fundamental value, respective malfunctioned power unit is identified, isolated and removed from service with bi-directional bypassing switch. Several switching technique topologies were applied to the cascaded H-bridge 13 level STATCOM and they are compared with THD spectrum study and identify the technique which gives the best performance.

II. Multilevel Converter

The converter is a power electronic circuit which converts the alternating current into the direct current. Now a days multilevel converters are emerging a new breed of high power switching applications. Multilevel converter consists of several switches, used in industrial applications, Railway Traction Drives and Electrical Vehicle etc. The converter is classified into voltage source and current source. The voltage source consists of multilevel converter and 2-level voltage converter. In this paper we are implementing multilevel with multiple DC sources.

The multiple DC sources with cascaded H-bridge design are implemented. Basically, multilevel inverters are

E-ISSN 2581 – 7957
P-ISSN 2277 – 3916

DOI: 10.32377/cvrjst1719

classified as Diode Clamped, Flying Capacitor and Cascaded H- Bridge. Of the above, Cascaded H-Bridge converter is the best one to choose because it requires less number of the components in each switching levels. In this paper we are applying Cascaded H-Bridge Multilevel converter (CHB-MLC) [5] which is internal design of a STATCOM.

III. Modulation Techniques

The output voltage of multilevel inverter is obtained using level shifted modulation technique. The PWM include n carrier waveforms for (m-1) level in which magnitude, frequency of waveform is same as that of grid taking sinusoidal waveform as reference for comparison. After comparing, the output signals using comparator are transmitted to the IGBT.

A. Phase Disposition PWM

Figure 2 shows the output characteristics of carrier signal arrangement using PDPWM technique. In this context the entire (n-1) carriers for n level converter are in phase. For thirteen levels three phase multilevel converter we get 12 carrier waveforms which are in phase with same amplitude & frequency.

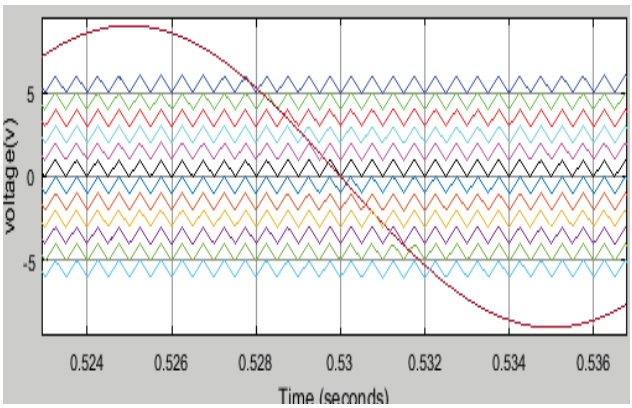

Figure 2. Carrier signal arrangement for PDPWM technique

B. Phase Opposition Disposition (PWM)

In this modulation technique, the output of the carrier signal is above the zero axis with frequency and amplitude in phase with each other. For 180 degree phase shift electrically between frequency and amplitude, same carrier signal is shifted below zero axis. The proposed method has 12 carrier signals to be modulated with the fundamental sinusoidal signal taken as reference is shown in figure 3.

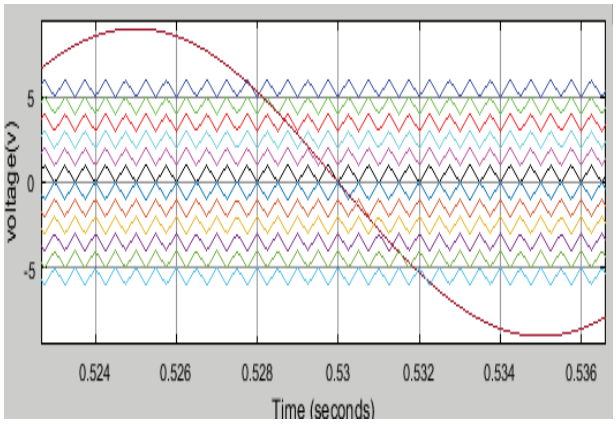

Figure 3. Carrier signal arrangement for PODPWM technique

C. Alternate Phase Opposition Disposition PWM

This modulation technique results in carrier signal out of phase with its next carrier waveform by 180 degree with same frequency & amplitude. Complete phase sequence of thirteen level converter with 12carriers and one reference wave form are shown in Figure 4.

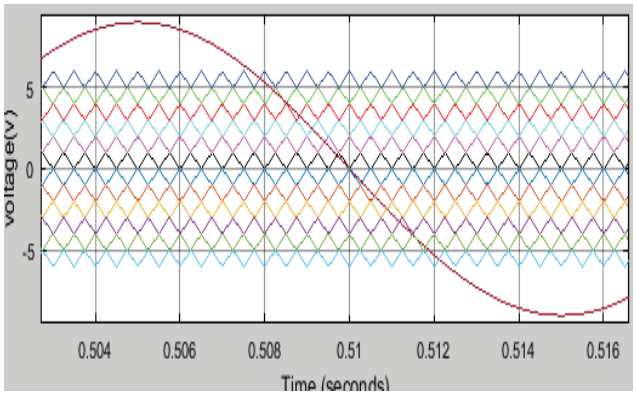

Figure 4. carrier signal arrangement for APODPWM technique

IV. Fault Analysis

The number of switches in the cascaded 13-level STATCOM is more when compare to the conventional control topologies. This is suitable in increasing faults in switching due to the continuous switching operation. This mode of operation results in malfunction of each switch in either of open or close states. The cell with switch faults is shown in below figure 5. The fault detection [7] of any IGBT can be detected by the comparison of capacitor DC voltages to a reference value.

E-ISSN 2581 – 7957
P-ISSN 2277 – 3916

CVR Journal of Science and Technology, Volume 17, December 2019
DOI: 10.32377/cvrjst1719

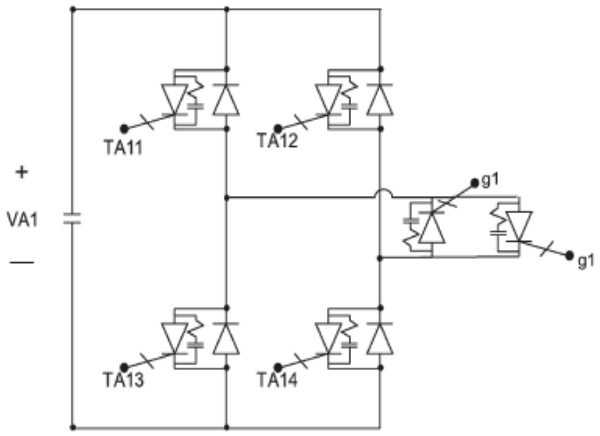

Figure 5. Cell with fault switch

Open circuit fault can be detected if the voltage across the capacitor rises to an infinite value. With dip in the voltage of the system, there is a predominant effect on the performance of STATCOM. An open circuit switch fault is able to avoid by controlling the gate current for the respective switch. In case of any short circuit switch fault, the capacitors will rapidly discharge to zero thereby avoiding the malfunction by using two-way switch.

V. Simulink Model and Results

In figure 6, the complete MATLAB model with STATCOM is shown. The complete system diagram with two buses (V-I measurement) connected one at source side and the other on load side.

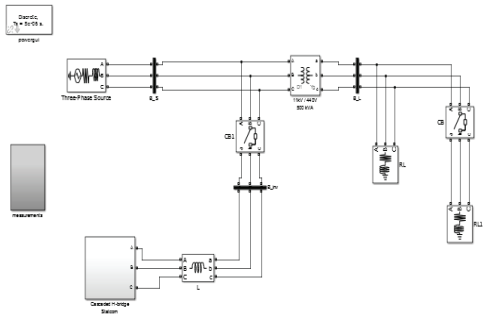

Figure 6. MATLAB model with STATCOM

The internal design of a STATCOM which is 13-level cascaded H-bridge is shown in figure 7. Multilevel STATCOM having 6 H-bridges in each phase to synthesize a staircase waveform is simulated. The converter legs are said to be identical and modular.

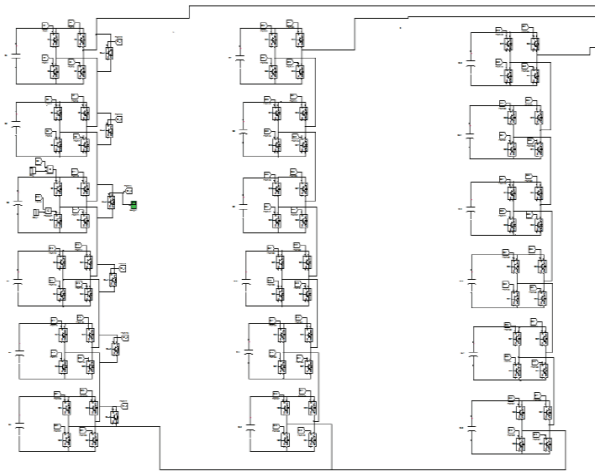

Figure 7. 13-Level Cascaded STATCOM Circuit Design in Simulink

Each H-bridge contains four power electronic switches which are IGBTs with an anti-parallel diode to avoid circulating currents. Each full bridge generates three level voltages (V, 0,-V). DC voltage balancing is obtained by incorporating DC source to each bridge. The Hybrid bridges are connected in a star model with the neutral at mid-point. In order to achieve steady output voltage, the voltages across all the direct current capacitors are to be maintained at a constant value. In this paper we are creating an open circuit and a short circuit switch faults randomly in phase A at third level of the converter which is connected in cascaded manner. The fault is created in circuit by a unit step function at a time interval t=0.5 seconds.

A. Short Circuit Switch Fault

The switch fault in any IGBT can be detected by comparing DC capacitor voltage to a reference value. Using unit step function at 0.5 seconds the fault has been injected into H-bridge.

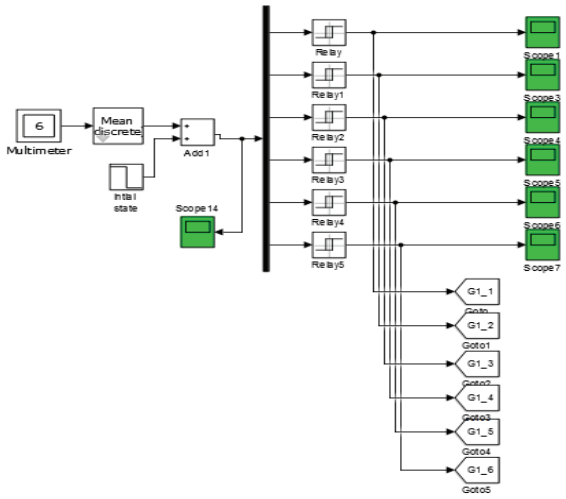

Figure 8. Control Circuit for Detection and Mitigation of the Open Circuit and Short Circuit

E-ISSN 2581 – 7957
P-ISSN 2277 – 3916

DOI: 10.32377/cvrjst1719

The relay feedback circuit is shown in figure 8. The circuit determines three sets of relays incorporated to generate pulses for each of the switches whose resistance is low. At 0.52 seconds the gate signal of cell 3 by-pass switch is generated as shown in figure 9.

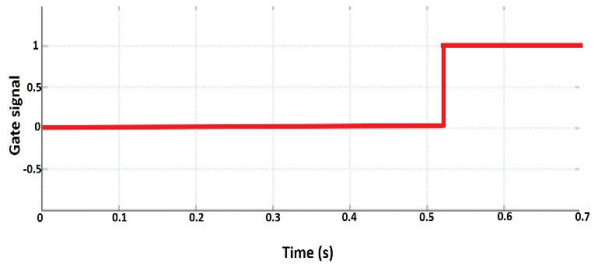

Figure 9. Gate signal generated by relay to by-pass cell No.3

During short circuit switch fault, the voltage across the direct current capacitor reduces to zero. In the figure 10 we can observe that all the voltages across the DC capacitor are same, except at the third hybrid bridge of phase A. This is due to that the voltage across it drops to zero at time interval 0.5 sec where the fault is detected.

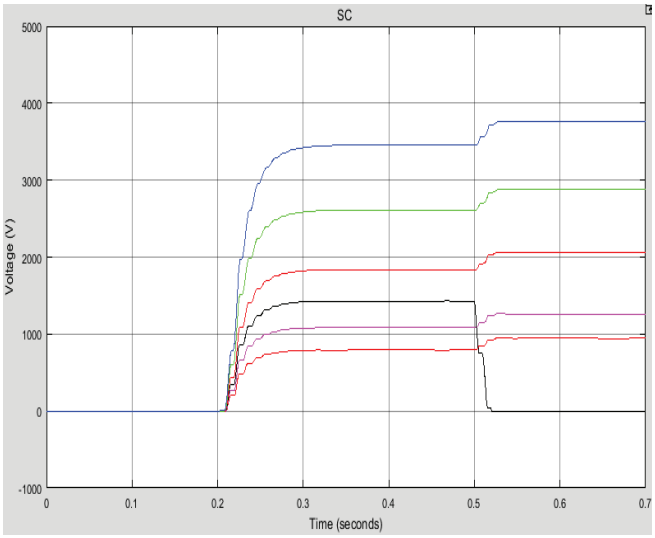

Figure 10. Capacitor voltages during short circuit fault.

Due to the existence of the fault in the system the per unit voltage of the system dropped to certain value. In order to mitigate the detected fault, a bidirectional switch is used to bypass the faulty H-bridge. This method of detection leads to pulse generation at certain signal level for gate bipolar transistor triggering and trips it ON for reduction in fault. The per unit voltages of all the three phases can be observed in figure 11. As soon as the fault is detected or identified, the feedback control circuit is integrated with respective change in the phase voltages as referred in figure 12.

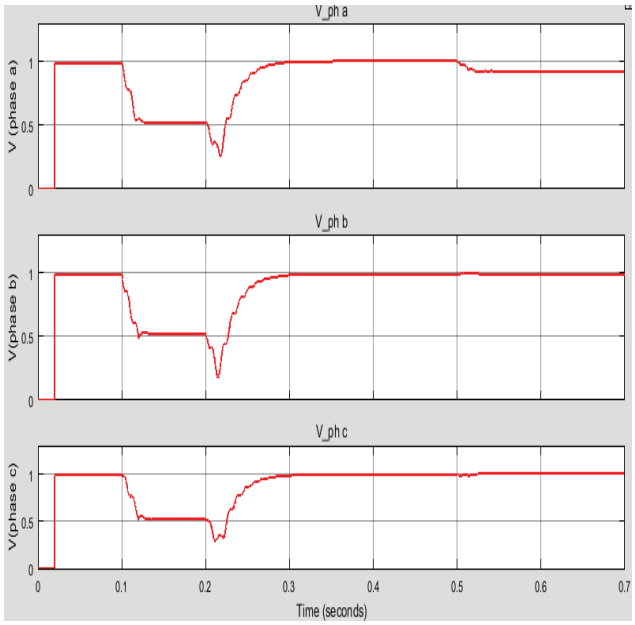

Figure 11. Magnitude of phase voltages during short circuit switch fault

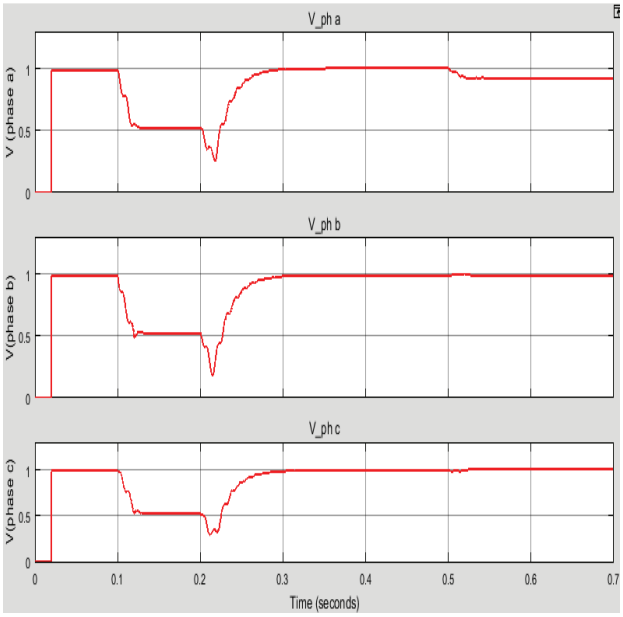

Figure 12. Magnitude of phase voltages in SC switch fault after feedback control circuit

B. *Open Circuit Switch Fault*

During open circuit condition, the potential difference across the capacitor on the direct current side increases to finite value. From the below figure 13 we can observe that all the voltages across the DC capacitor are same except the voltage across the 3rd H-bridge of phase A.

E-ISSN 2581 – 7957
P-ISSN 2277 – 3916

DOI: 10.32377/cvrjst1719

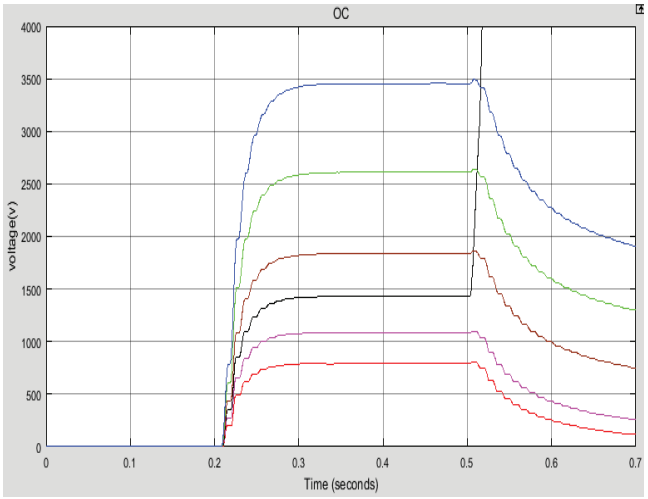

Figure 13. Capacitor voltages during open circuit fault condition.

The voltage across the 3rd H-bridge increases to finite value at t=0.5 sec that means at 0.5 sec the fault is detected. The per unit voltage values of capacitor during and after the open circuit fault can be seen in figure 13 and figure 14 during open circuit switch fault. Due to the existence of the fault in the system, per unit voltage of the system dropped down to certain value.

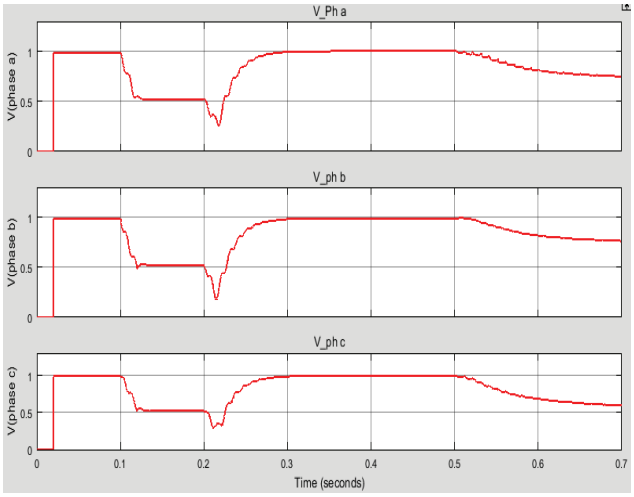

Figure 14. Magnitude of phase voltages during open circuit switch fault

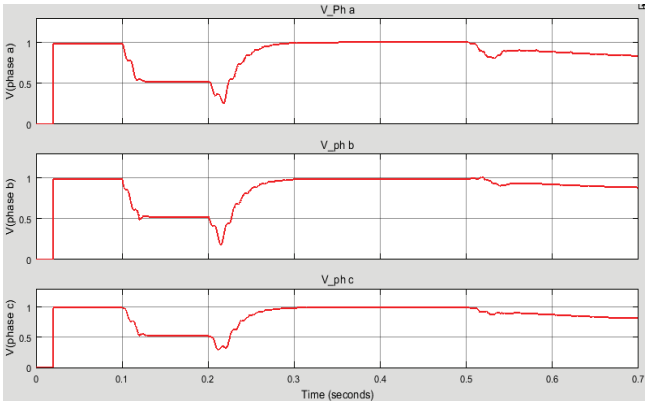

Figure 15. Magnitude of phase voltages in OC switch fault after feedback control circuit

For the injection of reactive power into the system the active power is completely maintained at zero so as to decrease the effect of source. At time interval 0.5sec there is a drop in the value of reactive power by 2MVAR which is due to the switching fault in the system in phase A.

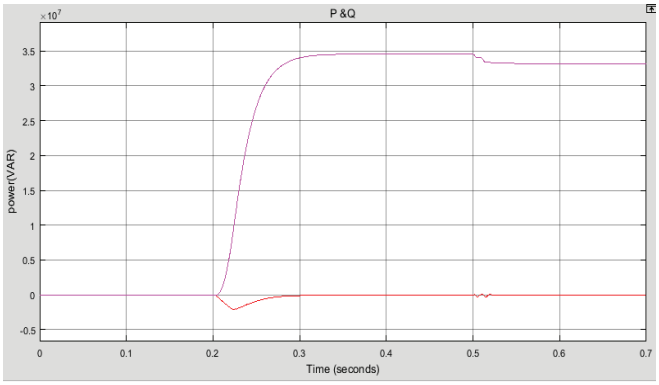

Figure 16. Active and Reactive power of STATCOM

C. *Results*

The following table I shows that comparison of percentage total harmonic distortion values of load voltages for different modulation methods before fault condition and after fault mitigation. From the below observation we can note that the total harmonic distortion in APOD is very less when compare to other PWM techniques.

TABLE I.
COMPARISON OF % THD VALUES OF LOAD VOLTAGES DIFFERENT PWM TECHNIQUES BEFORE, DURING AND AFTER FAULTS

S.NO	PWM TECHNIQUES	%THD LOAD VOLTAGES WITHOUT FAULTS	%THD LOAD VOLTAGES BEFORE FAULTS		%THD LOAD VOLTAGES AFTER FAULT MITIGATION	
			OC FAULT	SC FAULT	OC FAULT	SC FAULT
1	PD	4.26%	51.46%	5.57%	29.42%	5.57%
2	POD	4.78%	51.47%	5.60%	28.31%	5.60%
3	APOD	3.76%	51.26%	5.30%	28.10%	5.30%

VI. CONCLUSIONS

The switching faults in the proposed voltage source converter is detected and mitigated. The harmonic analysis is carried out using PD, POD, and APOD methods. Load voltages were compared by using respective mitigation techniques i.e. before faults and after faults. The THD after creating short circuit fault is said to be very minimal compared to that of open circuit condition and also it is observed that THD of APOD PWM technique is the lowest compared to the other two techniques.

CVR Journal of Science and Technology, Volume 17, December 2019
DOI: 10.32377/cvrjst1719

REFERENCES

[1] Sharad W. Mohod and Mohan V. Aware "A STATCOM-Control Scheme for Grid Connected Wind Energy System for Power Quality Improvement" Systems Journal, IEEE (Volume:4, Issue: 3)

[2] SINGH .M, Khadkikar, V. ; Chandra, A. ; Varma, R.K. "Grid Interconnection of Renewable Energy Sources at the Distribution Level at the Distribution Improvement Features" -IEEE Transactions on Power Delivery, (Volume:26 , Issue: 1)

[3] P. Lezana and G. Ortiz, "Extended operation of cascade multicell converters under fault condition," IEEE Trans. Ind. Electron., vol. 56, no. 7,pp. 2697–2703, Jul. 2009.

[4] P.Barriuso, J. Dixon, P. Flores, and L. Morán, "Fault tolerant reconfiguration system for asymmetric multilevel converters using bidirectional power switches," IEEE Trans. Ind. Electron., vol.56, no.4, pp.1300-1306, Apr.2009

[5] T. A. Meynard, M. Fadel, and N. Aouda, "Modeling of multilevel converters," IEEE Trans. Ind. Electron., vol. 44, no. 3, pp. 356–364, Jun. 1997.

[6] S.Wei, B. Wu, F. Li, and X. Sun, "Control method for cascaded H-bridge multilevel inverter with faulty power cells," in Proc. Appl. Power Electron. Conf. Expo., Feb. 2003, vol. 1, pp. 261–267.

[7] P. Lezana, J. Rodriguez, R. Aguilera, and C. Silva, "Fault detection on multicell converter based on output voltage frequency analysis," IEEE Trans. Ind. Electron., vol. 56, no. 6, pp. 2275– 2283, Jun. 2009.

[8] S. Khomfoi and L. Tolbert, "Fault diagnosis and reconfiguration for multilevel inverter drive using AI-based techniques," IEEE Trans. Ind.Electron., vol. 54, no. 6, pp. 2954–2968, Dec. 2007

E-ISSN 2581 – 7957
P-ISSN 2277 – 3916

CVR Journal of Science and Technology, Volume 17, December 2019
DOI: 10.32377/cvrjst1720

An Efficient Approach for Optimization of Nonlinearity Response in Linear Variable Differential Transformer

Dr. Santosh Kumar Sahoo
Assoc. Professor, CVR College of Engineering/ EIE Department, Hyderabad, India
Email: santosh.kr.sahoo@gmail.com

Abstract: **This paper proposes an efficient approach for optimization of non-linearity response reflected in output of Linear Variable Differential Transformer / in Linear Variable Differential Transducer (LVDT). Customarily, the non-linearity in LVDT was reduced by windings/coils tuning, which was very difficult to get fine tune. This problematic situation can overawe by implementation of the projected scheme. The Functional link artificial neural network (Fun-LANN) has been effectively implemented for nonlinear optimization of the senor's response. The effectiveness of the proposed method is demonstrated through MATLAB simulation and the response has validated with various nonlinear effects. The experimental analysis of the proposed scheme produces high sensitivity, good linearity and insensitivity to excitation variations.**

Index Terms: **LVDT, Fun-LANN, Optimization, Sensor, Tuning, Non-linearity.**

I. Introduction

In the field of engineering automation, transducer plays a vital role for measuring, monitoring, recording and control. Various environments are exposed to the transducers for performing the sensing activities. So, the response of the transducer is influenced by the excitation source and operating temperatures. Hence, it is highly necessary for optimizing the issues related to these factors, as a result the sensing element will be smarter enough for reduction of nonlinearity.

Linear Variable Differential Transformer / Linear Variable Differential Transducer (LVDT) is an electrical transformer used for measuring linear displacement. The LVDT converts a position or linear displacement into a proportional electrical signal. This LVDTs are broadly used for displacement, pressure, and flow measurements [1]. LVDT performance is affected by its geometrical structure, Primary and secondary coil arrangement, core material quality, current and frequency variation in excitation source and variation in operating temperature [2]-[3]. Furthermore, the aging factor of transducer is also inviting the nonlinearity. Due to these reasons, the transducers are limited for a particular usable span. The reported nonlinearity is a function of time and depends on several uncertain factors. The linearity is achieved [3] by considering the geometrical structure modification and same also realized by an introduction of twin series connected the secondary coils. Lately, some researchers [4]-[5] have considered the signal conditioning circuit for effective response. The LVDT displays nonlinearity with variation of core null position and at middle position it indicates linearity. By considering this, the proposed scheme is realized with Fun-LANN in order to better linear response.

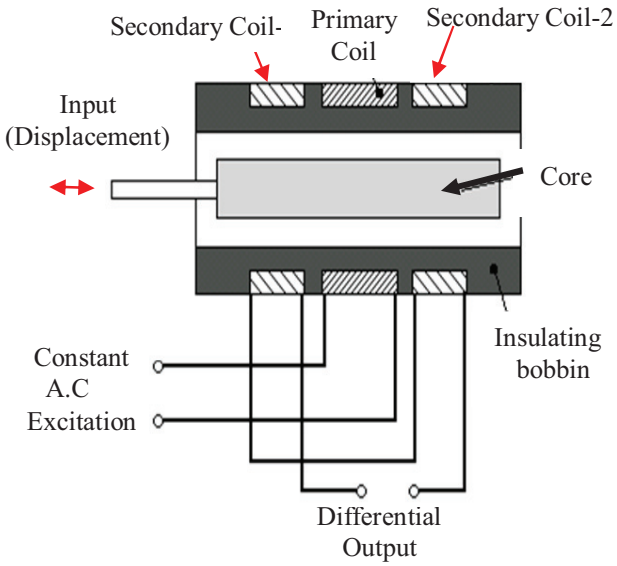

Figure 1. Schematic LVDT arrangement

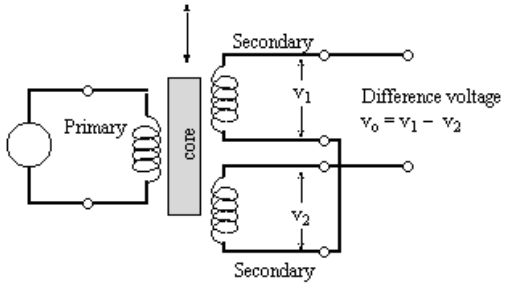

Figure 2. Electrical equivalent circuit arrangement for LVDT

LVDT consists of two coils namely Primary and Secondary. The Primary is excited externally by means of A.C. Excitation with a stable source and two secondary coils are connected in series opposition in order to provide single differential output. Schematic of LVDT arrangement is presented in figure 1. When an A.C. Supply excitation 'E_{AC}' with frequency 'F_S' is applied across primary coil and the core position with respect to primary and two secondary

E-ISSN 2581 – 7957
P-ISSN 2277 – 3916

DOI: 10.32377/cvrjst1720

windings, the developed output potential 'V_{Out}' is found across the secondary winding.

According to mutual induction principle, the induced potential in one secondary coil is presented in equation-1.

$$V_{\text{Secondary coil}} = V_{Sec} = -N\frac{d\phi}{dr} \quad (1)$$

Considering the primary current, the secondary voltage is as per equation-2. $$V_{Sec} = -M\frac{dI_{primary}}{dt} \quad (2)$$

In the above equation, the term 'N' represents number of turns in the secondary coil, 'ϕ' represents magnetic flux, $I_{Primary}$= Primary coil current. Similarly, when two secondary coils are connected in series opposition, the developed output can be presented in equation-3.

$$V_{OUT-Sec} = V_{Out-Sec1} - V_{Out-Sec2} = -(M_1 - M_2)\frac{dI_{primary}}{dt} \quad (3)$$

Where M_1 and M_2 are functions of displacement 'x'. Let $M_1 - M_2 = M(x)$. At certain range when the function is linear, $M(x) = kx$, as a result the displacement can be presented as per equation -4. $$x = \frac{V_{out-Sc}}{K dI_{\text{Primiary}/dt}} \quad (4)$$

The electrical equivalent circuit arrangement for LVDT is presented in Figure 2. In this arrangement, all the loss components are compensated and corresponding output voltage per unit displacement and phase angle are presented in equation -5 and equation-6.

$$\left|\frac{V_{Out-Secondary}}{V_{Input}}\right| \times \frac{1}{x} = \frac{KwR_m / \{(R_s + R_m)R_p\}}{\sqrt{\left[\{1 - w^2(\tau_m{}^2 + \tau_p\tau_s)\}^2 + w^2(\tau_p + \tau_s)^2\right]}} \quad (5)$$

$$\text{And } \phi = 90^0 - \tan^{-1}\frac{w(\tau_p + \tau_s)}{1 - w^2(\tau_m{}^2 + \tau_p\tau_s)} \quad (6)$$

Where $\tau_m = \frac{M_1 - M_2}{\sqrt{(R_m + R_p)R_p}}$ and $\tau_p = \frac{L_p}{R_p}$ $\tau_s = \frac{L_s}{R_s + R_m}$

With input excitation of V_{input}, operating frequency F_{Input} and meter resistance R_m. In all LVDT structure, there is some existence of nonlinearity due to some limitations. Hence, the proposed model is developed for overcome these limitations.

II. Proposed Experimental Setup

The Figure 3 represents an experimental setup for the proposed structure. In the given experimental setup presented in Figure 3, a stepper motor-controlled displacer is arranged for uniform movement of the LVDT core arm. The controller output tunes the displacement actuator as a result the core in LVDT is moved accordingly and then the nonlinear output of LVDT is again fed to Neural network model (NNM). Meanwhile the actuator output is also acting as setpoint value by the NNM. With the input and setpoint values, the NNM weights are revised in order to optimize an error. This NNM also enhances the linear response of the LVDT in a significant way. Researchers have found a useful alternative for artificial neural network as functional link artificial neural network (Fun-LANN) [6-7]. This Fun-LANN has advantages over ANN like it takes less computational time and a simple hardware structure.

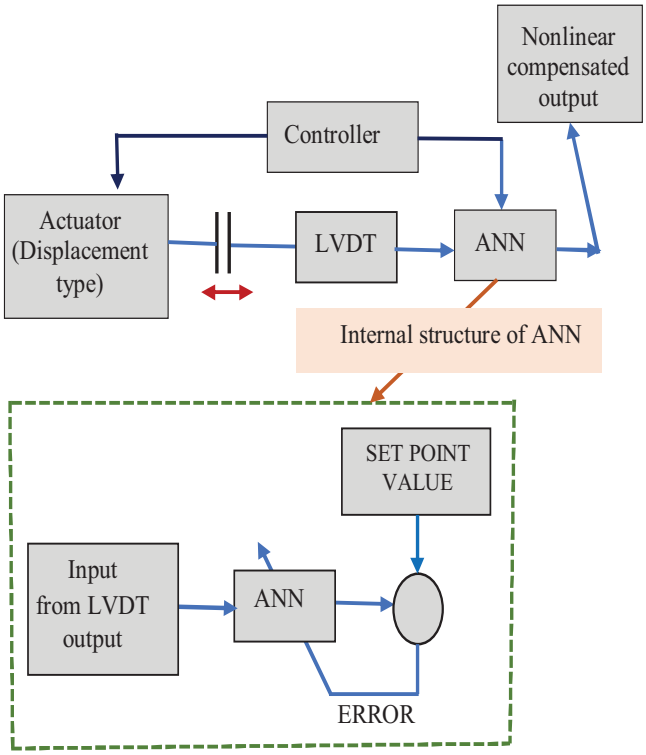

Figure 3. An experimental setup for the proposed structure

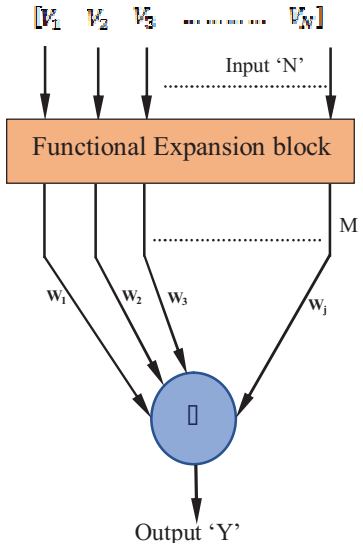

Figure 4. Simplified Fun-LANN structure

A simplified Fun-LANN structure is presented in Figure 4, where 'N' inputs are fed to the functional expansion block to generate M functionally expanded signals and these signals are combined with M-element weight vector to produce a single output.

In this article, a trigonometric functional expansion is preferred for Fun-LANN. If all the polynomials of x^{th} order with respect to an orthogonal system, the best approximation in the metric space is presented by the partial summation of Fourier series of x^{th} polynomial with respect to system.

E-ISSN 2581 – 7957
P-ISSN 2277 – 3916

DOI: 10.32377/cvrjst1720

Hence, the trigonometric polynomial basis function is expressed as per equation (7).

$$M=\{V_0, Sin(\pi V), Cos(\pi V), Sin(2\pi V), Cos(2\pi V) \ldots \ldots Sin(x\pi V), Cos(x\pi V)\} \quad (7)$$

The equation 7 signifies the compact representation of the function in mean square sense.

Let the LVDT output is extended functionally 'V_{Out}'. Now functionally extended 'M' vector is linearly joint with weight matrix by subsequent ways [8-9]

$$Y = \sum_{j=1}^{M} M_j w_j + \alpha \quad (8)$$

Where α= bias term and

$$M_j == \begin{cases} V_o & j = 1 \\ \sin(l\pi V_o), & j > 1, j \text{ even} \\ \cos(l\pi V_o), & j > 1, j \text{ odd} \end{cases} \quad (9)$$

Where $1 \leq l \leq x$, x is the order of expansion. Now the error signal can be defined as

$$E(n) = D(n) - \sum_{i=1}^{N} M_i w_i \quad (10)$$

Where $D(n)$ is set point value or desired signal or equivalent control signal applied to displacement actuator and 'n' is time index. Let the cost function 'ζ' as residual noise power and it is presented as [10] $\zeta = \epsilon[E^2(n)]$ (11)

The weight vector w_j may be adjusted as the per following in order to optimization of mean square error (MSE) ζ

$$w_{j+1} = w_j - \frac{\mu}{2} \nabla(n) \quad (12)$$

Where $\nabla(n)$ is an instantaneous estimation of gradient of ζ with respect to weight vector w_j.

Hence, $w_{j+1} = w_j + \mu E(n) M(n)$ (13)

Where 'μ' denotes the step size and it controls the convergence speed of the algorithm.

III. Experimental Simulation

Using experimental data sets, the response of the proposed model has been studied and this experimental data are collected from an LVDT with and without combination of the proposed model. The LVDT structure considered here having 3299 turns in the secondary coils, wound uniformly on each side isolated by Teflon ring. The core dia used in the proposed model is about 4.39 mm and length of core is about 4.6 mm. The primary coil excited by an excitation source of 10.5 V_{P-P} with operating frequency of 5.2KHz. Resistance of Primary winding is 267Ω and resistance of two Secondary coil are 423.5Ω and 412.8 Ω. The two secondary coils are wound in opposite directions (Series Opposition) for single differential output. The experimental measured values are presented in Table-1. The above data are normalized and utilized by Fun-LANN. The normalized LVDT output be considered as input to Fun-LANN and Fun-LANN output is equated with the normalized displacement as per Table-1data. Two experimental analysis are implemented with the same data set. The 1st test has performed through low functional expansion value (i.e $x = 9$) and in 2nd testing through high value of functional expansion (i.e $x = 109$). Figure-5 represents response of LVDT and the non-linear compensator for 1st test. Similarly, the figure-6 shows the same for high value of functional expansion (i.e $x = 109$).

From figure 4, it is concluded that there is substantial upgrading of linearity thru Fun-LANN founded compensator through a greater numeral of functional expansions.

TABLE I.
Experimental Measured Values

Sl. No	Displacement in mm	LVDT Output Voltage (V_o) in mV
1	-26	3.985
2	-24	3.852
3	-22	3.732
4	-20	3.723
5	-18	3.685
6	-16	3.584
7	-14	3.452
8	-12	3.212
9	-10	2.985
10	-8	2.125
11	-4	1.118
12	-2	0.952
13	-1	0.829
14	Null Position	0.185
15	1	0.812
16	2	0.978
17	4	2.975
18	8	2.145
19	10	2.998
20	12	3.412
21	14	3.652
22	16	3.784
23	18	3.885
24	20	3.926
25	22	3.981
26	24	3.982
27	26	3.985

TABLE II.
Comparison Of Experimental Measured Values

Sl. No	Displacement in mm	LVDT Output Voltage (V_o)	Output Voltage of proposed Model (LVDT with Fun-LANN) in mV
1	-26	3.985	4.985
2	-24	3.852	4.852
3	-22	3.732	4.732
4	-20	3.723	3.883
5	-18	3.685	3.868
6	-16	3.584	3.758
7	-14	3.452	3.652
8	-12	3.212	3.512
9	-10	2.985	3.525
10	-8	2.125	3.125
11	-4	1.118	2.118
12	-2	0.952	1.952
13	-1	0.829	1.829
14	Null Position	0.185	0.175
15	1	0.812	1.812
16	2	0.978	1.978
17	4	2.975	3.975
18	8	2.145	3.984
19	10	2.998	3.998
20	12	3.412	4.412
21	14	3.652	4.652
22	16	3.784	4.784
23	18	3.885	4.885
24	20	3.926	4.926
25	22	3.981	4.981
26	24	3.982	4.982
27	26	3.985	4.985

E-ISSN 2581 – 7957
P-ISSN 2277 – 3916

DOI: 10.32377/cvrjst1720

The proposed model (FANN) with 109 functional expansion is achieving better linearity.

Table II summarizes the comparison statement between the output response of LVDT with and without considering Fun-LANN (Proposed) model.

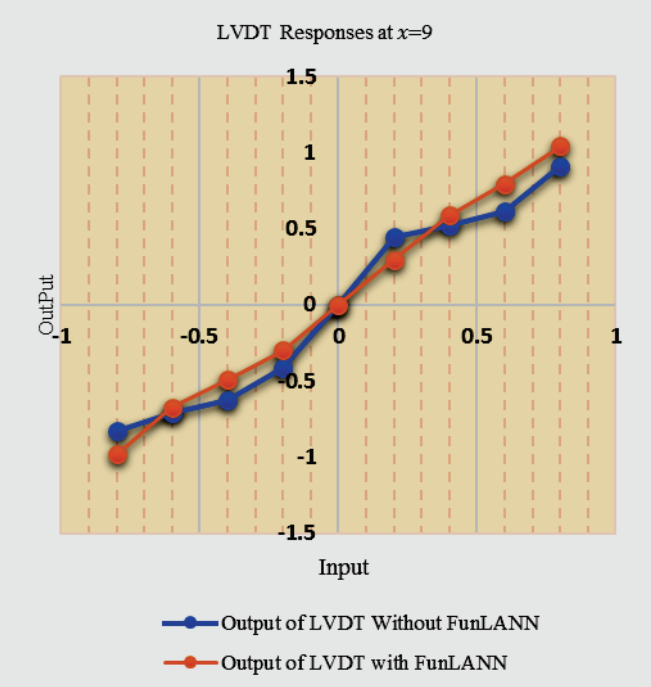

Figure 5. Response of LVDT at x=9

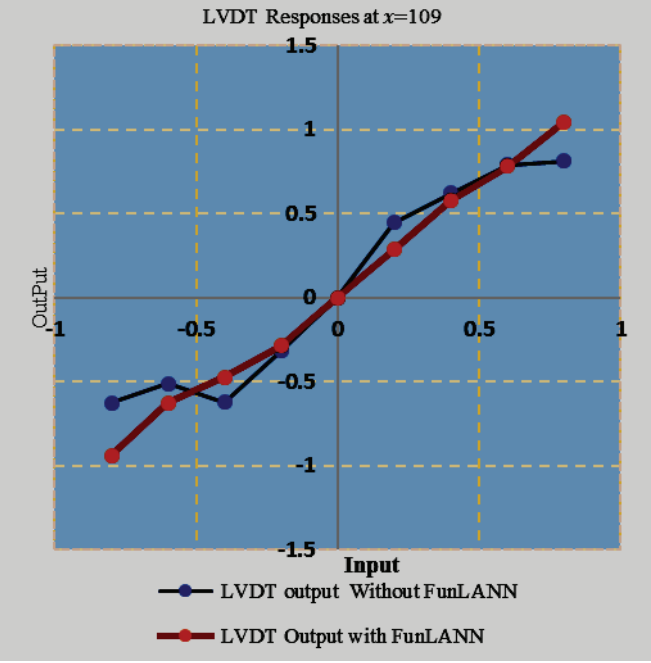

Figure 6. Response of LVDT at x=109

The response of the LVDT with and without considering the proposed scheme at various functional expansion values (i.e x=9 and x=109) are detailed in Table III and Table IV respectively. From these data, it is resolved that the proposed model has significant response in terms of linearity corresponding to input displacement variations.

TABLE III.
COMPARISON OF EXPERIMENTAL MEASURED VALUES AT x=9

Input Displacement	Output of LVDT Without Fun-ANN	Output of LVDT with Fun-LANN
-0.8	-0.825	-0.981
-0.6	-0.712	-0.675
-0.4	-0.621	-0.494
-0.2	-0.418	-0.297
0	0	0
0.2	0.445	0.298
0.4	0.521	0.589
0.6	0.612	0.795
0.8	0.912	1.045

TABLE IV.
COMPARISON OF EXPERIMENTAL MEASURED VALUES AT x=109

Input Displacement	LVDT output (mV) Without Fun-ANN	LVDT Output (mV) with Fun-LANN
-0.8	-0.625	-0.941
-0.6	-0.512	-0.625
-0.4	-0.621	-0.474
-0.2	-0.318	-0.287
0	0	0
0.2	0.445	0.288
0.4	0.621	0.579
0.6	0.792	0.783
0.8	0.812	1.045

IV. CONCLUSIONS

In this article, a simple and an effective way of designing the high linearity LVDT based displacement sensing structure is proposed. The proposed Fun-LANN is successfully applied for nonlinear optimization of the LVDT. The Detailed implementation procedure for training the Fun-LANN model is outlined properly. The proposed scheme also makes the sensing element smarter enough for auto-correction of nonlinear response. The proposed scheme is also suitable for nonlinear compensation of other sensing element.

REFERENCES

[1] C. D. Johnson and H. Al. Richeh, Highly accurate resistance deviation to frequency converter with programmable sensitivity and resolution, IEEE transactions on Instrumentation and Measurement, Vol.IM-35, pp.178-181,1986

[2] D. Patranabis, S. Ghosh and C. Bakshi, Linearizing transducers characteristics, IEEE Transactions on Instrumentation and Measurement, Vol.37, pp.66-69,1988

CVR Journal of Science and Technology, Volume 17, December 2019
DOI: 10.32377/cvrjst1720

[3] G. Bucci and C. Landi, Metrological characterization of a contactless smart thrust and speed sensor for linear induction motor testing, IEEE Transactions on Instrumentation and Measurement, Vol.45, pp.493-498, 1996

[4] Giovanni Bucci, Marco Faccio and Carmine Landi, New ADC with piecewise Linear Characteristics: Case Study-Implementation of a smart Humidity sensor, IEEE Transactions on Instrumentation and Measurement, Vol.49 (6), 2000

[5] J. M. Dias Pereira, O. Postolache and P. M. B. S. Girao, A Digitally programmable A/D Converter for smart sensor Applications, IEEE Transactions on Instrumentation and Measurement, Vol56(1),2007.

[6] Wu. Shang-The, Mo. Szu-Chieh and Wu. Bo-Siou, An LVDT based self-actuating displacement transducer, Sensors and actuators, Vol.142, PP.558-564,2008

[7] Hermann K P Neubert, "Instrument Transducers: An introduction to their performance and design", 2nd edition, Oxford University press.

[8] S. Haykin, "Neuraal Networks: A Comprehensive Foundation", Pearson Education Asia,2002.

[9] J. M. D. Pereira, O. Postolache and P. M. B. S. Giirao, "A digitally programmable A/D Converter for smart Sensors Applications, IEEE Transactions on Instrumentation and Measurement", Vol. 56, No.1, 2007

[10] Giovanni Bucci, Marco Faccio, and Carmine Landi, "New ADC with piecewise Linear characteristic: Case Study-Implementation of a smart humidity sensor", IEEE transactions on Instrumentation and Measurement, Vol.49, No.6, 2000.

E-ISSN 2581 – 7957
P-ISSN 2277 – 3916

CVR Journal of Science and Technology, Volume 17, December 2019
DOI: 10.32377/cvrjst1721

Virtually Transcribed and Restrained Robotic System

P. Choudesh Varma [1], G. Venkateswarlu [2], K.Uday[3]
[1] Asst. Professor, CVR College of Engineering/EIE Department, Hyderabad, India
Email: choudesh82@gmail.com
[2] Asst. Professor, CVR College of Engineering/EIE Department, Hyderabad, India
Email: venkigummadilli@gmail.com
[3] Asst. Professor, CVR College of Engineering/EIE Department, Hyderabad, India
Email: kaparthiuday@gmail.com

Abstract: **Robotic technologies are being used in various sectors for performing different tasks. In these technologies Pre defined actuator control programming techniques are used to perform desired tasks in the selected filed instead of human beings. But, Robotic control programming needs to be changed & reconfigured to change the control action & nature of working. So, there is no reliable technology to avoid reprogramming the robot. So, this paper presents development of artificial replicator to avoid reprogramming the robot for different situations, tasks such as bomb diffusion and sensitive surgery, taking readings from an active volcano or scientific analysis at radiation affected areas. In this proposed work, the wireless flexible gloves (emulator) are designed; which are integrated with flex, accelerometer, force, tilt, temperature sensors & also peltier modules and these sensors's output are connected to Arduino board & calibrated into the real nature of signal using Arduino programming. This Arduino with Wi-Fi shield communication is used to interact wirelessly with replicator-Robot. The desired control actions are recommended to robot by emulator moments through wearing gloves. The movements of robot hand wrist, fingers, forearm, head, elbow and shoulder can be controlled by advanced version Fx-5U PLC(Programmable Logic Controller).This PLC has the feature of industry internet protocol so emulator can be easily communicated with robot. Melsoft GX-Works-3 programming software is being to develop the algorithm for manipulation of emulator commands to actuator control signals. Here PLC executes actuator control Ladder programming with the speed of 40ns.**

Index Terms: **Robotics emulator, replicator, actuator, virtual, wireless glove.**

I. Introduction

This robotics system is built both virtually and physically, which is controlled by human with replicate actions [1]. There is no direct human development. In this robotic system, parts of robot are similar to a human body(such as hands, fingers), which are controlled by natural movements of human body, and those movements are sensed through the glove worn by the human whose actions are to be replicated & recorded for the further use. One human can control several hands by replicating these devices, which will be a breakthrough for many problems in the fields of Biomedical, Defense [2], Industry and manufacture of hand made goods. This proposal's first priority is to effectively create exact movements in the robot just as that of the person controlling it & also other main features of this innovation, include feeling the object located miles away, perform human operations on the object, replicate human actions and repeat them when ever needed.

All the programming and effective controlling is done with the help of PLC (Programmable Logic Controllers) which is power saving, efficient and multifunctional. The special feature of the V-TARRS (Virtually -Transcribed and Restrained Robotic System) is that, it gives exact pressure and force, which are being applied through gloves at a particular location, these are read by replicator. For example cutting a vegetable, two different vegetables have two different structure and density, so V-TARRS Robot will be intelligently built [3] to apply appropriate pressures for appropriate tasks.

II. System Design And Methodology

V-TARRS basically have two different sections, one is transmission section & another one is receiving section. Transmission section has wireless gloves with integration of sensors & Wi-Fi shield. Receiving section has robot electro mechanical elements with PLC. V-TARRS can be divided into three major blocks,

A. Transcribed set up-replicator,
B. Programmed controller block (which includes PLC) and
C. Emulator.

A. Transcribed set up-replicator

It is the robotic electro mechanical arrangement (shown in Figure1) which includes the physical replica of human hand and fingers with additional extensions which can extend robot's radius of reach, the robot's movements are made with the help of compressor pipes similar to the human nerve system in arms and with the help of the servo actuators mechanism. 2 Amps & 5 Amps servo driver circuits are used to drive the shoulder movements of robot. On to the robotic hands, sensory elements are attached [4], which can detect the presence of the object, applied force & it's temperature. Figure 2 represents the real-time developed model of robot-transcribed setup. The camera set up to this robot arrangement helps operator to properly see the surrounding of the robot. The data from these sensing elements & actuators are connected to the PLC. This controller is communicated to the emulator through TCP (Transmission Control Protocol) and feature of TCP enables us to obtain the data between emulator & replicator from anywhere around the globe.

E-ISSN 2581 – 7957
P-ISSN 2277 – 3916

DOI: 10.32377/cvrjst1721

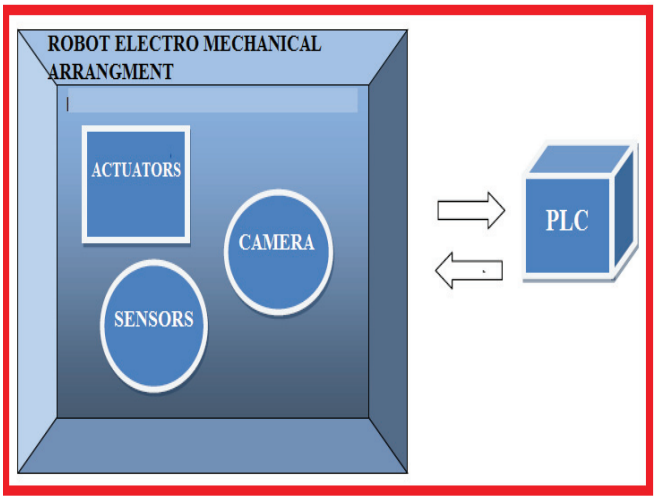

Figure 1. Elements of Transcribed setup

Figure 2. Developed model of Transcribed setup

B. Programmed controller block

This block is located at Transcribed set up. This block mainly performs the control operations on the actuators of replicator. PLC [5] ladder programming is used to write the programming for manipulation of emulator signal into control actions of robot. The Wi-Fi (transmitter + receiver) modules are located at the both ends, at the emulator side (to send the data to PLC and receive the transcribed set up's data), and one at the transcribed set up (for the robot to receive the data from the emulator and send data to emulator block).

CASE 1: Medical surgery using V-TARRS technology

i. In this case, if a person is needed to get operated immediately but the doctor is not available or he may be in the other location, then this technology comes into picture as shown in Figure3.

ii. The doctor who is in other country or in any remote location he just sits in the emulator setup and he controls the robot present in the operation theatre.
The robot which presents their acts according to movements by the emulator (flexible gloves) and these robot movements can be observed by the doctor through a monitor.
iii. The PLC programming [6] is done in such a way that maximum accuracy is maintained and if there is any power cut during the process there are additional batteries placed which make the operation to continue.

CASE 2: Bomb diffusion by armed forces:

i. While diffusing a bomb [4] V-TARRS robot can be sent to the location and the robot can be operated by military person who is sitting in a distant location and the bomb can be diffused without putting himself into any risk through the emulator commands, which transmits the movements or actions of the operating person to the robot over internet protocol. This emulator is integrated with multiple sensors to detect the entire hand movements of the operator. This assures the life of those people 100%.
ii. The robotic hands operate according to how the military personally operates and the whole operation can be viewed through a monitor as camera used in the V-TARRS.

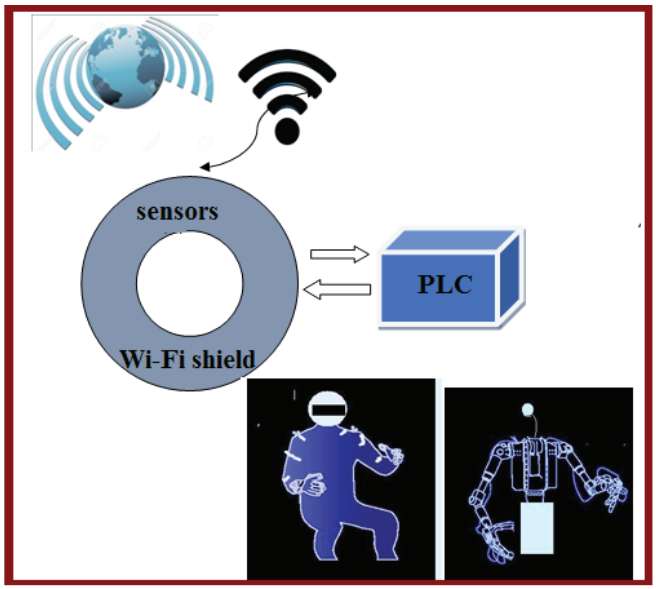

Figure 3. Graphical view of doctor operating patient using v-TARRS Technology

C. Emulator block

This is the area where human interaction is directly involved, human will wear gloves which will read the movements of fingers & hand movements in all respective degrees of freedom as shown in Figure4, and this is possible by using the sensor elements like piezo resistive and force sensors. It also contains peltier module, which enables human feel the object which the robot (operator is controlling) is holding even from miles away. The HMI (Human Machine Interface) [7] enables us perform control operations on the robot while failure of glove sensors.

E-ISSN 2581 – 7957
P-ISSN 2277 – 3916

DOI: 10.32377/cvrjst1721

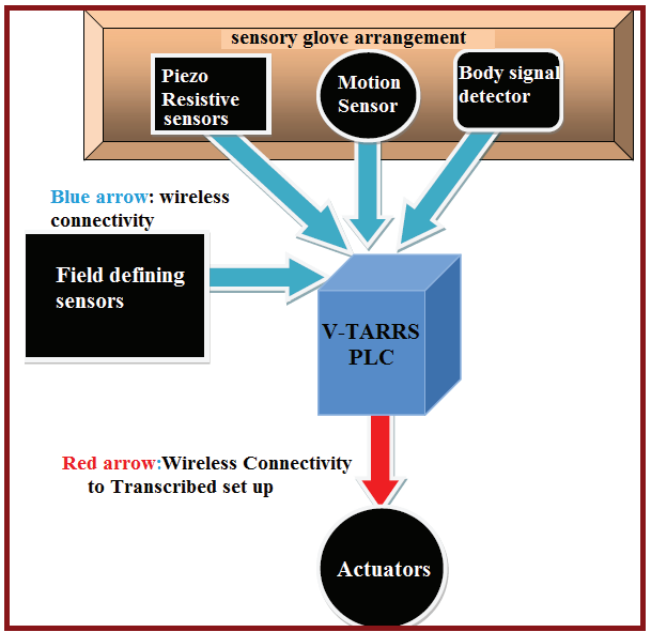

Figure 4. Elements of Emulator block.

III. Innovation And Theme Highlights

Problem statement

- For bomb diffusing and sensitive surgery, human hand expertise is needed. Now, there is no reliable technology which can diffuse any kind of analog bombs.
- Although for the surgeries, robotic surgical technology is available, it requires a lot of pre operation calibration and settings are required, and in case of emergencies, wasting much time is unaffordable.
- Virtual robotic system is a design, which can be controlled both virtually and physically by humans, and replicate actions whenever needed and where ever want to apply, where humans cannot involve directly.
- Here the robotic system, parts of which are similar to human assets, is controlled by natural human arm movements.
- The movement is sensed through the glove worn by the human whose actions are to be replicated or recorded for the further use.
- This virtual robotic system can be interfaced with web technology application hence helping the person to perform operations quickly and effectively.

Innovation

- Here a new technology is being introduced which includes both human and robot technology.
- This is new because all the tasks cannot be performed by artificial intelligence itself, even if it is possible it may not be effective as human beings think instantaneously when compared to robot as robot intelligence is limited.
- So, by using this V-TARRS, the robot can be made to work according to human interference [4] from a remote location.
- By using wireless technology, precious lives of people can be saved, who daily involve in dangerous situations.
- If a person is of lack of time and he is immediately wanted to get operated but the doctor is in some distant place, then using this V-TARRS, the delay can be reduced.

Theme highlights

- V-TARRS could become an industrial revolution, where people cannot reach, V-TARRS can.
- Handloom industries which preserve national heritage can be uplifted.
- Industrial workers who have lost their limbs or legs but have required skill set might find employment again, they can work through robots they can walk through the simulation of V-TARRS.
- The filtering lung of V-TARRS purifies the air, foams placed in these lungs absorb harmful air components and this could prevent the industrial environment from getting polluted.
- V-TARRS will be helpful when the skill set of certain human is needed but where human cannot reach, V-TARRS can be sent as a substitute.
- V-TARRS, will surely make a huge impact once it's being used in Coal Mining, Handloom Industries, Semi-Automatic Power Plants, Chemical and Pharmaceutical Industries.

IV. Hardware & Software

This section describes about major hardwares used like PLC, HMI, sensors, and Signal conditioning circuits. It gives detailed description of role of each &specifications.

Programmable Logic Controller:

A PLC is a real-time system as outputs are changed according to inputs within bounded time otherwise unintended operation result occurs [10]. In this paper, the system sequence of operation is controlled by FX5U-32M PLC & programmed by ladder diagram using MELSOFT GX works-3 software. Table.I represents the specifications of FX5U-32M PLC, Which have Consistency, Reliability, increased Productivity, Accuracy & easy to modify wiring when control contents are changed.

Features of GX WORKS3 MELSOFT

- ✓ Simple drag and drop
- ✓ Flexible register programming
- ✓ Easy visualization and confirm changes in program
- ✓ Motion control CPU hardware can be simulated
- ✓ Easy maintenance
- ✓ Reduction in downtime and high productivity.
- ✓ Easy error rectification and monitoring.

E-ISSN 2581 – 7957
P-ISSN 2277 – 3916

CVR Journal of Science and Technology, Volume 17, December 2019
DOI: 10.32377/cvrjst1721

TABLE I.
SPECIFICATIONS OF FX5U 32M –PLC

TYPE		FX5U-32M
I/O range		32
CPU performance	LD	Max. 40 ns
	MOV	100 ns
Memory size	Program	64k steps
Power		AC85-264V
High speed counter	1-Phase counter	200kHz 6ch 10kHz 2ch
	2-phase counter	100kz 3ch 5kHz 1ch
Pulse output		200kHz 4 axis(open collector) Simple linear interpolation
Memory card interface		SD card
Communication Port		Ethernet port, RS 485 1ch
Analog	Input(resolution)	2ch (12-bit)
	Output(resolution)	1ch (12bit)
Real time clock		Retained upto 10 days with capacitor
Service power supply(24V DC)		400 mA
Expansion board slot		1 slot
Adapter	Communication expandability	2
	Analog expandability	4

Human Machine Interface (HMI)

In this system, operators are also allowed to control the robot actions through Graphical Operating Terminal (GOT) while predefined actions are required. Developed graphical screens are shown from Figure 5 to Figure 7. Some limited actions only can be done by the operator through graphical operating terminal or Human Machine Interface (HMI). GT Designer 3 software is used for the development of HMI screens [8].

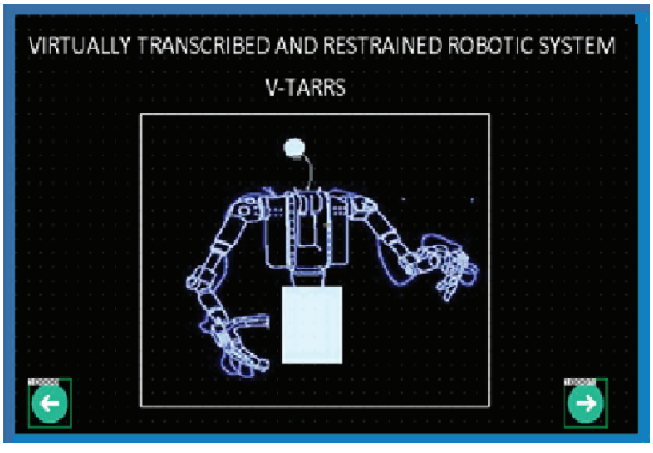

Figure 5. Basic display of HMI screen

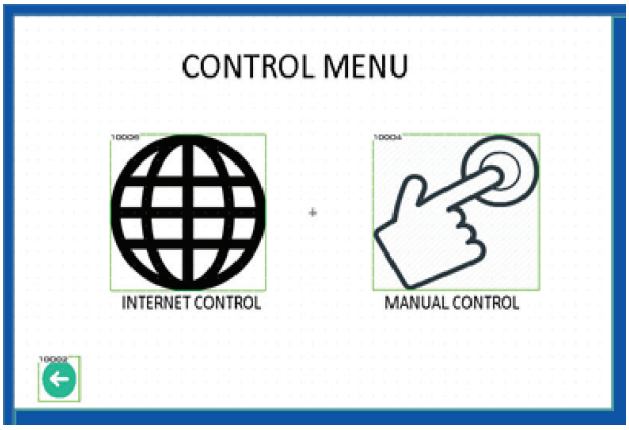

Figure 6. Operation that can be performed using HMI

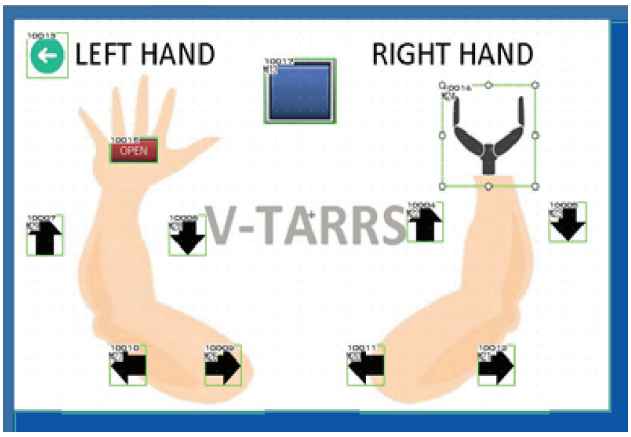

Figure 7. Manual Control in various directions

Alternative approach to analog to digital converter

As FX-5U PLC is used for calibration & control applications, it has only two analog inputs. But in this proposed work, many sensors are being used whose output is of analog in nature. In order to make PLC [9] understand this analog signal, Voltage Controlled Oscillator (VCO) is used to produce digital output i.e. converting analog signal into frequency signal and are making PLC to read those frequency signals using SPD (Special Programming Device) High speed function.

Here, JMK wireless camera module is being used (shown in Figure8) for monitoring and one more camera are being used is webcam for video conference. This wireless camera is adjustable for 50 to 100 meters' communication range. It is mainly suitable for small size mobile robots. Image can be transmitted wireless acquired by the robot to the PC and do the image processing as well as robot actuator control. It can work in wireless and wired mode. Wireless camera is powered by 9V battery or 9V DC adapter. Receiver can be powered by 9V / 12V DC adapter.

E-ISSN 2581 – 7957
P-ISSN 2277 – 3916

DOI: 10.32377/cvrjst1721

Figure 8. Wireless Camera and Receiver module

Specifications of force sensors

1. Size: 1/2" (12.5mm) diameter active area by 0.02" thick.
2. Resistance range: Infinite/open circuit (no pressure), 100KΩ (light pressure) to 200Ω (max. pressure).
3. Force range: 0 to 20 lb. (0 to 100 Newtons) applied evenly over the 0.125 sq in surface area.
4. Power supply: Uses less than 1mA of current (depends on any pullup/down resistors used and supply voltage).

Flex sensors

Flex sensors also called as bend sensors, which measure the amount of deflection caused by bending of human fingers, wrist moments through gloves. There are various ways of sensing deflection, from strain-gauges to hall-effect sensors. Signal Conditioning Circuit (SCC) is required to convert the change of the resistance into voltage [10] with respect to the change of movements of the wearied gloves.

The impedance buffer in the Basic flex sensor circuit, (SCC-Figure 9) is a single sided operational amplifier, which is used with these sensors because the low bias current of the op amp reduces error due to source impedance of the flex sensor as voltage divider. A potentiometer can be added to the circuit to adjust the sensitivity range.

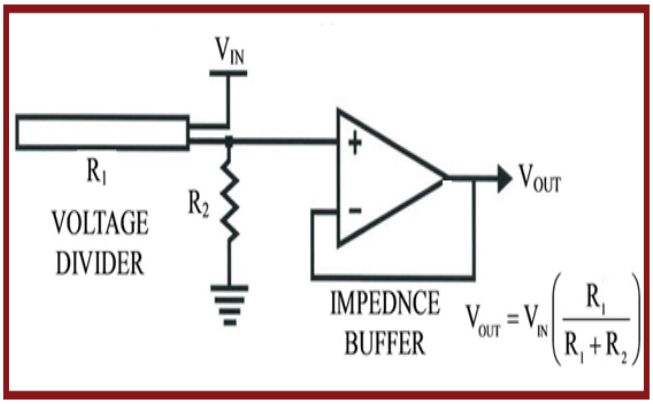

Figure 9. Basic Flex sensor signal conditioning circuit

Mechanical Specifications:
-Life Cycle: >1 million
-Height: 0.43mm (0.017")
-Temperature Range: -35°C to +80°C.
Electrical Specifications:
-Flat Resistance: 25K Ohms
-Resistance Tolerance: ±30%
-Bend Resistance Range: 45K to 125K Ohms (depending on bend radius)
-Power Rating: 0.50 Watts continuous. 1 Watt Peak.

Arduino with Wi-Fi shield

In this proposed work, Arduino Uno is being used to calibrate the Flex, tilt, force & proximity sensors, which are integrated with gloves to detect the various movements of hand as shown in Fig.10.Each glove is integrated with six flexible sensors, one tilt sensor, five force sensors & one proximity sensor.

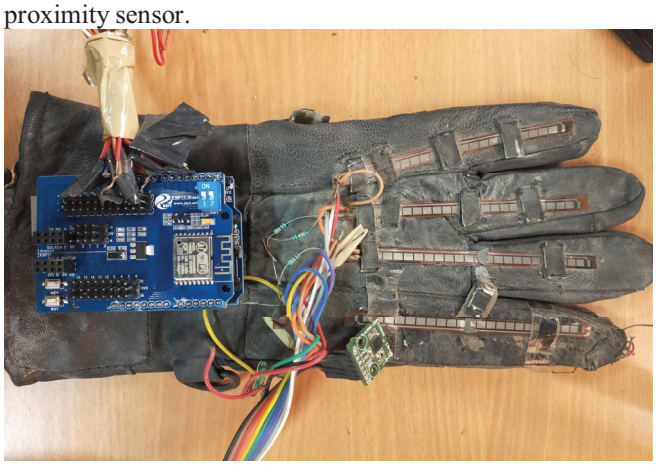

Figure 10. Emulator with Arduino & integrated sensors

All these sensors output is calibrated into the real nature of the signal by using special programming software Arduino IDE. The calibrated data is to be transmitted to the robot or Transcribed block wirelessly. So in this work, low-cost WiFi shield-WizFi210 is connected with Arduino uno board through the serial communication protocol. It operates with standard 802.11 b/g/n access points at speed up to 11 Mbps. Where WizFi210 shield has been set to act as a TCP/IP server to communicate robot & address of server is maintained as 192.168.43.150.

V. IoT Application

Here, UBIDOTS cloud connectivity is being used for wireless and IoT (Internet of Things) application. With the help of this cloud, data can be sent and received wirelessly. It is an open source IoT platform. It also stores the previous actions & manipulations done by the operator [11]. In this UBIDOTS, variable actions are created and assigned these actions to the actuators as shown in Figure 11. Sensor readings also can be monitored through these variables. A code is written in C Language for sending and retrieving the data from the variables.

E-ISSN 2581 – 7957
P-ISSN 2277 – 3916

CVR Journal of Science and Technology, Volume 17, December 2019
DOI: 10.32377/cvrjst1721

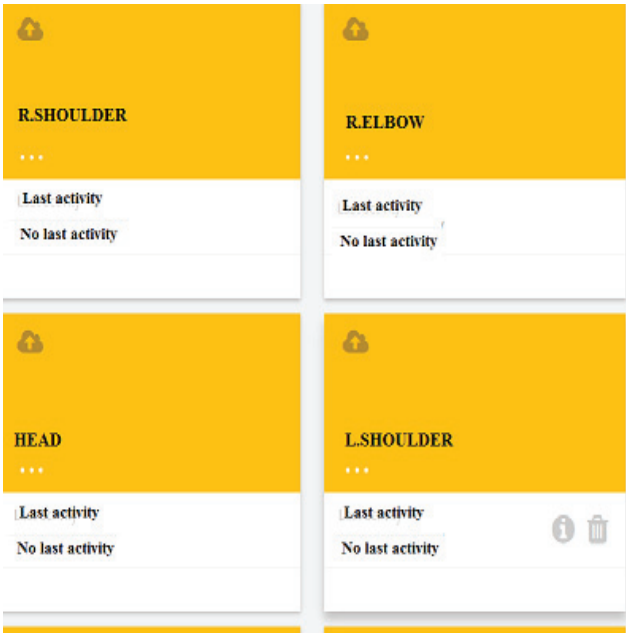

Figure 11. Variables created in UBIDOTS

VI. Results

Emulator has been designed in the desired configurations & established communication successfully between emulator & transcribed block by TCP protocol. Different movements & commands were given through emulator by wearing gloves, where robot replicated all the movements given by emulator as shown in figure 12 & 13. This proposed work has been implemented experimentally in the automation laboratory. In this work, various parameters were recorded like force applied by emulator & replicator on the object, linearity of flex sensors with respect to replicator movements. The comparison of force generated on the object by fingers of emulator & replicator produces ±1.3% to ±1.7% range of the error (98.3% to 98.7% range of accuracy). These errors are mainly caused by Hysteresis losses generated by replicator servo mechanisms. Table. II & Table.III represent the numerical comparison of forces generated on object by various fingers of emulator & replicator and it produces ±1.4% of linearity.

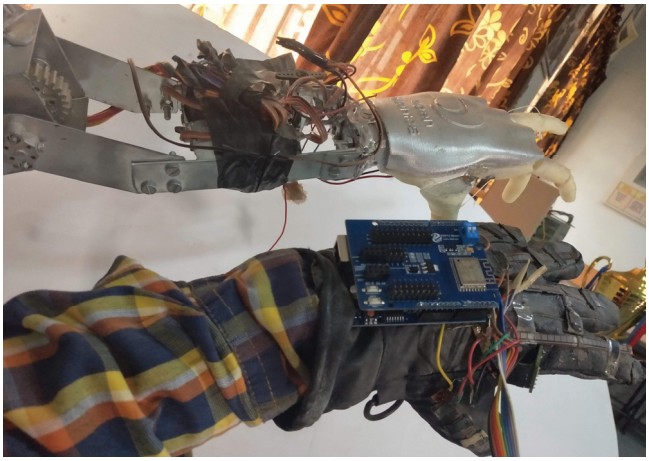

Figure 12. Right hand movement of emulator & replicator

Figure 13. Two hands movement of emulator & replicator

TABLE III.
FORCE COMPARISON OF EMULATOR & REPLICATOR-LEFT HAND

Force (Newton) measurement, left hand-Emulator					
	Little finger	Ring finger	Middle finger	Index finger	Thumb
Average	38.2	45.4	63.6	64.0	122.3
Force measurement, left hand (N)-Replicator					
	Little finger	Ring finger	Middle finger	Index finger	Thumb
Average	38.73	46.4	62.77	63.13	120.3
Error	+1.40%	+1.40%	-1.30%	-1.35%	-1.62%

TABLE III.
FORCE COMPARISON OF EMULATOR & REPLICATOR-RIGHT HAND GRIPPER

Force (Newton) measurement, Right hand gripper-Emulator		
	finger-1	finger-1
Average	110.2	109.2
Force measurement, right hand gripper (N)-Replicator		
	Gripper finger-1	Gripper finger-2
Average	108.7	107.7
Error	-1.30%	1.37%

VII. Future Scope & Applications

This proposed work has wide range of applications, it can be used in military for bomb diffusing, risk firing in the space missions, surgeries, handmade good production, and it can be applied in industries for smart production where the human actions have to be repeated especially in the areas where automation is not available. In the future by using

these kind of devices like V-TARRS, physically challenged people can be helped to overcome daily challenges by making V-TARRS controlled through voice commands. Physically challenged people can simply move the artificial limbs just by speaking to the V-TARRS, or by connecting it to nervous system. BIO METRIC protection can be implemented and V-TARRS can be secured and limited to only one person.

VIII. Conclusions

Interfacing of flex, accelerometer and other sensors to Arduino & PLC along with signal conditioning circuits was successfully accomplished and acquired data from field devices has been calibrated into physical movements using SPD (Special Programming Device), PWM (Pulse Width Modulation) and basic ladder functions in PLC. The prototype servo motors for driving robotic arm elbow, wrist & finger movements were successfully driven by PLC output module with the help of PWM programming functions. HMI screen layouts have been developed and the wireless network communication has been successfully established between emulator & replicator. Enough efforts were carried out to establish Internet of Things using Arduino with Wi-Fi shield.

References

[1] H.Oyama and F.Wako ”Evaluation of a virtual reality system for medicine” IEEE International conference on virtual systems & Multimedia, Geneva, Switzerland, 06 August 2002.

[2] Abdul Kadir Bin Motaleb, Mohammad Busayeed Hoque, and Md. Ahsanul Hoque “Bomb disposal robot”. International Conference on Innovations in Science, Engineering and Technology (ICISET), IEEE publisher, Dhaka, Bangladesh, 16 February 2017.

[3] I. H. Lin, C. Y. Liu, and L. C. Chen, "Evaluation of Human-Robot Arm Movement Imitation", Proceedings of 8th Asian Control Conference (ASCC), *PP. 287-292, 2011.*

[4] Takumi Kawasetsu, Takato Horii, Hisashi Ishihara, and Minoru Asada “Flexible Tri-Axis Tactile Sensor Using Spiral Inductor and Magneto rheological Elastomeric” IEEE Sensors Journals, volume18, PP: 5834 - 5841 July 15, 2018.

[5] Bolton, W, “Programmable logic controllers”, Access Online via Elsevier, 2009.

[6] Skulavik Tomas, Kopcek Michal, and Kopeekova Alena “Fuzzy control of robotic arm implemented in PLC”, 9th International Conference on Computational Cybernetics (ICCC),IEEE,Publisher, Tihany, Hungary, 03 October 2013.

[7] AmarBanerji , M. Tabassum , D. Venkatesh, and Manjit Singh.“An interactive GUI for dual-robot command console” Annual IEEE India conference, volume 1, 2008.

[8] Lai Wei and Huosheng Hu**”** EMG and visual based HMI for hands-free control of an intelligent wheelchair”, World Congress on Intelligent Control and Automation, IEEE Publisher Jinan, China, 7-9 July 2010.

[9] Chung, C. A, ‘A cost-effective approach for the development of an integrated pc-plc-robot system for industrial engineering education’, IEEE Transactions on Education ,Volume: 41 , Issue: 4 ,PP- 306 – 310, Nov 1998 .

[10] D.Roy Choudhury and Shail B Jain, ”Linear Integrated Circuits”, 2nd Edition, New Age International (P) Limited, PP-56-58.

[11] Federico Montore, Luca Bedogu, and Luciano Bononi”A collaborative Internet of things Architecture for smart cities and Environmental monitoring”,.IEEE Internet of things Journal, volume: 5,issue 2,PP- 592 - 605 ,April 2018.

E-ISSN 2581 – 7957
P-ISSN 2277 – 3916

CVR Journal of Science and Technology, Volume 17, December 2019
DOI: 10.32377/cvrjst1722

Design and Implementation of FIR Filter using Low Power and High Speed Multiplier and Adders

O. Venkata Krishna
Assoc. Professor, CVR College of Engineering/EIE Department, Hyderabad, India
Email: venkatakrishna.odugu@gmail.com

Abstract: **The Finite Impulse Response (FIR) filter is robust and high stable architecture rather than Infinite Impulse Response (IIR) Filter for the speech and image processing applications. In this paper, a high speed and low power FIR filter is designed and implemented using Radix-4 modified Booth Multiplier and Carry Look Ahead (CLA) adder. The Booth multiplier reduces the accumulation computation time in the multiplication of filter inputs and coefficients. CLA is used to reduce the critical path delay of the normal Ripple carry adder, which is used for the addition for the FIR filter. The 8-tap direct form FIR filter is implemented using Booth multiplier and CLA, and it is simulated and synthesized. The delay and power corresponding to these blocks are computed and presented. The utilization summary with respect to target FPGA of the each and every block is also presented.**

Index Terms: **FIR, CLA, Booth multiplier, FPGA, HDL, Verilog and Low Power.**

I. Introduction

Digital filters are most frequently used for the speech processing, image processing and video processing applications. These digital filters are of two types Finite Impulse Response (FIR) filters and Infinite Impulse Response (IIR) filters. The FIR filter is preferred for the above applications due to the simplicity of the design and of high stability. The following expression (1) represents the N-tap FIR filter.

$$y[n] = a_0 x[n] + a_1 x[n-1] + a_2 x[n-2] + \cdots \quad (1)$$

Where a_0, $a_1 \ldots a_n$ are the coefficients of the filter and x[n] and y[n] are the input and outputs of the FIR filter respectively.This FIR filter can be designed in many ways, like such as direct form, transpose form and hybrid forms. The block diagram of direct form FIR filter is shown in figure1.

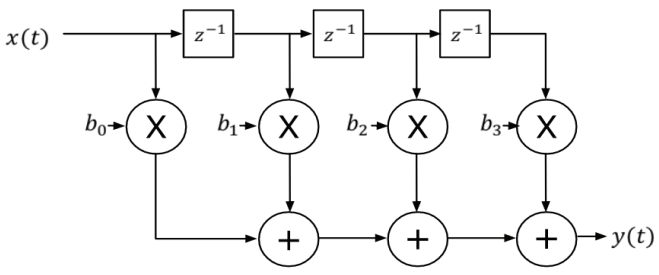

Figure 1. Block diagram of FIR filter

One of the important hardware blocks in the FIR filter is multiplier, this is used to generate the product of filter coefficients and inputs. There are different types of multipliers such as, Array multiplier, Booth's multiplier and Wallace tree multiplier, which are mostly used for the VLSI design. The other blocks are adders and delay elements. The D Flip-flops are used as delay elements in the filter, the adders are basically, Carry Look Ahead Adder (CLA) and Carry Save adders (CSA) are used in the implementation of the FIR architecture.

For the low power and high performance the optimization can be done in block level. The optimized multiplier and adders can reduce the delay and power as well as area also. For the low power, the CLA adder and Booth multipliers are used in this work.

II. Booth Multiplier Implementation

The performance of the FIR filter depends mainly on multiplier. Hence, the optimized multiplier is implemented in this section. For the purpose of the low power and less area, the booth multiplier is selected for the implementation. This approach reduces half of the accumulations and hence overall area, delay reduced.

Generally, the multiplication of two binary numbers requires partial product generation, reduction of partial products and final addition of partial products. For these operations, multiplier takes long time and more hardware. The Booth multiplier which is based on the Booth's Algorithm introduced by "Andrew Donald Booth" can be used for the reduction of delay [1]. There are radix-2 and radix-4 Booth multipliers available. The radix-2 Booth multiplier requires more additions compared to radix-4 multiplier. In this work radix-4 Booth multiplier (Modified Booth multiplier) is implemented and used for the design of FIR filter.

The Booth's concept is applicable for both signed and unsigned numbers. The figure 2 and figure 3 shows the flowchart of the radix-4 Booth's algorithm for unsigned and signed numbers respectively.

The booth multiplier multiplies two binary words with length of N x N or any length. Both the numbers signed or unsigned and combination of two types of numbers can be applied as the inputs for the multiplier. Multiplication means partial product generation, shifting and final addition. The Radix-4 modified Booth Multiplier reduces the number of partial products into half [2] [3].

E-ISSN 2581 – 7957
P-ISSN 2277 – 3916

CVR Journal of Science and Technology, Volume 17, December 2019
DOI: 10.32377/cvrjst1722

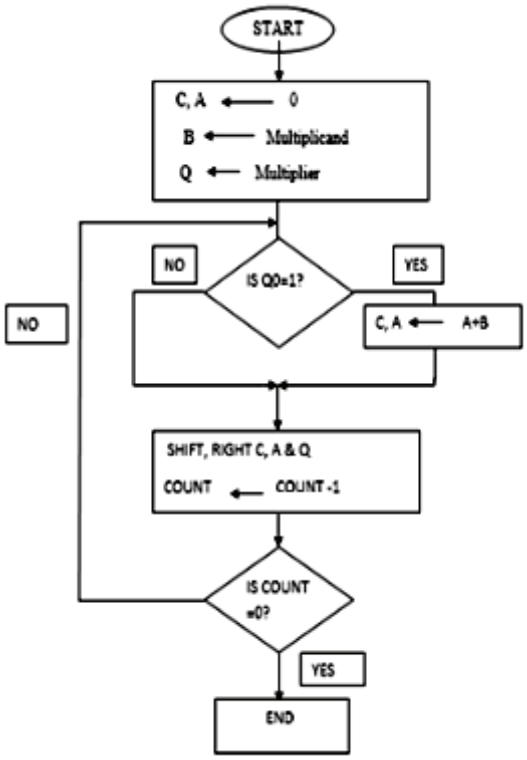

Figure 2. Booth's algorithm flowchart for the unsigned numbers.

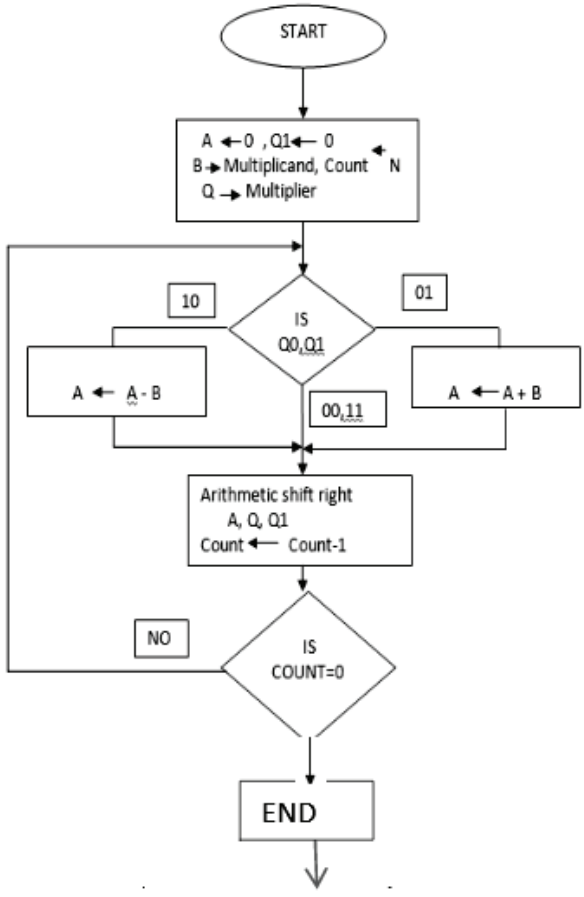

Figure 3. Booth's Algorithm in flow chart for the signed numbers.

The flow charts are converted into the logic structure, which consists of control logic, 2's compliment logic circuit, partial product register, adder and shifting circuits. The hardware structure of the radix-4 modified Booth multiplier [4] [5], is shown in figure 4. The same structure is also implemented and synthesized using Xilinx ISE tool. The RTL schematic view is shown in the figure 5.

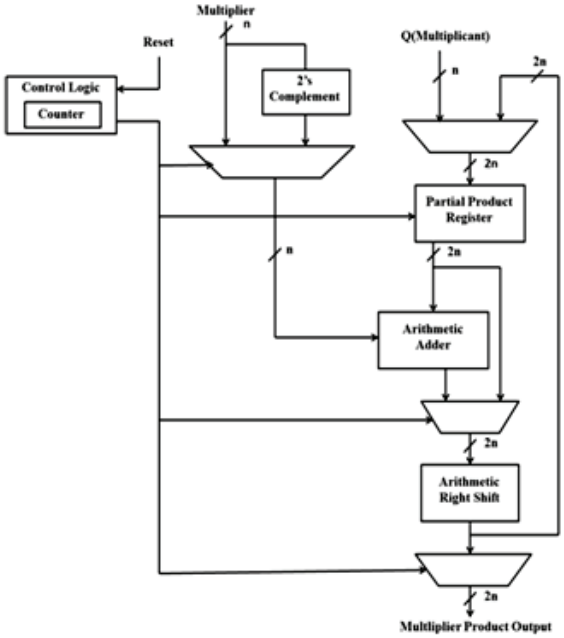

Figure 4. General architecture of Radix-4 Booth multiplier

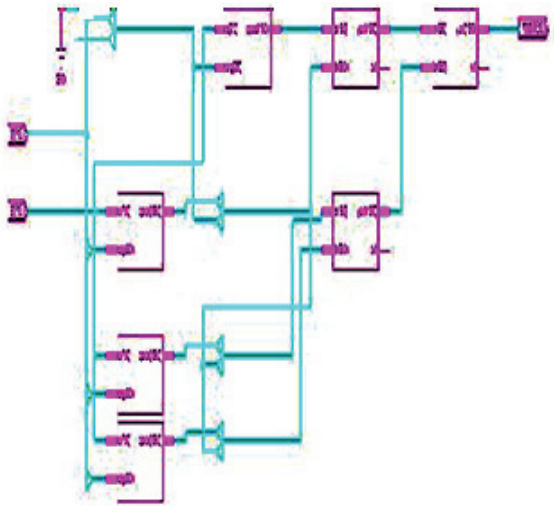

Figure 5. RTL view of Radix-4 Booth multiplier

The synthesis report of the radix-4 Booth multiplier is represented in the table I. This tables reports the hardware utilization for the Booth multiplier with respect to target device as Vertex Pro FPGA. The delay and power values for the Booth Multiplier are shown in the results section.

E-ISSN 2581 – 7957
P-ISSN 2277 – 3916

DOI: 10.32377/cvrjst1722

TABLE I.
DEVICE UTILIZATION SUMMARY OF BOOTH MULTIPLIER FOR THE TARGET DDEVICE VERTEX PRO FPGA

Device Utilization Summary (estimated values)			
Logic Utilization	**Used**	**Available**	**Utilization**
Number of Slice Registers	75	64000	0%
Number of Slice LUTs	278	64000	0%
Number of fully used LUT-FF pairs	74	193	38%
Number of bonded IOBs	132	640	20%
Number of BUFG/BUFGCTRLs	3	32	9%
Number of DSP48Es	80	256	31%

III. IMPLEMENATION OF CLA

Many High speed adder architectures are available for the implementation of Addition, such as Carry Select, Carry Save, Carry Skip and Carry Look Ahead adders (CLA). The CLA is a robust structure that reduces the hardware and improves the speed.

The CLA overcomes the carry rippling delay and also overcomes the latency problem in normal Ripple carry adder. The CLA adder depends on the carry generating term and carry propagate terms of the Full adder. In this, the carry is calculated for the possible carry bits and next it calculates the sum using appropriate hardware. Hence the delay is reduced with respect to the addition computation [6]. The architecture of the 4-Bit CLA is shown in the figure 6.

The CLA operation depends on the propagate terms and generate terms of the full adder. The propagate and generate terms of the full adder is considered as given in the equations (2) and (3).

$$Pi = Ai \oplus Bi \tag{1}$$

$$Gi = Ai.Bi \tag{2}$$

The modified full adder sum and carry out are calculated with the help of the following equations (4) and (5) in CLA adder [7] [8].

$$Ci+1 = Gi + (Pi.Ci) \tag{4}$$

$$Si = Pi \oplus Ci \tag{5}$$

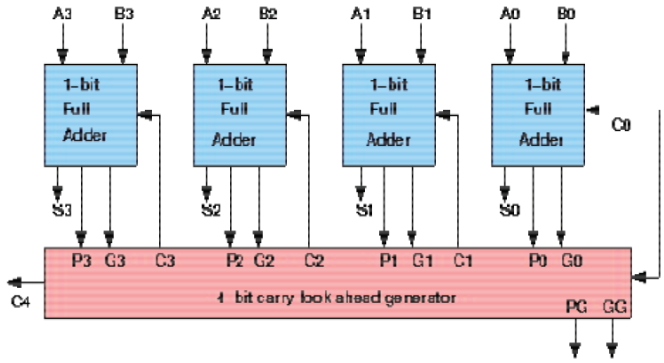

Figure 6. General Architecture of the CLA

As per the above architecture, the HDL code is written to design the 16- bit CLA and simulated. The same HDL code is also synthesized using Xilinx ISE Tool. The RTL view of the 16-bit CLA as shown in the figure 7. The synthesis report of the CLA is shown in the table II.

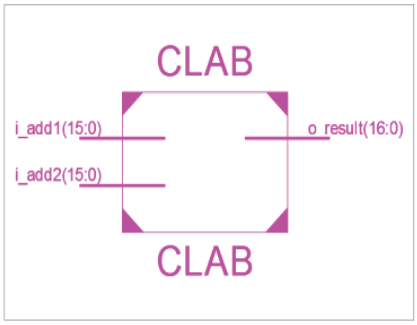

(a)

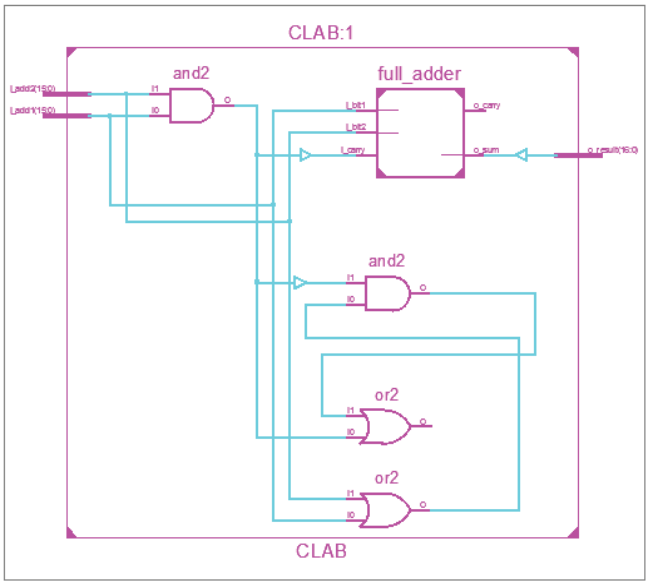

(b)

Figure 7. RTL view of (a) the 16-bit CLA symbol (b) internal RTL view of 16-bit CLA

E-ISSN 2581 – 7957
P-ISSN 2277 – 3916

DOI: 10.32377/cvrjst1722

TABLE II.
DEVICE UTILIZATION SUMMARY OF CLA FOR THE TARGET DEVICE VERTEX PRO FPGA

Device Utilization Summary (estimated values)			
Logic Utilization	**Used**	**Available**	**Utilization**
Number of Slice LUTs	29	64000	0%
Number of fully used LUT-FF pairs	0	193	0%
Number of bonded IOBs	132	640	20%

IV. IMPLEMENTATION OF FIR FILTER

The 8-Tap FIR filter is designed and implemented using Booth multiplier and CLA. The block based direct form FIR architecture [9] [10] selected and coded using HDL in Xilinx ISE tool and synthesized. The block based concept is introduced for the parallel proceeding for the FIR filter to reduce the delay [11]. In this work 4 inputs are grouped as block and applied to filter input [12] [13].The parallel processing also reduces the power consumption of the FIR filter [14]. The RTL view and the simulated output of the FIR filter is shown in the figure 8 and figure 9 respectively.

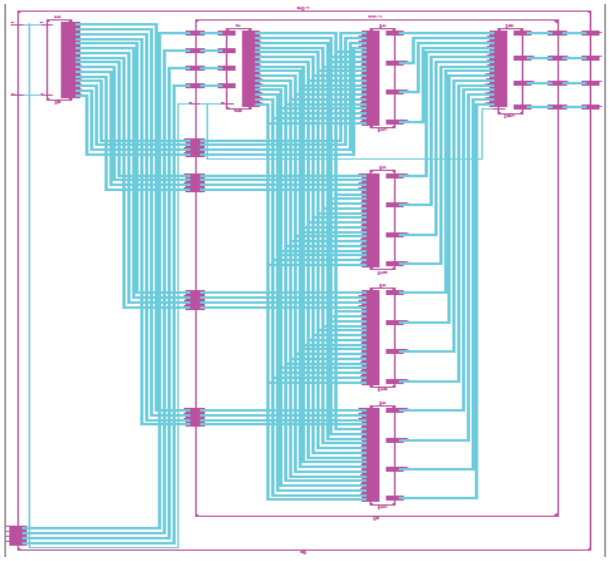

Figure 8. RTL Schenatic view of 8-tap FIR Filter

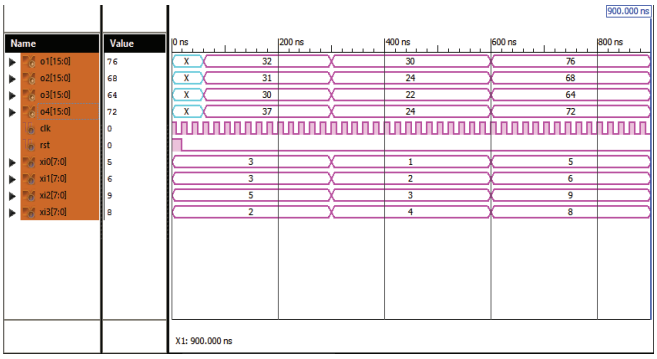

Figure 9. Simulated output results of FIR Filter for the random inputs.

The utilization summary report of the 8-tap block based FIR filter using Xilinx software is shown in the table III. Total 80 DSP blocks are required for the entire FIR filter. The total LUTs and LUT-FF pairs are 192 and 128 utilized for the 8-tap FIR filter. The input output blocks are 98 in total.

TABLE III.
DEVICE UTILIZATION SUMMARY OF FIR FILTER FOR TARGET DEVICE VERTEX PRO FPGA

Device Utilization Summary (estimated values)			
Logic Utilization	**Used**	**Available**	**Utilization**
Number of Slice Registers	129	64000	0%
Number of Slice LUTs	192	64000	0%
Number of fully used LUT-FF pairs	128	193	66%
Number of bonded IOBs	98	640	15%
Number of BUFG/BUFGCTRLs	1	32	3%
Number of DSP48Es	80	256	31%

V. RESULTS

In this section, the Radix-4 Booth multiplier and 16-bit CLA power consumption, area and delay are tabulated. The proposed 8-tap FIR Filter architecture is based on Booth multiplier and CLA adder power consumption, area and delay are computed using RTL compiler from CADENCE Tools. The TSMC 180nm CMOS technology is also used for synthesis of the FIR filter. Here, the same Xilinx HDL code is also synthesized using RTL compiler and it can be optimized. The RTL complier also generates the area, power and delay reports of the proposed 8 tap FIR filter. The table IV shows the area, delay and power of the FIR filter and important blocks of the FIR filter. In the previous section, Xilinx results corresponding to 8-tap FIR filter are discussed.

TABLE IV.
VLSI PARAMETERS OF FIR FILTER AND OTHER INTERNAL BLOCKS.

Name of the structure	Area (μm^2)	Delay (ns)	Power (μW)
CLA Adder	24544	8.371	6076
Booth Multiplier	38659	27.198	8906
8-tap FIR Filter	91925	35.391	16967

CVR Journal of Science and Technology, Volume 17, December 2019
DOI: 10.32377/cvrjst1722

VI. Conclusions

The 8-tap FIR filter is designed and implemented using high speed adder and high speed multiplier. The Radix-4 modified Booth multiplier and 16-bit CLA adder is considered for the implementation of high speed block based direct form 8-tap FIR filter, which is used for the digital signal processing applications. The VLSI parameters, such as area, delay and power for the optimized 8-tap FIR filter are calculated and presented. The summary report of the hardware utilization with respect to target FPGA also generated and presented in this paper for Booth multiplier, CLA adder and FIR filter. The HDL code is written and simulated, synthesized using Xilinx and RTL Compiler from CADENCE also.

References

[1] Oscal T.-C.Chen, Sandy Wang, and Yi-Wen Wu, "Minimizat ionof Switching Activities of Partial Products for Designing Low-Power Multipliers", IEEE Transactions on VLSI Systems,vol. 11, no. 3, June 2003.

[2] Shiann-RongKuang and Jiun-Ping Wang "Design of powerefficient configurable booth multiplier" IEEE Trans. CircuitsSyst. I Regular Papers vol. 57, no.3, pp. 568-580, March2010.

[3] TusharV.More, Dr.R.V.Kshirsagar, "Design of Low PowerColumn Bypass Multiplier using FPGA" IEEE journal of solid-state, circuits, vol 31,pp 1535-1546,July 2011.

[4] Akanksha Sharma, Akriti Srivastava, Anchal Agarwal, Divya Rana ,SonaliBansa "Design and Implementation of Booth Multiplier and Its Application Using VHDL. International Journal of Scientific Engineering and Technology, Volume No.3 Issue No.5, pp: 561 –563,May2014.

[5] A.RamaVasantha,M.Sai Satya Sri" Design and Implementation of FPGA Radix-4 Booth Multiplication Algorithm" in International Journal of Research in Computer and Communication Technology, Vol 3, Issue 9, September – 2014.

[6] JagannathSamanta, MousamHalder, Bishnu Prasad De "Performance Analysis of High Speed low Power Carry Look-Ahead Adder"International Journal of Soft Computing and Engineering (IJSCE) ISSN: 2231-2307, Volume-2, Issue-6, Jan-2013.

[7] Fu -Chiung Cheng Stephen H. Unger "Delay - Insensitive Carry - Look ahead Adders" ManojKumar,Sandeep K. AryaandSujataPandey "Single bit full adder design using 8 transistors " International Journal of VLSI design & Communication Systems (VLSICS) Vol.2, No.4, December 2011.

[8] M.C.B. Osorio, C.A. Sampaio, A. I. Reis, R.P. Ribas., etc.al. "Enhanced 32 - bit Carry Look Ahead Adder using Multiple Output Enable-Disable CMOS Differential Logic". SBCCI, pp. 181-185, 2004.

[9] A. Umasankar and N. Vasudevan," Designa and Analysis of Various Slice Reduction Algorithm for Low Power and Area Efficient FIR Filter", ICCTET13, IEEE Conf. july 2013.

[10] R. Mahesh and A. P. Vinod, "New reconfigurable architectures for implementing FIR filters with low complexity," IEEE Trans. Computer.-Aided Design Integr. Circuits Syst., vol. 29, no. 2, pp. 275–288, Feb. 2010.

[11] S. Y. Park and P. K. Meher, "Efficient FPGA and ASIC realizations of a DA-based reconfigurable FIR digital filter," IEEE Trans. Circuits Syst. II, Exp. Briefs, vol. 61, no. 7, pp. 511–515, Jul. 2014.

[12] B. K. Mohanty and P. K. Meher, "A high- performance FIR Filter Architecture for Fixed and Reconfigurable Applications," IEEE Trans. on VLSI systems, vol. 24, issue 2, pp.444 –452, 2016.

[13] A. P. Vinod and E. M. Lai, "Low power and high-speed implementation of FIR filters for software defined radio receivers," IEEE Trans. Wireless Commun., vol. 7, no. 5, pp. 1669–1675, Jul. 2006.

[14] J. Park, W. Jeong, H. Mahmoodi-Meimand, Y. Wang, H. Choo, and K. Roy, "Computation sharing programmable FIR filter for low-power and high-performance applications," IEEE J. Solid State Circuits, vol. 39, no. 2, pp. 348–357, Feb. 2004.

E-ISSN 2581 – 7957
P-ISSN 2277 – 3916

CVR Journal of Science and Technology, Volume 17, December 2019
DOI: 10.32377/cvrjst1723

Design and Analysis of the Sleeve Ejection System in Injection Molding Die for Trolley Wheel

Neeraj Kumar Jha[1] and Bhavya Sri Tadiparthi[2]
[1]Assoc. Professor, CVR College of Engineering/ Mechanical Engg. Department, Hyderabad, India
Email: neerajjha.me@gmail.com
[2]B. Tech. Student, CVR College of Engineering/ Mechanical Engg. Department, Hyderabad, India
Email: bhavyatadiparthi@gmail.com

Abstract: **Plastic is a commonly used engineering material. Properties like availability, less weight, moldability and corrosion resistance are a few among many desirable properties, due to which most of our usable products are made of plastic. This vital use encourages manufacturing industries to make plastic products in large scale. The industries are able to meet this demand and supply requirement, using various methods of processing plastics. All the methods and tools for processing plastics contribute to mass production. Injection molding dies are one among the many tools used for processing plastics to the required shape. Usually it is very easy to learn and perform the injection molding method to obtain plastic products. But to achieve quality components in mass production, one needs proper implementation of each die-set element in an injection molding die. Ejection of component from the die cavity is one phase in injection molding process and it has similar importance like all other phases. This paper aims at implementation of sleeve ejection system for plastic trolley wheels. Software used for modeling of parts is UG Nx 9.0 and that for the simulation of process parameters is Autodesk Moldflow Adviser 2015. Stress and deformation analysis is done by ANSYS 16.0 version.**

Index Terms: **Moldability, Mass Production, Tool, Plastic Mold, Die, Ejection, UG Nx 9.0, Autodesk Moldflow Adviser 2015**

I. Introduction

Injection molding process is similar to hot chamber die casting. A barrel (cylinder) is heated to promote melting. The pallets or granules are fed into the heated cylinder, and the melt is forced into a split-die chamber, either by hydraulic plunger or by the rotating screw system of an extruder [1]. This split-die is termed as injection molding die or mold. They are aligned and clamped together. This is the first phase of injection molding process, known as clamping. Pressurized flow of the plastic melt into the mold is another phase and this phase of the injection molding process is called as injection. After the die cavity is filled, it is allowed to cool for curing of plastic melt into shaped cavity of the mold, this phase is known as cooling. In the last phase of the process, molds are opened and the solidified part is ejected out of the mold cavity, thus this phase is called ejection [2]. This is the end of one cycle of the injection molding process. Molds are then closed again and the process is repeated. The process can be optimized by analyzing all the dependent and independent variables involved within [3].

An injection molding die is a systematic arrangement of a number of different parts or elements, assembled together to accomplish each phase without any error. Most of such elements were illustrated in Figure 1. To achieve mass production, time consumed by each phase is kept as small as possible. Thus, a designer plans and designs element for each phase effectively. There are different conditions and situations associated with each phase, which must be addressed wisely. The complexity related to ejection phase is slightly related to change of form of plastic material inside the mold cavity. As plastic solidifies in the mold cavity it shrinks on the core which forms it. This shrinkage makes the molding difficult to remove. Thus, there must be proper provision by which molded part can be positively ejected from the mold cavity. Such provision is called as ejector system and this is situated behind the fixed die block in an injection molding die set.

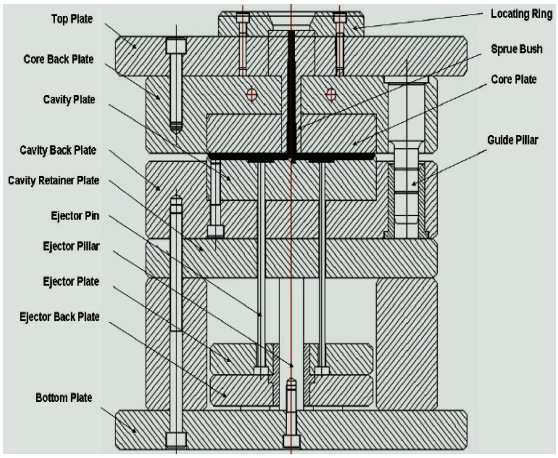

Figure 1. Elements of an Injection Molding Die
(Source: researchgate.net)

The design of an effective ejector system is planned in three parts viz. ejector grid, ejector plate assembly and method of ejection. Ejector grid is a part of the mold which supports the mold plate and provides sufficient space into which the ejector plate assembly can be fitted and operated. The ejector plate assembly is that part of the mold to which the ejector element is attached. The assembly is contained in a pocket, formed by the ejector grid, directly behind the mold plate. The method of ejection is about several ejection techniques by which a component can be ejected from the mold cavity [4]. Few basic ejection techniques are pin ejection, sleeve ejection, bar ejection, blade ejection, air ejection, stripper plate ejection etc. These ejectors remain hiding on mold surface till the phase of solidification. After solidification as the die opens, they advance to push the component away from the cavity. The selection of a suitable

E-ISSN 2581 – 7957
P-ISSN 2277 – 3916

CVR Journal of Science and Technology, Volume 17, December 2019
DOI: 10.32377/cvrjst1723

ejection technique depends mainly on the shape and size of molding. But one type of ejection technique is not restricted to be used in one particular type of molding [5]. Required strength, economy and easiness of manufacturing are among few other factors which must be considered before deciding the ejection technique. Due to ease in manufacturing and installation, pin ejectors are widely used in ejection technique. But a pin ejector usually leaves impression and sometimes additional material deposition called boss, on the surface of the component. Figure 2 represents one such component, trolley wheel. Ejector bosses can be easily seen on its surface. Such marks are usually undesirable, especially if the appearance of the component is an important aspect.

Figure 2. Ejection Marks of Pin Ejection on Trolley Wheel

Incorrect size and wearing, as well as chopping of the ejector pin tips cause such ejector marks and bosses. This is one of the limitations of the pin ejection system. Another aspect of avoiding pin ejection is related to strength, which can be observed from Figure 3. Ejectors need to apply ejection force on the solidified component in the mold cavity so that the component comes out of the cavity, overcoming the friction of mold walls and shrinkage on core. This force is distributed on the number of ejectors employed for ejection. Due to shape, size and available space constrains, less number of big size ejectors cannot be deployed. Thus, a number of small size ejectors are used for uniform ejection of the component. For their movement, holes are made in the mold and inserts. Higher number of ejectors implies to more number of holes in die, and inserts resulting a decrease in their strength.

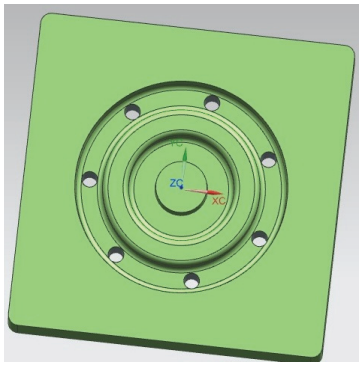

Figure 3. Holes in a Die for Pin Ejection

Proper product design along with correct study of shrinkage behavior of the components like trolley wheel indicates that a single sleeve ejector can be sufficient for such component rather than using multiple pin ejectors. In sleeve ejection method the molding is ejected by means of a hollow ejector pin, termed as sleeve. It is used preferably for circular moldings, moldings with usually local circular bosses and to provide ejection around a core pin forming a round hole in molding. This implementation not only decreases complexity in the die design but also contributes to low cost of die manufacturing.

II. Product Design

An effective mold design begins with proper product design of the part to be molded. In the product design phase a product is observed for its manufacturability by a particular process of manufacturing. By considering various design considerations and product specification a part was redesigned and corresponding to that its mold was prepared [6].The modeled product for this research work is as shown in Figure 4.

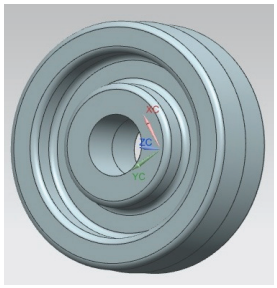

Figure 4. Modeled Trolley Wheel for Analysis

Figure 5 represents various dimensions and geometry of the component. The dimensions of the modeled product for this research work were taken from one of the standard dimension followed by the manufacturers. Then it was further modified by providing appropriate fillet and drafts in the direction of ejection. The component dimension was slightly modified in terms of hub diameter and mass reduction groove. Table I represents few specifications related to the modeled product.

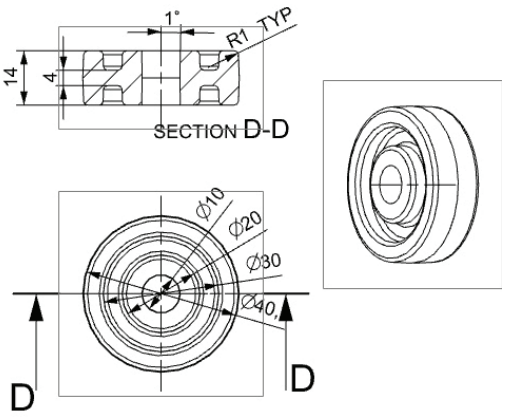

Figure 5. Dimensional Details of the Component (All dimensions are in mm)

E-ISSN 2581 – 7957
P-ISSN 2277 – 3916

CVR Journal of Science and Technology, Volume 17, December 2019
DOI: 10.32377/cvrjst1723

TABLE I.
PRODUCT SPECIFICATION

Part Name	Trolley Wheel
Material	Polypropylene
Part Volume	12828.28 mm^3
Surface Area	8172 mm^2
Mass	15.4 gm

By observing geometry and profiles of the component, horizontal plane of symmetry was considered as parting plane. This arrangement of parting plane was suitable according to design considerations of designing of plastic molds. Thus the expected position of component against mold opening and closing is shown in Figure 6.

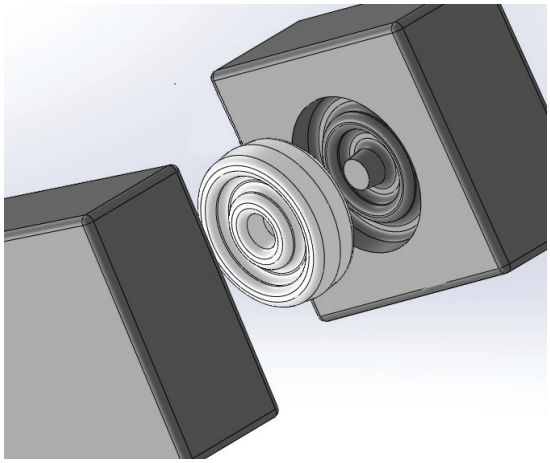

Figure 6. Position of the Component in Die and Expected Direction of Ejection

By the observation of the component profile, it can be understood that it has sufficient wide hub area near to the central hole. As the central hole is inbuilt profile of the component, cure pin will be implemented in the mold to achieve the hole in the component. Sufficient surface available in hub area can be used as resting area of ejector sleeve for sleeve ejection of the component. But before proceeding for designing of the ejection system, we should ensure that the phases prior to ejection are intact. Thus, we should see that the component is perfectly in condition prior to ejection. For this purpose we will perform simulation of injection molding for the component. Polypropylene is preferred for this purpose because it is one of the preferable materials for making trolley wheels. Few of the important characteristics of polypropylene (PP) are enlisted in Table II.

TABLE II.
MATERIAL SPECIFICATION
POLYPROPYLENE (PP)

Density	946 kg/m³
Melting Point	160 °C
Formula	$(C_3H_6)_n$
Type	Thermoplastic
Flexural Strength	40 N/mm²
Shrinkage	1-2.5% mm/mm
Tensile Strength	32 N/mm²
Injection Temperature	140-160 °C
Heat Deflection Temperature	100 °C
Specific Gravity	0.91

For process parameter selection, specifications from an injection molding machine were taken. So that further trial results would be compared after development of such ejection system which we are being considered in this research article. Before starting simulation, it is always desirable to consider part shape, size material and machine capacity in to account [7]. Common specifications of available injection molding machine is shown in Table III.

TABLE III.
MACHINE SPECIFICATION
(TEXPLASST 1HD, PT LAB, CVRCE)

Shot Capacity	2 – 45 gms / shot
Plunger Diameter	25 mm
Stroke Lenght	450mm
Clamping Capacity	6.0 Tons
Injection Pressure	80 kg/cm^2
Heating Capacity	1.5 kw
Total Installed Power	3.7 kw
Total Shut Height	100 - 450mm

Based on above mentioned process parameters and material properties, process simulation was performed with help of Autodesk Moldflow Adviser 2015 software. The obtained results were indicated in Figure 7 and Figure 8. Confidence of fill indicates possibility of filling of die cavity in conventional injection molding conditions [8]. Weld lines emerges if there is no proper fusion of polymer flow front due to design features like, hole, ribs etc. [9]. Indicated and other obtained results clearly show that there is no defect in the component like weld line of air entrapment which may become problem for implementing sleeve ejection of the component.

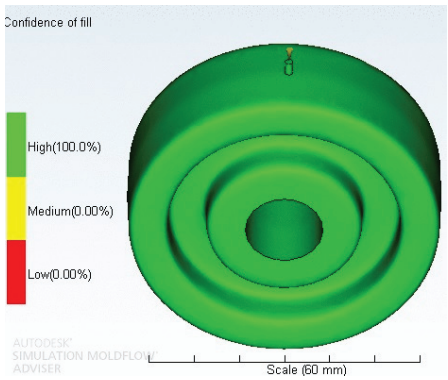

Figure 7. Confidence of Filling Prediction

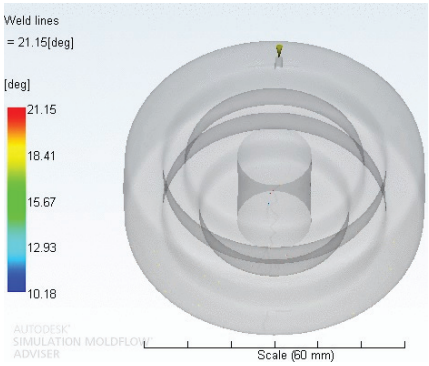

Figure 8. Weld Line Prediction

E-ISSN 2581 – 7957
P-ISSN 2277 – 3916

DOI: 10.32377/cvrjst1723

III. Ejection Force Calculations and Sleeve Ejector Design

In molding, no part can be ejected from the mold cavity till it acquires sufficient rigidity. During solidification, polymer shrinks inside the mold and internal stress builds up [10]. The solidified component shrinks on the core or on the inserts. Thus an ejection system should overcome the frictional forces caused due to shrinkage [11].

A. Calculation of Ejector Force

To calculate ejection force, based on various material properties, an equation is developed by experiments [12], which is shown below.

$$Fe = \frac{\alpha\,(Tm - Te)EA\,\mu}{\left(\frac{D}{2t} - \frac{D\,\gamma}{4t}\right)} \qquad (1)$$

Where,

Fe = Ejection Force (N)
α = Coefficient of thermal expansion for molding material (/°C)
Tm = Melting temperature of molding material (°C)
Te = Ejection temperature of molding material (°C)
E = Young's modulus of material at Te (N/cm^2)
A = Area of contact between core and molding in direction of ejection (cm^2)
μ = Coefficient of friction between molding material and core material
D = Diameter of core (cm)
γ = Poisson's ratio of molding material
t = Thickness of mold (cm)

The required values of above mentioned parameters for our situation are collected from various sources and arranged in Table IV. Ejection temperature is taken as 20°C by considering the ideal condition that the mold is being cooled by cooling lines to reduce solidification time of the component.

TABLE IV.
Values of Parameters

α	8 X 10^{-5} cm (cm/°C), standard
Tm	152 °C, standard
Te	20 °C, standard
E	1.32 X 10^5 N/ cm^2, standard
A	2.17 cm^2 from software
μ	0.3, standard
D	1 cm, measured
γ	0.42, standard
t	0.7 cm in one half, measured

$$Fe = \frac{8\times10^{-5}\times(152-20)\times1.32\times10^{5}\times2.17\times0.3}{\left(\frac{1}{2\times0.7} - \frac{1\times0.42}{4\times0.7}\right)}$$

$$Fe = 1608\,N \text{ (Approximately)}$$

B. Validation of Result

Thus approximately 1608 N force was required to push the component away from the cavity. As the maximum shrinkage was occurring on core and nearby area was also sufficient to implement ejector sleeve, we must check the possibility of damage in our component by this type of ejection. For this purpose ANSYS 16.0 version was used to analyze our component for any possibility of localized deformation on our component and result is displayed in Figure 9 and Figure 10. The component was fixed in core area and load of 1608 N if applied in distributed manner on hub area. As we can observe that negligible deformation has occurred, the result indicated that the component can be ejected by sleeve ejector.

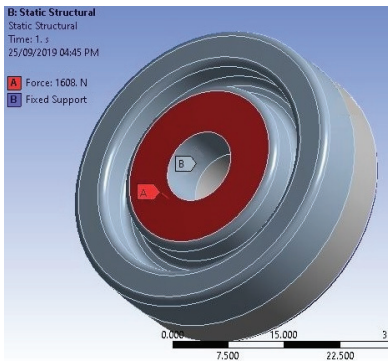

Figure 9. Applied Load Position

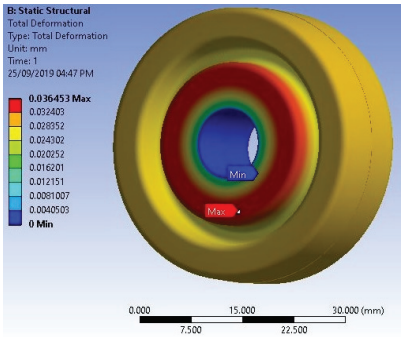

Figure 10. Effect of Ejection Force on Deformation Pattern of the Component

C. Design of Sleeve Ejector

Sleeve ejectors are always employed in two parts viz. core pin which is surrounded by ejector sleeve. They usually have common basic design but their dimensions and profiles can be specific based on particular application. Ejector sleeve and core pins generally have sliding fit [13]. This fit additionally acts as venting medium [14]. Inner diameter of core pin slides on outer surface of the core pin. Nitriding is done to harden them up to 65-70 HRC. Core hardness is usually kept in the range of 45-55 HRC. Otherwise due to wear, clearance will increase on contact surface causing flash in molding. Hot working tool steel is most proffered material used for making ejector sleeve. Overall manufacturing is possible by turning operations, for profiled heads milling is done. One possible design of ejector sleeve and core pin, corresponding to our requirement is shown in Figure 11 and in Figure 12 respectively.

E-ISSN 2581 – 7957
P-ISSN 2277 – 3916

CVR Journal of Science and Technology, Volume 17, December 2019
DOI: 10.32377/cvrjst1723

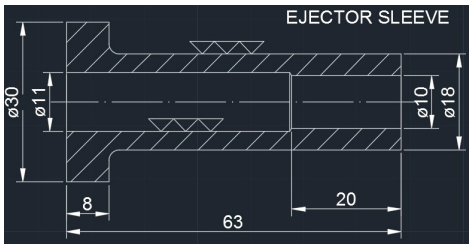

Figure 11. Ejector Sleeve
(All dimensions are in mm)

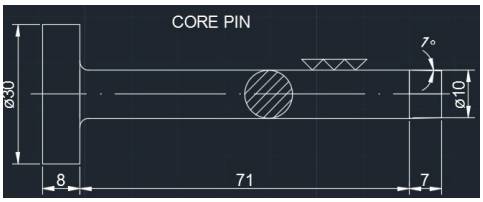

Figure 12. Core Pin
(All dimensions are in mm)

One can observe Figure 13 to understand the arrangement of sleeve ejector in combination with other parts of mold assembly. In this figure, part number 1 and 3 indicates ejector sleeve and core pin respectively. Part number 2 is mold plate. Part number 4 and 5 are ejection plates which cause sleeve to move during ejection. Part number 6 is termed as core retainer plate. Ejection gap is maintained as amount of travel of ejection plates. Usually it is kept more than the length of deepest cavity in the mold, so that the component can be fully pushed out of the mold cavity.

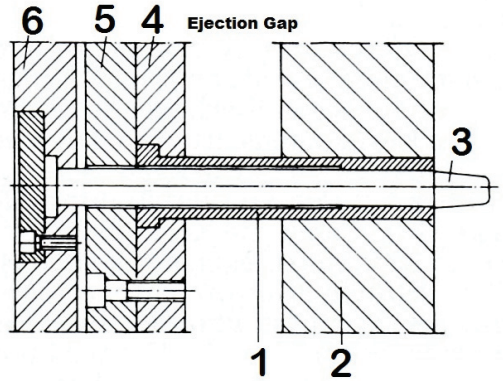

Figure 13. Ejector Assembly

IV. Ejection Simulation

When a number of movable parts come together, it is necessary to compare and observe their relative position and dimension. Assembly and simulation of sleeve ejector assembly is done with help of UG Nx 9.0 software.

A. Assembly

Figure 14 indicates partial assembly of sleeve ejection system along with component and mold inserts. For the sake of simplicity of observation, other plates, viz. die block, ejector plates etc are not shown. One can visualize top half and bottom half of die (kept transparent), component in die cavity, fixed core pin and sleeve ejector.

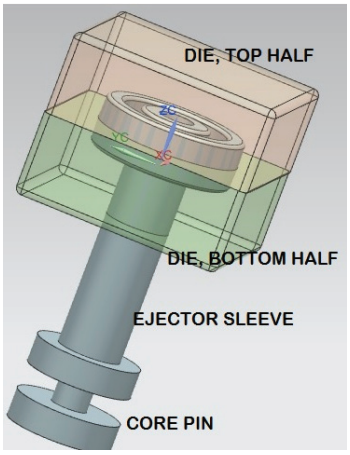

Figure 14. Modeled Assembly of Sleeve Ejection System

Assembly of sleeve ejection system can be observed in a set of images indicated in Figure 15.

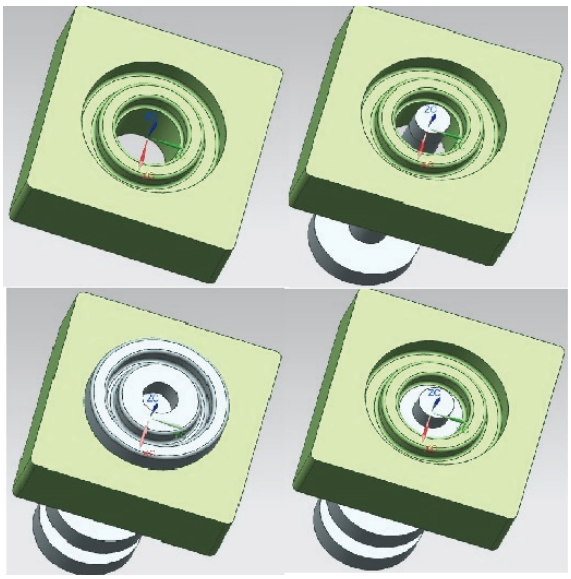

Figure 15. Sequence of Sleeve Ejector Assembly

In Figure 15, fitting of core pin in bottom die insert and fitting of ejector sleeve and placement of component are shown in clockwise sequence. From this figure it is shown that an ejector sleeve in retarded position acts as the surface of the mold. After mold filing and solidification, it advances to push the solidified component away from cavity while the core pin remains stationary at its place. One must understand that the similar profile of bottom half of die is in top half also. But in top half of die the core is inbuilt and ejection of a part from top half is taken care of by sufficient high die opening force.

B. Simulation

By Figure 16, an attempt is made to visualize simulation of sleeve ejection system. The left side image shows initiation of ejection. Top half of the die is removed. The ejector sleeve is at its position and the component is still in bottom half. In the right side image advance of ejector

E-ISSN 2581 – 7957
P-ISSN 2277 – 3916

DOI: 10.32377/cvrjst1723

sleeve and ejection of the component from die cavity can be observed.

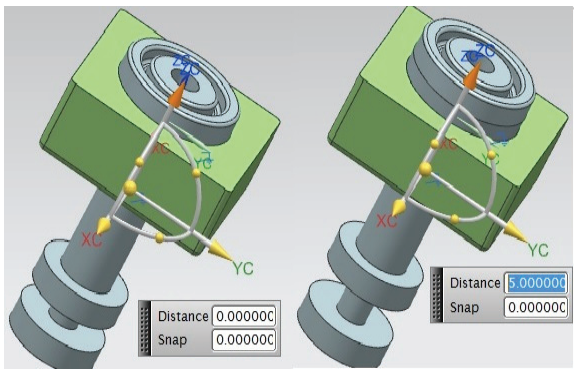

Figure 16. Ejection Simulation up to 5mm Advance of Ejector Sleeve

Travel of ejection sleeve is indicates as 5 mm i.e. component is still 2 mm inside the cavity. Figure 17, shows 10 mm ejector sleeve advance, which is more than sufficient for the required ejection gap of 7 mm and hence the component is ejected completely out of mold cavity.

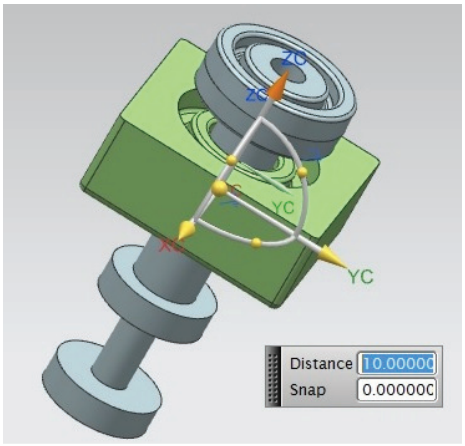

Figure 17. Ejection Simulation up to Sufficient Ejection Gap

V. Conclusions

There are a number of process variables in injection molding, which must be controlled to obtain a defect free plastic component. Years of research in combination with design innovations are overcoming most of them. It is additional responsibility of a tool designer to find innovative solutions for the difficulties coming in his way of tool design. Innovation allows a designer to combine his experience with new learning. Conventionally used ejector pins for ejection purpose is more versatile. But that is not the only solution for each ejection requirement. For smaller and specifically of circular profiled component, sleeve ejection is easy and economical solution. It can be concluded that for large and unsymmetrical components, importance of pin ejection system can't be ignored but at the same time the drawbacks of such systems can be avoided by other innovative ejection techniques. The tool and method discussed in this report is just an approach towards avoiding problems occurred in molded parts due to pin ejection system. A better and more innovative approach can find even more suitable and simple solution for this and many other situations.

References

[1] Neeraj Kumar Jha, P V Ramana, "*Design Methodology and Analysis of Double Cavity Metal-Plastic-Insert Injection Molding Die for Push Board Pin*". CVRJST, Vol. - 14, pp. 91-96, 2018.

[2] Hamdy Hassan, Nicolas Regnier, Guy Defaye, "*A 3D study on the effect of gate location on the cooling of polymer by injection molding*", International Journal of Heat and Fluid Flow, pp. 1218–1229, 30-2009.

[3] Ciprian Ciofu, Daniel Teodor Mindru, "*Injection And Micro Injection Of Polymeric Plastics Materials: A Review*", International Journal of Modern Manufacturing Technologies, ISSN 2067–3604, Vol. V, No. 1, 2013.

[4] Technical committee, *Technical Directory on Design and Tooling for Plastics*, Central Institute of Plastic Engineering & Technology. pp. 43-64, 1970.

[5] Samson Teklehaimanot, "Simulation and Design of a plastic injection Mold", Degree Thesis,PTE 2011.

[6] Y.-M. Deng , D. Zheng , B.-S. Sun & H.-D. Zhong, "*Injection Molding Optimization for Minimizing the Defects of Weld Lines*", Polymer-Plastics Technology and Engineering, 47:9, pp. 943-952, 2008

[7] Md. Jamsheed, Md. AaqibRahman, M.A Moyeed,G.M.SayeedAhmed, "*Design and Analysis of Plastic Injection Mould for CAM BUSH with Submarine Gate*", Materials Today: Proceedings 2, pp. 2083 – 2093, 2015

[8] N. Sreenivasulu, Dr. D. Ravikanth, " *Injection Moulding Tool Design Manufacturing, Estimation and Comparison of L&T Power Box Side Panel Using Plastic Materials HDPE, ABS, PP and PC*", IOSR Journal of Mechanical and Civil Engineering (IOSR-JMCE) Volume 8, Issue 3,pp. 23-32, 2013

[9] Mohd Hilmi Othman, Shazarel Shamsudin , Sulaiman Hasan and Mohd Norhafiz Abd Rahman, "*The effects of injection moulding processing parameters and mould gate size towards weld line strength*" , Advanced Materials Research Vols 488-489 , pp. 801-805, 2012

[10] Struik, L.C.E, "*Orientation effects and cooling stresses in amorphous polymers*", Polym. Eng. Sci.. vol. 18:10 pp. 799-811, 1978

[11] António José Vilela Pontes, "*Shrinkage And Ejection Forces In Injection Moulded Products*" Universidade Do Minho, pp. 20-29, 2002

[12] Neil Hopkinson , Phil Dickens, "*Study of Ejection Forces In The AIM™ Process*", De Montfort University,Leicester, UK, pp. 65-78, 1998

[13] Kavin Kumar S, Ravi kumar M, "*Tool Design for Injection Moulding With Basic Parameters*", International Research Journal of Engineering and Technology, Volume: 06 Issue: 03, pp. 1316-132, 2019

[14] Vikram Bhargava, "*Robust Plastic Product Design- A Holistic Approach*," Tooling Considerations, pp. 115-159, 2018

E-ISSN 2581 – 7957
P-ISSN 2277 – 3916

CVR Journal of Science and Technology, Volume 17, December 2019
DOI: 10.32377/cvrjst1724

Energy and Exergy analysis of a Power Plant and Adoption of OPCAN Power Box for Improving Productivity

Mr. A. Suresh[1] and Dr. Manjeet Kharub[2]
[1]Asst. Professor, CVR College of Engineering/Mechanical Engg. Department, Hyderabad, India
Email: suri0341@gmail.com
[2]Asst. Professor, CVR College of Engineering/Mechanical Engg. Department, Hyderabad, India
Email: manjeetkharub@gmail.com

Abstract: **Most of the electric energy which the world has utilized is generated from coal or gas based on thermal power plants. These power plants have increased the pollution to the maximum extent. In addition to this the population on the world has multiplied as well as their needs. Therefore, there is a scope for the enhancement of the power plants. All these factors have helped to write this research paper. It is based on the thermal power plant located in Ramagundam of Telangana state, India. Power plant performance evaluation is one of the important processes towards the optimization of its performance. Here in this research power plant performance is evaluated based on first law of thermodynamics (energy analysis) and second law of thermodynamics (exergy analysis) and after that organic rankine cycle based opcan power box is introduced in the power plant. By adopting it the performance of the plant is calculated, after that a comparison is made among the efficiencies with energy analysis, exergy analysis and plant efficiency after, before installation of the opcan power box. For all the components the exergy analysis based efficiency is less than efficiency based on energy analysis. The efficiencies of boiler, turbine using energy analysis are more compare with exergy analysis. In addition to this the efficiency of power plant before installation of opcan power box is calculated as 45% and after the installation of the opcan power box it is computed as 46.07%. It indicates that for a 500MW capacity power plant an extra electricity of 6.7MW power is produced without altering the input fuel quantity. The net increase of efficiency of 1.07% indicates that 2-3 % of reduced pollutants.**

Index Terms: **energy analysis, exergy analysis, opcan power box, efficiency**

I. Introduction

Electricity is one of the important source of energy to the mankind. Most of the electric energy producing using the conventional sources those are actually making huge lose to the environment. This is the main reason behind the development of the un conventional sources of energy. But the amount of unconventional energy produced is not at all sufficient to the mankind because of many reasons. On the other hand, there is a equal responsibility to reduce the pollutants from the existing conventional coal or gas based thermal power plants. This research paper has focused exactly on this issue to reduce the amount of harmful gases from the power plants for per unit electricity generation. This is achieved by analyzing the power plant performance using energy analysis and then exergy analysis. By doing these analyses the exact picture of power balance has obtained. After archiving the exact picture of power distribution using the energy balance. A new discovery of opcan power box is attached to the existing power plant. The net effect of this installation is critically analyzed for performance evaluation. This in turn shows a significant amount of power outcome. If a plant can produce a megawatt of electricity with the same input and output quantities, it is a welcoming situation to the mankind. Here in this case the plant could produce an extra electricity of about 6.7MW with a 500MW power plant.

The analysis is carried out on coal based thermal power plant located in Ramagaundam of Telangana state in India. As a part of the existing research the first step to carry out the work is energy analysis. The energy analysis is a systematic process of analyzing the energy interactions in the system using the thermodynamic principles. Basically, the energy analysis is works on the principle of first law of thermodynamics; it is a law of conservation of energy. During the analysis only boiler and turbine are considered for the analysis because of the priority of these machines. After finding the efficiencies of individual machines the overall efficiency is calculated. After that the exergy analysis is made to the boiler and turbine. Exergy analysis concerns with the available part of the energy. The efficiency of boiler and turbine using exergy analysis are dropped down compared with the energy analysis.

On the other hand, there are many numbers of scholars working over the betterment of the power plants performance or efficiency. Acharya Chirag al [1] in their paper suggested that process parameters must be divided based on the priority basis and out of them those which are making the maximum effect must be separated as decision parameters and they must be analyzed using the perato's principle. And during the analysis the pump work may be neglected as compared with the boiler and turbine. I. S. Jacobs al [2] have found that working over the efficiency calculations will enhance the power plant performance in a better way than many other methods. And they have yielded a solution by optimizing the input energy through the boiler from economizer.

Plant performance relies on the performance of the components in it. Hence there is a significant importance made on the components of the power plants such as boiler and turbine. As a part of that it is emphasized that the available energy is a critical parameter to be analyzed to

E-ISSN 2581 – 7957
P-ISSN 2277 – 3916

CVR Journal of Science and Technology, Volume 17, December 2019
DOI: 10.32377/cvrjst1724

calculate the efficiency. Hence at first the boiler and turbine efficiencies are calculated based on the input and output energy values. Then they are compared for the understanding of difference among the values.

After that the organic rankine cycle based opcan power box is used to lift the power output of the power plant. Basically, opcan power box is a set of construction to use the exhaust heat to produce electricity. This machine utilizes the n-pentane as the working fluid. And it is best suited for the power plants based on the working principle of thermal energy. Because the working fluid that is used in the opcan power box has the property to get vaporized at low temperatures compared with the water. By making this analysis the power plants efficiency is improved by about 1.07%. This is a significant value because of no extra fuel input and no pollution from the power plant. And the box can operate with less noise and low space compared to the conventional power plant. The detailed methodology and work is briefed below.

II. Experimentation

The work is an outcome of critical analysis of the power plant components and as well as the effect of mounting the opan power box for the exiting power plant. The detailed methodology is given in figure 1.

Nomenclature:

Q=Heat input in kJ/kg
W= Work input in kJ/kg
P= Pressure in bar
T = Temperature in ^{o}C
h = enthalpy in kJ/kg
s = entropy in Kj/kg
x= dryness fraction
m_f = mass flow rate in kg/sec
C_v = Specific heat in kJ/kg
ε = specific energy in kJ/kg
$\varepsilon_{k.e}$ = exergy due to velocity (or) kinetic energy in Kj/kg
$\varepsilon_{p.e}$ = exergy due to potential energy in kJ/kg
ε_{ph} = physiccal exergy in kJ/kg
V = Volume in m^3/kg
dh = change in enthalpy
ds = change in entropy
dP = change in pressure
dV = change in volume
dT = change in temperature
η = efficiency
h_f- is the specific enthalpy of the saturated fluid
h_g- is the specific enthalpy of the saturated gas/vapor
h_{fg}- is the difference of the specific enthalpy values of the substances
E= physical exergy

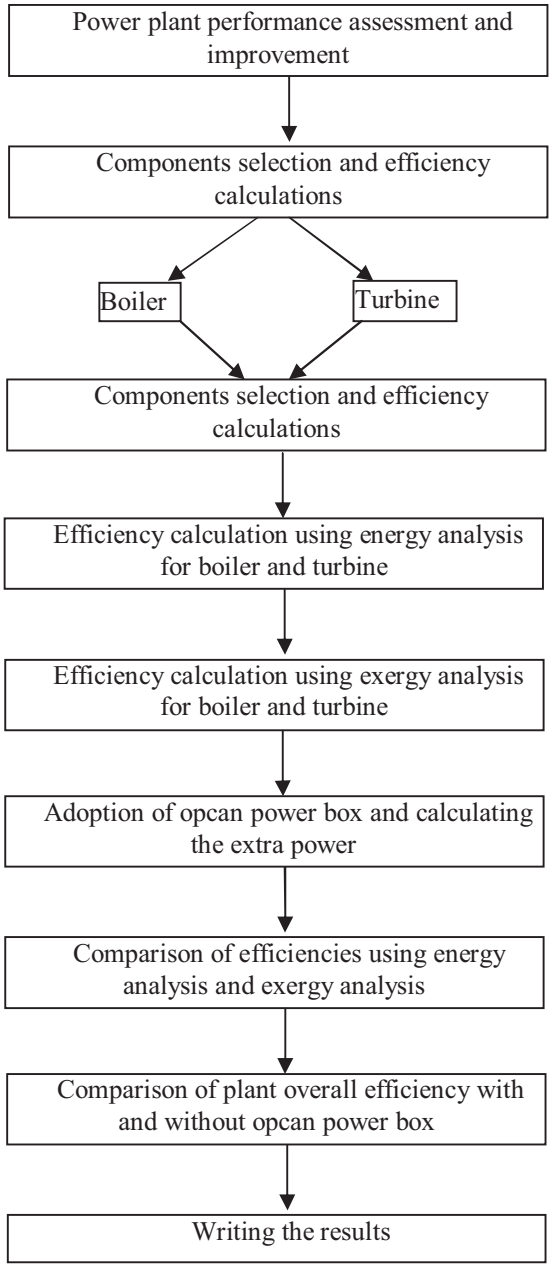

Figure 1: Flow chart describing the methodology of work

III. Analysis

The energy and exergy analysis is made by the following assumptions.

- The working parameter values for the power plant usually vary based on the seasonal variations and here the values are considered in winter season.
- The auxiliary power consumption is fixed value and will not vary.
- There are no miscellaneous effects affecting the plant performance.

A. Energy Analysis

Considering 1 kg of fluid:
Applying steady flow energy equation to boiler, turbine, condenser and pump.

E-ISSN 2581 – 7957
P-ISSN 2277 – 3916

CVR Journal of Science and Technology, Volume 17, December 2019
DOI: 10.32377/cvrjst1724

1 For boiler (as control volume),

$h_{f4} + Q_1 = h_1$

$Q_1 = h_1 - h_{f4}$

2. For turbine (ascontrol volume),

$h_1 = W_T + h_2$ where W_T =turbine work

$W_T = h_1 - h_2$

3. For condenser,

$h_2 = Q_2 + h_{f3}$

$Q_2 = h_2 - h_{f3}$

4. For the feed pump,

$h_{f3} + W_p = h_{f4}$

$W_P = h_{f4} - h_{f3}$

5. Rankine cycle efficiency:

$\eta_{Rankine} = W_{net} / Q_1$

$= \{(h_1-h_2)-(h_{f4}-h_{f3})\} / (h_1-h_{f4})$

The feed pump handles liquid water which is incompressible which means with increase in pressure its density or specific volume undergoes a small change .Using general property relation for reversible adiabatic compression, it can be taken as TdS =dh-Vdp

Since dS=0

Therefore dh=vdp

$\Delta h = v\,\Delta p$

$h_{f4} - h_{f3} = V_3(p_1 - p_2)$

When p is in bar & V is in m^3/kg, then it becomes

$h_{f4} - h_{f3} = V_3(p_1-p_2) \times 10^5$ J / kg

The feed pump term ($h_{f4}-h_{f3}$) being a small quantity in comparison with turbine work, W_T, is usually neglected, especially when the boiler pressures are low.

Then $\eta_{Rankine} = h_1-h_2 / h_1-h_{f4}$

Properties of steam are shown in the below table I:

TABLE. I

PROPERTIES OF STEAM IN 500MW NTPC POWER PLANT

S No	Pressure	Temperature	Enthalpy	Dryness fraction
1	P_1=160 bar	T_1=450°C	h_1=2600 kJ/Kg	
2	P_1'=160 bar	T_1'=540°C	h_1'=3420kJ/Kg	
3	P_2=50 bar	T_2=350 °C	h_2=3060 kJ/Kg	
4	P_2'=50 bar	T_2'=540°C	h_2'=3540 kJ/Kg	
5	P_3=2 bar	T_3=130 °C	h_3=2710 kJ/Kg	
6	P_4=1 bar	T_4= 70 °C	h_4=2585.505 kJ/Kg	x= 0.96
7	P_5=1 bar	T_5= 70°C	h_5= 419.5 kJ/Kg	
Note: All the values are taken from the 500MW unit of NTPC				

Boiler:

The water from reservoir from reservoir entered in to the economizer from the sump or reservoir. Hence point 1 (here after shown as h_1, s_1,P_1 etc) can be considered as the economizer exit. The fluid then goes to the drum where purification of stream and also separation takes place. After that the steam enters into super heater, the exit of it is considered as point (1'), then the steam is supplied to High pressure turbine, from there, as the steam is expanded it is again sent in to boiler for reheating by reheaters. Then the steam is sent in to Low pressure turbine.

Briefly the boiler consists of Economizer coils, super heater coils and reheater coils. The heat quantity given to the boiler will be by burning of coal with the air in the furnace and that will be equal to mass flow rate of the coal multiplied by the calorific value.

The calorific value of the coal that is using there is C_V= 4000 kCal / Kg

= 956.93 kJ /Kg

And the mass flow rate of the coal will be (m_f) = 320 T/hr = 1152 Kg / sec

So the input power given to the boiler = (m_f)*C_V = (1152 Kg / sec) x (956.93 kJ /Kg) = 1102383.36 kJ /sec = 1102.383 kW

And due to this input power the water gets converted in to steam , so totally in the three forms energy transfer will be there , viz,

i) Economizer

Change in enthalpies (h_1-h_2) = 2220.3 kJ / kg

ii) Super heater

Change in enthalpies (h'_1-h_1) = 780 kJ / kg

iii) Re heater

Change in enthalpies (h_2-h'_1) = 360 kJ / kg

Then the boiler efficiency is given by η = ({dh *m_f }of economizer) / (input energy {mf*CV})

= (2220.3 x 430.55) / (1102383.36)

= 86.7 %

Turbine:

In the turbine there are two stages will be there,

viz., i) High pressure turbine

ii) Low pressure turbine

The net work done by the High pressure turbine = m_f *(h'_1-h_2)

= {1550*18 /5}*{360}

= 2008800 kW

The net work done by the Low Pressure turbine = m_f *(h'_2- h_4)

= {1550*18 /5} * {954.916}

= 5328431.28 kW

And the input energy is = {(h_5-h_1)*m_f} of combustion products + {{(h_1'-h_1)*m_f} energy of super heated steam}+ {{(h_2-h_2')*m_f} energy of re heated steam}

= [{320*18/5} *{4000/4.18}] + [{1550 x18/5}*{780}] + [{1550*5/18}*{480}]

= 1102392.345 + 4352400+2287800 kW

= 7742592.345 kW

Therefore, $\eta_{Turbine,\ I\ law}$ = (net work generated by HPTurbine) / (heat supplied to the steam to run the HPTurbine)

= ((2008800+532841.28) / 7742592.345)

= (7337231.28 / 7742592.345)

=0 .94 = 94 %

Condenser:

From the data the mass flow rate of the steam at the inlet of the turbine = 334.35 Kg/ sec with the temperature of 70 deg C.

E-ISSN 2581 – 7957
P-ISSN 2277 – 3916

DOI: 10.32377/cvrjst1724

The input quantity = m_f * h_{fg} = 334.8*2431 = 813898.8 kW

In the condenser the rate of heat transfer will be equal to: (m_f) * C_p * dT

= 4868.106*4.2*40 = 817841.8 kW

Therefore the effectiveness of the condenser = (input quantity / output quantity) = 0.995

Pump:

The pump work has been neglected. And more over there is auxiliary power consumption (A.P.C), which includes the power required to run the plant in all the sectors.

And that will be equal to: 6%

Note: A.P.C. includes power given to all fans, households of the plant, pump etc.

A. Energy balance

Energy balance includes the balancing of input and output energies.

The input energy for the total plant is = (m_f) * C_V = (1152 Kg / sec) * (956.93 kJ /Kg)

= 1102383.36 kJ /sec = 1102.383 MW

And the output will be: 500MW constant.

Then the overall efficiency of the plant will be equal to: (500 / 1102.383) = 45%

Thermal efficiency: $\{((h'_1-h_2)-(h'_2-h_4)) / ((h_1-h_5)-(h_2-h_2))\}$ = 37%

And the Auxiliary Power Consumption = 30 MW = (30 / 500) = 6%

And the heat transfer losses due to bad insulation = (approximately) = 2%

The power loss in condenser is equal to: 440.15MW = (approximately) = 40%

And finally the power loss by flue gases will be equal to = 15% (remaining) .

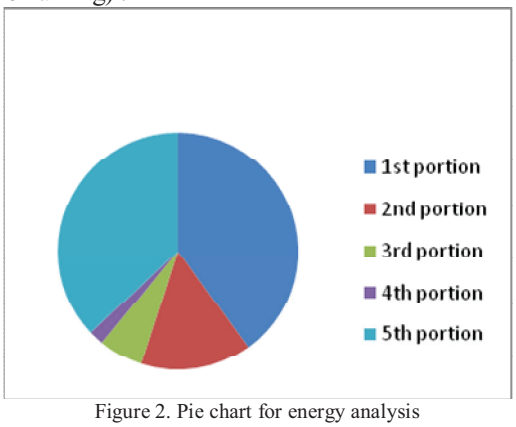

Figure 2. Pie chart for energy analysis

Portion 1 : Condenser losses = 40%
Portion 2 : Flue gases losses = 15%
Portion 3 : A.P.C. = 6%
Portion 4 : Heat Transfer losses = 2%
Portion 5 : Net power = 37%

B. Exergy analysis

The exergy analysis is the combination of the First and Second laws of thermodynamics. In this analysis the heat does not have the same value as the work, and the exergy losses represent the real losses of work. When analyzing novel and complex thermal systems, experience needs to be supplemented by more rigorous quantitative analytical tools [1,2]. Exergy analysis provides those tools and it helps in locating weak spots in a process. This analysis provides a quantitative measure of the quality of the energy in terms of its ability to perform work and leads to a more rational use of energy. In general, the specific exergy denoted by "ε" is calculated using the equation as given below.

$$\varepsilon=\varepsilon_{k.e}+\varepsilon_{p.e}+\varepsilon_{ph}+\varepsilon_{ch}$$

Where, $\varepsilon_{k.e}$ and $\varepsilon_{p.e}$ are exergy due to velocity (or) kinetic energy and exergy due to potential energy respectively. ε_{ph} is physiccal exergy i.e. exergy due to temperature difference and pressure difference with respect to the reference point and ε_{ch} is chemical exergy (i.e due to reactions). In the present analysis, it is assumed that the exergy due to kinetic energy and potential energy are negligible. Also, for the exergy calculations, the atmospheric temperature and pressure are taken respectively as 30ºC and 101.325kPa.

Exergetic performance analysis is based on second law of thermodynamics. The results obtained from such an analysis can be used as a guide for diminishing the irreversibilities in the power plants and thereby enhancing their performances [3,4]. In fact, exergy is a thermodynamic indicator that shows the transformation potential and convertible limit of an energy carrier to maximum theoretical work under the conditions imposed by an environment at given pressure and temperature. In this exergetic performance analysis exergy efficiency and exergy destruction rate of both plant and plant component are determined. In addition, exergy losses per unit power output in the plants are defined and used as a new exergetic performance criterion.

For control volume of any plant component at steady-state conditions, a general equation of exergy destruction rate derived from the exergy balance can be given as equation number 1[8].

$$\dot{E}x_D = \sum(\dot{E}x)_{in} - \sum(\dot{E}x)_{out} + \left[\sum\left(\dot{Q}(1-\frac{T_o}{T})\right)_{in} - \sum\left(\dot{Q}(1-\frac{T_o}{T})\right)_{out}\right] \pm \dot{W} \quad (1)$$

Where the first two terms of right hand side represent exergy of streams at entry and exit the control volume. The third and fourth terms are the exergy related to heat transfer by heat. Q represents heat transfer rate across the boundary of the system at a constant temperature of T. The last term is work transfer rate to or from the control volume. In this study, only physical exergy by mass flows crossing the control volume is considered and given as equation number 2[9].

$$\dot{E}x = \dot{m}[(h-h_o)-T_o(s-s_o)] \quad (2)$$

Where, h and s represent specific enthalpy and entropy, respectively [5,6]. In the exergetic performance analysis, exergy efficiency gives a measure of the performance of a system or a component. Exergy efficiency of the components in the investigated power plants is defined based on product and fuel approach [7].

E-ISSN 2581 – 7957
P-ISSN 2277 – 3916

CVR Journal of Science and Technology, Volume 17, December 2019
DOI: 10.32377/cvrjst1724

The exergy analysis or second law efficiency results are computed as follows. In addition to it the opcan power box calculations are also shown below.

Boiler:

The exergy efficiency of the boiler is calculated as follows
input power = (486.11* {(13000-7000)) – (298) *(160-150)) =1468.05MW
output power =(430.55*{(2905)-298*(5.3521-1.3027)}) = 730.183 MW
Hence the efficiency is = output / input = 49.7%

Turbine:

There are two parts in the turbine. Hence exergy analysis is to be done individually.
For HPT: efficiency:
Input = ((3420-104.9)-(298)*(6.4481-.3664)) = 1502.75 kJ / kg
Output= ((3060-104.9)-(298*96.45-.3664)) = 1142.1 kJ /kg
Efficiency = 76 %
For LPT: efficiency:
Input = ((3540-104.9)-(298*(7.09-.366))) = 1429.56 kJ /kg
Output = ((2585.084-104.9)-(298*(7.358-.366)) = 398.952 kJ / kg
Efficiency = 27.9 %
Therefore the total turbine second law efficiency is equal to:
Total input: 1502.75 + 1429.56 = 2932.31 kJ /kg
Total output: 1142.1 + 398.952 = 1541.052 kJ /kg
Total efficiency: (1541.052 / 2932.31) = 52.5%

Condenser:

In the condenser the heat Balance equation is:
$Ex_1 = m[(h-h_o)-T_o(s-s_o)]$, here $h=h_f+x*h_{fg}$
Therefore, at T=70°C &P= 1bar
From steam tables h_f = 293.0kJ/kg , h_{fg} =2333.8kJ/kg , s_f=0.955k J/kgK, s_{fg}=6.800kJ/kgK
$Ex_1 = m[(h-h_o)-T_o(s-s_o)]$
=334.84[(2533.448-417.5)+70(7.483-1.3037)] =853.362kJ/kgK
Ex_2 = 334.84[(2333.8-293)-70(6.800-0.955)] =820.341kJ/kgK
Ex_3 = 334.84[(2459-417.5)–30(8.13236-1.3027)] =752.348kJ/kgK
The temperature at Ex_4 is not known hence it must be found out by the following procedure. From the plant the value of m = 6450.9 kg / sec
Then the equation is = $mC_p (T_4 – T_3)$ = mass flow rate $*h_{fg}$
Then T_4=60.13°C
Ex_4 =334.84[(2353.6-417.5) – 60.13(7.022-1.3027)
=763.435kJ/kgK
Exergy=Ex_4-Ex_3 / Ex_2 –Ex_1
=0.3357
η =33.57%
The concept to use this opcan power box in the power plant is to produce more power with the same input. This box will be kept at exit of the Low pressure turbine, so that it can utilize that waste heat from steam and water mixture.

Salient features of the OPCAN power box:
One box can produce 750kW of power.
The maximum efficiency of opcan box is 60%.
With the 1200kW input power it can produce 750kW power.
The input power (ex: compressor) needed to one box = 45kW
The mass flow rate of the steam at the exit of the Low pressure turbine will be = 334.8 Kg/sec.
Hence Q =$m_f * h_{fg}$ = 334.82* 2431kW
= 813996 kW
And that quantity Q = m*cp*dt
=> 813996 = m x0.8 x 40
=> m= 29071.28 kg / sec

IV. Opcan Power Box Installation

The power boxes can be kept individually by supplying the steam to them. In order to install the opcan power boxes the steam required for each box must be calculated. After that based on the available steam number of boxes to be installed will be known.
Therefore steam required for one box is = m * Cp* dT = Q(heat supplied)
=> m *0.8 *40 = 1200
=> m = 37.5 kg / sec.
Then the no of power boxes that can be adopted = 334.8 / 37.5 = 9
Hence the total extra power produced is = 9 * 750 = 6750kW = 6.7 MW.

V. Results

First law of thermodynamic efficiency is calculated to the main components of power plant viz., boiler, turbine, condenser. After calculating the first law efficiency, second law of thermodynamic efficiency known as exergytic efficiency has been calculated. Based on the outcomes of efficiencies it is found that second law efficiency is less than that of first law efficiency. The detailed outcomes of the efficiencies of first law and second law are compared in the below figures. Figure 3 shows the boiler and turbine efficiencies as per the energy and exergy analysis.

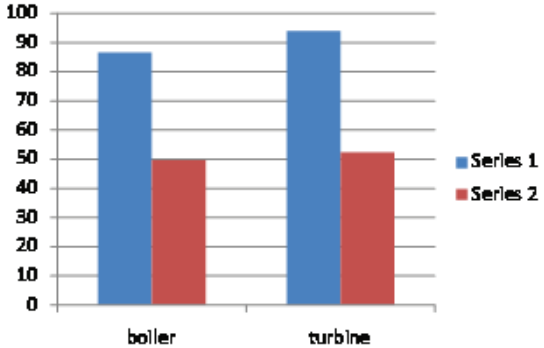

Figure 3. Comparison of I and II law efficiencies applied to boiler and turbine

The boiler efficiency as per energy analysis is 86.7% shown in blue color in figure 3 and as per exergy analysis it is 49.7% shown in blue color in figure 3. Similarly, for turbine the efficiencies as per energy and exergy analyses are 94% (blue color) and 52.5% (red color) shown in figure 3 respectively. Series 1 in blue color indicates the efficiency as per energy analysis and series 2 in red color indicates the efficiency as per exergy analysis.

CVR Journal of Science and Technology, Volume 17, December 2019
DOI: 10.32377/cvrjst1724

As discussed above, to the existing power plant setup the opcan power boxes are added to produce the extra power from the waste heat, which use escape out to the atmosphere through the chimneys. By installing the opcan power boxes it has been calculated that 6.7MW of extra power can be produced.

The opcan power boxes are easy to install and maintain hence these can be adopted with ease and less effort. During the process of energy conversion from the waste heat into useful form of electric energy no flue gases will be emitted. This process is economic as well as useful for the mankind to overcome the electricity needs. The efficiency calculations are given below.

Before installing the opcan power boxes

$$\eta_{overall} = 500 / 1100.4 = 45\ \%$$

After installing the opcan power boxes

$$\eta_{overall} = 506.7 / 1100.4 = 46.07\ \%$$

Increase in efficiency = 1.07 %

% of increase in efficiency = 2.37

The comparison of efficiencies of the power plant with and without using of opcan power boxes is given below in the figure 4.

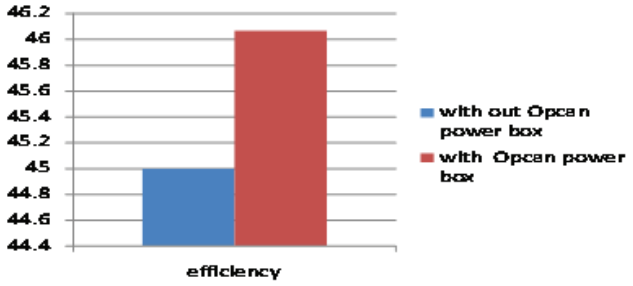

Figure 4. Comparison of efficiency with and without installing opcan power box.

The blue color bar indicates the efficiency of the power plant without using the opcan power box and the red color bar shows the efficiency of the power plant after installing the opcan power box. It can be observed from the above figure that there is an increase of efficiency of 1.07. This is a significant value for a thermal power plant, hence it is advisable to adopt the opcan power boxes to the existing thermal power plants for increasing the efficiency.

VI. Conclusions

From the above research it can be concluded that the efficiency calculated based on energy analysis for boiler and turbine are more compared to the same done by the exergy analysis. And by installing the opcan power boxes there is significant amount of improvement in the output quantity of power production. 6.7MW extra power production per 500MW power plant will make an arena for the existing power plants to modify and install the opcan power box for the efficient power production and also as already it is emphasized that as there is no extra input quantity of coal or gas are used in this hence the pollution also reduces. At the end there is a lot of scope for this technology in future to overcome the power demand and reduce the pollution problems.

References

[1] Acharya Chirag1, Prof. Nirvesh Mehta2 , Prof. Jaspal Dabhi3, Research paper on Analysis of Boiler losses to improve Unit heat rate of coal fired thermal power plant. International Journal of Advance Engineering and Research Development (IJAERD) Volume 1, Issue 5, May 2014, e-ISSN: 2348 - 4470 , print-ISSN:2348-6406

[2] I. S. Jacobs and C. P. Bean, “Fine particles, thin films and exchange anisotropy,” in *Magnetism*, vol. III, G. T. Rado and H. Suhl, Eds. New York: Academic, 1963, pp. 271–350.

[3] G. Eason, B. Noble, and I. N. Sneddon, “On certain integrals of Lipschitz-Hankel type involving products of Bessel functions,” Phil. Trans. Roy. Soc. London, vol. A247, pp. 529–551, April 1955.

[4] J. Clerk Maxwell, *A Treatise on Electricity and Magnetism*, 3rd ed., vol. 2. Oxford: Clarendon, 1892, pp.68–73.

[5] Vikas Bavane, Pooja Rindhe, Energy Analysis of Thermal Power Plant , International Journal of Research in Advent Technology (IJRAT) (E-ISSN: 2321-9637) Special Issue National Conference “CONVERGENCE 2017”, 09th April 2017

[6] Y. Yorozu, M. Hirano, K. Oka, and Y. Tagawa, “Electron spectroscopy studies on magneto-optical media and plastic substrate interface,” *IEEE Transl. J. Magn. Japan*, vol. 2, pp. 740–741, August 1987 [Digests 9th Annual Conf. Magnetics Japan, p. 301, 1982].

[7] M. Young, *The Technical Writer's Handbook*. Mill Valley, CA: University Science, 1989.

[8] Joong Yong Yi, Kyung Min Kim, Jongjun Lee and Mun Sei Oh, Exergy Analysis for Utilizing Latent Energy of Thermal Energy Storage System in District Heating, Energies 2019, 12, 1391; doi:10.3390/en12071391

[9] MSK. Tony Suryo U, Eflita Yohana, Syarif Dwi Priyanto, Ignatius Apryando M. and Tauviqirrahman, Energy and Exergy Analysis of Steam Power Plant 3rd Unit PT PLN (PERSERO) Centre Unit Generation Tanjung Jati B Use BFP-T Modification Cycle, E3S Web of Conferences 125, (2019) https://doi.org/10.1051/e3sconf/2019125 ICENIS 2019 13003 13003

E-ISSN 2581 – 7957
P-ISSN 2277 – 3916

CVR Journal of Science and Technology, Volume 17, December 2019
DOI: 10.32377/cvrjst1725

Design and Analysis of Shock Absorber using ANSYS Workbench

C. Sai Kiran
[1]Asst. Professor, CVR College of Engineering/Mechanical Engg. Department, Hyderabad, India
Email: csaikiran001@gmail.com

Abstract: **In this paper, a shock absorber is designed and analyzed which is useful for damping shock impulse and dissipating kinetic energy. Shock absorber is a critical part of the suspension system, which is used to connect the vehicle to the wheels. The purpose of the work is to model a shock absorber which will be able to improve the ride quality by reducing the amplitude of disturbances caused by a bump road. Shock absorber is designed in CREO software. Analysis of shock absorber was performed by using ANSYS software and this analysis helps to predict the shock absorber failure when an external load acts on it.**

Index Terms: **Shock absorber, Shock impulse, Von-mises stress, ANSYS.**

I. Introduction

Whenever any vehicle crosses a bump on the road, shock impulse is generated which will affect the passengers travelling in the vehicle Therefore, shock absorber or damper is a critical part of a suspension system used to dissipate kinetic energy and damp shock impulse. Without shock absorbers, the vehicle will bounce ride. A shock absorber absorbs sudden shocks generated by the uneven surface of the road and makes the ride smooth and comfortable.

Johnson et al. [1] has created a shock absorber design for carrying loads of a vehicle. The shock absorber is modelled in CATIA V5 software. Structural analysis is performed by varying the material in ANSYS Mechanical APDL software. After modelling the shock absorber, boundary conditions are applied. Von-mises stress and deformation values are observed in the results.

Sudarshan et al. [2] has developed a new methodology which allows designing the components of a shock absorber by using FEM. In production of shock absorbers, it is difficult to know the accuracy of shock absorber which doesn't fail. The shock absorber is modelled by using CAD software and analysed in ANSYS workbench by considering the weight of vehicle. In the results, deflection and stress induced in the shock absorber are observed.

Bhasha et al. [3] has designed a 3D model of shock absorber by using CATIA V5 R21 and changed the thickness of spring. A shock absorber reduces the effect of shocks while travelling on a rough road and increases the ride comfort and quality by reducing the amplitude of disturbances. Structural and modal analysis is performed on shock absorber by considering different materials for spring by using ANSYS software. Structural analysis was performed to validate the strength of the shock absorber. To determine the displacements for different frequencies, modal analysis was performed.

Chavhan et al. [4] has designed a shock absorber of pleasure vehicle. The shock absorber is modelled using Pro-E software. By using ANSYS software, static and dynamic analysis is performed by changing materials for spring. In ANSYS, the results of deflection and von-mises stress are observed.

Mallesh et al. [5] has designed a 3D model of shock absorber by using CATIA V5 20 software and structural analysis of shock absorber is performed by using ANSYS 15.0 software. Suspension system consists of springs and dampers for passenger's safety and for a comfortable ride. A shock absorber consists of spring, top and bottom part. The loads are applied on shock absorber to know the results of total deformation, equivalent stress and equivalent strain.

Mohan et al. [6] has modelled a shock absorber using Pro/ENGINEER software. Structural and modal analysis is performed by considering the vehicle weight and person weight. Modal analysis is performed to know the displacements and frequencies for number of mode shapes.

Achyut et al. [7] has designed a 3D model of shock absorber by using Pro/ENGINEER software. Shock absorber consists of a sliding piston in a cylinder. The cylinder can be filled by either fluid or air. Analysis is performed in ANSYS. The results of natural frequency, total deformation and shear stress are observed.

Manga et al. [8] has modelled a shock absorber using CATIA V5 R20. A shock absorber uses a soft spring for controlling the rate of suspension movement in response to bumping. Structural and modal analysis of shock absorber is performed by using ANSYS. Modal analysis is performed for different frequencies to understand deformations for ten different mode shapes.

Prasad et al. [9] has focused on developing new correlate methodologies which enables to design different parts of a shock absorber by FEM tools. All the different parts of shock absorbers are modelled and assembled in CAD software. Structural analysis is performed in ANSYS 13.0 software.

Christopher et al. [10] has designed and analysed the shock absorber performance by varying the diameter of the spring. The modelling of shock absorber is performed by using Pro-E and analysis by using ANSYS software. The analysis is performed by considering number of persons, different loads and bike mass.

Durmus et al. [11] has created a shock absorber model by using CATIA software. Modal and structural analyses are performed by considering different materials for shock absorber. The analysis is performed by considering four person's weight, vehicle weight and different loads. The

E-ISSN 2581 – 7957
P-ISSN 2277 – 3916

DOI: 10.32377/cvrjst1725

results were analysed and optimized in Minitab software by using Taguchi method.

Sunil et al. [12] has designed a 3D model of a shock absorber with helical spring and wave spring by using CREO software. Structural and modal analysis is performed by considering the bike and passengers weight by using ANSYS software. To determine the strength of the shock absorber, structural analysis is performed. Modal analysis is performed to determine the displacements and frequency of each number of mode shapes.

Ramanjaneyulu et al. [13] has designed the shock absorber of hero honda bike by using Solidworks software. By considering different loading conditions, structural and modal analysis is performed by using ANSYS software.

Akhil et al. [14] has modelled a shock absorber with different tapper angles for a spring by using CATIA-V5. To determine stresses and deflections, structural analysis is performed. The results are compared with existing spring model to verify the best spring design of shock absorber.

Chatterjee et al. [15] has modelled a shock absorber in Solidworks. The analysis of the shock absorber is performed in Abaqus and Ansys software. Shear stress and deflection results are observed to suggest the best material.

A. Different Types of Shock Absorber

Shock absorbers connect vehicles to its wheels. A shock absorber is coupled with a spring to convert sudden shock waves into oscillatory motion. Shock absorbers provide a comfortable ride and stability to the vehicle on the uneven surface of the road[1].

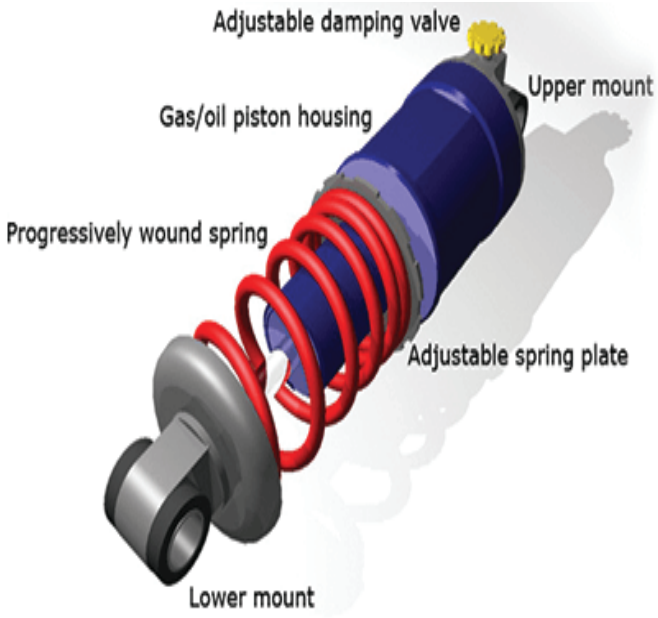

Figure 1. Shock Absorber and its Parts

Shock absorber is represented in Fig. 1. The main parts of a shock absorber are spring, adjustable spring plate, gas/oil piston housing, damping valve, upper and lower mount[2]. Some of the important types of shock absorbers are given below [3]:

1. Mono tube damper shock absorber.
2. Twin tube damper shock absorber.
3. Air shock absorber.
4. Electric shock absorber.

B. Working Principle of a Shock Absorber

Whenever a vehicle hits a bump on the road, the spring of the shock absorber to coil and uncoil. The energy of the spring is transferred to the shock absorber through the upper mount, down through the piston rod and into the piston.

The working principle of a shock absorber is shown in Fig. 2. The shock absorber works in extension cycle and the compression cycle. In the extension cycle, the piston moves upwards. In the compression cycle, the piston moves down and compresses the spring. The compression cycle controls the vehicle's unsprung weight and extension cycle controls the sprung weight of the vehicle.

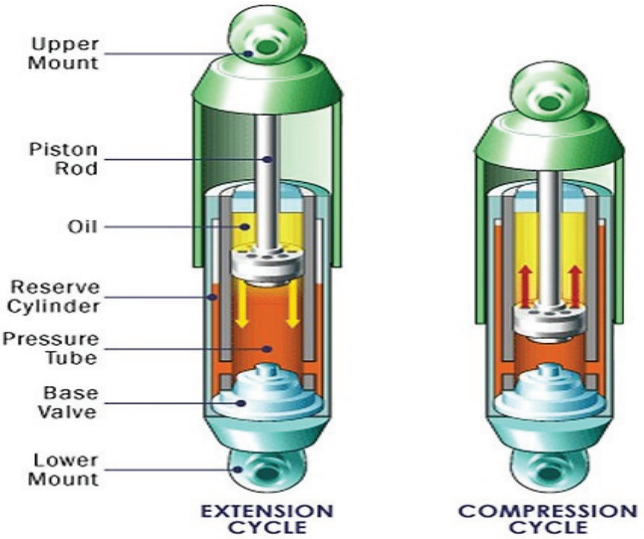

Figure 2. Working Principle of a Shock Absorber

C. Shock absorber Material

Shock absorbers are generally made of materials which are very strong and suitable to withstand heavier impact loads on it. Carbon steel, Stainless steel and Aluminum alloy are the materials[8] selected for shock absorber as shown in Table I.

TABLE I.
MATERIAL PROPERTIES OF STEEL

S. No	Properties	Carbon Steel	Stainless Steel	Aluminum Alloy
1.	Density (Kg/m^3)	7,870	7,850	3,630
2.	Young's Modulus (GPa)	205	203	77.9
3.	Yield Strength (MPa)	360	310	279
4.	Tensile Strength (MPa)	440	510	344
5.	Poisson's Ratio	0.29	0.275	0.327

II. MODELLING AND FINITE ELEMENT ANALYSIS

A. Shock absorber Model

The important parts of a shock absorber are upper mount, piston rod, cylinder and lower mount. All the different parts of the shock absorber are modelled separately in CREO software and all the individual parts of the shock absorber are assembled in the CREO as shown in Fig. 3

E-ISSN 2581 – 7957
P-ISSN 2277 – 3916

CVR Journal of Science and Technology, Volume 17, December 2019
DOI: 10.32377/cvrjst1725

Figure 3. Assembled Model of Shock Absorber in CREO

B. Elememt Type

The element type selected for shock absorber is SOLID 186. It is a 20-node higher order solid element which has three degrees of freedom per node. The three degrees of freedom are nodal x, y and z translations.

It exhibits quadratic displacement behavior and have spatial orientation. SOLID 186 support large strain capabilities, plasticity, large deflection, hyper elasticity, stress stiffening and creep. SOLID 186 have capability for simulating deformations of incompressible elastoplastic materials and incompressible hyper-elastic materials.

C. Meshing

In meshing, the created 3D model is divided into the certain number of divisions or elements for accurate analysis result. By applying meshing on the model, we can determine the effectiveness and efficiency of any analysis. An automated mesh is generated on the created model which is shown in Fig. 4.

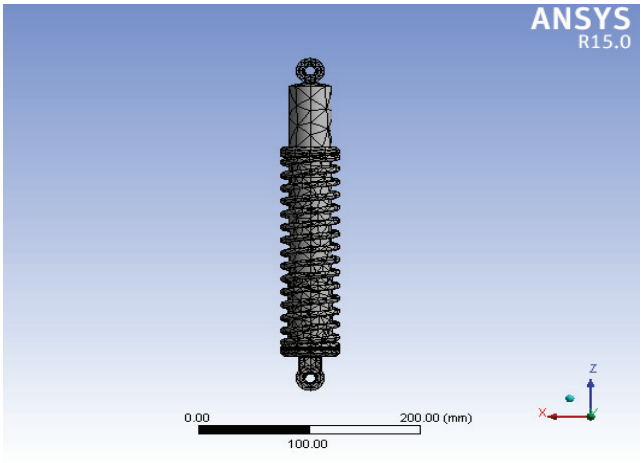

Figure 4. Meshing of Shock Absorber

In the automatic mesh, a fine mesh is applied to achieve precise and accurate results. Instead of using a fine mesh on all the components of the model, coarse mesh is applied on larger area and fine mesh is applied only on the area of higher stress concentration.

D. Applying Loads

On the lower mount of the shock absorber, a fixed support is assigned to withstand the forces acting on the shock absorber as shown in Fig. 5.

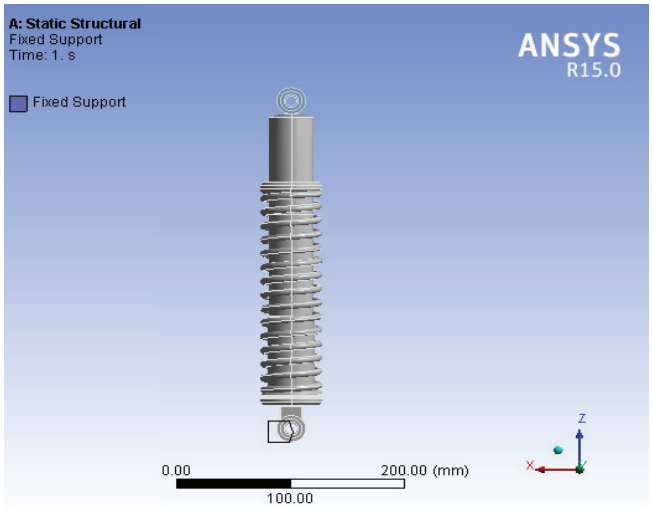

Figure 5. Fixed Support on the Lower Mount of Shock Absorber

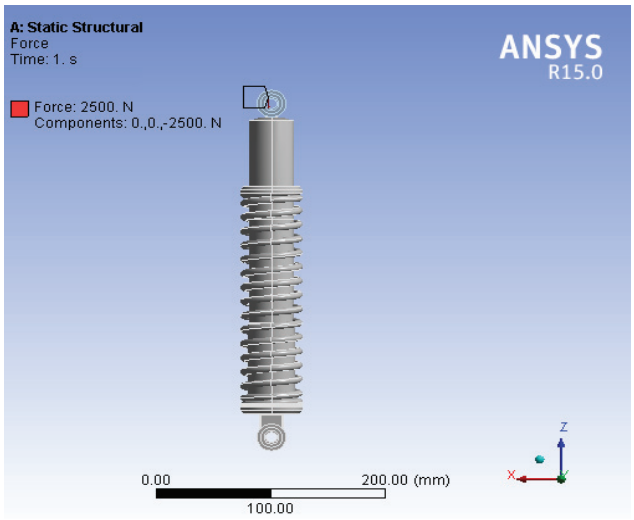

Figure 6. Applying Force on Upper Mount of Shock Absorber

Whenever a certain external load is applied on the upper mount of a shock absorber, the shock absorber cylinder moves down and compresses the spring. For applying the load on the shock absorber, the weight of the vehicle with passengers is calculated in Kg and the weight is converted into force. A force of 2500 N is applied on the upper mount of the shock absorber[4] as shown in Fig. 6.

III. Results And Discussions

After assigning fixed support on the lower mount and applying the static load on the upper mount of the shock

E-ISSN 2581 – 7957
P-ISSN 2277 – 3916

CVR Journal of Science and Technology, Volume 17, December 2019
DOI: 10.32377/cvrjst1725

absorber, structural analysis is performed on the shock absorber for three different materials in ANSYS workbench to determine the total deformation and von-mises stress. The following results were observed in the analysis.

A. Total Deformation of Shock absorber

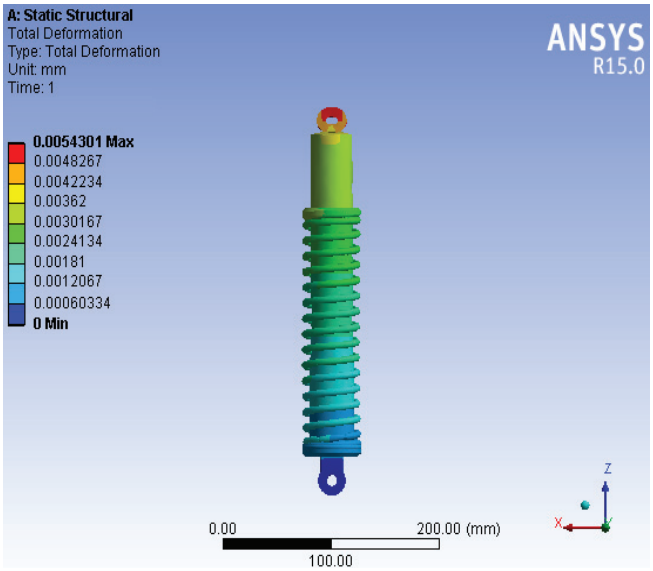

Figure 7. Total Deformation of Carbon Steel Material

After performing structural analysis by applying the load on shock absorber for carbon steel material, a maximum total deformation of 0.0054 mm and the minimum total deformation of 0 mm are observed from the Fig. 7.

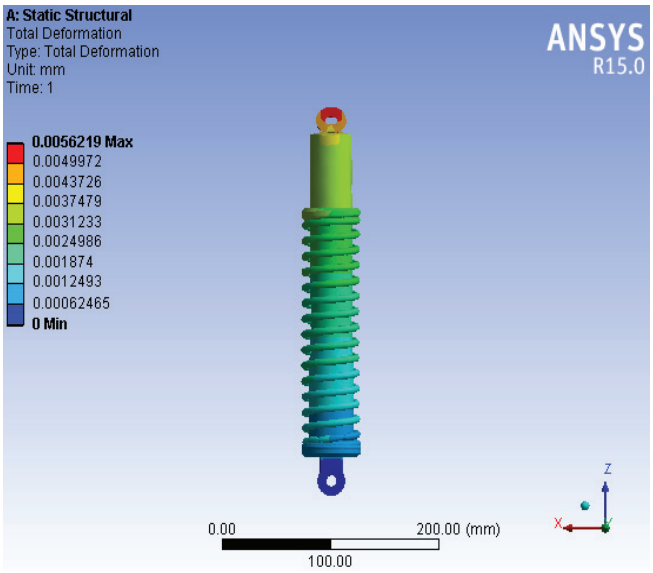

Figure 8. Total Deformation of Stainless Steel Material

After performing structural analysis by applying the load on shock absorber for stainless steel material, a maximum total deformation of 0.0056mm and the minimum total deformation of 0 mm are observed from the Fig. 8.

After applying the load on shock absorber, structural analysis is performed on aluminum alloy material. A maximum total deformation of 0.0152mm and the minimum total deformation of 0 mm are observed from the Fig. 9.

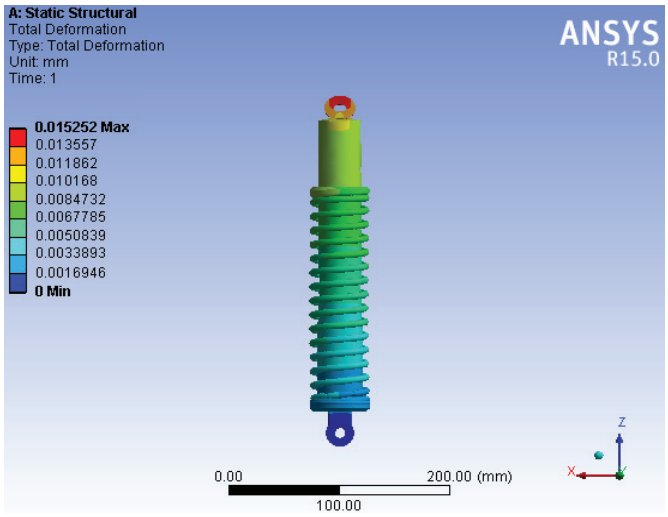

Figure 9. Total Deformation of Aluminum Alloy Material

B. Von-mises Stress of Shock absorber

After performing structural analysis by applying the load on shock absorber for carbon steel material, maximum von-mises stress of 21.09MPa and minimum von-mises stress of 0.0197Pa are observed from the Fig. 10.

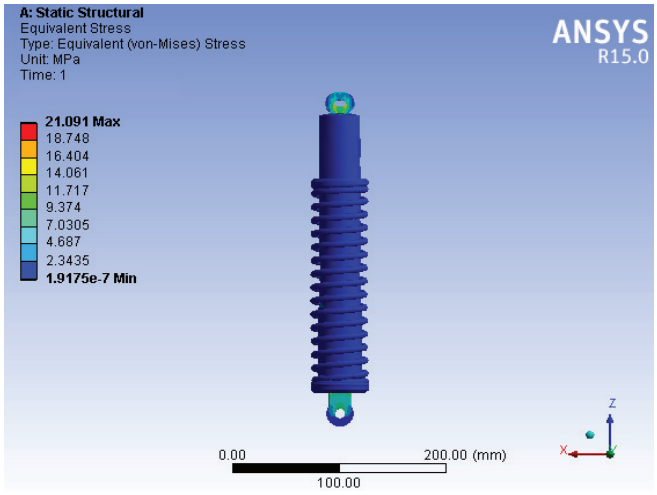

Figure 10. Von-mises Stress of Carbon Steel Material

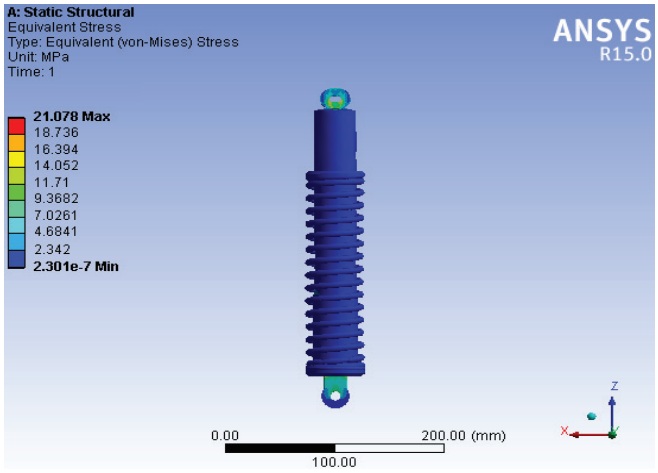

Figure 11. Von-mises Stress of Stainless Steel Material

E-ISSN 2581 – 7957
P-ISSN 2277 – 3916

CVR Journal of Science and Technology, Volume 17, December 2019
DOI: 10.32377/cvrjst1725

After performing structural analysis by applying the load on shock absorber for stainless steel material, maximum von-mises stress of 21.07MPa and minimum von-mises stress of 0.2301Pa are observed from the Fig. 11.

After performing structural analysis by applying the load on shock absorber for aluminum alloy material, maximum von-mises stress of 21.05 MPa and minimum von-mises stress of 0.025Pa are observed from the Fig. 12.

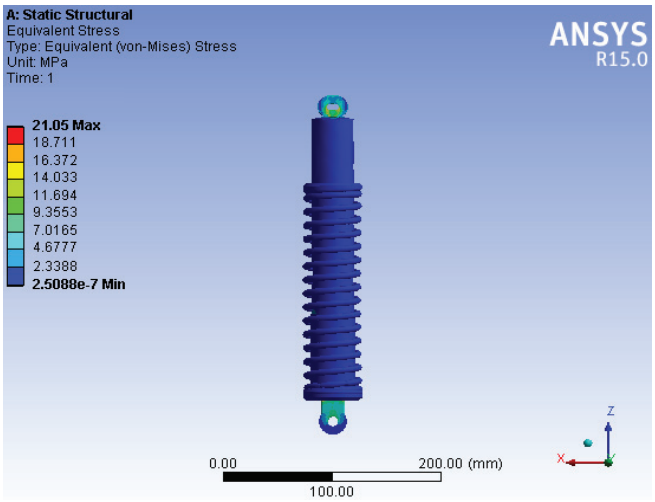

Figure 12. Von-mises Stress of Aluminum Alloy Material

After performing structural analysis by applying the load on shock absorber, the graph of total deformation for three different materials is observed from the Fig. 13.

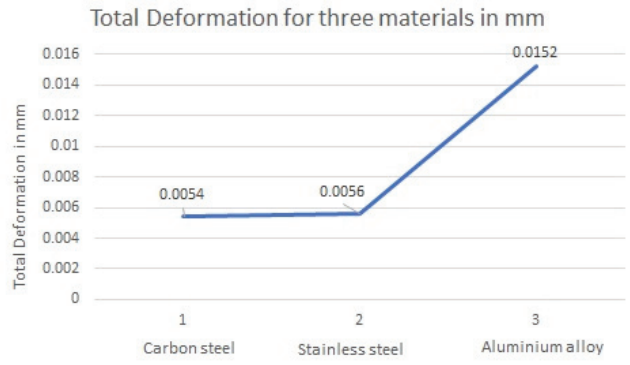

Figure 13. Total Deformation Graph for Different Materials

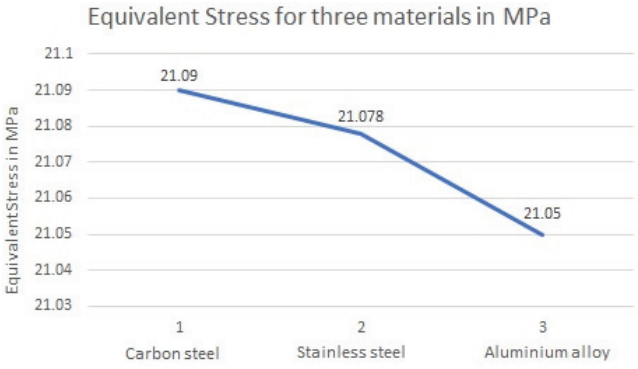

Figure 14. Equivalent Stress Graph for Different Materials

After performing structural analysis by applying the load on shock absorber, the graph of von-mises stress for three different materials is observed from the Fig. 14.

IV. Conclusions

In this paper, CREO software is used for modelling the shock absorber and analysis of shock absorber with a force of 2500 N is analysed by using ANSYS software. The von-mises stress and total deformation of the shock absorber are analysed.

TABLE II.
Results Comparison for Shock Absorber Material

Material	Total Deformation (mm)	Equivalent Stress(MPa)
Carbon Steel	0.0054	21.09
Stainless Steel	0.0056	21.078
Aluminum Alloy	0.0152	21.05

From the Table II, it is observed that the maximum total deformation is observed in aluminium alloy and the minimum total deformation is observed in carbon steel material. Maximum von-mises stress is observed in carbon steel and the minimum von-mises stress is observed in aluminium alloy material. The values of von-mises stress and total deformation of the shock absorber are within the limits. Therefore, modelled shock absorber has long life and safe to use.

In future scope, different dimensions for a shock absorber can be modelled by considering advanced materials like composites and by assigning different loading conditions for performing analysis.

References

[1] Johnson, Davis Jose and Anthony Tony, "Design and analysis of a shock absorber," *International Journal of Scientific and Engineering Research*, vol. 7, Issue 3, ISSN 2229-5518 pp. 19–23, March 2016.

[2] Sudarshan Martande, Y. N. Jangale and N. S. Motgi, "Design and analysis of shock absorber," *International Journal of Application or Innovation in Engineering and Management*, vol. 2, Issue 3, ISSN 2319-4847 pp. 195–199, March 2013.

[3] A. Chinnamahammad Bhasha, N. Vijay Rami Reddy and B. Rajnaveen, "Design and analysis of shock absorber," *International Journal of Engineering and Technology*, vol. 4, Issue 1, pp. 201–207, January 2017.

[4] G. R. Chavhan, S. W.Burande and Dr. L. P. Dhole, "Analysis of shock absorber using different material of spring," *International Journal of Advanced Engineering Technology*, vol. 5, Issue 4, pp. 19–21, December 2014.

[5] Mallesh Jakanur, and Dr. S. Chakradhar Goud, "Structural static analysis of shock absorber," *International Journal of Advance Research in Science and Engineering*, vol. 5, Issue 8, pp. 248–255, August 2016.

[6] Pinjarla Poornamohan, and T. Lakshmana Kishore, "Design and analysis of shock absorber," *International Journal of Research in Engineering and Technology*, vol. 1, Issue 4, pp. 578–592, December 2012.

[7] Achyut P. Banginwar, Nitin D. Bhusale and Kautuk V. Totawar, "Design and analysis of shock absorber using FEA

CVR Journal of Science and Technology, Volume 17, December 2019
DOI: 10.32377/cvrjst1725

tool," *International Journal of Engineering Research and Development*, vol. 10, Issue 2, pp. 22–28, February 2014.

[8] Manga Hymanjali, Elumagandla Surender, and Nalla Suresh, "Design and analysis of shock absorber," *International Journal of Innovative Science and Research Technology*, vol. 3, Issue 8, pp. 420–430, August 2018.

[9] V. Hari Prasad, Upparpalli Guna, and Dr. D. Vijayaganapathy, "Design and analysis of a shock absorber spring for automobiles," *International Journal of Pure and Applied Mathematics*, vol. 120, Issue 6, ISSN 1314-3395 pp. 3955–3963, June 2018.

[10] J. Prince Jerome Christopher, and R. Pavendhan, "Design and analysis of two-wheeler shock absorber coil spring," *International Journal of Modern Engineering Research*, pp. 133–140.

[11] Durmus Ali Bircan, and Abdul kadir Yasar, "Design, analysis and optimization of a shock absorber," *Journal of Agricultural Machinery Science,* vol. 10, Issue 4, pp. 293–299, August 2014.

[12] K. Raminaidu, K. Sunil Ratna Kumar, E. Venkateshwar Rao, and Ch. Lakshmi Pornima, "Design and analysis of wave spring for motar cycle shock absorber," *Anveshana's International Journal of Research in Engineering and Applied Sciences*, vol. 3, Issue 2, ISSN-2455-6300, pp. 171–176, February 2018.

[13] S. Ramanjaneyulu, B. Geetha Chandra Sekhar, and R. Rama Krishna, "Design, modeling and performance analysis of psd shock absorber using ansys," *International Journal of Current Engineering and Scientific Research*, vol. 5, Issue 4, ISSN-2393-8374, pp. 68–80, 2018.

[14] Gopireddy Akhil Kumar Reddy, and Dr. G. Maruthi Prasad Yadav, "Modeling and analysis of two wheeler shock absorber for optimum performance," *International Journal of Engineering Trends and Applications*, vol. 5, Issue 2, ISSN-2393-9516, pp. 7–13, March 2018.

[15] Sitangshu Chatterjee, and Subash Nandy, "Optimization of a shock absorber using finite element analysis," *International Journal of Science, Engineering and Technology Research*, vol. 7, Issue 8, ISSN: 2278-7798, pp. 564–568, August 2018.

E-ISSN 2581 – 7957
P-ISSN 2277 – 3916

CVR Journal of Science and Technology, Volume 17, December 2019
DOI: 10.32377/cvrjstxxxx

Template for the Preparation of Papers for Publication in CVR Journal of Science and Technology

First Dr.A. Author[1] and Second B. Author[2]
[1]Designation, Name of Institution/Department, City, Country
Email: first.author@hostname1.org
[2]Designation, Name of Institution/Department, City, Country
Email: second.author@hostname2.org

Abstract: **These instructions give you basic guidelines for preparing camera-ready papers for CVR College journal Publications. Your cooperation in this matter will help in producing a high quality journal.**

Index Terms: **first term, second term, third term, fourth term, fifth term, sixth term**

I. Introduction

Your goal is to simulate the usual appearance of papers in a Journal Publication of the CVR College. We are requesting that you follow these guidelines as closely as possible. It should be original work. Format must be done as per the template specified. Diagrams with good clarity with relevant reference within the text are to be given. References are to be cited within the body of the paper. Number of pages must not be less than five with minimum number of 4000 words and not exceeding eight pages. The journal is published in colour. Colours used for headings, subheadings and other captions must be strictly as per the template given in colour.

A. Full-Sized Camera-Ready (CR) Copy

Prepare your CR paper in full-size format, on A4 paper (210 x 297 mm or 8.27 x 11.69 in). No header or footer, no page number.

Type sizes and typefaces: Follow the type sizes specified in Table I. As an aid in gauging type size, 1 point is about 0.35 mm. The size of the lowercase letter "j" will give the point size. Times New Roman has to be the font for main text. Paper should be single spaced.

Margins: Top and Bottom = 24.9mm (0.98 in), Left and Right = 16 mm (0.63 in). The column width is 86mm (3.39 in). The space between the two columns is 6mm (0.24 in). Paragraph indentation is 3.7 mm (0.15 in).

Left- and right-justify your columns. Use tables and figures to adjust column length. On the last page of your paper, adjust the lengths of the columns so that they are equal. Use automatic hyphenation and check spelling. Digitize or paste down figures.

For the Title use 24-point Times New Roman font, an initial capital letter for each word. Its paragraph description should be set so that the line spacing is single with 6-point spacing before and 6-point spacing after. Use two additional line spacings of 10 points before the beginning of the double column section, as shown above.

TABLE I.
TYPE SIZES FOR CAMERA-READY PAPERS

Type size (pts.)	Appearance		
	Regular	Bold	Italic
6	Table caption, table superscripts		
8	Tables, table names, f irst letters in table captions, figure captions, footnotes, text subscripts, and superscripts		
9	References, authors' biographies	Abstra ct	
10	Section titles ,Authors' affiliations, main text, equations, first letters in section titles		Subheading
11	Authors' names		
24	Paper title		

Each major section begins with a Heading in 10 point Times New Roman font centered within the column and numbered using Roman numerals (except for REFERENCES), followed by a period, two spaces, and the title using an initial capital letter for each word. The remaining letters are in SMALL CAPITALS (8 point). The paragraph description of the section heading line should be set for 12 points before and 6 points after.

Subheadings should be 10 point, italic, left justified, and numbered with letters (A, B, …), followed by a period, two spaces, and the title using an initial capital letter for each word. The paragraph description of the subheading line should be set for 6 points before and 3 points after.

For main text, paragraph spacing should be single spaced, no space between paragraphs. Paragraph indentation should be 3.7mm/0.21in, but no indentation for abstract & index terms.

II. Helpful Hints

A. Figures And Tables

Position figures and tables at the tops and bottoms of columns. Avoid placing them in the middle of columns. Large figures and tables may span across both columns. Leave sufficient room between the figures/tables and the main text. Figure captions should be centered below the figures; table captions should be centered above. Avoid placing figures and tables before their first mention in the

E-ISSN 2581 – 7957
P-ISSN 2277 – 3916

DOI: 10.32377/cvrjstxxxx

text. Use the abbreviation "Fig. 1," even at the beginning of a sentence.

To figure axis labels, use words rather than symbols. Do not label axes only with units. Do not label axes with a ratio

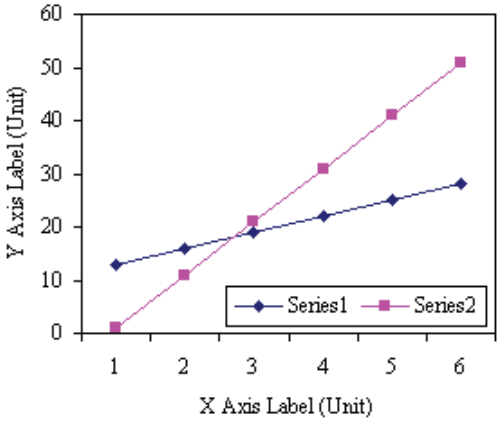

Figure 2. Note how the caption is centered in the column.

of quantities and units. Figure labels should be legible, about 8-point type.

All figures, tables and references must be cited in the text.

Please indicate the broad area/specializations into which the research paper falls, in the covering letter/mail to the Editor, so that reviewers with those specializations may be identified.

B. References

Number citations consecutively in square brackets [1]. Punctuation follows the bracket [2]. Use "Ref. [3]" or "Reference [3]" at the beginning of a sentence:

Give all authors' names; use "et al." if there are six authors or more. Papers that have not been published, even if they have been submitted for publication, should be cited as "unpublished" [4]. Papers that have been accepted for publication should be cited as "in press" [5]. In a paper title, capitalize the first word and all other words except for conjunctions, prepositions less than seven letters, and prepositional phrases. Good number of references must be given.

Latest references in the area must be included and every refence must be cited in the text of the research article.

C. Footnotes

Number footnotes separately in superscripts [1, 2, ···]. Place the actual footnote at the bottom of the column in which it was cited, as in this column. See first page footnote as an example.

D. Abbreviations and Acronyms

Define abbreviations and acronyms the first time they are used in the text, even after they have been defined in the abstract. Do not use abbreviations in the title unless they are unavoidable.

E. Equations

Equations should be left justified in the column. The paragraph description of the line containing the equation should be set for 6 points before and 6 points after. Number equations consecutively with equation numbers in parentheses flush with the right margin, as in (1). Italicize Roman symbols for quantities and variables, but not Greek symbols. Punctuate equations with commas or periods when they are part of a sentence, as in

$$a + b = c \ . \qquad (1)$$

Symbols in your equation should be defined before the equation appears or immediately following. Use "(1)," not "Eq. (1)" or "equation (1)," except at the beginning of a sentence: "Equation (1) is ..."

F. Other Recommendations

Use either SI (MKS) or CGS as primary units. (SI units are encouraged.) If your native language is not English, try to get a native English-speaking colleague to proofread your paper. Do not add page numbers.

III. Conclusions

The authors can conclude on the topic discussed and proposed, future enhancement of research work can also be briefed here.

References

[1] G. Eason, B. Noble, and I. N. Sneddon, "On certain integrals of Lipschitz-Hankel type involving products of Bessel functions," Phil. Trans. Roy. Soc. London, vol. A247, pp. 529–551, April 1955.

[2] J. Clerk Maxwell, *A Treatise on Electricity and Magnetism*, 3rd ed., vol. 2. Oxford: Clarendon, 1892, pp.68–73.

[3] I. S. Jacobs and C. P. Bean, "Fine particles, thin films and exchange anisotropy," in *Magnetism*, vol. III, G. T. Rado and H. Suhl, Eds. New York: Academic, 1963, pp. 271–350.

[4] K. Elissa, "Title of paper if known," unpublished.

[5] R. Nicole, "Title of paper with only first word capitalized", *J. Name Stand. Abbrev.*, in press.

[6] Y. Yorozu, M. Hirano, K. Oka, and Y. Tagawa, "Electron spectroscopy studies on magneto-optical media and plastic substrate interface," *IEEE Transl. J. Magn. Japan*, vol. 2, pp. 740–741, August 1987 [Digests 9th Annual Conf. Magnetics Japan, p. 301, 1982].

[7] M. Young, *The Technical Writer's Handbook*. Mill Valley, CA: University Science, 1989.

[8] T. Ali, B.K. Subhash and R.C. Biradar, "A Miniaturized Decagonal Sierpinski UWB Fractal Antenna", PIERS C, vol. 84, pp. 161-174, 2018.

E-ISSN 2581 – 7957
P-ISSN 2277 – 3916

In the next issue (Vol 18, June 2020)

1.	*Effect of Mineral Admixture, W/B Ratio and Elevated Temperature on Strength of Lightweight Expanded Clay Aggregate*	*V. Sravan, T. Manoj, Prof. M. V. Seshagiri Rao*
2.	*Influence of Temperature on the Fracture Parameters of Basalt Fiber Concrete*	*N. Shiva kumar, Prof. T. Muralidhara Rao*
3.	*Analysis of Beam-Column Joints Using FEM Method*	*Ch Harika, Prof. N. Murali Krishna*
4.	*Implementation of 2x2 MIMO-OFDM System using NI-USRP and LabVIEW*	*Prof. Yedukondalu Kamatham, Naveen Talati*
5.	*A Cluster Head Routing Protocol for Improving Network Lifetime in Wireless Sensor Networks*	*Gaurav Sharma*
6.	*Optimal supplementary controller design for IPFC in order to damp low- frequency Oscillations in power systems*	*Prof. Shankarappa F Kodad, Dakka Obulesu, Manjunatha S C*
7.	*Cascaded H-Bridge Inverter for Wind Driven Isolated Squirrel Cage Induction Generators*	*G. Manohar, K Chiranjeevi*
8.	*Machine Vision Based Color Recognition by Robotic Arm Using LabVIEW*	*Y. Divya, C. Pramod Kumar*

ABOUT THE COLLEGE

CVR College of Engineering (A UGC Autonomous Institution) was established in the year 2001, and its fourteenth batch of students graduated from the College. This college is on a roll with the recent ***NIRF*** *ranking of 132 in the Country, followed by record placements.*

The College was the ***first*** *college in Telangana that was promoted by NRI technology professionals resident in the US. The NRI promoters are associated with cutting-edge technologies of the computer and electronics industry. They also have strong associations with other leading NRI professionals working for world-renowned companies like IBM, Intel, Cisco, Facebook, AT&T, Google and Apple who have agreed to associate with the College with a vision and passion to make the College a state-of-the-art engineering institution.*

The college has many accomplishments and to name a few, it obtained ***NBA Tier 1 accreditation for its UG Programs, NAAC 'A' grade, UGC autonomous status, National Employability Award*** *for seventh year in a row and received a very high rating by several ranking agencies including the most recent Education World ranking of third best college in Telangana and Outlook magazine, rating CVR CE, one among the* ***top 100 colleges in the country****, and* ***AAAA grade*** *from Careers 360. The college received the* ***ISTE Best Engineering College award*** *and, the Director Dr. K. Rama Sastri, the ISTE Lifetime Achievement Award in 2017.*

The college received Rs. 2.87 crores from New Gen IEDC of the DST. Faculty members are working on Rupees One crore worth projects with funding from the AICTE, UGC and ISRO.

The college has been creating records year after year. With more than 100 companies visiting CVR and more than 750 placements for the 2018-19 academic year, it is the highest among the peer group of colleges. The highest offer of Rs. 30.25 Lakh PA was bagged by 7 students and close to 25 students got offers higher than Rs. 10 Lakh PA. About 65 offers are higher than Rs. 7 Lakh PA and another 60 offers are higher than Rs. 5 Lakh PA. With this, CVR became the leading college in entire Telangana in terms of the offers with higher salaries. CVR has made huge progress in a short span of time and was preferred by the students and parents during the EAMCET counseling this year and is among the top 3 colleges in the state.

In keeping with the current global emphasis on green and eco-friendly energy generation, 360kW Solar PV plant has been installed on the campus to meet the power requirements of the college to a significant extent.

CALL FOR PAPERS:

Papers in Engineering, Science and Management disciplines are invited for Publication in our Journal. Authors are requested to mail their contributions to Editor, CVR Journal of Science and Technology (Email Id: journal@cvr.ac.in). Authors can also submit their papers through our online open journal system(OJS) www.ojs.cvr.ac.in or www.cvr.ac.in/ojs Papers are to be written using a Standard Template, which may be obtained on request from the Editor. It is also available on the college website www.cvr.ac.in

.

CVR JOURNAL OF SCIENCE AND TECHNOLOGY

CVR COLLEGE OF ENGINEERING

(UGC Autonomous- Affiliated to JNTU Hyderabad)
Mangalpalli (V), Ibrahimpatnam (M),
R.R. District, Telangana - 501510
http://cvr.ac.in